PROCEEDINGS OF PAPERS

UNIVERSITY OF NIŠ
FACULTY OF OCCUPATIONAL SAFETY
Department of Preventive Engineering
Noise and Vibration Laborotory

"POLYTECHNICA" UNIVERSITY OF TIMISORA
FACULTY OF MECHANICAL ENGINEERING
Department of Mechanics and Vibration
Noise and Vibration Laboratory

27th INTERNATIONAL CONFERENCE

NOISE & VIBRATION

20 - 21, October 2022.
Niš, Serbia

27th INTERNATOINAL CONFERENCE

NOISE AND VIBRATION

PROCEEDING OF PAPERS

Niš, October 20-21, 2022.

Publisher: *University of Niš, Faculty of Occupational Safety*
For the publisher: *Prof. Srđan Glišović, Ph. D.*
dean

Editors of proceeding of papers:
Prof. Dragan Cvetković, Ph. D.
Prof. Vasile Marinca, Ph. D.
Prof. Nicolae Herisanu, Ph. D.
Prof. Momir Praščević, Ph. D.
Prof. Darko Mihajlov, Ph. D.

All paper published in the Proceedings of papers are reviewed in peer-review process.

Printout: "Unigraf X-copy" Niš

No. of copies: 120

ISBN: 978-86-6093-111-7

CIP - Каталогизација у публикацији

Народна библиотека Србије, Београд

534.83(082)
62-752(082)
614.872(082)
628.517(082)

INTERNATIONAL Conference Noise and Vibration (27 ; 2022 ; Niš)

Proceeding of Papers / 27th International Conference Noise and Vibration, Niš, October 20-21, 2022. ; [organizer University of Niš, Faculty of Occupational Safety of Niš, Department of Preventive Engineering, Noise and Vibration Laboratory [and] "Politechnica" University of Timisoara, Faculty of Mechanical Engineering, Department of Mechanical Engineering, Noise and Vibration Laboratory] ; [editors Dragan Cvetković ... [et al.]]. - Niš : University Faculty of Occupational Safety, 2022 (Niš : Unigraf X-copy). - 187 str. : ilustr. ; 30 cm

Tekst štampan dvostubačno. - Tiraž 120. - Bibliografija uz svaki rad.

ISBN 978-86-6093-111-7

а) Бука -- Зборници б) Вибрације -- Зборници

COBISS.SR-ID 77168905

ORGANIZER

University of Niš

Faculty of Occupational Safety

Department of Preventive Engineering

Noise and Vibration Laboratory

www.znrfak.ni.ac.rs

"Politechnica" University of Timisoara

Faculty of Mechanical Engineering

Department of Mechanical Engineering

Noise and Vibration Laboratory

www. http://www.mec.upt.ro

AUSPICE

Republic of Serbia

Ministry of Education, Science and Technological Development

www.mpn.gov.rs

GENERAL SPONSOR

Brüel & Kjær

an HBK company

CONFERENCE REVIEW

1st Yugoslav Conference	Belgrade	1978
2nd Yugoslav Conference	Belgrade	1979
3rd Yugoslav Conference	Belgrade	1980
4th Yugoslav Conference	Belgrade	1981
5th Yugoslav Conference	Belgrade	1982
6th Yugoslav Conference	Belgrade	1983
7th Yugoslav Conference	Belgrade	1984
8th Yugoslav Conference	Belgrade	1985
9th Yugoslav Conference	Belgrade	1986
10th Yugoslav Conference	Belgrade	1987
11th Yugoslav Conference & 1st International Conference	Belgrade	1988
12th Yugoslav Conference	Belgrade	1989
13th Yugoslav Conference	Niš	1991
14th Yugoslav Conference & 2nd International Conference	Niš	1993
15th Yugoslav Conference & 3rd International Conference	Niš	1995
16th Yugoslav Conference with international participation	Niš	1998
17th Yugoslav Conference with international participation	Niš	2000
18th Yugoslav Conference with international participation	Niš	2002
19th Conference with international participation	Niš	2004
20th Conference with international participation	Tara	2006
21st Conference with international participation	Tara	2008
22nd Conference with international participation	Niš	2010
23rd Conference and 4th International Conference	Niš	2012
24th International Conference	Niš	2014
25th International Conference	Tara	2016
26th International Conference	Niš	2018
27th International Conference	Niš	2022

PROGRAM COMMITTEE

Prof. Dragan Cvetković, Ph. D.
University of Niš, Faculty of Occupational Safety – chairman

Prof. Vasile Marinca, Ph. D.
"Politehnica" University of Timişoara, Romania – co-chairman

Prof. Momir Praščević, Ph. D.
University of Niš, Faculty of Occupational Safety – chairman

Prof. Giangiacomo Minak, Ph. D.
University of Bologna, Italy

Prof. Nicolae Herisanu, Ph. D.
"Politehnica" University of Timişoara, Romania

Prof. Vasile Bacria, Ph. D.
"Politehnica" University of Timişoara, Romania

Prof. Tihomir Trifunov, Ph. D.
National Military University „Vassil Levski“ of Veliko Turnovo, Bulgaria

Prof. Nikola Holeček, Ph. D.
Environmental Protection College, Velenje, Slovenia

Prof. Valentina Golubović-Bugarski, Ph. D.
Faculty of Mechanical Engineering, Banja Luka, Rep. of Srpska

Prof. Pero Raos, Ph. D.
Faculty of Mechanical Engineering, Slavonski brod, Croatia

Prof. Ivana Kovačić, Ph. D.
University of Novi Sad, Faculty of Technical Sciences

Prof. Zoran Perić, Ph. D.
University of Niš, Faculty of Electronic Engineering

Prof. Dejan Ćirić, Ph. D.
University of Niš, Faculty of Electronic Engineering

Prof. Zlatan Šoškić, Ph. D.
University of Kragujevac, Faculty of Civil and mechanical Engineering in Kraljevo

Prof. Snežana Ćirić Kostić, Ph. D.
University of Kragujevac, Faculty of Civil and mechanical Engineering in Kraljevo

Prof. Aleksandar Cvjetić, Ph. D.
University of Belgrade, Faculty of Minig and Geology

Prof. Koleta Zafirova, Ph. D.
Faculty of Technology and Metallurgy, Skopje, North Macedonia

ORGANISITION COMMITTEE

Prof. Darko Mihajlov, Ph. D.
University of Niš, Faculty of Occupational Safety – chairman

Prof. Nicolae Herisanu, Ph. D.
"Politehnica" University of Timişoara, Romania – co-chairman

Prof. Vasile Marinca, Ph. D.
Politehnica" University of Timişoara, Romania

Prof. Miomir Raos, Ph. D.
University of Niš, Faculty of Occupational Safety

Prof. Branko Radičević, Ph. D.
University of Kragujevac, Faculty of Civil and mechanical Engineering in Kraljevo

Prof. Nebojša Bogojević, Ph. D.
University of Kragujevac, Faculty of Civil and mechanical Engineering in Kraljevo

Prof. Mladena Lukić, Ph. D.
University of Niš, Faculty of Occupational Safety

Emir Ganić, Ph. D.
University of Belgrade, Faculty of Transport and Traffic Engineering

Marko Ličanin, MSc
University of Niš, Faculty of Occupational Safety

CONFERENCE SECRETARIAT

Prof. Darko Mihajlov, Ph. D. - technical secretary

Prof. Mladena Lukić, Ph. D.

Prof. Milica Nikodijević Đorđević, Ph. D.

Aleksandra Petković

Rodoljub Avramović

Srđan Cvetković

CONTENT

University of Nis
Faculty of Occupational Safety

„Politechnica“ University of Timisoara
Faculty of Mechanical Engineering

27th International Conference

NOISE AND VIBRATION

Niš, 20 - 21. 10. 2022.

INVITED PAPERS

University of Nis
Faculty of Occupational Safety
„Politechnica“ University of Timisoara
Faculty of Mechanical Engineering
27th International Conference
NOISE AND VIBRATION
Niš, 20 - 21. 10. 2022.

ON THE CONCEPT OF QUASI-ZERO STIFFNESS FOR VIBRATION ISOLATION PURPOSES

Ivana Kovacic[1]

[1]Centre of Excellence for Vibro-Acoustic Systems and Signal Processing, Faculty of Technical Sciences, University of Novi Sad, Novi Sad, Serbia

Abstract - *This work summarizes some of author's results achieved in the field of vibration isolation related to the beneficial use of a quasi-zero stiffness property. The focus is on two models that contain springs which incline as they extend: one in 2D and one in 3D. The conditions for their tuning to achieve quasi-zero stiffness are presented. The expressions for the corresponding restoring force are also given, with the emphasis on its approximate pure cubic form. Further, some dynamic phenomena in such externally excited systems are shown, including bifurcation sets and distinctive amplitude-frequency diagrams. A few other mechanical models from the literature that follow the previous work and can have quasi-zero stiffness are presented, as well as their practical realization.*

1. INTRODUCTION

Passive vibration isolation is one of the routes for mitigating undesirable vibration [1]. Transmissibility in linear vibration isolators with various types of damping has widely been explored [2], yielding clear identification of the associated disadvantages. Among them is the fact that the transmissibility of a harmonically excited linear mass-spring system becomes lower than unity only when the ratio of the forcing frequency and the system's natural frequency if higher than $\sqrt{2}$ (Fig. 1). This vibration-isolation region should be as wide as possible. One strategy for this to be achieved is to lower the natural frequency, which can be accomplished by low static stiffness, but this undesirably causes large static deflections.

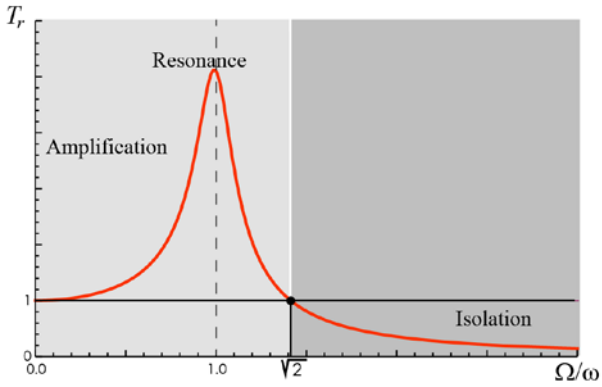

Fig. 1 *Characteristic regions in the transmissibility-frequency diagram of a harmonically excited linear mass-spring system*

Last several decades have opened new avenues for progress for overcoming this issue via intentional use of geometric stiffness nonlinearity, which includes the concept of quasi-zero stiffness (QZS) as well [3, 4].

This work briefly overviews this concept in Section 2, presenting author's results related to the spring models that can be adjusted to have a QZS characteristic in 2D and 3D [5-11]. In Section 3, certain phenomena associated with their dynamic behaviour are illustrated. In Section 4, some other mechanical models from the literature that can be adjusted to have a QZS characteristic are presented. In addition, practical realizations of several QZS systems that cite author's work are given.

2. QZS: MODELLING AND TUNING

One of the mechanical models adjustable to have a QZS characteristic is shown in Fig. 2. It consists of a vertical spring of stiffness k_v attached to two oblique springs of stiffness k_0 whose length in the underformed state is l_0, while their length in the horizontal position is labelled by a.

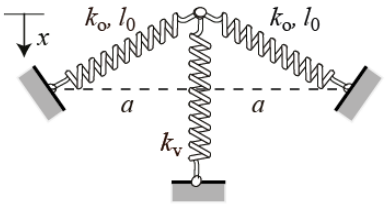

Fig. 2 *Three-spring model for achieving QZS in 2D*

The idea is to corelate the geometric parameters with the stiffness parameters so that the corresponding force-deflection curve has a horizontal tangent at the static equilibrium position, as shown in Fig. 3. This QZS condition is achieved when $\alpha = \frac{\gamma}{2(\gamma-1)}$, where $\alpha = k_o/k_v$ and $\gamma = a/l_0$ [6, 7].

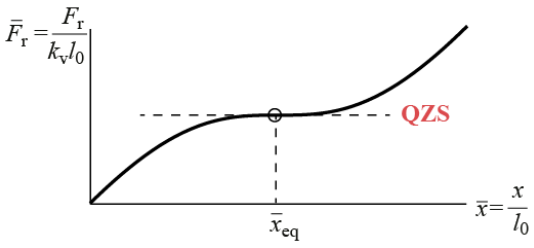

Fig. 3 *Force-deflection curve of a system from Fig. 2 with a QZS characteristic*

The resulting restoring force can then be approximated by a pure cubic expression $F_r \approx \alpha \bar{x}^3/\gamma^3$, where $\bar{x}$ stands for the non-dimensional displacement from the equilibrium position. The comparison between this pure cubic approximation for the QZS restoring force and its exact expression is plotted in Fig. 4. It is seen that the curve has a horizontal tangent at the origin as in Fig. 4, as well as that the approximation can be treated as valid for smaller displacements around this position.

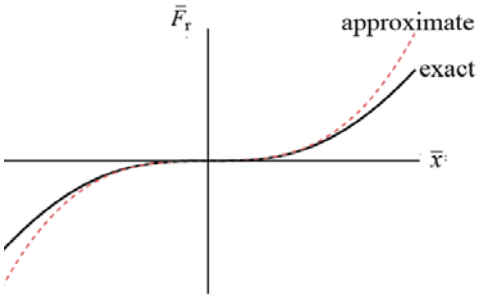

Fig. 4 *Comparison between the exact expression and pure cubic approximation for the restoring force for the QZS system from Fig.2*

Similarly, one can arrange and adjust a system of springs in 3D to achieve the desirable QZS characteristic. One such possible case is shown in Fig. 5, consisting of four mutually orthogonal springs at the static equilibrium position. Their stiffness is k, the length in the undeformed position d_0, and the length at the equilibrium position d. The QZS condition is achieved for $d_0 = d$, while the approximated non-dimensional restoring force can then be written down as $\bar{F}_r \approx 2d_0\bar{z}^3/d$, where $\bar{z}$ overbar stands for the non-dimensional displacement from the equilibrium position [8, 9]. Note that the comparison between this pure cubic approximation and the exact expression for the restoring force has a similar form as shown in Fig. 4.

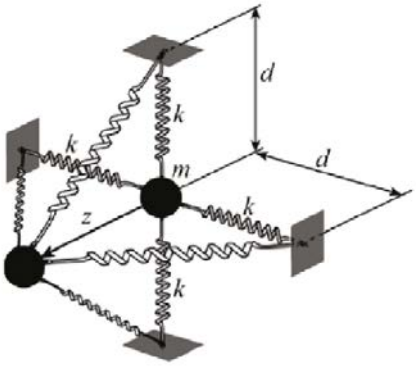

Fig. 5 *Four-spring model for achieving QZS in 3D*

3. ON CERTAIN DYNAMIC PHENOMENA APPEARING IN QZS SYSTEMS

It is shown in the previous section how springs can be arranged, and their properties tuned to achieve the QZS property. This section will present some interesting dynamic phenomena that they can exhibit when put in use.

3.1 QZS system in 2D

First, the case of a one degree-of-freedom QZS vibration isolator from Fig. 2 is considered and it is assumed to be under an asymmetric excitation comprising a constant force f_0 and harmonic time-varying force $f_1 \cos \Omega t$. It is shown in [10] analytically and confirmed numerically that this system can exhibit bifurcations related to different shapes of their frequency-response curves (FRCs), where five different regions I-V in the f_0 -Ω plane can be distinguished (Fig. 6b). It is seen that this bifurcation set comprises two cusps that intersect mutually. The five regions identified are characterized by different bending of the FRCs, different number of multiple solutions (fixed points) in certain frequency regions and multiple amplitude jumps [10]. Thus, in the regions I and V, two jumps for one value of f_0 can be appear: one jump-up and one jump-down point; in the regions II-IV four jumps for one value of f_0 can exist, but they appear differently with respect to each other in terms of the increase or decrease of the amplitude. The example of the FRCs corresponding to the regions II and V are presented in Fig. 7a and 7b, respectively, with the jumps indicated by the vertical arrows). It is also interesting that in the regions I-IV, the peak is directed towards right hand-side as in the hardening nonlinear oscillator [5], while in the region V, the peak is directed towards left hand-side (see Fig. 7b) as in the softening nonlinear oscillator. Thus, the external constant excitation changes the response from hardening to softening, which is an interesting phenomenon.

This system can also exhibit period-doubling bifurcations and chaos [11], which need to be taken into consideration when making a choice of a suitable operating regime.

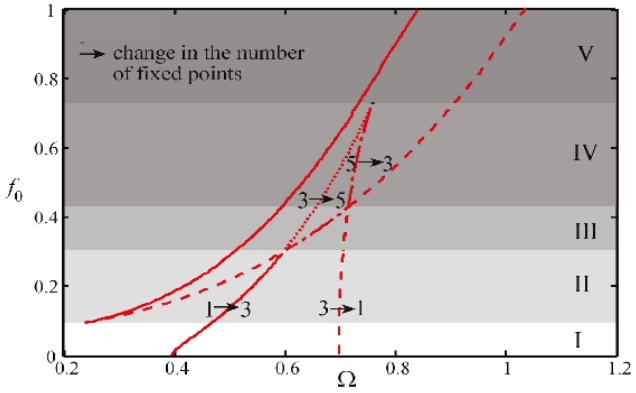

Fig. 6 *Bifurcation set containing two cusps (one directed down, the other directed up) for the asymmetrically excited 2D QZS system*

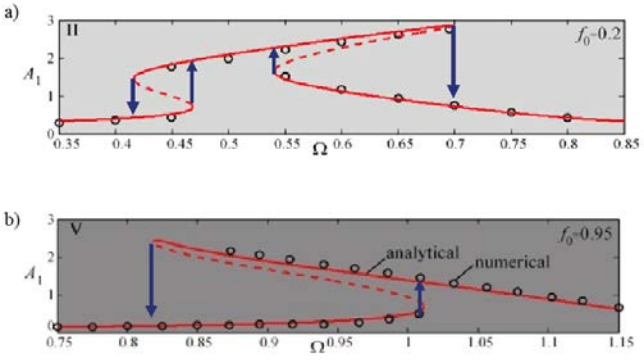

Fig. 7 *Typical shapes of the FRCs corresponding to a) region II and b) region III from Fig. 6 (solid line – stable analytical results, dashed line – unstable analytical results, circles – numerical results) with the jump points indicated by the vertical arrows*

3.2 QZS system in 3D

Second, the case of a QZS vibration isolator from Fig. 5 is considered when it is attached and driven harmonically by a linear oscillator [8, 9]. It is found analytically and confirmed numerically that as a result of the change of the coefficient of pure cubic nonlinearity γ, five different regions can be distinguished in the γ-Ω bifurcations set (Fig. 8), influencing the shapes of the corresponding FRCs [8, 9].

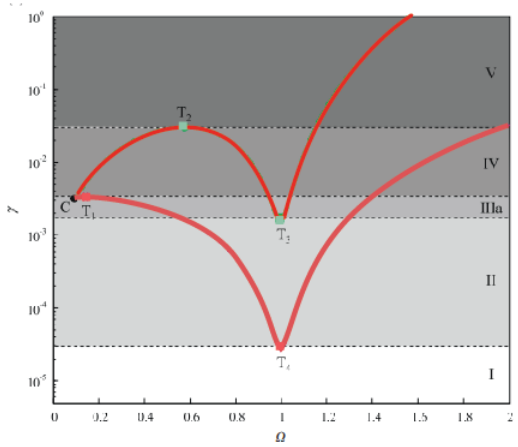

Fig. 8 *Bifurcation set containing two cusps (both directed down) for the 3D QZS attached to a linear oscillator*

In the region I, the FRC is continuous and single-valued, while in other regions it is multi-valued. In the regions II and IV, the FRC consists of a continuous part and a closed detached part, which can be positioned above it (region II) or inside it (region IV), as shown in Fig. 9. The latter is associated with a lower steady-state amplitude, and is, thus, desirable in practice.

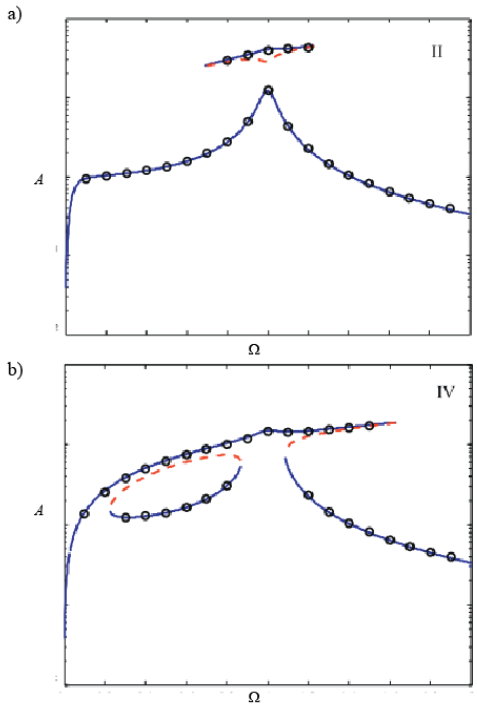

Fig. 9 *Typical shapes of the FRCs corresponding to a) region II and b) region IV from Fig. 8 (solid line – stable analytical results, dashed line – unstable analytical results, circles – numerical results)*

4. ON SOME OTHER QZS MODELS AND THEIR PRACTICAL REALIZATIONS

Besides the configuration in which QZS is achieved via obliques springs, other mechanical models do exist in the literature and some of them are shown in Fig. 10, based on the results from [3]. They include rods and springs (Fig. 10a), beams/arches (Fig. 10b), pendula with springs and a plate (Fig. 10c), cam-roller mechanisms (Fig. 10d), etc.

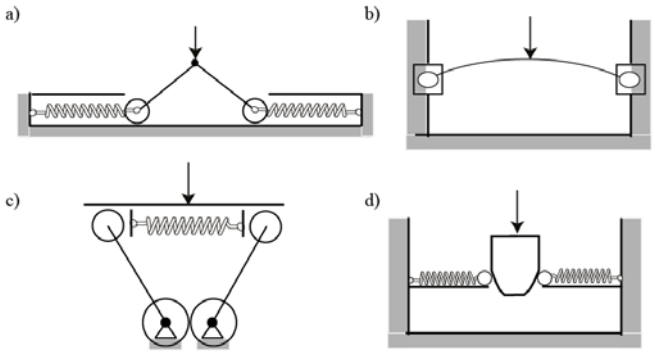

Fig. 10 *Other mechanical models of systems that can be adjusted to have QZS*

During the last decade numerous QZS systems have practically been realized. Many of them have been published as a follow-up to the author's work [6], which has received several hundred citations so far. They include the use of magnets, X-shaped structures, cam-roller mechanisms, origami-inspired foldable cylinders, composite plates, etc. A few of them are presented in Fig. 11 as illustrative examples.

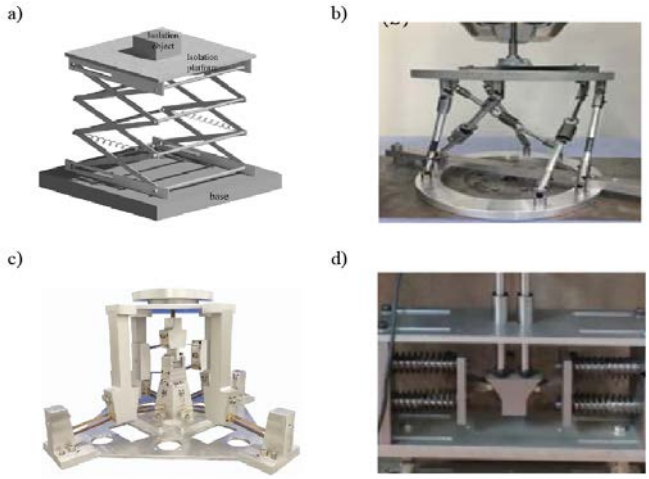

Fig. 11 *Practical realization of QZS systems from: a) [12], b) [13], c) [14], d) [15]*

5. CONCLUSIONS

The concept of quasi-zero stiffness has been presented. It is illustrated on two mechanical models comprising arrangements of springs whose deformations introduce geometric nonlinearities into the restoring force and the equations of motion. Certain characteristics of these springs can be adjusted to achieve a QZS configuration at the equilibrium position. The benefits of such configurations for nonlinear vibration isolation have been pointed out. In a system with one degree of freedom, these benefits involve widening the isolation region and achieving a smaller stiffness at larger displacements. In a system with two degrees of freedom, a

detached part of the FRC can appear inside the main continuous resonance curve, having a smaller steady-state amplitude than the co-existing stable solution at the same frequency. It should be noted that in both models, these beneficial effects are related to particular values of the systems' parameters. Variations of systems' parameters can lead to a diversity of nonlinear phenomena, which is a challenge to be taken care of in practical applications. A few other mechanical models and practical realizations of the QZS systems have been presented as well.

REFERENCES

[1] E.I. Rivin, *Passive Vibration Isolation*, New York: ASME Press, 2003.

[2] J.E. Ruzicka, T.E. Derby, *Influence of Damping in Vibration Isolation*, Washington DC: TSVI Centre, US Department of Defense, 1971.

[3] P. Alabudzev, I. Gritchin, L. Kim, G. Migirenko, V. Chon, P. Stepanov, *Vibration Protecting and Measuring Systems with Quasi-Zero Stiffness*, New York: Hemisphere Publishing, 1989.

[4] Ch.Ch. Liu, X.J. Jing, S. Daley, F.M. Li, "Recent advances in micro-vibration isolation", *Mech. Syst. Signal Pr.*, vol. 56–57, 2015, pp. 55-80.

[5] I. Kovacic, M.J. Brennan (Eds), *The Duffing Equation: Nonlinear Oscillators and their Behaviour*, Chichester: John Willey & Sons, 2011.

[6] I. Kovacic, M.J. Brennan, T.P. Waters, "A study of a nonlinear vibration isolator with quasi-zero stiffness characteristic", *J. Sound Vib.*, vol. 315, 2008, pp. 700-711.

[7] A. Carrella, M.J. Brennan, I. Kovacic, T.P. Waters, "On the force transmissibility of a vibration isolator with quasi-zero-stiffness", *J. Sound Vib.*, vol. 322, 2009, pp. 707-717.

[8] G. Gatti, M.J. Brennan, I. Kovacic, "On the interaction of the responses at the resonance frequencies of a nonlinear two degree-of-freedom system", *Physica D*, vol. 239, 2010, pp. 591-599.

[9] G. Gatti, I. Kovacic, M.J. Brennan, "On the response of a harmonically excited two degree-of-freedom system consisting of linear and nonlinear quasi-zero stiffness oscillators", *J. Sound Vib.*, vol. 29, 2010, pp. 1823-1835.

[10] I. Kovacic, M.J. Brennan, B. Lineton, "Effect of a static force on the dynamic behaviour of a harmonically excited quasi-zero stiffness system", *J. Sound Vib.*, vol. 325, 2009, pp. 870-883.

[11] I. Kovacic, G. Rega, M. Zukovic, "On the influence of a constant force on the appearance of period-doubling bifurcations and chaos in a harmonically excited pure cubic oscillator", *Chaos Solit. Fract.*, vol. 45, 2012, pp. 1531-1540.

[12] X.T. Sun, X.J. Jing, J. Xu, L. Cheng, "Vibration isolation via a scissor-like structured platform", *J. Sound Vib.*, vol. 333, 2014, pp. 2404-2420.

[13] S. Ishida, K. Suzuki, H. Shimosaka, "Design and experimental analysis of origami-inspired vibration isolator with quasi zero-stiffness characteristic", *J. Vib. Acoust.*, vol. 139, 2017, art. no 051004-1.

[14] Z.F. Zhou, Y.Z. Gao, L.N. Sun, W. Dong, Z.J. Du, "A bistable mechanism with linear negative stiffness and large in-plane lateral stiffness: design, modeling and case studies", *Mech. Sci.*, vol. 11, 2020, pp. 75–89.

[15] M. Li, W. Cheng, R. Xie, "A quasi-zero-stiffness vibration isolator using a cam mechanism with user-defined profile", *Int. J. of Mech. Sci.*, vol. 189, 2021, art. no 105938.

University of Nis
Faculty of Occupational Safety
„Politechnica“ University of Timisoara
Faculty of Mechanical Engineering
27th International Conference
NOISE AND VIBRATION
Niš, 20 - 21. 10. 2022.

ANALYTICAL INVESTIGATION TO AN OSCILLATOR WITH CUBIC NONLINEARITY AND HARMONIC RESTORING FORCE

Nicolae Herisanu[1], *Vasile Marinca*[1]

[1] Politehnica” University of Timisoara, Faculty of Mechanics, Romania, nicolae.herisanu@upt.ro

Abstract - *An approximate analytical periodic solution to large amplitude oscillations of a conservative single-degree-of-freedom oscillator is proposed. Comparisons between approximate analytical and numerical results reveal the remarkable accuracy of the proposed analytical approach. An example is presented to describe the solution methodology and to illustrate the usefulness and effectiveness of the Optimal Auxiliary Functions Method (OAFM).*

1. INTRODUCTION

In the last years, there has been a great deal of interest in physical and mechanical oscillatory systems which are often governed by nonlinear differential equations. In some cases, it is possible to replace a nonlinear differential equation by corresponding linear one that approximates the original equation closely to give useful results. Often such linearization is not feasible and for this situation, the original nonlinear differential equation itself must be directly dealt with.

In general, study of nonlinear differential equations is restricted to a variety of special classes of equations and the method of solution usually involves a limited number of techniques to achieve analytical approximations to the solution.

There are some approaches for approximating solutions of a nonlinear oscillatory system. The most common and widely applied methods for nonlinear differential equations are perturbation procedures. These methods involve the expansion of a solution to a differential equation in a series taking into account a small parameter [1], [2].

New analytical techniques should be developed to overcome this assumption of small parameters. Some extensions of Lindstedt-Poincare perturbation method to strongly nonlinear systems have been proposed [3], [4]. The harmonic balance method [1], [2] is a procedure which uses a truncated Fourier series, but it is very difficult to construct higher-order approximations. Lau and Cheung [5] presented the incremental harmonic balance method.

A mixture of methodologies has been reported in the attempt to develop new techniques, such as the homotopy perturbation method [7], the variational iteration method [8], the homotopy analysis method [9], the optimal homotopy asymptotic method [10] and so on.

In this work, we apply the Optimal Auxiliary Functions Method (OAFM) to find periodic analytical solutions to a nonlinear oscillator with cubic and harmonic force. In this approach, a finite number of unknown parameters and auxiliary functions appear and the approximate solution obtained through the proposed method rapidly converges to the exact solution.

2. THE OPTIMAL AUXILIARY FUNCTIONS METHOD

In order to introduce the OAFM [11-15], we consider the nonlinear differential equation

$$L[x(t)]+N[x(t)]=0 \tag{1}$$

in which time t is the independent variable, $x(t)$ is an unknown function, L is a linear operator and N is a nonlinear operator.

The corresponding boundary/initial conditions are

$$B\left[x(t),\frac{dx(t)}{dt}\right]=0 \tag{2}$$

For nonlinear differential equations, it is known that an exact solution is often very hard or even impossible to be found. According to OAFM procedure, the approximate solution of Eqs. (1) and (2) has the form

$$\bar{x}(t)=x_0(t)+x_1(t) \tag{3}$$

where the initial approximation $x_0(t)$ and the first approximation $x_1(t)$ will be determined as follows. Inserting Eq. (3) into Eq. (1), it results in

$$L[x_0(t)]+L[x_1(t)]+N[x_0(t)+x_1(t)]=0 \tag{4}$$

The initial approximation $x_0(t)$ is obtained from the linear equation

$$L[x_0(t)]=0,\quad B[x_0(t),\frac{dx_0(t)}{dt}]=0 \tag{5}$$

and the first approximation is obtained from the nonlinear equation

$$L[x_1(t)]+N[x_0(t)+x_1(t)]=0;\quad B\left[x_1(t),\frac{dx_1(t)}{dt}\right]=0 \tag{6}$$

The last term from Eq. (6) is expanded as

$$N[x_0(t)+x_1(t)]=N[x_0(t)]+\sum_{k\geq 1}\frac{x_1^k(t)}{k!}N^{(k)}(x_0(t)) \tag{7}$$

To avoid the difficulties that appear in solving the nonlinear differential Eq. (6) and also to accelerate the rapid convergence of the first approximation $x_1(t)$ and implicitly of

the approximate solution $\bar{x}(t)$ instead of the last term arising in Eq. (6) we propose another expression, such that Eq. (6) can be written as

$$L[x_1(t)] = \sum_{i=1}^{p} C_i F_i(t) \tag{8}$$

$$B\left[x_1(t), \frac{dx_1(t)}{dt}\right] = 0 \tag{9}$$

where F_i(t) are known auxiliary functions depending on $x_0(t)$ and on the functions which appear into the composition of $N[x_0(t)]$, or are combinations of such expressions. In other words, $x_0(t)$ and $N[x_0(t)]$ are "sources" for the auxiliary functions F_i.

These auxiliary functions are not unique and it should be emphasized that we have a large freedom to choose them.

The parameters C_i which appear in the expression (8) can be optimally identified via rigorous mathematical methods such as the collocation method, Galerkin method, the least square method, Ritz method, or minimizing the square residual error:

$$J(C_1, C_2, ..., C_p) = \int_{(D)} R^2(t, C_1, C_2, ..., C_p) dt \tag{10}$$

where

$$R(t, C_1, C_2, ..., C_p) = L[\bar{x}(t)] + N[\bar{x}(t)] \tag{11}$$

and $\bar{x}(t)$ is given by Eq. (3).

The values of the parameters C_i, i=1,2,…,p are obtained from the system:

$$\frac{\partial J}{\partial C_1} = \frac{\partial J}{\partial C_2} = ... = \frac{\partial J}{\partial C_p} = 0 \tag{12}$$

By this novel procedure, the approximate solution $\bar{x}(t)$ is well determined after identification of the optimal values of the initially unknown convergence-control parameters C_i. It will be proved that our procedure is a very powerful tool for solving nonlinear problems without assuming the presence of small parameters into the initial Eqs. (1) and (2).

3. APPLICATION OF THE OPTIMAL AUXILIARY FUNCTIONS METHOD

We will illustrate the applicability, the accuracy and effectiveness of the proposed approach by comparing the analytical approximate periodic solution with numerical integration results.

In what follows, we consider the oscillator with cubic and harmonic restoring force of the form:

$$\ddot{u} + au^3 + b\sin u = 0 \tag{13}$$

with the initial conditions

$$u(0) = A, \quad \dot{u}(0) = 0 \tag{14}$$

Making the transformation

$$\tau = \Omega t, \quad u(t) = Ax(\tau) \tag{15}$$

the Eq. (13) can be rewritten as

$$x'' + \frac{aA^2}{\Omega^2} + \frac{b}{A\Omega^2}\sin Ax = 0 \tag{16}$$

and the initial conditions (14) become

$$x(0) = 1, \quad x'(0) = 0 \tag{17}$$

where primes denote differentiation with respect to τ and Ω is the frequency of the system described by the governing equation (13).

Taking into account the nonlinear differential equation (16), we can identify the linear and nonlinear operators of the forms

$$L[x(\tau)] = x'' + x \tag{18}$$

$$N[x(\tau)] = \frac{aA^2}{\Omega^2}x^3 - x + \frac{b}{A\Omega^2}\sin Ax \tag{19}$$

We suppose the approximate solution of Eq. (16) under the form

$$\bar{x}(\tau) = x_0(\tau) + x_1(\tau) \tag{20}$$

in which the initial approximation $x_0(\tau)$ is obtained from Eq. (5):

$$x_0'' + x_0 = 0, \quad x_0(0) = 1, \quad x_0'(0) = 0 \tag{21}$$

whose solution is

$$x_0(\tau) = \cos\tau \tag{22}$$

Inserting Eq. (22) into Eq. (19), one can get

$$N[x_0(\tau)] = X\cos\tau + Y\cos 3\tau + Z\cos 5\tau \tag{23}$$

where

$$\begin{aligned} X &= \frac{3aA^2}{4\Omega^2} - 1 + \frac{b}{\Omega^2}\left(1 - \frac{A^2}{8} + \frac{A^4}{192}\right) \\ Y &= \frac{aA^2}{4\Omega^2} + \frac{b}{\Omega^2}\left(-\frac{A^2}{24} + \frac{A^4}{384} - \frac{A^6}{15360}\right) \\ Z &= \frac{A^4}{1920} - \frac{A^6}{46080} \end{aligned} \tag{24}$$

Taking into account Eqs. (22) and (23), as it is known in the frame of OAFM procedure [11], we have many possibilities to define the auxiliary functions since these are not unique. More precisely, some example of such functions in this case could be

$$\begin{aligned} &F_1(\tau) = C_1(X\cos\tau + Y\cos 3\tau), \\ &F_2(\tau) = 2C_2\cos 2\tau(X\cos\tau + Y\cos 3\tau), \\ &F_3(\tau) = 2C_3\cos 4\tau(X\cos\tau + Y\cos 3\tau), \\ &F_4(\tau) = 2C_4\cos 6\tau(X\cos\tau + Y\cos 3\tau) \end{aligned} \tag{25}$$

or

$$\begin{aligned} &F_1(\tau) = C_1(Y\cos 3\tau + Z\cos 5\tau); \\ &F_2(\tau) = 2C_2\cos 2\tau(Y\cos 3\tau + Z\cos 5\tau); \\ &F_3(\tau) = 2C_3\cos 4\tau(Y\cos 3\tau + Z\cos 5\tau); \end{aligned} \tag{26}$$

or

$$F_1(\tau) = C_1 X \cos\tau;$$
$$F_2 = 2C_2 \cos 2\tau X \cos\tau;$$
$$F_3 = 2C_3 \cos 4\tau X \cos\tau; \quad (27)$$
$$F_4 = 2C_4 \cos 6\tau X \cos\tau$$

or yet

$$F_1(\tau) = C_1(X\cos\tau + Z\cos 5\tau);$$
$$F_2(\tau) = 2C_2 \cos 2\tau(X\cos\tau + Y\cos 3\tau); \quad (28)$$
$$F_3(\tau) = 2C_3(Y\cos 3\tau + Z\cos 5\tau)$$

and so on. If we consider only the auxiliary function given by Eq.(25), the first approximation can be obtained from Eqs. (8) and (9):

$$x_1'' + x_1 = (C_1 + 2C_2\cos 2\tau + 2C_3\cos 4\tau +$$
$$+ 2C_4\cos 6\tau)(X\cos\tau + Y\cos 3\tau) \quad (29)$$
$$x_1(0) = x_1'(0) = 0$$

After some simple manipulations,Eq.(29) can be rewritten in the form

$$x_1'' + x_1 = [(C_1 + C_2)X + (C_2 + C_3)Y]\cos\tau + [(C_2 + C_3)X +$$
$$+ (C_1 + C_4)Y]\cos 3\tau + [(C_3 + C_4)X + C_2 Y]\cos 5\tau + \quad (30)$$
$$+ (C_4 X + C_3 Y)\cos 7\tau + C_4 Y\cos 9\tau$$

Avoiding the presence of secular terms in the last expression needs

$$(C_1 + C_2)X + (C_2 + C_3)Y = 0 \quad (31)$$

From Eqs.(24) and (30), we obtain the frequency as

$$\Omega^2 = \frac{3}{4}aA^2 + b\left(A - \frac{A^2}{8} + \frac{A^4}{192}\right) + \frac{C_1 + C_3}{C_1 + C_2}\left[\frac{1}{4}aA^2 + \right. \quad (32)$$
$$\left. + b\left(-\frac{A^2}{24} + \frac{A^4}{384} - \frac{A^6}{15360}\right)\right]$$

Taking into consideration Eq.(32) we find the solution

$$x_1(\tau) = \frac{1}{8}[(C_2 + C_3)X + (C_1 + C_4)Y](\cos\tau - \cos 3\tau) +$$
$$+ \frac{1}{24}[(C_3 + C_4)X + C_2 Y](\cos\tau - \cos 5\tau) + \quad (33)$$
$$+ \frac{1}{48}(C_4 X + C_3 Y)(\cos\tau - \cos 7\tau) +$$
$$+ \frac{1}{80}YC_4(\cos\tau - \cos 9\tau)$$

From Eqs. (14), (20), (22) and (33) one can get the approximate solution of Eqs. (13) and (14):

$$\bar{u}(t) = A\cos\Omega t + \frac{A}{8}[(C_2 + C_3)X + (C_1 + C_4)Y](\cos\Omega t -$$
$$- \cos 3\Omega t) + \frac{A}{24}[(C_3 + C_4)X + C_2 Y](\cos\Omega t - \cos 5\Omega t) + \quad (34)$$
$$+ \frac{A}{48}(C_4 X + C_3 Y)(\cos\Omega t - \cos 7\Omega t) +$$
$$+ \frac{A}{80}YC_4(\cos\Omega t - \cos 9\Omega t)$$

where X and Y are given by Eq. (24) and Ω is obtained from Eq. (32).

A numerical example is further developed to prove the accuracy of the obtained analytical solution. Using a set of values for the physical parameters involved in the governing equation (a=0.01, b=0.01, c=-0.03, A=2), following the procedure described avove one obtains the optimal values for the convergence-control parameters:

$$C_1 = -0.05739952196359245,$$
$$C_2 = 0.05995231441797591,$$
$$C_3 = 0.12989255935357402, \quad (35)$$
$$C_4 = 0.21888144594401138$$

and therefore the approximate analytical solution is well defined and ploted in Fig.1 in comparison with numerical integration results.

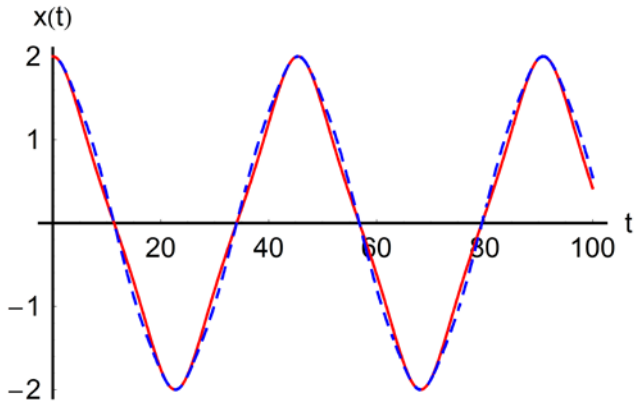

Fig. 1 *Comparison between analytical and numerical solutions in the considered case:* ——— *numerical,* _ _ _ _ *analytical*

4. CONCLUSIONS

In this work we present analytical and numerical solution to nonlinear oscillator with cubic and harmonic restoring force. To validate the approximate solution obtained through OAFM, it is necessary to analyze the time response.

From Fig.1 it can be seen that the error of the approximate is very good in comparison with numerical integration solution. OAFM accelerates the convergence of the approximate analytical solution of nonlinear oscillator and lead to a very good approximate value for the frequency.

Our approach is independent of any small or large parameters. The construction of the first iteration is different from any other traditional approaches, especially concerning the presence of the auxiliary functions and some initially unknown convergence-control parameters.

In the construction of Eqs. (8) and (30), respectively, it is not necessary the presence of the entire nonlinear function and therefore our proper construction led to simplifications of calculus in a considerable manner.

The optimal convergence-control parameters ensure a fast convergence of the approximate solutions using only the first iteration, being identified using rigorous mathematical procedures.

The main advantage of OAFM is the possibility to optimally control and adjust the convergence of the solutions by means of the auxiliary functions. A very good agreement was found between the approximate analytical solutions and numerical integration results, which proves the validity of our technique and emphasizes that this method is very efficient in practice.

REFERENCES

[1] A.H. Nayfeh and D. T. Mook, *Nonlinear oscillations*, New York:Wiley, 1979.

[2] P. Hagedorn, *Nonlinear oscillations*, Oxford:Claredon, 1988.

[3] Y.K. Cheung, S.H. Chen, S.L. Lau, "A modified Lindstedt-Poincare method for certain strongly nonlinear oscillators", *Int. J. Nonlin. Mech*, vol. 26, pp. 367-378, 1991.

[4] B.S. Wu, C.W. Lim, P.S. Li, „A generalization of the Senator-Bapat method for certain strongly nonlinear oscillators", *Phys. Lett. A*, vol. 341, pp.164-169, 2005.

[5] S.L. Lau, Y.K. Cheung, „Amplitude incremental variational principle for noninear vibration of elastic system", *ASME J. Appl. Mech.*, vol.48, pp.959-964, 1981.

[6] J.H. He, „Homotopy perturbation method for solving boundary value problems", *Phys. Lett. A*, vol. 350, pp.87-88, 2006.

[7] K. Huseyn, R. Liu, „An intrinsic multiple-scale harmonic balance method for nonlinear vibration and bifurcation problems", *Int. J. Nonlinear Mech.* Vol.26, pp.727-740, 1991.

[8] D. Slota, „Direct and inverse one-plane Stepan problem solved by the variational iteration method", *Comp. Math. Appl.*, vol. 54, pp.1139-1146, 2007.

[9] S.J. Liao, *Homotopy analysis method in nonlinear differential equations*, Cham:Springer, 2012.

[10] V. Marinca, N. Herisanu, *The Optimal Homotopy Asymptotic Method. Engineering Application*, Heidelberg:Springer, 2015.

[11] V. Marinca, N. Herisanu, B. Marinca, *Optimal Auxiliary Functions Method for Nonlinear Dynamical Systems*, Cham: Springer, 2021.

[12] N. Herisanu, V. Marinca, G. Madescu, „Application of the Optimal Auxiliary Functions Method to a permanent magnet synchronous generator", *Int. J. Nonlin. Sci. Numer. Simul.*, vol. 20, pp.399-406, 2019

[13] N. Herisanu, V. Marinca, G. Madescu, F. Dragan, „Dynamic response of a permanent magnet synchronous generator to a wind gust", *Energies*, vol. 12, Art.No. 915, 2019

[14] V. Marinca, N. Herisanu, „Optimal Auxiliary Functions Method for a Pendulum Wrapping on Two Cylinders", *Mathematics*, vol.8(8), Art.No.1364, 2020

[15] N. Herisanu, V. Marinca, „An effective analytical approach to nonlinear free vibration of elastically actuated microtubes", *Meccanica*, vol. 56(4), pp.813-823, 2021

University of Nis
Faculty of Occupational Safety

„Politechnica“ University of Timisoara
Faculty of Mechanical Engineering

27th International Conference

NOISE AND VIBRATION

Niš, 20 - 21. 10. 2022.

NOISE

University of Nis
Faculty of Occupational Safety
„Politechnica“ University of Timisoara
Faculty of Mechanical Engineering
27th International Conference
NOISE AND VIBRATION
Niš, 20 - 21. 10. 2022.

AUTOMATIC NOISE EVENT CLASSIFICATION BASED ON IMMISSION DIRECTIVITY

Jure Murovec[1], Luka Čurović[1], Anže Železnik[1], Jurij Prezelj[1]

[1] University of Ljubljana, Faculty of Mechanical Engineering, Slovenia, jure.murovec@fs.uni-lj.si

Abstract - *Environmental noise measurements are often performed to determine and evaluate the contribution of the selected source to the overall noise level. Since noise pollution reduction is most effective at the source itself, its identification is critical. Continuous noise measurements are, in practise, the only credible source of information. The cost of the current approach is high due to expensive equipment, long measurement time, and the need for trained personnel. To fully automate the measurement, we need to simplify the identification of the main noise sources and make the exclusion of residual and background noise more efficient. By combining unsupervised learning, psychoacoustic, and spatial features, we present a device capable of determining the contribution of each noise source to the total noise level.*

1. INTRODUCTION

Environmental noise is a dynamic and complex process. The temporal, amplitude, frequency, and location diversity, as well as the simultaneous operation of different sources, determine the complexity of dealing with the negative effects of environmental noise on humans [1-4].

The non-periodicity of many noise sources in the environment means that we are dealing with variations in sound pressure levels on different time scales [5,6]. On the one hand, we can record sound impulses with a duration of less than one second, and on the other hand, we observe changes in sound pressure levels in the time frame of seasons due to meteorological changes and various human activities [7].

Environmental noise measurements are often performed to determine and evaluate the contribution of the selected source to the overall noise level. Since noise pollution reduction is most effective at the source itself, its identification is critical. The problem arises when the noise source in question generates sound pressure levels comparable to or even lower than those of other sources.

The time of operation and thus of noise generation is usually random. This means that personnel must always be present during measurements to record working conditions and eliminate random sound events from the environment. One of the common measurement techniques is to listen to the entire recording of the measurement in the laboratory [8,9]. The next way to determine the contribution of the selected noise source is to exclude it. Then, the sound pressure level of the background and residual sources during operation and non-operation of the selected source is compared, which allows indirectly calculating its contribution to the total level. The third technique is based on the principle of improving the signal-to-noise ratio by getting close enough to the noise source in question, Fig. 1.

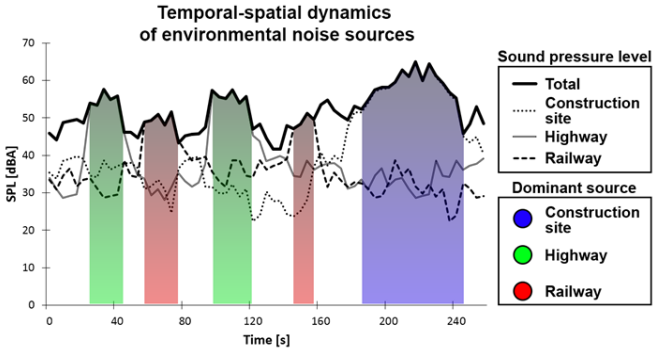

Fig. 1 *Sound pressure levels from multiple sources. Measurements with a single microphone can only record the combined sound pressure level.*

All of the above techniques have their limitations. Some noise sources cannot be turned off or consist of a large number of uncorrelated sources. Examples of such noise sources are large industrial plants, ports, railroad stations, refineries, airports, construction sites, etc. Another problem that usually occurs is the simultaneous operation of multiple noise sources that significantly affect the overall sound level at the measurement point (MP).

Noise propagation modelling, together with sound power measurements provides good estimates of the contributions of the various sources to the total sound pressure level at a given MP. When modelling software is used, control measurements are required, the sound power of all sources and their operating times must be determined, and their geometry, terrain topography, etc. must also be known. The uncertainty of calculations is especially large when working with different software packages and propagation models. Their constant updating, as well as the updating of standards and laws, contribute to the variability of the results at the administrative level. Therefore, noise modelling can only be used as a tool to extrapolate measurements from multiple measurement locations to a larger area, which is confirmed by many studies, [4,10,11].

For the above reasons, continuous noise measurements are in practise the only credible source of information. The cost of such an approach is high due to expensive equipment, long measurement time, and the need for trained personnel. If we want to fully automate the measurement of environmental noise, we need to simplify the identification of the main noise sources and make the exclusion of residual and background

noise more efficient. Humans are very good at perceiving and judging the general characteristics of the surrounding sound field. The computer does not have sufficient capacity to handle this. Therefore, the development of computational methods to automatically extract this information holds great potential for a variety of applications. The development of an environmental noise classification system that mimics as closely as possible the way trained personnel work should be the next logical step. By automatically determining the contribution of each noise source to the total noise level, a significant amount of manual work can be saved. Personnel classify noise events based on the noise level threshold (which may be similar to the background noise level), the direction of the noise source, and subjective noise recognition capabilities.

2. AUTOMATIZATION OF NOISE MEASUREMENTS

The use of acoustic cameras for rapid localization and visualization of sound sources in devices has become very popular in industrial applications and acoustic research. Many approaches for detecting the direction of sound sources derive from this. Microphone arrays are either too large with too many microphones for permanent acoustic sensing, or unusable in the low frequency range. The use of microphone arrays in environmental noise measurement is more or less limited to specific cases and for the formation of a synthesized signal to increase the signal-to-noise ratio [12-14]. A small microphone has been developed for monitoring environmental noise and detecting dominant sources, and its use is presented in this paper.

In order to build a practical apparatus for automatizaton of environmental noise measurements, an algorithm has been created from classical delay-and-sum beamformig and differential microphone array. Environmental noise measurements are performed under far-field conditions, which leads to simplification of sound wave propagation. In the free field, the distances between the MP and the noise sources are many times larger than the wavelengths of the lowest generated frequencies. We can assume that sound propagates in two dimensions, parallel to the ground. Therefore, only the azimuthal direction of arrival (DOA) of the sound events is of interest [15-17].

The proposed system consists of a small horizontal circular 4-channel microphone array (⌀ = 30 mm), an A/D converter (sampling frequency of 192 kHz), and a computer to process the information. The four microphones measure the sound field simultaneously and their signals are processed to localise the sound source in a two-dimensional plane. By taking advantage of the delay-and-sum algorithm (DAS) and the average square difference function (ASDF) and combining all six pairs of microphones according to the principle of differential microphone arrays, we have developed the delay, subtract, and sum (DSS) method of microphone signals. For each individual microphone pair, the average squared difference of the acquired signals is first calculated and then summed with all other pairs, [9,17-20].

The detection of DOA within the 125 ms (also known as the »fast« time constant) allowed the expansion and implementation of features in the spatial domain. The equivalent sound pressure level $L_{A,eq,T}$ can be correlated with the sum of all noise sources surrounding the immission point in time interval T. For each integration time, the array calculates and stores the most dominant direction of noise immission surrounding the MP and assigns the value of the instantaneous sound pressure level (SPL). The discovery of this principle led directly to the development of a new concept in acoustics: Immission directivity, [9, 17-20]. It gives us a unique insight into the temporal-spatial dynamics of noise. The expanison of commonly used $L_{A,eq}$ into the spatial domain helps to uncover the acoustic environment in more detail and subsequently allows an easier identification of dominant noise sources. Imission directivity is defined by the Eq. 1:

$$L_{A,eq,T} = 10\log\left[\frac{1}{T}\int_0^T\int_0^{2\pi} 10^{\frac{L_p(t,\varphi)}{10}} d\varphi dt\right] \qquad (1)$$

Immission directivity can distinguish between different scenarios with multiple noise sources around the MP. A single value of $L_{A,eq}$ cannot distinguish the different contributions of each noise source and is in some sense insufficient for an adequate investigation of the acoustic environment of enviromental noise. In such cases, more detailed measurements are required to correctly identify the dominant noise source. The concept of immission directivity helps to avoid lengthy and costly measurements that require trained personnel and additional post-processing of the results. A simulated example of three noise sources with different contributions to the total sound pressure level is shown in Fig. 2. Although all three scenarios have an $L_{A,eq}$ of 64 dB, the nature of the noise sources in each example is very different.

In Fig. 2.a all three noise sources are relatively large, as indicated by the wider lobes of the immission directivity. Their individual contributions to the $L_{A,eq}$ are roughly comparable, with noise source 1 (direction 36°) being the largest contributor by a small margin. In contrast, the example in Fig. 2.b shows that noise source 3 is the largest contributor, radiating from a point relative to the MP, implying that it is either a very small noise source or a very distant one. Although its L_p is the lowest, its nearly uninterrupted operation (P = 0,85) outweighs the contributions to $L_{A,eq}$ from the other two noise sources. Fig. 2.c shows the third example, where noise sources 1 and 2 occur with similar probabilities of occurrence, the latter having a higher L_p at the immission point. The parameters used in the simulation in Fig. 2 are listed in Table 1.

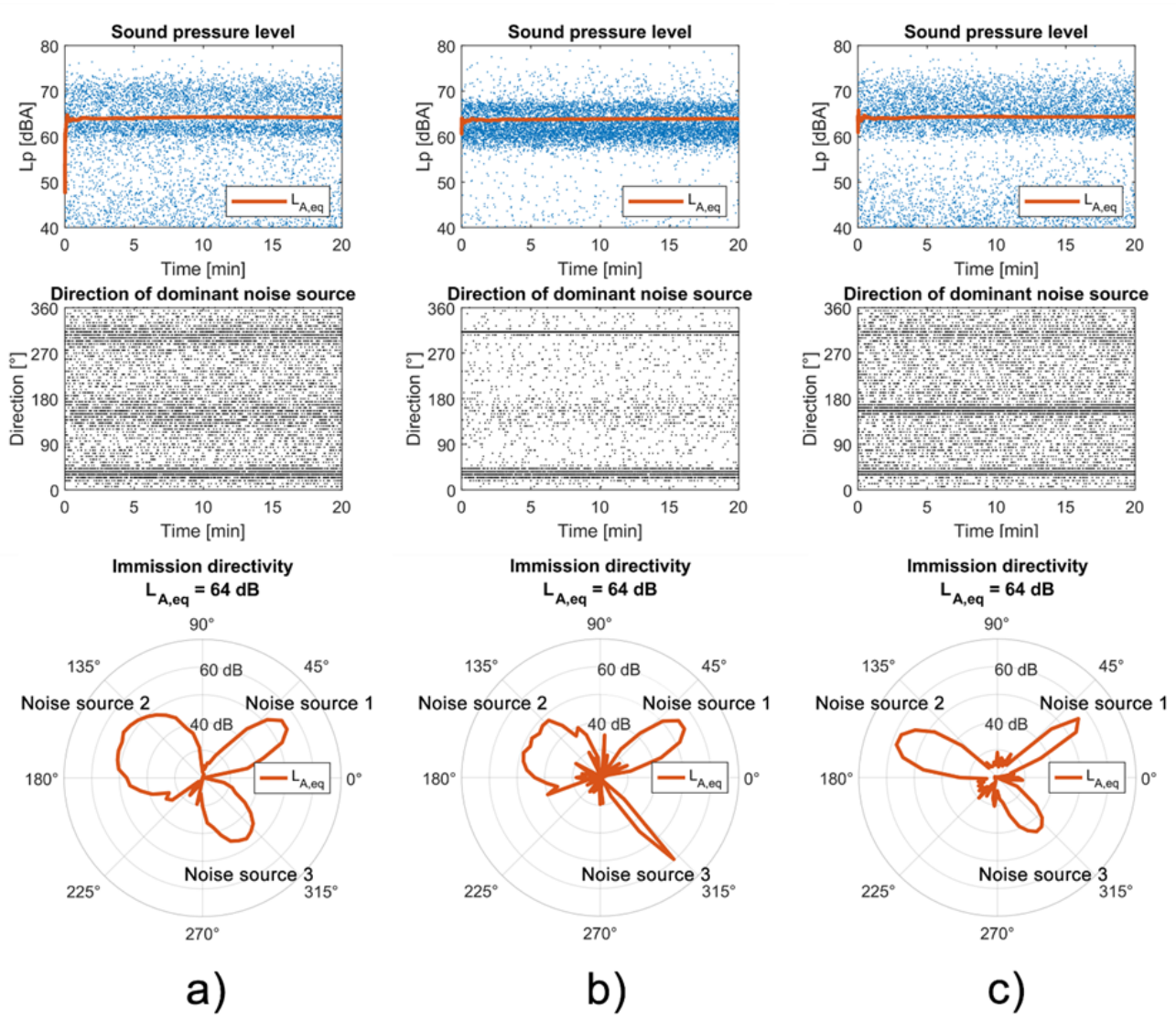

Fig. 2 *Different scenarios in which the MP is surrounded by three noise sources that have different values for L_p at the immission point, probability of occurrence, and relative size. L_p and the direction of dominant noise source are plotted against time and the immission directivity is calculated for each scenario.*

Table 1 *Parameters for simulations of immission directivity*

		Noise source 1	***Noise source 2***	***Noise source 3***
a)	L_p	*65 ± 5 dB*	*70 ± 2 dB*	*62 ± 1 dB*
	Prob. of occur. P	*0,3*	*0,15*	*0,2*
	DOA	*36° ± 6°*	*162° ± 18°*	*312° ± 12°*
b)	L_p	*65 ± 5 dB*	*70 ± 4 dB*	*62 ± 2 dB*
	Prob. of occur. P	*0,25*	*0,05*	*0,85*
	DOA	*36° ± 6°*	*162° ± 18°*	*312° ± 1°*
c)	L_p	*65 ± 2 dB*	*70 ± 3 dB*	*62 ± 1 dB*
	Prob. of occur. P	*0,25*	*0,2*	*0,1*
	DOA	*36° ± 3°*	*162° ± 6°*	*312° ± 9°*

The compatibility of pairing the presented acoustic sensor with the calibrated Type 1 sound level meter (SLM) allows traceability of the SPL values of immission directivity to the units of SI, which means that the results obtained with this new concept can be used as legally valid.

By omitting the calculation of the equivalent level, we can apply the principle of immission directivity to another new feature: Source dominance Θ. The array compares the calculated values from all directions around the MP within each integration time of 125 ms. We use the polar diagram of the immission directivity as an indicator to determine the dominance of the noise source. When there is no obvious noise source around the MP and only background noise is present, the immission directivity plot points in all directions and approaches circular shape. As the dominance of the source increases, the diagram becomes more and more asymmetrical and the value of the dominance of the noise source Θ increases. It is defined by the Eq. 2:

$$\Theta = 1 - \frac{\sum_{i=1}^{D} \frac{\sum ASDF_i^{-1}}{\sum ASDF_{max}^{-1}}}{D} \qquad (2)$$

D defines the number of directions observed by the array, where $\sum ASDF_{max}^{-1}$ is the maximum value within all observed directions. If only background noise is present, the source dominance Θ approaches 0 as the sum of $\sum ASDF^{-1}$ values of all directions is close to D. If we have a dominant source around the measurement point, the same sum approaches 1 and so does the value of source dominance Θ. This feature opens

the possibility to filter all parts of the measurement where there is no distinct dominant source. The amount of irrelevant data for noise source classification is thus significantly reduced, which speeds up the computation of features for identifying noise sources and their individual contribution to the total noise level. In addition, the synthesized signal from multiple microphones provides an improved signal-to-noise ratio (SNR), which naturally improves the detection of noise sources. Fig. 3 shows three different examples of noise source dominance Θ. Example A shows a very dominant source - the beam pattern is narrow. In example B, where there is no distinct noise source, the beam pattern approaches a circular shape, so the value of Θ is close to 1. The third example, labeled C, shows a noise source that is located in a different direction and is somewhat less dominant than example A. The introduction of the spatial domain into environmental noise measurements allows us to automate the measurement process more effectively.

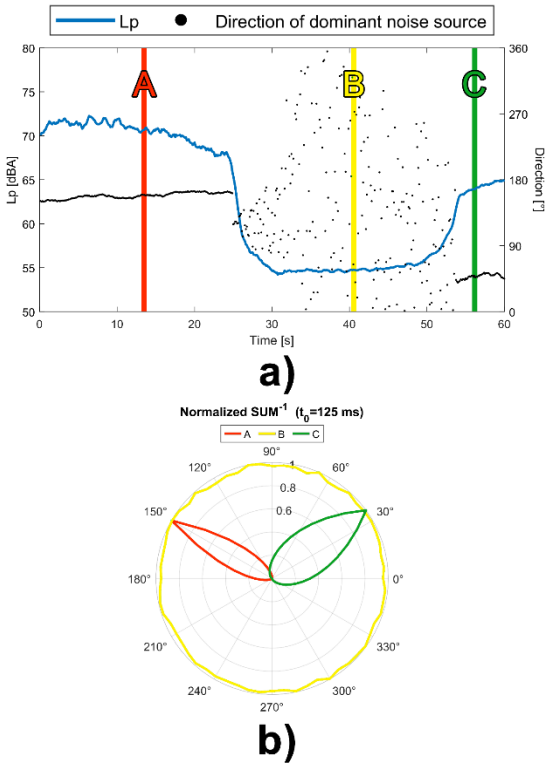

Fig 3. *a) Direction of the dominant noise source and sound pressure level plotted against time, b) Source dominance for three different examples.Font styles for typewriting equation*

Virtually all classification algorithms have implemented a combination of different features from the acquired signals. Initially, attempts focused on developing a universal method for classifying all possible noise sources, but this proved impossible. In recent years, neural networks have been shown to be very accurate and usually outperform other classification algorithms [21-23]. The problem with deep neural networks is the large amount of input data for learning and the time required to fine-tune the classifier. Moreover, the algorithms are developed or learned for a specific type of noise source to achieve the best possible performance. In general, artificial neural networks are divided into two main categories: supervised and unsupervised. Self-organizing maps (SOMs) are competitive and unsupervised feed-forward type training networks. There is no training data and no expected results for the learning process. SOMs discover and exploit statistical similarities in the input space data, which they automatically cluster into different classes. The automatic addition or subtraction of neurons of the self-organising map makes the model more complex compared to the classical SOM with fixed structure, but the growing self-organising network (GSOM) provides a significant advantage in classifying the unknown structure of the acquired data. Hans-Ulrich Bauer and Thomas Villmann were the first to describe and define the GSOM in 1997 [24]. The growing self-organising network is an extension of the Kohonen SOM algorithm that adjusts the topology of the output space in addition to the weights of the neurons in the input space.

Studies have shown that unsupervised learning is comparable to other classification methods in terms of computational efficiency and clustering. Real-time use is cited as an advantage, since no prior database is required for recognition learning [25,26]. In numerous reviewed journal publications, unsupervised neural network learning for sound recognition is not as widely used as supervised learning. This is due to the specific classifications that recognize known, predictable sounds. However, some approaches based on unsupervised learning have been developed to process larger data sets of sound signals. In addition to identifying noise sources in water [27,28], some researchers have used SOM to model or predict noise in the environment, focusing on traffic noise, and have also addressed direct classification of general noise sources in urban environments [29-34].

While part of the research deals with classification itself, the other part focuses on feature extraction. Psychoacoustics is the science of human perception of sound. It studies the relationship between sensory perception (psychology) and physical variables (physics) [35]. Although psychoacoustic features are used to some extent outside their original purpose, they have hardly been used in any environmental noise source classification system. However, their specificity, importance, and applicability in the field of environmental noise have been demonstrated in many studies in recent years [36-40], and they are also implemented in the standard ISO /TS 12913-2: 2018.

In addition to the recorded sound, the derivative and log dt/dp of the recorded signal were also used in the presented study. The simplest method of Newton's difference quotient was used for numerical differentiation of the recorded sound signal, while log dt/dp is a nonlinear signal transform that acts as a decompressor. It amplifies small changes in the signal while attenuating larger ones. The above signal processing techniques were demonstrated in one of our previous studies, [41]. Seven features are extracted from each of three different inputs for classification. The psychoacoustic features of loudness, fluctuation strength, sharpness, tonality, and roughness are joined by crest factor and zero crossings. The final feature vector consists of 21 values and represents the input space for GSOM.

To mimic the human ability to spatially filter the acoustic environment (i.e., the Cocktail-Party effect), we have done much research and development in recent years in the area of microphone arrays for measuring environmental noise [9,17-20,42,43]. The implementation of the spatial domain to environmental noise measurements offers exceptional potential for more efficient identification of individual sources and clearer representation of the temporal and spatial dynamics of enviromental noise. In this paper, we present a

state-of-the-art approach for identifying environmental noise sources.

Multiple microphones in the form of an array mimic the use of our two ears. Simultaneous observation or listening in all directions on a plane parallel to the ground allows the implementation of immission directivty and source dominance Θ. This opens the possibility of filtering noise events and sources before feature extraction for classification purposes. In addition, the synthesized signal provides an improved signal-to-noise ratio (SNR), which naturally improves noise source detection. The amount of input data for classification is significantly reduced. The implementation of GSOM provides a broadly applicable device, as each environmental noise measurement is unique. Unexpected or residual noise sources cannot contaminate the data and thus the classification because the classifier is not trained, i.e., learning is unsupervised. Since we wanted to mimic human actions and track trends of environmental noise measurements, we used psychoacoustic features because they directly describe human perception of sound. Manipulation of the sound signal (its derivative and log dt/dp) was used to obtain two additional inputs for computing single-valued features (psychoacoustic features, crest factor, and zero crossing). Such an approach captures the most important characteristics of noise sources while reducing the dimensionality of the input data. All of the above methods enable the classification and identification of noise sources in real time.

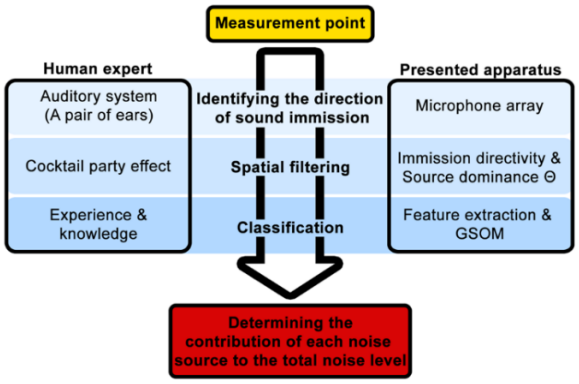

Fig. 4 *Determening the contribution of each noise source to the total noise level with the presented apparatus.*

The introduced elements of the device allow faster, more reliable, more objective and less expensive measurements. This is a step towards improving our health and the environment in which we live. By combining unsupervised learning, psychoacoustic and other features based on spatial domain, a apparatus is presented that is capable of determining the contribution of each noise source to the overall noise level (Fig. 4). Modernising the measurement approach indirectly reduces noise pollution and its effects on human well-being and health. The direct inclusion of spatial domain in the measurement of environmental noise represents a paradigm shift in the way we control noise pollution and exposure.

3. EXPERIMENT

The measurement was made near the vicinity of the train station Moste. In addition to passing trains, noise sources from the Aquafil industrial complex and the container terminal were also present, both located northeast of the MP. The array was placed near a gravel road used by residents as an access road to their gardens and tool sheds.

Based on the immission directivity in Fig. 5.d, we can distinguish two directions from which most of the sound was emitted: 24° and 270°. In general, we can say that most of the noise came from the directions south and northeast. In Fig. 5.a the data of the whole measurement are presented, and a clear short-term increase of the sound pressure level can be seen, which coincides with the dispersion of the dominant direction and the increase of the value of the source dominance Θ. These sound events are due to unloading of containers, gardening and other sound pulses impulse noise. The feature Θ was generally the lowest of all three measurements because much low-frequency noise was present. Despite the obvious non-stationarity of the detection of the dominant direction, it can be seen from the time course of the whole measurement that the immission of the noise came to a large extent from the NE.

In Fig. 5.b, showing the time course of the sound pressure level, the dominant direction and the dominance of the source Θ in the area between the 262nd and 265th minute of the measurement, we can clearly distinguish the impulse sound and the moving train. With a gradual increase in the level and the source dominance Θ, as well as a steady change in the dominant direction, the sound event can be recognized as the passage of the train south of the MP.

As a threshold for spatial filtering, we chose a value of 0.1 for source dominance Θ and an angle of 9° for stationarity of sound arrival direction. The classification into the individual classes depending on the time of measurement and the sound pressure level can be seen in Fig. 5.c. The area at the beginning of the measurement can be seen in which the data points of classes 5 and 8 dominate. Clearly visible are also all short-time ranges with increasing levels, mainly defined by class 7.

Table 2 *Calculated values of $L_{A,eq}$ for each class from spatially filtered data recorded at MP3*

Source	$L_{A,eq}$	Source	$L_{A,eq}$
Class 1	61,9 dB	Class 7	64,7 dB
Class 2	52,4 dB	Class 4	57,0 dB
Class 3	58,9 dB	Class 6	55,6 dB
Class 5	52,3 dB	Class 8	52,3 dB
All classes collectively	**57,8 dB**	**Entire measurement**	**54,4 dB**

The data had to be analysed by arranging the classified data points in four polar plots, as shown in Fig. 5.d. With the exception of direction 24°, the train noise occurred in the range between 225° and 315°, and was predominantly assigned to class 7. Individual deviations or misclassifications to other classes resulted from other impulse noise and the operation of the container terminal machinery. These noise sources were represented by the most data points and were grouped into classes 2 and 4. The second most data points were assigned to classes 3 and 6, which were later identified as low-frequency impulse noises, emitting from the railroad tracks and the container terminal site.

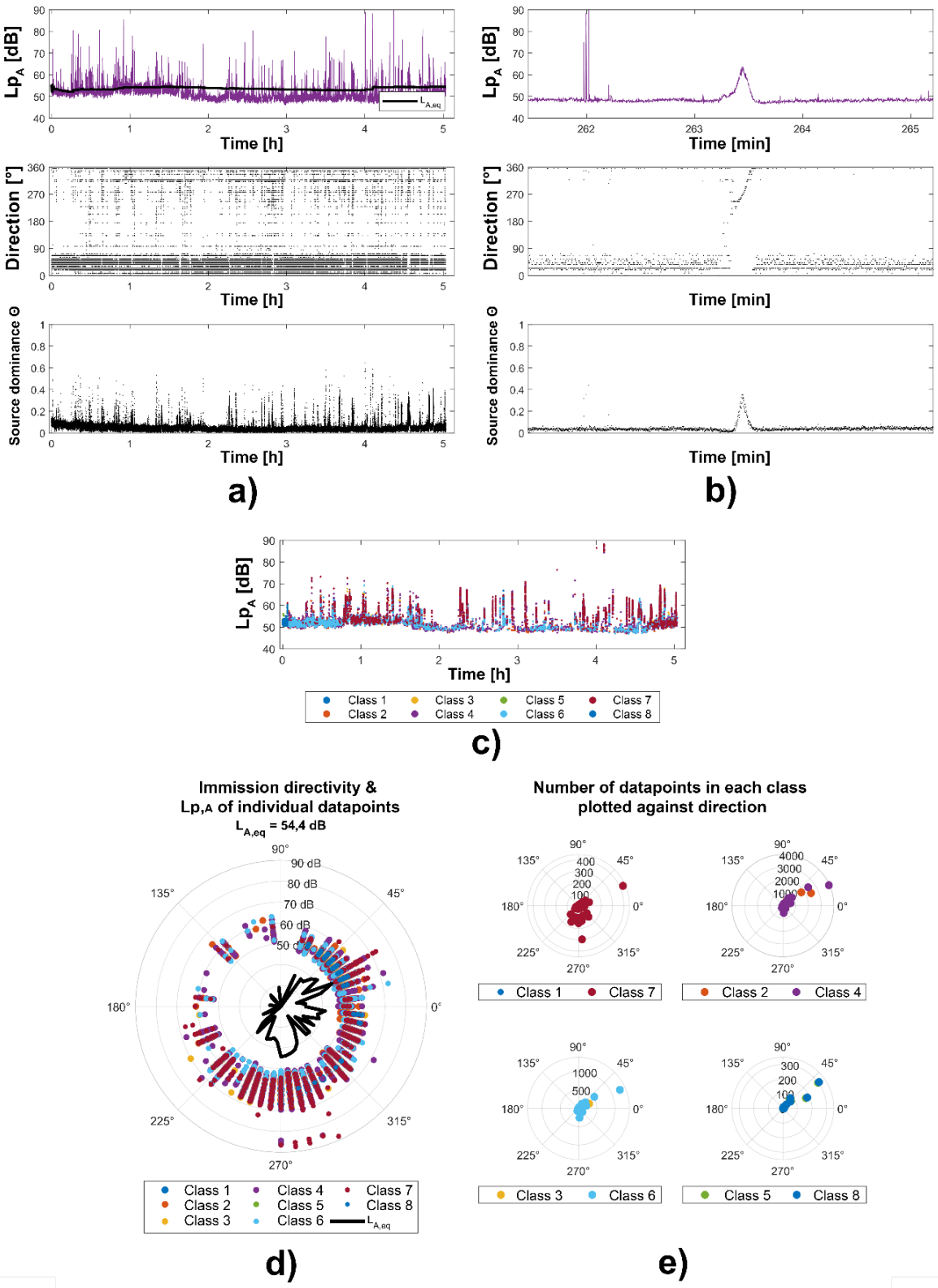

Fig. 5 *Recorded data of $L_{p,A}$ direction and source dominance Θ from MP3 of: a) The entire measurement, b) Train pass-by. Classified data points from MP3 plotted against: c) Time and $L_{p,A}$, d) Direction and $L_{p,A}$ (together with immission directivity), d) direction by their total number in each.*

Due to filtering of data points of the recorded sound pressure level where the value of source dominance Θ was less than 0.1, we excluded noise with a lower sound pressure level from the calculation of the equivalent value, resulting in a 3.4 dBA higher $L_{A,eq}$ compared to the value calculated on the basis of the whole measurement. With the exception of classes 1 and 7, all other values in Table 2 are at a similar level to the total equivalent of the filtered measurement. The low-frequency noise, most likely from the container terminal and the Aquafil industrial complex, can be assigned to classes 5 and 8. The

lower decibel values are the result of A-weighting, which reduces the influence of low frequencies. Although a clearer presentation of the classification would be desirable, it can be seen from the immission directivity, that the noise arrived mainly from two directions: the south and the northeast. Using spatial filtering, we were able to excluide 81% of the data points, which is comparable to the data filtering of MP1 and MP2.

4. DISCUSSION

In order to properly assess the in situ measurements, we compared the results of the equivalent values of the sound pressure level obtained with the prototype system with those obtained by manually marking individual parts of each of the three measurements. The technique of listening and marking is very time-consuming and prone to error, especially for long-term measurements in a noisy, highly dynamic acoustic environment. It should be noted that the classification of entire measurement with the prototype system took only of 3 minutes, while the manual marking of the measurements took more than an hour on average. The results of the comparison are shown in Table 3.

Table 3 *$L_{A,eq}$ for each identified noise source from all three measurements*

Train station Moste	$L_{A,eq}$	
	System	**Manually**
Train (C1 & 7)	64,7 dB	64,9 dB
Aquafil (C5 & 8)	55,8 dB	51,6 dB
Container terminal (C2 & 4)	56,4 dB	53,0 dB
Low frequency impulse noise (C3 & 6)	52,3 dB	52,9 dB
Entire measurement	**57,8 dB**	**54,4 dB**

The differences in the equivalent level values obtained level between the two approaches are inherent, since it is practically impossible to obtain exact values. In both cases, individual parts of the measurement are selected for the calculation of the equivalent level values, which means some loss of recorded data. In the case of manual filtering, what matters most is the accuracy of selection and judgment when listening to the entire five-hour recording and selecting representative parts of the measurement. On the other hand, the system is more prone to errors in quieter sources, (too) large sources and fast moving sources near the MP, which are excluded from the calculations.

Noise measurements in the vicinity of Moste train station revealed the greatest deviation of $L_{A,eq}$ in the noise of the Aquafil industrial complex. Probably, this is a consequence of the low-frequency noise, which affects the non-stationarity of the direction and is particularly noticeable at low sound pressure levels. Something similar can be observed in the results of the container terminal. It can be concluded that these two sources are also the reason for the difference between the equivalents of the whole measurement, which was 3.4 dBA.

5. CONCLUSION

The proposed system was found to be effective in determining the contributions of individual noise sources to the overall noise level, especially for long-term measurements. A typical environmental noise measurement was performed and four noise sources were detected and classified. We obtained results with the system that approximate those obtained manually. The calculated equivalent level values in conjunction with the immission directivity correctly identified the main noise sources for all three measurements, which was the main objective. The presented apparatus has shown that it will soon be able to replace conventional measurements by trained personnel, which are costly, time-consuming and prone to human errors. In the future, further measurements will be performed in different acoustic scenarios and the stationarity of the detected dominant direction of the sound immission will be investigated in more detail. Full integration with the SLM is also one of the priorities. Further tests of the system are needed, which will give us a better understanding of its shortcomings and suitability for integration with other applications, such as production line quality control, cavitation detection, acoustic imaging, etc.

REFERENCES

[1] Bocanegra, Johan Augusto, et al. "A novel approach to port noise characterization using an acoustic camera." Science of The Total Environment 808 (2022): 151903.

[2] Čurović, Luka, et al. "Impact of COVID-19 on environmental noise emitted from the port." Science of The Total Environment 756 (2021): 144147.

[3] López-Pacheco, et al. "A method for environmental acoustic analysis improvement based on individual evaluation of common sources in urban areas." Science of the total environment 468 (2014): 724-737.

[4] Kogan, Pablo, et al. "A Green Soundscape Index (GSI): The potential of assessing the perceived balance between natural sound and traffic noise." Science of the total environment 642 (2018): 463-472.

[5] Zannin, Paulo Henrique Trombetta, et al. "Evaluation of environmental noise generated by household waste collection trucks." Journal of Environmental Assessment Policy and Management 20.04 (2018): 1850010.

[6] Liguori, Consolatina, et al. "Accurate estimation of the environmental noise through sampling approach: selection of the measurement time." IEEE Transactions on Instrumentation and Measurement (2018):1006-1013.

[7] B. Berglund, T. Lindvall, Community Noise, Center for Sensory Research, Švedska (1995).

[8] P.Maijala, et al., Environmental noise monitoring using source classification in sensors, Applied Acoustics, Vol.129, (2018), pp. 258–267.

[9] J.Prezelj, Directivity measurements of environmental noise immission, Euronoise 2018, Crete, pp.711–717.

[10] Faulkner, Jon-Paul, et al. "Estimating the harmful effects of environmental transport noise: An EU study." Science of The Total Environment 811 (2022): 152313.

[11] Morillas, Juan Miguel Barrigón, et al. "A review of the measurement procedure of the ISO 1996 standard. Relationship with the European Noise Directive." Science of the Total Environment 565 (2016): 595-606.

[12] Chiariotti, Paolo, et al.. "Acoustic beamforming for noise source localization–Reviews, methodology and applications." Mechanical Systems and Signal Processing 120 (2019): 422-448.

[13] Xing, Hongyan, and Xu Yang. "Sound source localization fusion algorithm and performance analysis of a three-plane five-element microphone array." Applied Sciences 9.12 (2019): 2417.

[14] Aldeman, Matthew, and Ganesh Raman. "Effects of array scaling and advanced beamforming algorithms on the angular resolution of microphone array systems." Applied Acoustics 132 (2018): 58-81.

[15] Tiana-Roig, Elisabet, Finn Jacobsen, and Efrén Fernández Grande. Beamforming with a circular microphone array for localization of environmental noise sources. The Journal of the Acoustical Society of America 128.6 (2010): 3535–3542.

[16] Al-Sheikh, Bahaa, et al. "Sound source direction estimation in horizontal plane using microphone array." 2013 IEEE Jordan Conference on Applied Electrical Engineering and Computing Technologies. IEEE, 2013. https://doi.org/10.1109/AEECT.2013.6716479

[17] Murovec, Jure, et al. "Microphone array based automated environmental noise measurement system." Applied Acoustics 141 (2018): 106-114.

[18] Prezelj, J., et al. Estimation of Noise Immission Directivity using small Microphone Array. Universitätsbibliothek der RWTH Aachen, 2019.

[19] Murovec, Jure, et al. Environmental noise event classification based on self-organizing map using psychoacoustic features and spatial filtering. Universitätsbibliothek der RWTH Aachen, 2019.

[20] Prezelj, Jurij, et al. "A novel approach to localization of environmental noise sources: Sub-windowing for time domain beamforming." Applied Acoustics 195 (2022).

[21] Zhao, Wen, and Bo Yin. "Environmental sound classification based on adding noise." 2021 IEEE 2nd International Conference on Information Technology, Big Data and Artificial Intelligence, Vol. 2. IEEE, 2021.

[22] Demir, Fatih, et al. "A new deep CNN model for environmental sound classification." IEEE (2020)

[23] Cao, Jiuwen, et al. "Urban noise recognition with convolutional neural network." Multimedia Tools and Applications 78.20 (2019): 29021-29041.

[24] Bauer, H-U, et al. Growing a hypercubical output space in a self-organizing feature map. IEEE Transactions on Neural Networks 8.2 (1997): 218–226.

[25] Saki, Fatemeh, and Nasser Kehtarnavaz. Real-time unsupervised classification of environmental noise signals. IEEE/ACM Transactions on Audio, Speech, and Language Processing 25.8 (2017): 1657–1667.

[26] Sukhwal, Abhilasha, and Mahendra Kumar. Comparative study of different classifiers based speaker recognition system using modified MFCC for noisy environment. 2015 International Conference on Green Computing and Internet of Things. IEEE, 2015.

[27] Rako, Nikolina, et al. Mapping underwater sound noise and assessing its sources by using a self-organizing maps method. The Journal of the Acoustical Society of America 133.3 (2013): 1368–1376.

[28] Zak, Andrzej. Kohonen networks as hydroacoustic signatures classifier. Proceedings of the 9th WSEAS International Conference on Neural Networks. World Scientific and Engineering Academy and Society, 2008.

[29] Cammarata, G., et al. Self-organizing map to filter acoustic mapping survey in noise pollution analysis. Proceedings of 1993 International Conference on Neural Networks (IJCNN, Japan). Vol. 2. IEEE, 1993.

[30] Oldoni, Damiano, et al. Context-dependent environmental sound monitoring using SOM coupled with LEGION. The 2010 International Joint Conference on Neural Networks (IJCNN). IEEE, 2010.

[31] Valero, Xavier, et al. Support vector machines and self-organizing maps for the recognition of sound events in urban soundscapes. 41st International Congress and Exposition on Noise Control Engineering (Inter-Noise-2012). Institute of Noise Control Engineering, 2012.

[32] Ricciardi, Paola, et al. Sound quality indicators for urban places in Paris cross-validated by Milan data. The JASA 138.4 (2015): 2337–2348.

[33] Can, Arnaud, and Benoit Gauvreau. Describing and classifying urban sound environments with a relevant set of physical indicators. The Journal of the Acoustical Society of America 137.1 (2015): 208–218.

[34] Oldoni, Damiano, et al. The acoustic summary as a tool for representing urban sound environments. Landscape and Urban Planning 144 (2015): 34–48.

[35] Zwicker, Eberhard, and Hugo Fastl. Psychoacoustics: Facts and models. Vol. 22. Springer Science & Business Media, 2013.

[36] Engel, Margret Sibylle, et al. "A Review of the Use of Psychoacoustic Indicators on Soundscape Studies." Current Pollution Reports 7.3 (2021): 359-378.

[37] Moehler, Ulrich, Christine Huth, and Manfred Liepert. "Case studies on the application of psychoacoustic methods for traffic noise." Forum Acusticum. 2020.

[38] Genuit, Klaus. "Binaural measurement and psychoacoustic analysis—An advantage for the environmental noise research." The Journal of the Acoustical Society of America 145.3 (2019): 1752-1753.

[39] Hoffmann, Alice, and Wolfgang Kropp. Auralization of simulated tyre noise: Psychoacoustic validation of a combined model. Applied Acoustics 145 (2019)

[40] Van den Berg, Frits. "Wind Farm Noise Management Based on Determinants of Annoyance." (2022).

[41] Murovec, Jure, et al. "Psychoacoustic approach for cavitation detection in centrifugal pumps." Applied Acoustics 165 (2020): 107323.

[42] Prezelj, Jurij, and Wolfgang Fellner. "System for Automatic Noise Source Identification and Classification." Patent, G01H 11.00: 24518.

[43] Lipar, Primož, et al. "Automatic recognition of machinery noise in the working environment." Strojniški vestnik-Journal of Mechanical Engineering 61.12 (2015)

University of Nis
Faculty of Occupational Safety
„Politechnica“ University of Timisoara
Faculty of Mechanical Engineering
27th International Conference
NOISE AND VIBRATION
Niš, 20 - 21. 10. 2022.

TECHNICAL GUIDELINES FOR THE INSTALLATION OF A HEAT PUMP FOR PROTECTION AGAINST EXCESSIVE ENVIRONMENTAL NOISE

Nikola Holeček

Faculty of Environmental Protection, Velenje, Slovenia, nikola.holecek@outlook.com

Abstract - *A worrying fact is that our environment is increasingly exposed to noise, which is primarily due to accelerated urbanization. Despite the growing trend of increasing noise exposure, awareness of excessive noise exposure is also rising in Europe. When dealing with increased noise levels, we must be aware that they are easiest to eliminate at the planning stage, of course, if we are aware of these problems and anticipate them in a timely manner. Outdoor heat pump units are just one small source of environmental noise out of many. However, as there are more and more of them from year to year, there has been an increase in the number of complaints about their noise in recent years. Their noise comes to the fore especially in places where residential buildings are placed close together. When installing outdoor heat pump units, it is therefore advisable to decide on the location and location of the unit, as improper installation can cause a lot of problems for residents of the most congested nearby buildings. Abroad, there are also technical guidelines for the installation of a heat pump, the purpose of which is precisely to protect against excessive environmental noise. In Germany, this guideline is the TA Lärm (German: Technische Anleitung zum Schutz gegen Lärm), which also states the immission limit values for different areas. In addition, the technical guideline provides a simple method by which we can estimate the sound pressure level at a particular emission point based on the distance from the outdoor unit of the heat pump and its location.*

1. INTRODUCTION

The use of heat pumps (HP) is increasing for heating buildings and sanitary water, as they represent both an energy-efficient and a clean and environmentally friendly heating alternative. There are mainly three types of HP: water/water, soil/water and air/water. The biggest problem in terms of noise is still the air/water heat exchanger (Fig. 1), as most models also have an external unit, which represents an additional burden in the already high environmental noise load. From the user's point of view, the noise in the other versions (water/water and earth/water) can also be problematic if the unit is located close to living and sleeping areas.

The problem of excessive exposure to noise is becoming more relevant every day. The World Health Organization has recently issued new guidelines regarding environmental noise, thereby drawing attention to the urgent problem revolving around it once again [1]. Excessive levels of environmental noise can also cause serious health problems [2], such as cognitive impairment, sleep disturbances, tinnitus and even cardiovascular disease. In the same report, they also estimated that at least 1 million healthy years of life are lost annually in Western Europe countries precisely because of environmental noise. (A year of healthy life lost is represented by a DALY (Disability-Adjusted Life Year).

a) b)

Fig. 1 *Air/water heat pumps: a) an example of heating heat pumps from a domestic manufacturer, b) an external heat pump unit installed in the area in front of a residential building*

2. NOISE EMITTED BY HEAT PUMPS

External heat pump units represent only one minor source of environmental noise among many. Nevertheless, in recent years there has been an increased number of complaints about their noise, because of the increased number of them. Their noise comes to expression, especially in places where residential buildings are close together. As far as the noise of external air/water type HP units is concerned, the dominant sources are the noise of the compressor and the fan (Fig. 2). During pump operation, both aerodynamic noise and structural noise are generated. Aerodynamic noise is the result of fan operation. Fan noise depends on the type of fan itself and the functioning conditions. In heat pumps, the axial fan is most commonly used. It turns out that fan noise is the lowest when fan efficiency is the highest. The frequency content of the fan's aerodynamic noise primarily depends on the speed of operation and the number of blades. The higher the number of blades and speed, the higher the sound frequency of the fan will be dominant. The main source of vibrations in the outdoor unit is the compressor, where the vibrations transmit throughout the entire construction of the outdoor unit. This generates structural noise, the amplitude of which only depends on the quality of the vibration isolation under the compressor and the shape of the entire structure itself. Compressor vibrations also depend on the operating speed and the pressure difference in the system itself, which the compressor must overcome during operation. The most

modern HPs allow both variable fan speed and variable compressor speed. Therefore, depending on the operating mode, both the frequency content of the noise, as well as the amplitude of it, change. Despite the variability of the compressor and fan operation, each heat pump will have tonal components even in the lower frequency range between 10Hz and 250 Hz. This is exactly why the noise of heat pumps is often associated with low-frequency noise or infrasound [3].

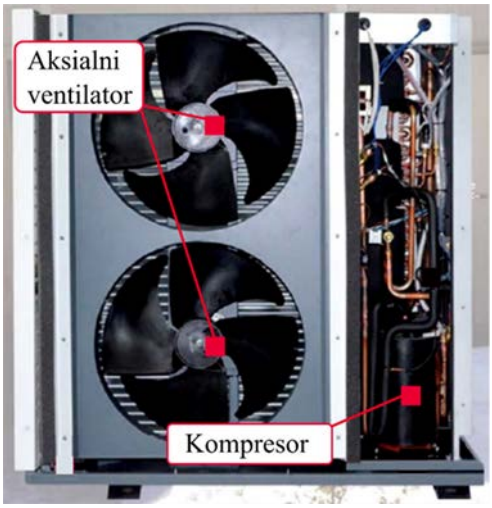

Fig. 2 *External unit of HP without protective cover*

Heat pumps must be marked with an energy label, which is an important tool for consumers to better understand and compare the energy efficiency of appliances. In addition, the energy label contains information about the relevant functions of the devices, as well as information about the noise level of the product itself. The energy label for household appliances was introduced for the first time in 1994. The primary purpose of the energy label is to simply show the energy efficiency of the appliance and thereby encourage the customer to buy energy-efficient products. Which also indirectly encourages the development of technologies that enable low energy consumption. An example of a HP energy label is shown in Figure 3. In the lower-left corner, we can see information on the noise level of the external and internal units of the heat pump. The quantity used to list the noise level of appliances is A-weighted sound power and has the unit decibel [dB]. However, we must be careful when understanding this parameter and it should not be confused with the sound pressure level. The sound power of any source is independent of the room and the distance from where it is installed. This is why it is used to declare the noise level. The sound pressure depends on both the room in which the device is located and the distance from the source. Despite all the advantages of using sound power to characterise noise, we must be aware of the limitations. Two different products can have identical sound power but completely different noise characteristics [4]. The noise of one may be acceptable to us, while the sound of the other may feel disturbing or unpleasant. This is why it is recommended for the end user to check the noise of the device during functioning before the purchase, if possible.

3. THE PROBLEM OF LOW-FREQUENCY NOISE

The effect of excessive noise on the human body is already a well-known field. Excessive levels of environmental noise are also proven to cause serious health problems [2], such as cognitive impairment, sleep disorders, tinnitus and even cardiovascular diseases. Despite all of the problems, unlike other environmental stressors, noise pollution, especially in the urban environment, is increasing daily.

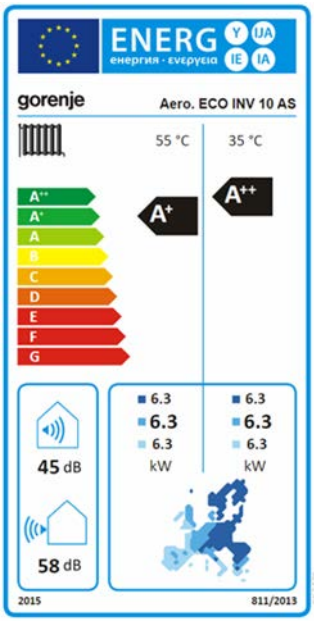

Fig. 3 *Energy label of the Gorenje Aero ECO INV 10 AS heat pump*

The problem of low-frequency noise has been known for some time, but there are relatively few measures or interventions in this area. We are talking about low-frequency noise in the frequency range between 10 Hz and 250 Hz. It should be pointed out that noise in this low-frequency range only becomes audible at high sound pressure levels. Nevertheless, it has been proven that humans can perceive low-frequency noise below the level of hearing in one way or another [5, 6]. Low-frequency noise in the urban environment is often described as a constant deep annoying noise or even shaking and can also be detected by people based on the body's vibrations or surroundings [6].The main problem with low-frequency noise is its long wavelength (noise at a frequency of 50 Hz has a wavelength of 6.8 m at 20°C). Therefore, it is difficult to suppress, and it spreads rapidly in all directions and can be heard over great distances. There has already been a lot of research on the impact of low-frequency noise on people, and it turns out that at first, with short-term exposure, the noise is only annoying, but it is accompanied by quite a few secondary symptoms, such as headache, concentration problems, rapid heartbeat and problems with sleeping. Research on the long-term impact of daily exposure to low-frequency noise on human health has not yet been conducted by the WHO, despite repeated exposure to low-frequency noise as an environmental stressor. Current research consists only of individual case studies and laboratory experiments on small samples and short exposures to low-frequency noise. Because of this, the exact impact of prolonged exposure to low-frequency noise is currently unknown.

4. PRIMARY MEASURE: CORRECT PLACEMENT OF HEAT PUMPS IN THE ROOM

The most effective measures to reduce noise are primary measures, where we can reduce noise in the source. Even before purchasing HP, it is recommended to inquire noise level of the model in question and to opt for a quieter and more efficient model, despite the likely higher price. During the actual installation of the HP, possible increased noise levels can be avoided by following simple measures. Most are achieved by just setting up the HP.

Abroad, there are also technical guidelines for setting up a heat pump, the purpose of which is precisely protective against excessive environmental noise. In Germany, this guideline is TA Lärm [10] (German: Technische Anleitung zum Schutz gegen Lärm), in which the immission limit values for different areas are also indicated. In addition, the technical guidelines provide a simple method that can be used to estimate the sound pressure level at a specific emission point based on the distance from the heat pump's outdoor unit and its location. The noise emission rating is calculated using the following equation and Fig. 4:

$$L_r = L_{WA} + K_T + K_0 - 20\log(s_m) - 11\text{dB} + K_R, \quad (1)$$

where L_{WA} = A-weighted sound power, K_T = addition due to accented tones, K_0 = addition due to mounting method (see Fig. 5), s_m = distance from the outdoor unit to the emission point, and K_R = supplement due to the increased sensitivity of people in individual periods of the day.

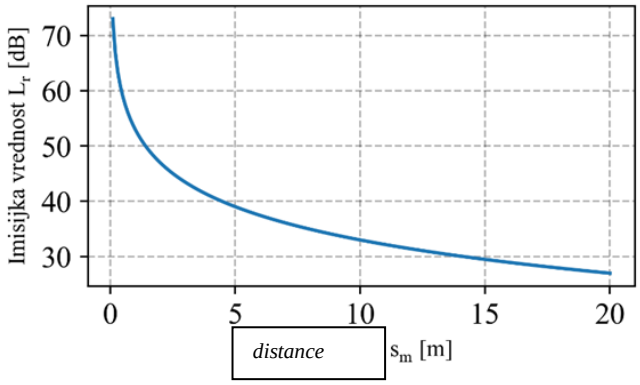

Fig. 4 *Emission value L_R of the sound pressure as a function of the distance from the source*

Additional recommendations and an interactive calculator of the emission value are available on the website [19].

4.1. Example of calculation of the emission value

Use of informative calculation on a simple example. Let's take the data from the energy label shown in Fig. 3. The declared sound power of the outdoor unit is equal too. Let's assume that the heat pump is installed close to the building and is additional (see Fig. 5.b). By taking these parameters into account, we can calculate the emission value of the sound pressure depending on the distance from the source, see Fig. 4. (Information on the supplement due to accented tones is not available for the specified type of outdoor unit and the allowance due to increased sensitivity has not been taken into account). Minimum distance of the heat pump would be determined based on the limit emission value. According to the TA Lärm guideline, the minimum emission value at night is 35 dB; in the assumed conditions, the outdoor unit should be located at least 8 m from the nearest emission point.

If possible, the outdoor unit should be at least 3m or more away from the nearest reflective surface. Figure 3a shows the best placement of the outdoor unit, and Figure 3b shows the worst possible placement, where the outdoor unit is placed on two sides close to the reflective surfaces.

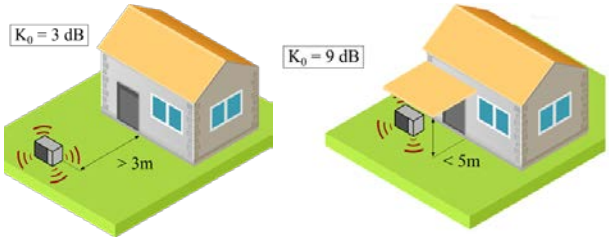

a) b)

Fig. 5 *Example of spatial placement of the heat pump outdoor unit: a) best placement, b) worst placement in the room*

5 HEAT PUMP NOISE LEGISLATION

On August 2, 2013, in Regulation 813/2013, the European Union set the limit values for the sound power of heat pumps. These values are valid from 2015 onwards. [15]

Table 1 *Sound power limit values of heat pumps from Regulation 813/2013 14*

	Indoor unit Sound power L_{WA}[dB]	Outdoor unit Sound power L_{WA}[dB]
Nominal heat power ≤ 6 kW	60	65
Nominal heat power > 6 kW and ≤ 12 kW	65	70
Nominal heat power > 12 kW and ≤ 30 kW	70	78
Nominal heat power > 30 kW and ≤ 70 kW	80	88

5.1 Noise legislation Slovenia

At this point, Slovenia does not yet have guidelines directly related to heat pumps. Thermal devices are limited by the Regulation on limit values of noise indicators in the environment. The regulation defines areas and noise limits in these areas [17].

Table 2 *Limit values of noise indicators in the environment [17]*

Noise protection zone	L_{day} [dB]	$L_{evening}$ [dB]	L_{nigt} [dB]
IV area	73	68	63
III area	58	53	48
II area	52	47	42
I area	47	42	37

I. The area of noise protection includes quiet outdoor areas, except for areas of transport infrastructure and areas of natural resources [17].

II. The area includes residential areas, and areas of central activities, such as areas for healthcare near hospitals, spas and recovery centres. The back surfaces that fall under II. the area is an area for tourism [17].

III. The area includes residential areas in the countryside, central areas of activities, areas of sports centres, green areas for rest, recreation and sports, cemeteries, and areas of scattered settlements and scattered construction [17].

IV. The area covers areas for industry, economic zones, transport infrastructure zones, energy infrastructure, communication infrastructure, environmental infrastructure, water infrastructure and mineral resources area. In addition, also areas of agricultural and forest land, except in quiet areas [17].

5.2 Noise legislation Austria

In Austria, heat pump noise must not significantly exceed the background noise level, and distance criteria are also provided depending on the installation circumstances. Maximum noise levels vary by region. Restrictions may apply to the boundary of a property or the frontage of a neighbouring property. When installing a heat pump, the neighbour must clarify the permissible external sound power with a legal expert who measures the sound of the surroundings, on a case-by-case basis. This introduces uncertainty about acceptable sound power levels [18].

5.3 Noise legislation Germany

In Germany, there are no restrictions on the sound power level of heat pumps. However, the TA Lärm (Technical Guidelines for Noise Protection) protects neighbours from excessively high emission levels. It determines the limit values that must be observed at the relevant point of emission (0.5 m in front of the open window of the room most in need of protection). For a residential area, the maximum level is 35 dB(A) at night (22-6 h). The most common place of installation is a common living area with a night limit of 40 dB(A). In general, the TA Lärm limits apply to the sum of the total noise emissions from each source on the site, not just to a single unit. If the sound pressure caused by the heat pumps is at least 6 dB(A) below the limit value, the accumulated forecast is not required [14].

Therefore, three methods of calculation can be used: taking into account all sources on the site, a general discount of 6 dB(A) on the limit value or only the sound pressure of the heat pump. The decision is made by the local authorities [18].

The sixth general administrative regulation for the federal emission control act adopted on August 26th, 1998 sets noise limit values for the protection of the general public and the surrounding area from the harmful effects of noise on the environment and the protection from harmful effects of noise on the environment [18].

The Bundesverband Wärmepumpe has developed an online tool that can be used to calculate whether limit values are met [18].

Table 3 *Noise limits during the day according to TA Lärm [18]*

Area	Time	Rating level [dB(A)]
Industrial estates		70
Industrial areas	Day	65
	Night	50
Urban area	Day	63
	Night	45
Central area	Day	60
	Night	45
Mixed residential area	Day	55
	Night	40
Clean Residential Area	Day	50
	Night	35

5.3.1 Bundesverband Wärmepumpe noise calculator

The sound calculator enables the evaluation of the noise emissions of air-to-water heat pumps, according to TA Lärm, during daytime operation periods of increased sensitivity and at night. With the calculation, it is possible to estimate noise emissions in rooms that need protection (relevant points of emission) on neighbouring properties or to determine the required distance from the heat pump [19].

The website is divided into sections for input. The following pictures are translated into Slovenian, the website is in German [19].

Fig 6 *Noise calculator I.* [19]

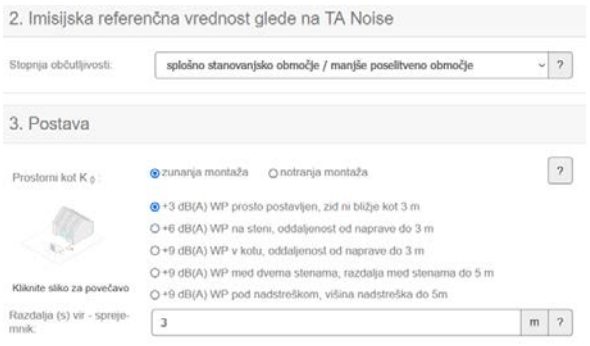

Fig. 7 *Noise calculator II. and III.* [19]

In the second area, the area where the pump will be installed is marked, in the third area, the location is marked and the distance from the buildings is entered. [19], Based on this data, the website indicates how much noise is below the standards or just exceeded them [19].

6. CONCLUSIONS

With increasing urbanisation, the burden on our environment intensifies. These incriminating factors include the excessive noise level that many people encounter every day. External units of heat pumps are also the source of environmental noise, the use of which increases day by day as they constitute an energy-efficient alternative to heating. Despite all the advantages the external units of heat pumps are the noise source and the additional burden to already existing high environmental noise load. Due to its sound profile and long-lasting operation, the noise of heat pumps is the major problem due to its sound profile and long-lasting operation.

The legislation related to the noise of heat pumps in Europe, especially in Germany and Austria is in general relatively well regulated, so we can soon expect changes at home as well. It would be a good choice or recommendation to follow German standards till Slovenia changes legislation. They also offer online tools that enable more consistent installation of heating devices.

7. REFERENCES

[1] World Health Organization (2018): Environmental Noise Guidelines for European region.

[2] URL: http://www.euro.who.int/__data/assets/noise-guidelines/eng.pdf?ua=1 .

[3] World Health Organization (2011): Burden of disease from Environmental noise.

[4] URL: http://www.who.int/quantifying_ehimpacts/publications/e94888.pdf?ua=1 .

[5] Baliatsas, C., van Kamp, I., van Poll, R., Yzermans, J. (2016): Health effects from low-frequency noise and infrasound in the general population: Is it time to listen? A systematic review of observational studies. *Science of the Total Environment*, vol. 557, str. 163–169.

[6] Mirowska, M., Mroz, E. (2000): Effect of low frequency noise at low levels on human health in light of questionnaire investigation. Proc. Inter-noise, vol. 5, str. 2809–2815.

[7] Zwicker, E., Fastl, H. (1983): A portable loudness meter based on ISO 532 B. Proc. *11th Int Congr Acoustics*, vol. 8, str. 135–137.

[8] Yost, W. A. (2015): Psychoacoustics: A Brief Historical Overview. *Acoustical Society of America*, vol. 11, str. 46–53.

[9] Swart, D. J., Bekker, A. (2019): The relationship between consumer satisfaction and psychoacoustics of electric vehicle signature sound. *Applied Acoustics*, vol. 145, str. 167–175.

[10] Volardi, G., Di Puccio, F., Forte, P., Mattei, L. (2019): Psychoacoustic analysis of power windows sounds: Correlation between subjective and objective evaluations. *Applied Acoustics*, vol. 134, str. 160–170.

[11] Moravec, M., Ižaríková, G., Liptai, P., Badida, M., Badidová, A. (2019): Development of psychoacoustic model based on the correlation of the subjective and objective sound quality assessment of automatic washing machines. *Applied Acoustics*, vol. 140, str. 178–182.

[12] Sechste Allgemeine Verwaltungsvorschrift zum Bundes-Immissionsschutzgesetz (Technische Anleitung zum Schutz gegen Lärm – TA Lärm), vom 26. August 1998 (GMBl Nr. 26/1998 S. 503).

[13] Bundesverband Wärmepumpe (BWP) (2019): Schall-rechner.

[14] URL: https://www.waermepumpe.de/schallrechner/

[15] Evropska Komisija. UREDBA KOMISIJE (EU) Št. 813/2013.; 2013.

[16] Holeček N, Bregar T. EMISIJA HRUPA ZUNANJE ENOTE TOPLOTNE ČRPALKE ZRAK-VODA. Published online 2019.

[17] Uradni list RS. Uredba o Mejnih Vrednostih Kazalcev Hrupa v Okolju.; 2018.

[18] HEAT PUMPS & SOUND ANNEXE

[19] Bundesverband Wärmepumpe. Zvočni kalkulator. Published 2021. Accessed August 19, 2022. https://www.waermepumpe.de/schallrechner/

BRÜEL & KJÆR
SOUND & VIBRATION
MEASUREMENTS

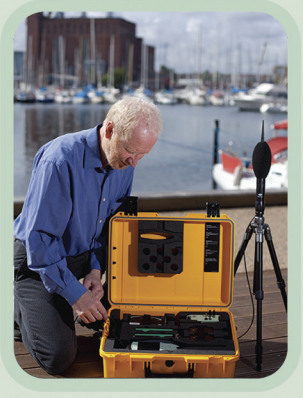

We help our partners and customers
measure and manage
the quality of sound and vibration
in products and enviroment

With more than 90 sales offices or local agents,
we provide immediate and comprehensive
customer support

Contact your local
sales representative:

RMS d.o.o.
Partizanske avijacije 12/3
11070 Novi Beograd, Srbija
Tel.: +381(0)11 2280 951
Fax: +381(0)11 2280 751
www.rms.rs

Brüel & Kjær
an HBK company

University of Nis
Faculty of Occupational Safety
„Politechnica“ University of Timisoara
Faculty of Mechanical Engineering
27th International Conference
NOISE AND VIBRATION
Niš, 20 - 21. 10. 2022.

STRATEGIC NOISE MAP OF THE CITY OF NIŠ, SERBIA - COMPARATIVE ANALYSIS OF NOISE EXPOSURE

Momir Prascevic[1], Darko Mihajlov[1], Marko Ličanin[1]

[1] University of Nis, Faculty of Occupational Safety, Serbia
e-mail: momir.prascevic@znrfak.ni.ac.rs

Abstract - *In the largest number of European cities and countries the third round of strategic noise mapping was completed in 2017, while the first strategic noise map for agglomerations in the Republic of Serbia was developed in 2019 for the city of Niš. The paper presents some of the results of the strategic noise map for the city of Niš and the results of noise exposure are compared with the data obtained for European cities in the strategic noise mapping process.*

1. INTRODUCTION

Environmental noise exposure with at least one in five people exposed to noise levels considered harmful to physical and mental health of the population requires measures to be taken to reduce the negative effects of environmental noise.

Reducing environmental noise to the recommended noise levels by the World Health Organization (WHO) is a key objective under the Seventh Environment Action Programme [1] and the Environmental noise Directive (END) [2].

The recommendations of the World Health Organization define the exposure levels above which an increase in negative outdoor noise effects on health occur. Reducing noise below these levels is strongly recommended

Table 1 *WHO recommendations* [3]

Noise indicator	Road	Rail	Air
L_{den}	53 dB	54 dB	45 dB
L_{nigh}	45 dB	44 dB	40 dB

The policy of the European Union on environmental noise reduction is based on the strategic noise mapping for:

- Major roads of more than 3 000 000 vehicle passages a year;
- Major railways of more than 30 000 train passages a year;
- Major airports of more than 50 000 movements a year;
- All road, railways airports and IPPC industrial sites within agglomerations of more than 100 000 inhabitants.

Based on the data collection, a noise model is created, which is validated and used to determine the noise exposure of population and building. With the described procedure, which represents strategic noise mapping, the following are determined:

- Number of people living in dwellings at the most exposed building façade that are exposed to noise levels in END recommended bands:
  - 55-59, 60-64, 65-69, 70-74 and 75 dB L_{den};
  - 50-54, 55-59, 60-64, 65-69 and 70 dB L_{night};
- Noise contour maps for major sources and agglomerations.

After strategic noise mapping, the areas with high noise levels are detected and analysed, noise management and mitigation measures are identified, including Involving stakeholders and consulting the public.

The described procedure represents noise action planning and results in noise action plans for noise protection that contain:

- Description of noise problems that need to be improved and identification of their geographical location;
- Description of measures taken to address noise problems including the protection of quiet areas;
- Estimates in terms of the reduction of the number of people affected;
- Description of public consultation.

The entire procedure from the strategic noise mapping to action plans, which is repeated in 5-year cycles, should result in:

- Reducing number of people exposed to noise;
- Reducing negative effects caused by environmental noise;
- Reducing health costs due to noise

The third round of strategic noise mapping in EU Member States was to be completed by 31 December 2017. After this deadline, the European Environmental Agency produced a report on environmental noise in Europe [4]. This report presents a comprehensive overview and analysis of environmental noise in Europe and is focused on the data officially reported by the 33 EEA member countries (the 28 EU Member States plus Iceland, Lichtenstein, Norway, Switzerland and Turkey), excluding Turkey, until 1 January 2019. For member countries that had not submitted data until

1 January 2019, an assessment was made based on the data submitted after the second round of strategic noise mapping.

The data presented in the EEA report [4] were compared with the data obtained by strategic noise mapping for the city of Niš.

2. ENVIRONMENTAL NOISE EXPOSURE IN EUROPE

The estimations of population exposure to environmental noise given in EEA report show that 112.8 million are exposed to L_{den} levels of 55 dB and higher due to road traffic, 21.6 million due to railway traffic, 4.2 million due to air traffic and 0.8 million due to industry. Therefore, 78.6 million are exposed to L_{night} levels of 50 dB and higher due to road traffic, 17.1 million due to rail traffic, 1.3 million due to air traffic and 0.4 million due to industry [4].

The levels of 55 dB L_{den} and 50 dB L_{night} are END thresholds.

These results show that at least 20% of Europeans are exposed to high L_{den} levels and more than 15% of Europeans are exposed to high L_{night} levels considering road traffic noise only, from which adverse health effects can occur [4]. Detailed data are given in Table 2.

Number of people exposed to various L_{den} and L_{night} noise bands is shown in Fig. 1 and Fig. 2.

The presented results indicate that road traffic is the biggest source of environmental noise, followed by railway, air and industrial noise.

In countries such as Finland, Germany, Norway, Sweden and the United Kingdom, the proportion of people exposed to road traffic noise across different cities (Fig. 3) in the same country is rather homogeneous. However, in southern and eastern European countries, the differences in the proportion of people exposed to noise differ greatly from city to city within the same country [4].

The proportional differences in exposure to railway noise across cities (Fig. 4) could be due to whether or not urban trams and light railways are included in the noise mapping [4].

Table 2 *Population exposure to environmental noise, based on areas covered by strategic noise maps in 2017, EEA-33 (Turkey not included)* [3]

	Noise source	Number of people exposed to $L_{den} \geq 55$ dB		Number of people exposed to $L_{night} \geq 50$ dB	
		Reported	Estimated	Reported	Estimated
Inside urban areas	Road	50.6	81.7	33.8	57.5
	Rail	7.9	10.7	6.0	8.1
	Air	2.2	3.1	0.6	0.9
	Industry	0.3	0.8	0.2	0.4
Outside urban areas	Road	21.8	31.1	14.2	21.1
	Rail	10.4	10.9	8.7	9.0
	Air	0.8	1.1	0.4	0.4

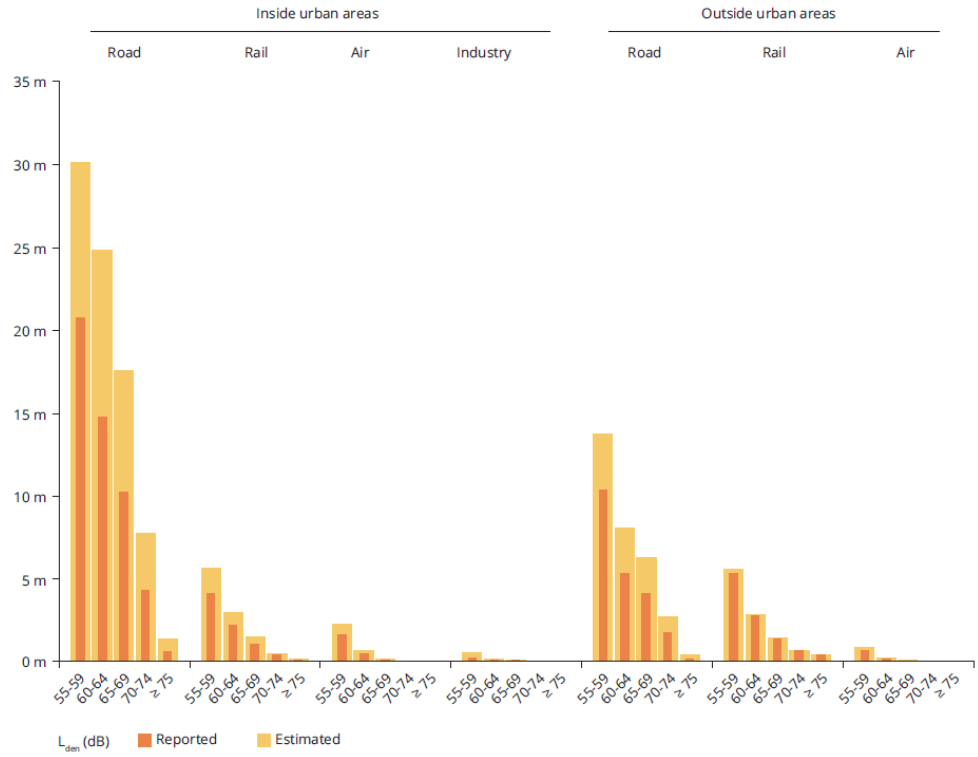

Fig. 1 *Number of people exposed to various L_{den} noise bands based on areas covered by strategic noise maps in 2017, EEA-33 (Turkey not included)* [4]

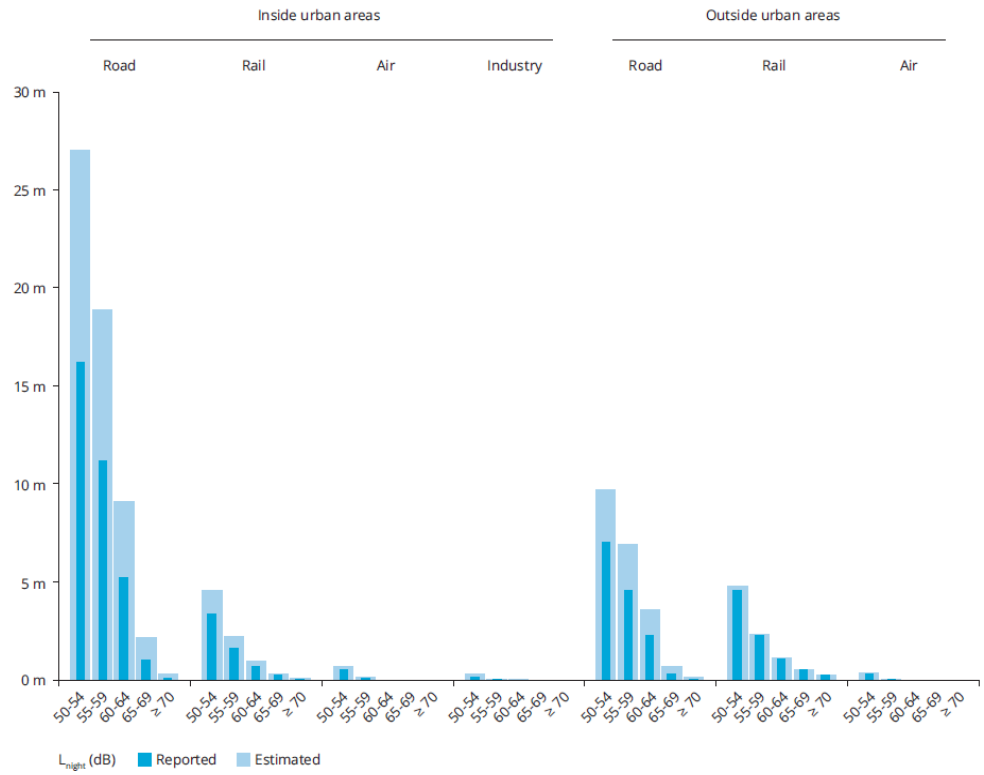

Fig. 2 *Number of people in million exposed to various L_{night} noise bands based on areas covered by strategic noise maps in 2017, EEA-33 (Turkey not included)* [4]

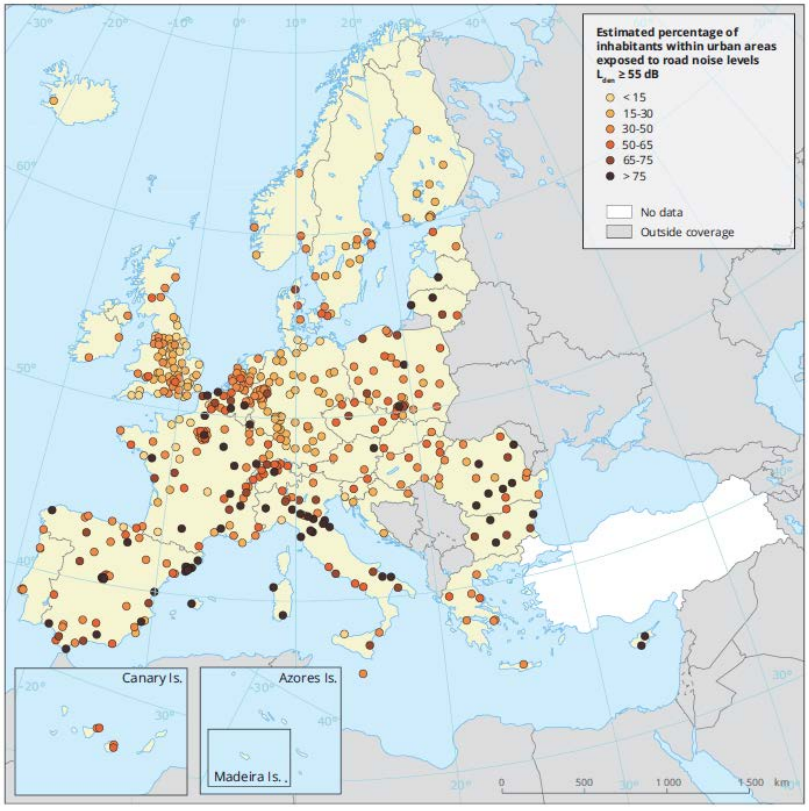

Fig. 3 *Percentage of inhabitants within urban areas, exposed to road noise levels $L_{den} \geq 55$ dB in 2017* [4]

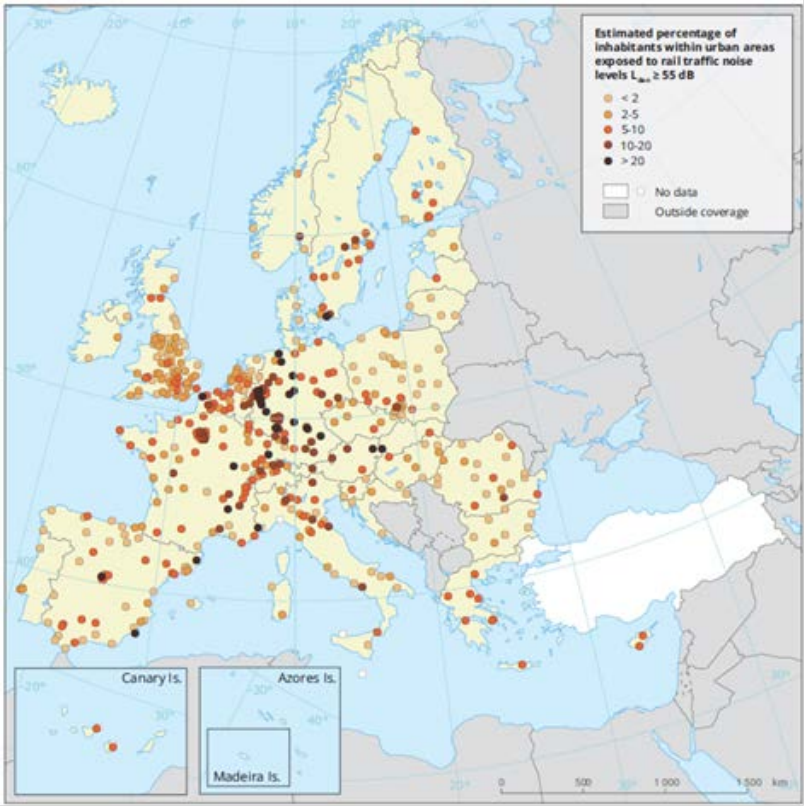

Fig. 4 *Percentage of inhabitants within urban areas, exposed to rail noise levels $L_{den} \geq 55$ dB in 2017 [4]*

3. ENVIRONMENTAL NOISE EXPOSURE IN THE WESTER BALKAN ACCESSION COUNTRIES

For the third round of strategic noise mapping in 2017, Bosnia and Herzegovina, Montenegro and North Macedonia have submitted information regarding all the noise sources to be mapped [4]. However, strategic noise maps have been delivered only for the city of Podgorica in Montenegro (Table 3).

Table 3 *Population exposure to environmental noise in Podgorica* [4]

Noise sources	$L_{\text{den}} \geq 55$ dB	$L_{night} \geq 50$ dB
Road	132 500 (71 %)	117 200 (63 %)
Rail	6 700 (4 %)	5 500 (3 %)

4. ENVIRONMENTAL NOISE EXPOSURE IN THE CITY OF NIŠ

The city of Niš is one of the five agglomerations in the Republic of Serbia that has the obligation, in accordance with the provisions of the END directive and national legislation, to develop strategic noise maps. Other agglomerations that have this obligation are Belgrade, Novi Sad, Kragujevac and Subotica.

Among the five agglomerations above the thresholds identified with the END directive, Niš was selected for strategic noise mapping within the project no. 14SER01/03/131 funded by the European Union, among the other things thanks to the availability of reliable and up-to-date input data.

Consultants of AECOM International Development Europe SL (Spain) carried out the process of strategic noise mapping for the city of Nis in 2018 and 2019. The final version of the strategic noise map was presented in 2019.

The calculation method CNOSSOS-EU:2015 is used for the first time for the strategic noise mapping of the city of Nis. This calculation method is established by EU directive 2015/996 [5] as a common calculation method for all strategic noise maps created after January 1, 2019. Therefore, this calculation method will be used in the fourth round of strategic noise mapping in European countries.

For the development of the strategic noise maps of the city of Niš, the noise levels were calculated inside the agglomeration area of total area of approximately 91.5 km^2, with approximately 225,500 inhabitants in approximately 100,700 dwellings. Strategic noise maps have been developed for road, railway and air traffic, industry and major road (Highway A5 Niš-Dimitrovgrad).

The noise contour maps in 5 dB noise level bands for all road, railways, Niš Constantine the Great airport and IPPC industrial site (City Heating Plant) within agglomeration are presented on Serbian Environmental Protection Agency web pages (www.sepa.gov.rs). Also, the noise contour maps for combined impact of all noise sources are presented. These noise contour maps are given in Fig. 5 and Fig. 6.

The results of strategic noise mapping, the assessment of areas, dwellings and people exposed to noise; the assessment of community noise annoyance and the exceedance of noise limit values in particular areas are presented in AECOM report [6] available at Serbian Environmental Protection Agency web pages. In this report is given the number of people living in dwellings at the most exposed building

façade that are exposed to noise levels in END recommended band value.

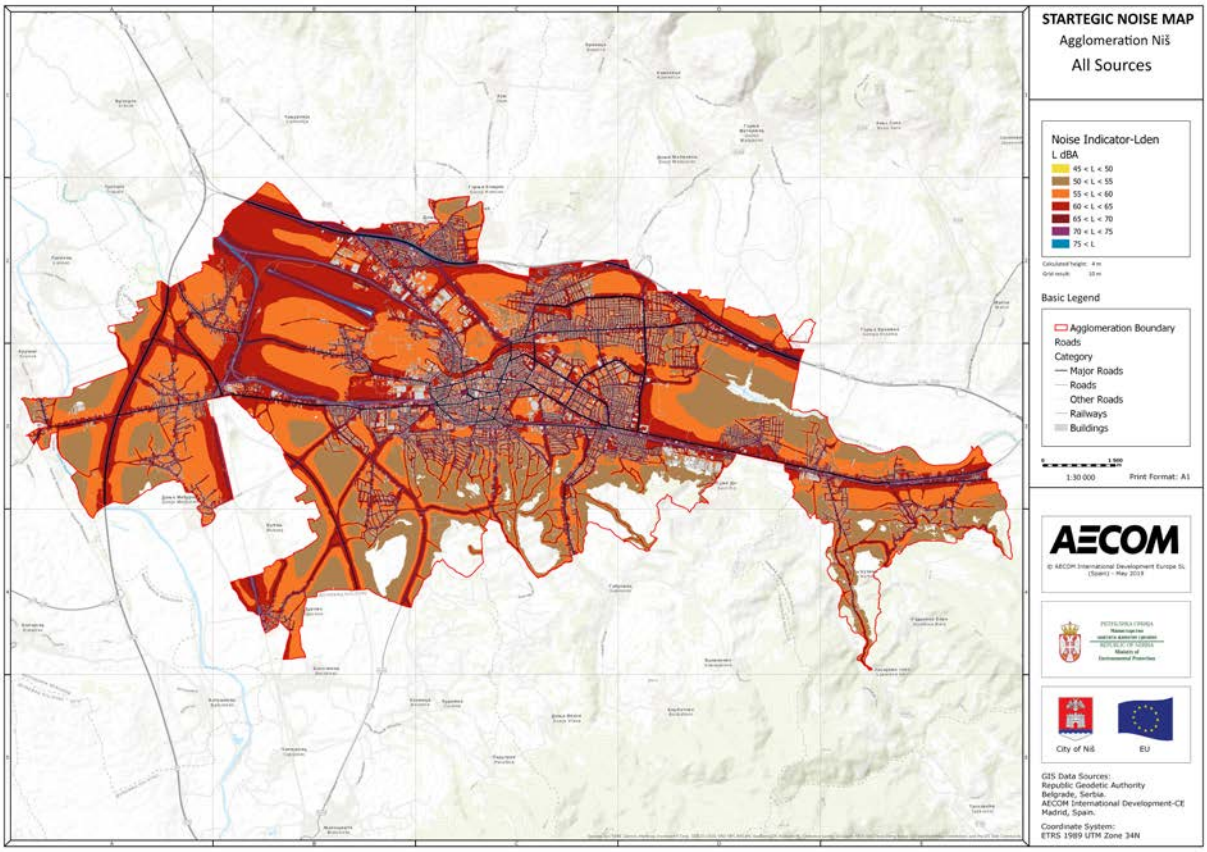

Fig. 5 *Noise contour map of the city of Niš – noise indicator L_{den} (all sources)*
www.sepa.gov.rs/slike/buka/orig300dpi/A2-21_Nis_Agglomeration_-_Combined-_Lden(300dpi)_-_EN.jpg

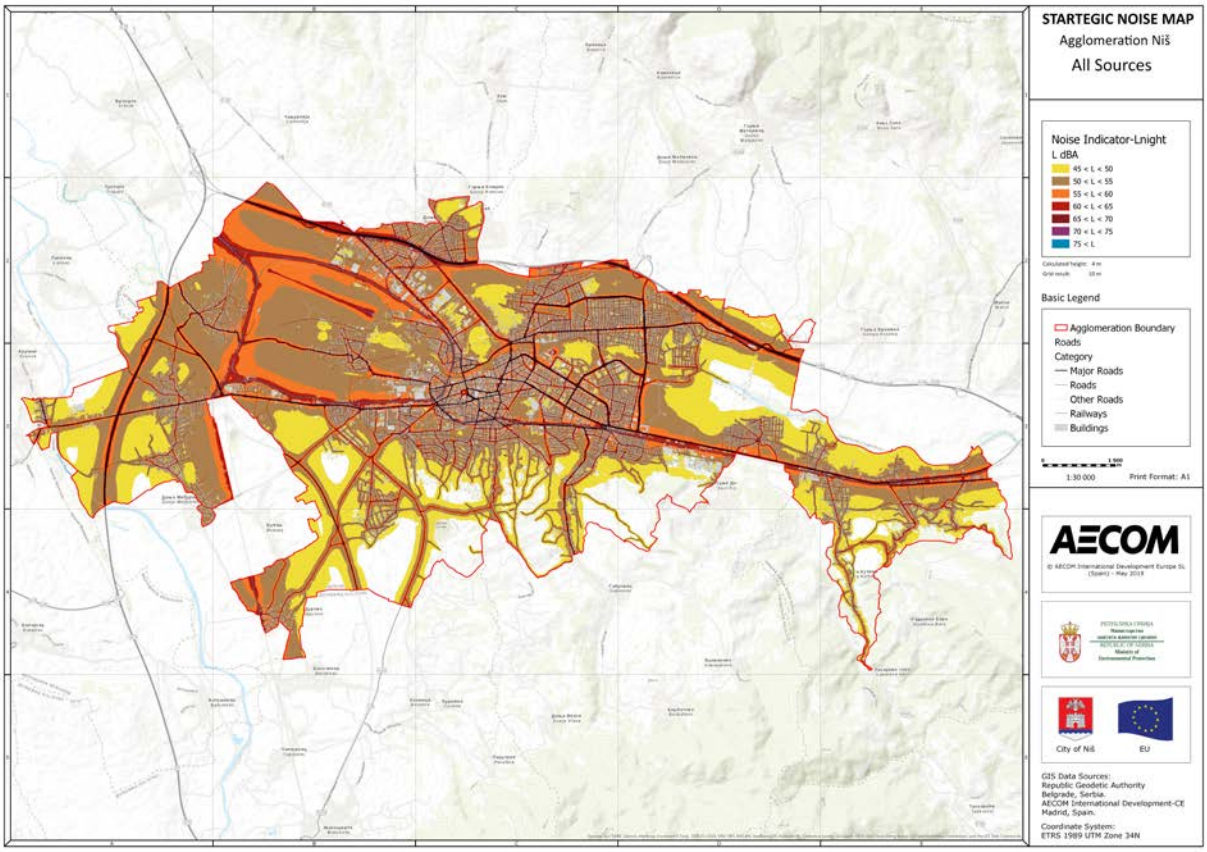

Fig. 6 *Noise contour map of the city of Niš – noise indicator L_{night} (all sources)*
www.sepa.gov.rs/slike/buka/orig300dpi/A2-21_Nis_Agglomeration_-_Combined-_Lden(300dpi)_-_EN.jpg

The estimations of population exposure to environmental noise given in AECOM report show that 198,200 are exposed to L_{den} levels of 55 dB and higher due to road traffic, 21,200 due to railway traffic, 100 due to air traffic and 300 due to industry. Therefore, 182,000 are exposed to L_{night} levels of 50 dB and higher due to road traffic, 18,000 due to rail traffic, 200 due to industry and nobody due to air traffic [5].

Number of people exposed to various L_{den} and L_{night} noise bands is shown in Fig. 7 and Fig. 8, respectively. (data source: AECOM report [5]).

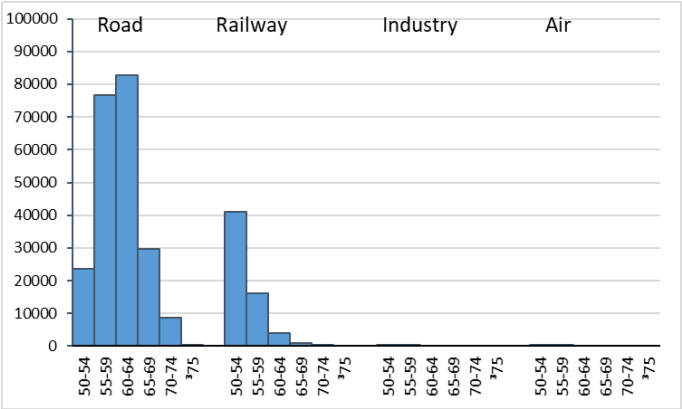

Fig. 7 *Number of people exposed to various L_{den} noise bands based on areas covered by strategic noise maps*

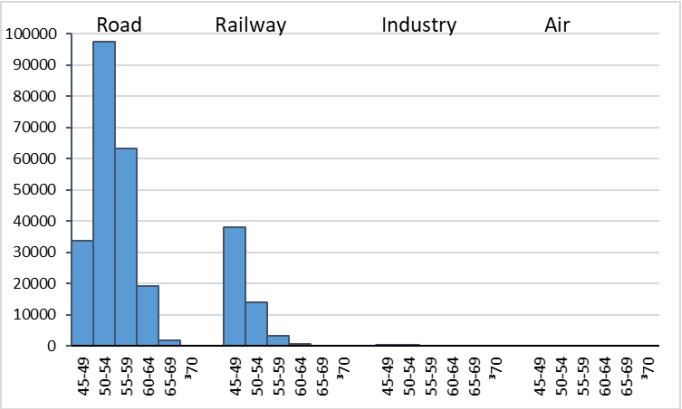

Fig. 8 *Number of people exposed to various L_{night} noise bands based on areas covered by strategic noise map*

These results show that at least 87.9% of population of the city of Niš are exposed to high L_{den} levels and more than 80.7 % of population of the city of Niš are exposed to high L_{night} levels considering road traffic noise only, from which adverse health effects can occur.

Regarding overall exposure from all sources, at least 88.6% of population of the city of Niš are exposed to high L_{den} levels and more than 80.7 % of population of the city of Niš are exposed to high L_{night} levels, from which adverse health effects can occur.

The presented results indicate that road traffic is the biggest source of environmental noise, followed by railway, air and industrial noise.

5. COMPARASION OF ENVIRONMENTAL NOISE EXPOSURE

The results of environmental noise exposure estimation for capital cities obtained after the third round of strategic noise mapping in EEA-33 countries are compared with the results of environmental noise exposure estimation in the city of Niš for road and rail traffic. Data for air traffic and IPPC industrial sites are excluded from the analysis because the exposure to noise from these sources in the city of Niš is insignificant.

The estimated percentage of people in capital EEA-33 cities exposed to road and rail traffic noise to L_{den} levels of 55 dB and higher and Lnight levels of 50 dB and higher shown in Fig. 7 and Fig. 8, respectively. Further, the figures show data for Podgorica (Montenegro) and Niš (Serbia).

Fig. 9 and Fig 10 shows the high variability in population exposure to noise due to road and rail traffic. The high variability in population noise may be results of the use of different noise level calculation method and different methodologies of strategic noise mapping (for example scope of traffic roads covered by noise model).

The third round of strategic mapping was carried out using the END recommended methods for noise level calculation or using the national methods. While for the city of Niš, the CNOSSOS method was used for the first time, which is mandatory for application from January 1, 2019.

The estimated percentage of people exposed to road traffic noise above the END threshold is highest in capital cities such as Nicosia, Vienna and Luxembourg as well as in the city of Niš. The estimated percentage of people who are exposed to road traffic noise above the END threshold in the city of Niš is significantly higher than the estimated percentage in Podgorica as a city of similar area and population.

Railway traffic is the second dominant noise source in the EEA-33 capital cities and in the city of Niš. The estimated percentage of people who are exposed to railway traffic noise above the END threshold is the highest in Bratislava, Vienna, Paris and Bucharest due to the developed network of city rail network. In Niš, a large percentage of people who are exposed to railway traffic noise above the END threshold was also identified, even though the city of Niš does not have a city rail network.

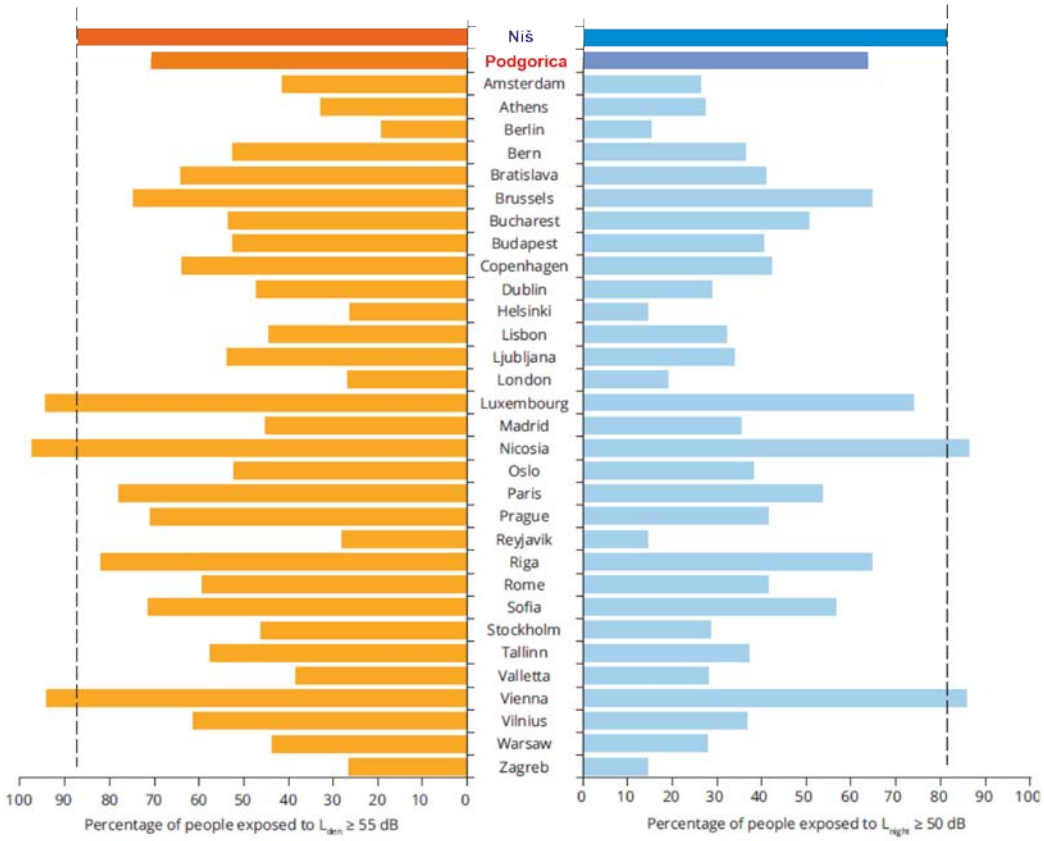

Fig. 9 *Percentage of people exposed to road traffic noise in capital cities and Niš (updated from [5] adding data for Podgorica and Niš)*

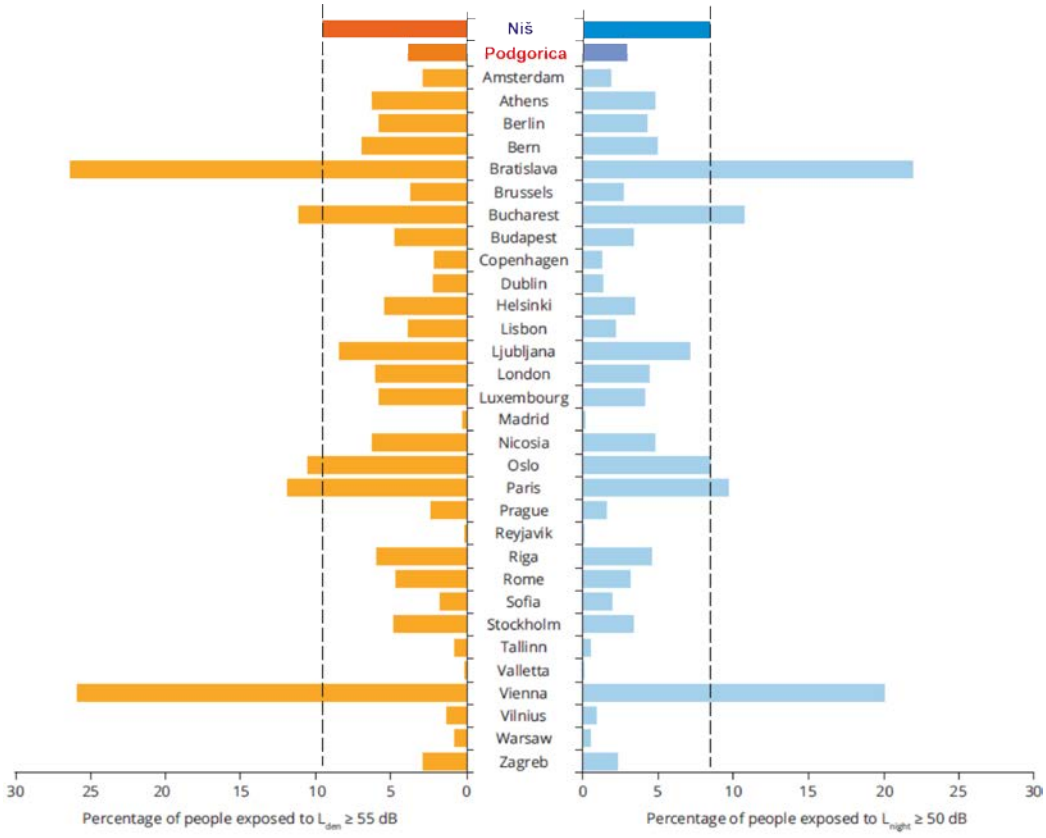

Fig. 10 *Percentage of people exposed to rail traffic noise in capital cities and Niš (updated from [5] adding data for Podgorica and Niš)*

6. CONCLUSION

The strategic noise mapping, which shows that a considerable percentage of the population is exposed to levels beyond the END thresholds for road traffic noise, highlights the importance of strategic noise mapping as a new approach to reducing harmful effects which identify and quantify to the noise problem. To tackle the noise problem, the city of Niš must very soon adopted noise action plans that will help protect people from environmental noise.

ACKNOWLEDGEMENT

The authors acknowledge the support of Ministry of Education, Science and Technology Development of Republic of Serbia to its institution through grant No. 451-03-68/2022-14/200148.

REFERENCES

[1] EU, Decision no 1386/2013/EU of the European parliament and of the council of 20 November 2013 on a General Union Environment Action Programme to 2020 'Living well, within the limits of our planet', OJ L 354, 28.12.2013, p.171-200, 2013

[2] EU, Directive 2002/49/EC of the European Parliament and of the Council of 25 June 2002 relating to the assessment and management of environmental noise (OJ L 189, 18.7.2002, p. 12-25), 2002.

[3] WHO, 2018, Environmental noise guidelines for the European region, WHO Regional Office for Europe, Copenhagen (http://www.euro.who.int/en/health-topics/environment-and-health/noise/publications/2018/environmental-noise-guidelines-forthe-european-region-2018), 2018

[4] EEA report, Environmental noise in Europe – 2020, ISBN 978-92-9480-209-5, doi:10.2800/686249, European Environment Agency, Denmark, 2020

[5] EU, Commission Directive (EU) 2015/996 of 19 May 2015 establishing common noise assessment methods according to Directive 2002/49/EC of the European Parliament and of the Council, (OJ L 168, 1.7.2015, p. 1-823), 2015.

[6] AECOM, Strategic noise map of Niš agglomeration (in Serbian), http://www.sepa.gov.rs/download/buka/Analiza_stanja_iz_podataka_strateskih_karata_Nis.pdf

University of Nis
Faculty of Occupational Safety
„Politechnica“ University of Timisoara
Faculty of Mechanical Engineering
27th International Conference
NOISE AND VIBRATION
Niš, 20 - 21. 10. 2022.

POSSIBLE DIFFERENCES IN THE CNOSSOS-EU IMPLEMENTATION BETWEEN DIFFERENT VERSIONS OF THE SAME SOFTWARE

Aleksandar Gajicki[1,2], Emir Ganić[3]

[1] PhD Student, University of Nis, Faculty of Occupational Safety, Serbia, aleksandar@gajicki.com
[2] Institute of Transportation CIP, Nemanjina 6,11000 Beograd, Serbia, aleksandar.gajicki@sicip.co.rs
[3] University of Belgrade, Faculty of Transport and Traffic Engineering, Serbia, e.ganic@sf.bg.ac.rs

Abstract – *The CNOSSOS-EU method for the determination and management of environmental noise is mandatory for use in all EU member states from 01.01.2019. The method is described and specified in Directive 2015/996/EC, however without precise guidance for its software implementation. In the paper, we compare the calculation results between two versions of the software, using the same acoustic model and CNOSSOS-EU method to see if there are any differences. The results obtained from a case study of one newly designed highway showed that the absolute difference in noise contour areas per 5 dB noise classes calculated by these two different versions of the same software was 3.49%, while the difference per one decibel was 29.7%.*

1. INTRODUCTION

Transport sector has tremendous positive impact on society, economy, as well as on employment and overall growth. Nevertheless, it comes at the price of many adverse effects on the environment, where environmental noise is considered to be one of the main negative consequences of transport. Environmental noise is defined as “unwanted or harmful outdoor sound created by human activities, including noise emitted by transport, road traffic, rail traffic, air traffic and from sites of industrial activity” [1].

At the European level, enormous efforts have been invested to address the issues of transportation noise and reduce its impact on the population. The main EU legislative instrument in relation to the environmental noise is Directive 2002/49/EC (the Environmental Noise Directive, “END”) [1]. It has been introduced 20 years ago with the aim to "achieve a common European approach to avoid, prevent or reduce the effects of exposure to environmental noise harmful for health, which includes annoyance; and to provide a basis for developing Community measures to reduce noise emitted by major sources, in particular road and rail vehicles and infrastructure, aircraft, outdoor and industrial equipment and mobile machinery“ [2]. In March 2020, the Annex III of Directive 2002/49/EC was amended by the Commission Directive (EU) 2020/367 [3], which introduced the new assessment methods for harmful effects of environmental noise.

The Environmental Noise Directive imposes the obligation for the development of strategic noise maps and noise action plans with the aim of avoiding, preventing and reducing the harmful effects of noise on public health. After 20 years of enforcement, both the implementation review and the evaluation of END have been done twice so far, addressing questions related to effectiveness, efficiency, coherence, relevance and EU added value [2]. In addition, common noise assessment methods (CNOSSOS-EU) for the determination of the noise indicators L_{den} and L_{night} have been adopted by the EC through the revision of Annex II of the END in 2015 [4-6]. CNOSSOS-EU has been developed to improve the consistency and the comparability of noise assessment results across the EU member states, providing a harmonized framework for assessment of each noise source covered by END.

Various authors analysed the differences in the results of noise modelling by comparing different software for the prediction of environmental noise [7,8]. The implementation of CNOSSOS-EU method is not clearly defined, therefore it is possible that there are differences between the software packages. The ISO/TR 17534-4:2020 provides an agreed interpretation of ambiguous aspects of the sound propagation part of CNOSSOS-EU:2015, a set of illustrative test cases along with reference solutions, and an example of a template form for the declaration of conformity for software manufacturers [9]. In addition, ISO 17534-1 describes quality requirements and measures to ensure the methodology for different quality assured software products to be able to produce the same results with an identical set of input data within a defined range of acceptable deviations [10].

The main objective of this study is to analyze the possible differences in the CNOSSOS-EU implementation between different versions of the same software using real-world case study. This paper is organised as follows. The methodology is briefly described in the Section 2, while the specifics of the case study are given in the Section 3. The obtained results are discussed in the Section 4, followed by the concluding remarks in the Section 5.

2. METHODOLOGY

For the analyses we used the same software in two different version. For the purpose of this paper, the name of a software is not relevant, so we will not list it. The „old“ version is from 2019, and the „new“ version is from 2021. Both versions are developed after 2015, when the Directive 2015/996/EC was already published.

The „new“ version has the Declaration of Conformity according to ISO 17534-1:2015, in conjunction with ISO/TR

17534-4:2019, which claims that the implementation of the calculation of sound propagation is in agreement with Section 2.5 of EU-Directive 2015/996/EU of 19 May 2015 in conjunction with the "Uniform and agreed interpretation of ambiguous definitions" of Clause 5 of ISO/TR 17534-4:2019. The „old" version does not have a Declaration.

The same acoustic model was used for the calculations. The model development for the road noise calculation was performed on the basis of the noise indicator calculation method specification (CNOSSOS-EU). The basic data required for acoustic analyses, planning of noise protection measures and road noise mapping are [11]:

- 3D Model Environment which consists of 3D surface model and 3D building heights;
- Road as noise source (carriageway centerline, technical and technological characteristics of road, traffic flow volume, traffic mix and traffic speed);
- Meteorological parameters (speed and wind frequency, average air temperature, average humidity and average atmospheric pressure), and
- Demographics data (identification of the noise sensitive objects).

Acoustic zoning was not implemented in the subject area. In order to be able to analyse noise impacts on the population and, if required, plan protection measures, it had to be assumed, in accordance with the Regulation on Noise Indicators, Limit Values, Noise Indicators Assessment Methods, Annoyance and Harmful Effects of Environmental Noise ("Official Gazette of the Republic of Serbia" No. 75/10) that the analysed corridor belonged to Zone 5 (city center, craft, trade, administrative zone with apartments, zones along highways and railways). The limit values of noise indicators for Zone 5 are as follows: L_{day} = 65 dB(A) for daylight period, $L_{evening}$ = 65 dB(A) for evening and L_{night} = 55 dB(A) for night period.

Only noise generated by road traffic was considered in calculations of noise indicators and in further analyses. Noise indicator for the night period was adopted as the parameter referent for further analysis. This decision was based on the fact that there are no measuring points, or areas where exceedances occur only in the day or evening period.

3. CASE STUDY OVERVIEW

The case study was based on the calculations for the corridor of 250 meters to the left and right from the centerline of the newly designed highway with total length of around 14.1 km.

The study area included one tunnel (approx. 270 m) and seven bridges (approx. 1100 m) on the route. The model covered an area of 7,732,982 m^2 and included 1,148 buildings. The noise indicators were calculated in a grid of 10 × 10 m and at the height of 2.25 meters above the ground. The calculations were done on a total of 77,391 grid points.

The measuring points used for the determination of noise levels on the facades of residential and other buildings were 0.5 meters in front of them. The noise indicators were calculated by using the first order of reflection, except for the measuring points on facades, where reflection from the buildings on which the measuring point is located was not considered. The analysis covered 417 noise-sensitive buildings. Table 1 shows the number of buildings and average size of household per settlement, from which the overall population affected by noise was estimated.

Table 1 *Population affected by noise per settlement*

Settlement	Number of buildings	Average size of household	Affected Population
Settlement 1	164	2.82	462
Settlement 2	126	3.05	384
Settlement 3	36	3.13	113
Settlement 4	62	3.26	202
Settlement 5	13	2.52	33
Settlement 6	16	3.40	54
Total	417	/	1,248

The noise indicators for the day, evening and night periods were calculated for 3,450 measuring points. All other input parameters for the noise calculation were exactly the same. Details of the 3D-model is shown on Fig. 1.

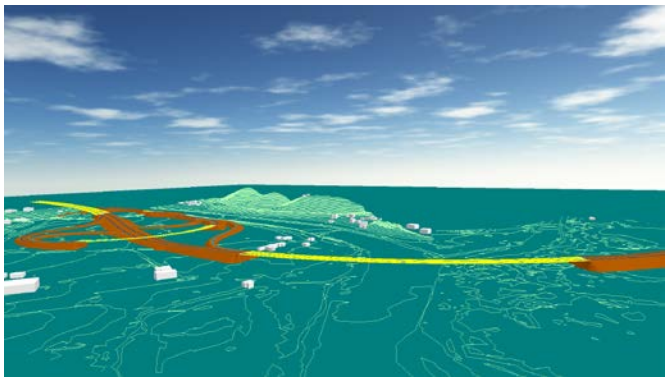

Fig. 1 *Details of the 3D model*

4. CALCULATION RESULTS

The first parameter that was calculated is the area covered by a certain noise class level. The total area included in the analysis was 7,732,982 m^2, noise classes start with 15 dB(A) and are divided into 5 dB steps. The distribution of area affected by noise class levels is shown in Table 2.

Table 2 *The distribution of area affected by noise*

Noise class	OLD Area		NEW Area		Difference (new-old)	
[dB(A)]	[m^2]	[%]	[m^2]	[%]	[m^2]	[%]
(15-20]	9491	0.12	24523	0.32	15032	0.19
(20-25]	36783	0.48	42712	0.55	5929	0.08
(25-30]	40384	0.52	26176	0.34	-14208	-0.18
(30-35]	28445	0.37	28072	0.36	-373	0.00
(35-40]	61338	0.79	73956	0.96	12618	0.16
(40-45]	324620	4.20	342899	4.43	18279	0.24
(45-50]	1371124	17.73	1281185	16.57	-89939	-1.16
(50-55]	2690588	34.79	2660192	34.40	-30396	-0.39
(55-60]	2027329	26.22	2047262	26.47	19933	0.26
(60-65]	606874	7.85	634367	8.20	27493	0.36
(65-70]	252796	3.27	283092	3.66	30296	0.39
(70-75]	283210	3.66	288546	3.73	5336	0.07
Total (absolute)	7732982	100	7732982	100	269832	3.49

There are differences in calculation results between the „old“ and the „new“ versions of software. In the column „Difference“ the minus sign indicates that the „old“ version have higher noise levels in a certain class and vice versa. The difference percentage is given in relation to the total surface area of the model.

The differences in noise coverage per 5 dB noise classes occur in an area of 269,832 m^2, which makes up 3.49% of the total surface area of the model.

The biggest differences were in the noise classes 45-50 dB(A) and 50-55 dB(A) where „old“ version covers a combined territory larger than 120,335 m^2 or 1.56% of the total area, and in the noise classes 60-65 dB(A) and 65-70 dB(A) where „new“ version covers a combined territory larger than 57,789 m^2 or 0.75% of the total area.

This difference is much more pronounced when the differences per one decibel are analysed. In such case, the positive differences occur in an area of 1,039,432 m^2 (13.4% of total), while negative differences occur in an area of 1,257,814 (16.3% of total). Therefore, the absolute difference in calculation results between the „old“ and the „new“ version of software for this case study amounts 29.7% of the total surface area of the model.

The second parameter that was calculated is the difference of noise indicators for day, evening and night periods between the "new" and the "old" versions by points of the terrain grid. Number of grid indicators per noise class is shown in Table 3.

Table 3 *Distribution of grid indicators by noise classes*

Noise class dB(A)		Lday	Levening	Lnight
> 25		30	30	30
15	20	355	355	355
10	15	115	115	115
5	10	264	264	264
4	5	318	318	318
3	4	510	511	510
2	3	601	599	600
1	2	882	884	883
0	1	27017	26999	27017
-1	0	44535	44554	44535
-2	-1	1253	1251	1253
-3	-2	525	525	525
-4	-3	345	345	345
-5	-4	207	207	207
-10	-5	396	396	396
-15	-10	29	29	29
-20	-15	9	9	9
-25	-20	0	0	0
< -25		0	0	0
Total		77,391	77,391	77,391

The absolute average difference between the „new“ and the „old“ version was 0.4 dB with standard deviation of 1.6 dB. There are 71,552 points (92.45% of total) with a difference of less than one decibel and 73,687 points with a difference of less than two decibels (95.21% of total).

Maximum calculated difference was 18.1 dB (minus sign) in the favor of the „old“ version, and 21.6 dB (plus sign) in the favor of the „new“ version.

The third parameter that was calculated is difference of noise levels on the facades of residential and other noise sensitive buildings (this refers to people dwelling and/or working in those buildings) for day, evening and night periods between the "new" and the "old" versions. The measuring points were established in the center of the facades on each of the floors. Maximum calculated difference was 13.3 dB in the favor of the „old“ version, and 9.7 dB in the favor of the „new“ version. The number of facade indicators per noise class is shown in Table 4.

Table 4 *Distribution of facade indicators by noise classes*

Noise class dB(A)	dB(A)	Lday	Levening	Lnight
10	9	1	1	1
9	8	3	3	3
8	7	3	3	3
7	6	6	6	6
6	5	18	18	18
5	4	24	24	24
4	3	29	29	29
3	2	34	34	34
2	1	76	76	76
1	0	591	592	591
0	-1	1857	1854	1855
-1	-2	320	322	322
-2	-3	139	139	139
-3	-4	87	87	87
-4	-5	66	66	66
-5	-6	60	60	60
-6	-7	38	38	38
-7	-8	32	32	32
-8	-9	25	25	25
-9	-10	12	12	12
-10	-11	14	14	14
-11	-12	8	8	8
-12	-13	4	4	4
-13	-14	3	3	3
Total		3450	3450	3450

There are 2,448 points (70.96 % of total) with a difference of less than one decibel. The average difference between the „new“ and the „old“ version was -0.8 dB with standard deviation of 2.2 dB. This parameter is essential because noise protection measures are planned based on the same. The result shows that the "new" version has lower calculated facade levels resulting in less noise protection measures being required.

Table 5 shows the number of people affected by noise per different noise classes for day, evening, and night periods. This estimation was done based on the maximum noise levels on a facade for each building. The calculated noise maps for the night period are shown graphically in Fig. 2a for the "old" version of the software and in Fig. 2b for the "new" one. The noise maps with the noise levels differences between the "new" and the "old" software version for the night period are shown in Fig. 3. Fig. 3a shows difference in levels where the "new" version has higher calculated noise levels compared to the "old" one (positive values), while the Fig. 3b shows difference in levels where the "old" version has higher calculated noise levels compared to the "new" one (negative values).

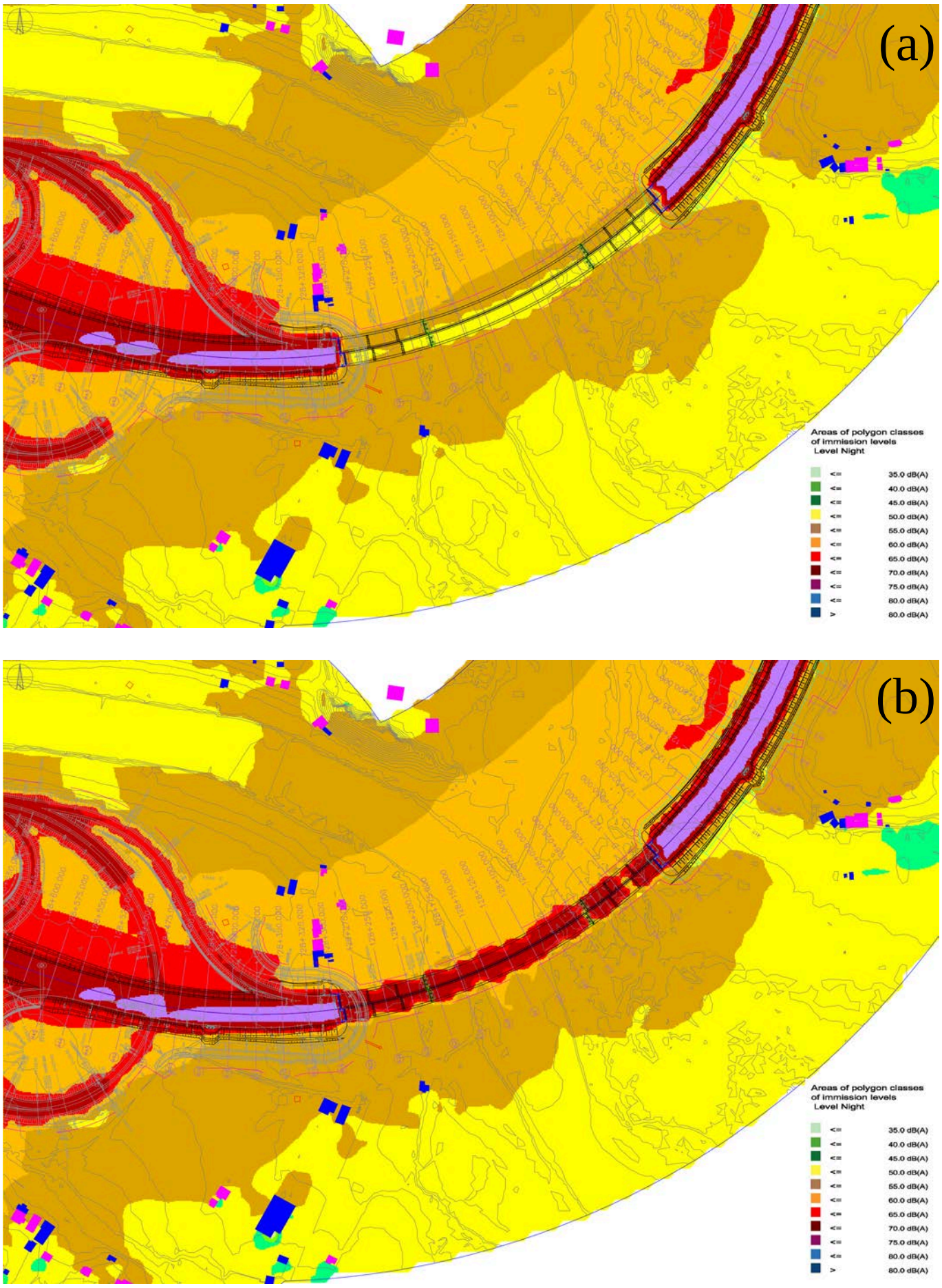

Fig. 2 *Noise maps calculated by two versions of the software (a) old version; (b) new version*

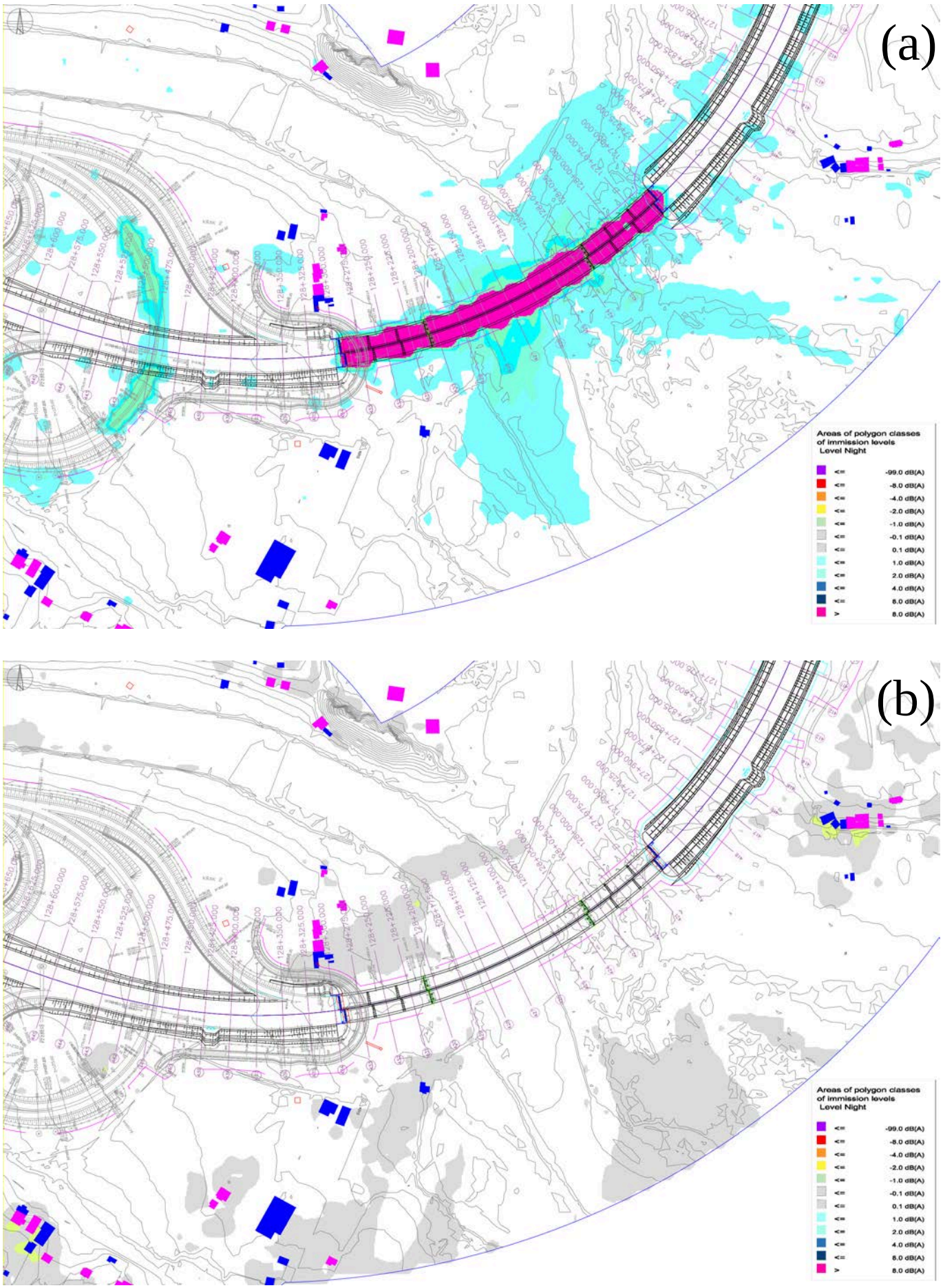

Fig. 3 *Differences between noise maps calculated by new and old versions of the software, (a) positive difference; (b) negative difference*

Table 5 *The distribution of population affected by noise*

Noise class	L_{day}			$L_{evening}$			L_{night}		
	Old	New	Difference (new-old)	Old	New	Difference (new-old)	Old	New	Difference (new-old)
[dB(A)]	[Num]	[Num]	[%]	[Num]	[Num]	[%]	[Num]	[Num]	[%]
(15-20]	0	0	0.0	0	0	0.0	0	0	0.0
(20-25]	0	0	0.0	0	0	0.0	0	0	0.0
(25-30]	0	0	0.0	0	0	0.0	0	0	0.0
(30-35]	0	0	0.0	0	0	0.0	0	3	0.3
(35-40]	0	0	0.0	0	3	0.3	3	3	0.0
(40-45]	3	7	0.3	3	6	0.2	28	55	2.2
(45-50]	25	49	1.9	40	59	1.5	274	236	-3.1
(50-55]	241	211	-2.4	306	289	-1.3	558	554	-0.4
(55-60]	563	563	-0.1	576	562	-1.1	328	340	1.0
(60-65]	353	353	0.0	284	281	-0.2	53	53	0.0
(65-70]	59	62	0.2	35	44	0.7	3	3	0.0
(70-75]	3	3	0.0	3	3	0.0	0	0	0.0
Total (abs.)	1248	1248	4.9	1248	1248	5.4	1248	1248	6.9

5. CONCLUSION

Calculations results show that there are differences in CNOSSOS-EU method implementation between the „old“ and the „new“ software version. The difference is particularly noticeable in facade noise indicators, which may lead to differences in the required protection measures for the same acoustic model and the same input parameters. These are all preliminary results and conclusions. It is necessary to conduct more detailed analyses in order to get the final conclusions about this issue. At this stage of research it is certainly recommended to use the latest version of the software, or at least version with Declaration of Conformity according to ISO 17534-1:2015.

REFERENCES

[1] European Commission , “Directive 2002/49/EC of the European parliament and the Council of 25 June 2002 relating to the assessment and management of environmental noise,” *Official Journal of the European Communities*, vol. 189, no. 12. pp. 12–25, 2002.

[2] European Commission, “Evaluation of Directive 2002/49/EC relating to the assessment and management of environmental noise. Executive Summary,” Brussels, Belgium, 2016.

[3] European Commission, “Commission Directive (EU) 2020/367 of 4 March 2020 amending Annex III to Directive 2002/49/EC of the European Parliament and of the Council as regards the establishment of assessment methods for harmful effects of environmental noise,” *Official Journal of the European Union L 67/132*, 2020.

[4] European Commission, “Commission Directive (EU) 2015/996 of 19 May 2015 establishing common noise assessment methods according to Directive 2002/49/EC of the European Parliament and of the Council,” *Official Journal of the European Union*, 2015.

[5] J.L.B. Coelho, K. Vogiatzis, G. Licitra, “The CNOSSOS-EU initiative: A framework for road, railway, aircraft and industrial noise modelling for strategic noise mapping in EU Member States,” in *18th International Congress on Sound and Vibration 2011, ICSV 2011*, 2011, pp. 789–795.

[6] S. Kephalopoulos and M. Paviotti, “Common Noise Assessment Methods for Europe (Cnossos-Eu): Implementation Challenges in the Context of Eu Noise Policy Developments and Future Perspectives,” in *The 23rd International Congress on Sound and Vibration*, 2016, July.

[7] M. Arana, R. San Martin, M. L. San Martin, and E. Aramendía, “Strategic noise map of a major road carried out with two environmental prediction software packages,” *Environmental Monitoring and Assessment*, vol. 163, no. 1–4, pp. 503–513, Apr. 2010, doi: 10.1007/s10661-009-0853-5.

[8] H. Puckeridge, T. Braunstein, and C. Weber, “Comparison of rail noise modelling with CadnaA & SoundPLAN,” in *Acoustics 2019, Sound Decisions: Moving Forward with Acoustics - Proc. of the Annual Conference of the Australian Acoustical Society*, 2019.

[9] International Organization for Standardization, *ISO/TR 17534-4:2020 Acoustics — Software for the calculation of sound outdoors — Part 4: Recommendations for a quality assured implementation of the COMMISSION DIRECTIVE (EU) 2015/996 in software according to ISO 17534-1*. 2020.

[10] International Organization for Standardization, *ISO 17534-1:2015(en) Acoustics — Software for the calculation of sound outdoors — Part 1: Quality requirements and quality assurance*. 2015.

[11] A. Gajicki, V. Babić, M. Prašćević, and D. Mihajlov, “Strategic noise maps for major roads – the first results in Serbia,” *FACTA UNIVERSITATIS, Series: Working and Living Environmental Protection*, vol. 12, no. 1, pp. 17–27, 2015.

University of Nis
Faculty of Occupational Safety
„Politechnica“ University of Timisoara
Faculty of Mechanical Engineering
27th International Conference
NOISE AND VIBRATION
Niš, 20 - 21. 10. 2022.

REALIZATION OF THE REAL-TIME LOW-COST NOISE MONITORING SYSTEM BASED ON RASPBERRY PI

Marko Ličanin[1], Momir Praščević[2], Darko Mihajlov[3]

[1] University of Nis, Faculty of Occupational Safety, Serbia, marko.licanin@znrfak.ni.ac.rs
[2] University of Nis, Faculty of Occupational Safety, Serbia, momir.prascevic@znrfak.ni.ac.rs
[3] University of Nis, Faculty of Occupational Safety, Serbia, darko.mihajlov@znrfak.ni.ac.rs

Abstract - *Noise monitoring is an integral part of modern city environmental urban planning and improvement of the wellbeing of the human population. Modern noise monitoring stations of the sufficient measurement precision and sensitivity class are quite expensive, meaning that only several points in the cities are usually assessed at the same time, reducing the resolution of the noise assessment. Since noise is a variable category, question arises is it possible to increase the number of measurement position without significantly increasing the cost of the noise monitoring. This paper addresses this issue by introducing a model of the low-cost noise monitoring system that could be deployed at many locations in the city and perform noise monitoring in much dense resolution. A solution based on the Raspberry Pi has been proposed, data processing, software and hardware components are presented.*

1. INTRODUCTION

There are several projects and attempts to create a noise monitoring system that can enable assessment of the noise in the urban area in higher resolution [1]. Each of these systems have different architecture and differ in the number and quality of noise parameters, as well as implemented acquisition of data. Although these systems are not of the highest precision, by deploying a large number of sensors or remote low-cost noise stations throughout the city, a much better overview of the noise change can be observer in opposed to having only few measurement locations with high-end measurement equipment [2,3]. System proposed in this paper is composed of separate sub-systems that communicates through web protocols and enables almost realtime data acquisition, processing and viewing [4]. These sub-systems are:

- Raspberry Pi as a Single Board Computer (SBC) that represent the main acquisition unit of the monitoring station;
- Data Server that handles data flow from the monitoring station to the remote PC;
- Backend Server that performs database ques;
- Frontend Server where Graphical User Interface (GUI) is implemented. Here, data change can be viewed on the dashboard.

Workflow of these systems has been explained and schematics presented.

2. HARDWARE

In the past decade SBCs such as Raspberry Pi (RPi) has gained a high popularity in many electronic projects. From the hobby enthusiast who used them in the small projects in the past, SBCs have paved the way into large industrial projects with very serious applications. Their hardware capabilities have developed significantly, bringing them very close to full size PCs with a size form factor of a credit card [5].

Hardware that has been used in this project is composed of RPi 4B as the main noise acquisition unit, Arduino microcontroller that handles other types of sensors (such as weather data), Micro-Electro-Mechanical Microphone (MEMS) in the 3D printed enclosure and PC that runs servers for data flow, storage and web services.

2.1 Microphone

MEMS microphones are getting better with each technology iteration. Their frequency response becomes reasonably flat in the range between 100 Hz and 10 kHz, which is for the most environment noise applications sufficient enough. Microphone used in this application is I^2S InvenSense INMP441 digital interface that outputs Pulse Code Modulation (PMC) data format, when fed the appropriate control signals. This sensor can measure noise levels between 30 dB and 120 dB, which is also sufficient for the outdoor noise monitoring. Below 30 dB digital self-noise is high and measurements are not valid [6].

MEMS microphone is connected to the RPi, where Python script is running and serving as a data driver. In order to protect the microphone an enclosure has been designed in SolidWorks and created using 3D printer. This can be seen in Fig 1. Printed model consists of two parts, first being the capsule that is fitted with a circular MEMS circuit board containing data pins, while the second part is intended for the microphone cable. This way, electronics is protected from the influence of the heat and moisture that will be present while monitoring station is placed outdoor for a longer period of time.

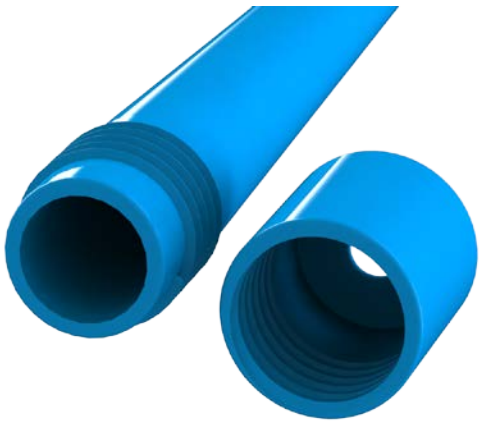

Fig. 1 *Microphone enclosure designed in SolidWorks for 3D printing*

2.2 Raspberry pi

In opposed to standard PCs, SBCs have dedicated ports (General Purpose Input Output – GPIO pins) that can be programmed according to the need of the designer, outputting the different form of signals, voltages and data. This has made them very close to the capabilities of microcontrollers that has been used in industry much longer, but having much greater processing power and peripherals. For instance, latest Raspberry pi 4 B features 8 GB of LPDDR4 RAM, Quad Core Cortex-A72 ARM 64-bit processor, 5 GHz wireless, Bluetooth 5.0, USB 3.0 Ports, two HDMI outputs and 40 pin GIPO header [5].

MEMS microphone is connected to the RPi where Python script is running (Fig. 2).

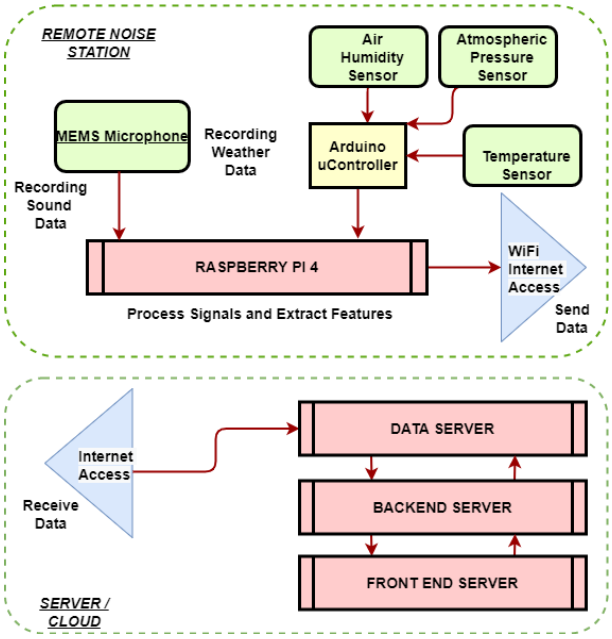

Fig. 2 *Schematic of the noise station sub-system and its components*

Through USB port, RPi is connected to Arduino microcontroller which handles the air humidity, atmospheric and temperature sensors. This can be further expanded with other types of sensors, such as for flammable gasses, air quality and similar [7].

When monitoring station starts running, it connects to the data streaming server through socket protocol and becomes ready to stream data. Python script then collects all the data and sends it to the server in the 1s interval.

3. SOFTWARE

Several programing languages and technologies has been used to implement the software part of the noise monitoring system. Noise monitoring station is realized on RPi and all of the processing has been done in Python programming language. Python is very suitable for the variety of applications, as it contains large pool of useful libraries that speed up the development process, ranging from communication with peripheral on a hardware level, up to the web development. Data streaming server and backend server are also realized in Python, where the latter uses a specialized Python framework called Django, which enables very fast and structured backend programing and database handling. Frontend server is realized in JavaScript framework called React that enables fast and efficient update of the data on web page.

Data is sent from the monitoring station to the data streaming server that stores the data into Postgree database. Frontend server where webpage dashboard is realized, performs requests through API (Application Programming interface Interface). Once the request is received by backend, it reads the appropriate data from database and serves the data response back to the frontend, which then updates the dashboard.

3.1 Data streaming

Pythons samples the data from MEMS at 48 kHz per second and send it to the buffer of 1 s data. This buffer is then transformed to the frequency domain using Fast Fourier Transform (FFT). Following the FFT, there is a brick wall filter implemented using parallel processing libraries in Python. This filter separates data into 1/3 octave bands, where each parallel process handles processing of a single band. This way, overall processing speed is significantly increased and data loss is avoided if next batch of samples arrives to the buffer before previous is being processed. Each of the 1/3 octave band data is A-weighted and Sound Pressure Level (SPL) is being calculated. Data from each band is then combined into a single data array and broad band 1s equivalent SPL calculated $L_{\mathrm{Aeq,1s}}$. Python script that sends a request to the Arduino which collects data from sensors, pack data into suitable format and returns the weather data to the RPi. Script than combines the weather data, 1/3 octave band data and broad band SPL data into single data stream which is then packed into appropriate binary format ready to be sent through the internet via socket protocol. Assuming that monitoring station is connected to the data streaming server, it sends the 1 s processed data to the server that handles it further. Then scripts take another raw data set from buffer and entire process repeats indefinitely. This process can be observed in Fig. 3.

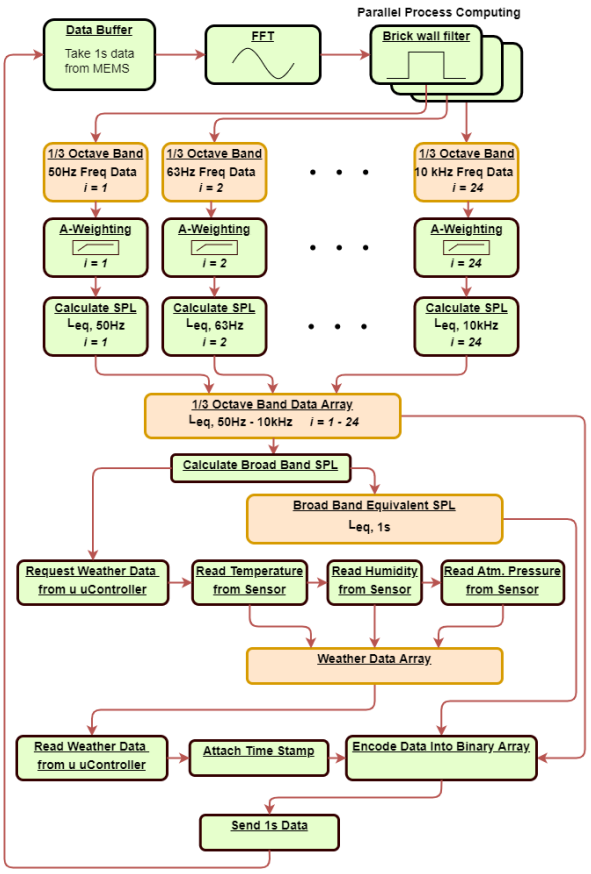

Fig. 3 *Schematic of the data streaming sub-system*

3.2 Backend and database

Software part for the backend sub-system is realized on the PC and it is implemented as Python Django technology [8]. It offers a structured way of handling data and serves it to the web client. First part of the Python script runs independently from Django server. It connects to the remote noise stations and receive data at the interval of 1 s. For the purpose of proof of concept, only one station is connecting to the data stream server, but intention is that it could handle the data from the large number of stations. These data are the decoded a written into Postgree SQL database that runs on it owns server.

On the Django backend server, there is a written API protocol that waits for the web client request. For now, there are two APIs written. First is used to fetch the 1s processed data, while second is used to obtain the data in bulk, typically used for presenting the noise change over time. For this purpose, it is set to the 200 database entries, but in the future, it can be programmed to fetch amount of data that can be specified at the client side and sent together with the API request. Once the request has been made, Django backend server creates the que and retrieve the data from the database. Then it creates the response and sends data to the web client from which request has been made.

In the future, once the system is further developed and improved, more API protocols will be written to manage different statistics. This is particularly important for environmental noise indicators for day, evening, night and 24 hrs noise disturbance (L_{day}, $L_{evening}$, L_{night} and L_{den}), where data is obtained from the accumulated data set in the database [9]. Some of the future work might include the realization of the mathematical or machine learning methods that will be able to predict the noise distribution and noise levels based on the available data. Once having a multiple monitoring station deployed throughout the city, it would be possible to create a dynamic noise map that will address the noise problems in much more details. This would also require building a more complex database structure with que optimization that could fetch the data at the same tame from multiple data tables and for Django to combine them into single complex data response to the web client. Work flow of the backend and database sub-system can be seen in Fig. 4

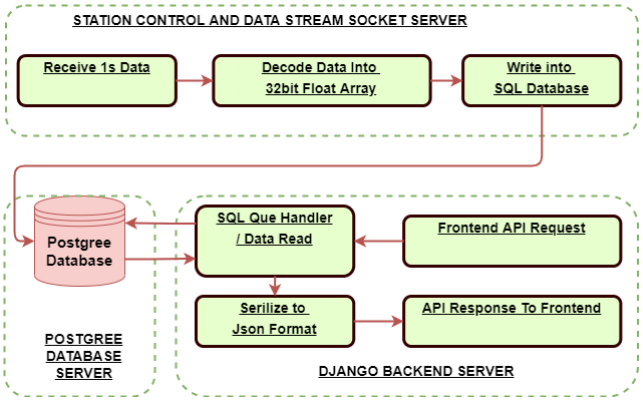

Fig. 4 *Schematic of the backend sub-system*

3.3 Frontend

Software of the frontend is realized on PC and it is implemented as the JavaScript React framework [10]. This is a very useful and advance technology for creating dynamic dashboards that have high refresh rate of the data. Problem with web client is that they tend to refresh entire web page once the data that is being viewed changes. This results in a slow responsive web presentation that is unable to handle the data change. This is particularly observable in dashboards where there is a lot of graphical data. It is where React shines, as it updates only JavaScript elements that are being changed, while the rest of the webpage remains static.

React is composed of the so-called components. Each graphical elements represent one component, that is furthermore separated into elements. Typical example of the element is a needle on the gauge graphic element, or a spline on time domain data. These elements will change with every data update, while the rest of the graphical element (axes, legend, background) does not refresh.

Components that are realized on the dashboard are 1/3 octave band frequency graph, instantaneous values of SPL gauge graphs ($L_{min,1s}$, $L_{max,1s}$, $L_{Aeq,1s}$, $L_{Aeq,1min}$), time range data and weather data. In the React, an API requests has been written with the time defined request occurring at 1s interval. In the future, request can be programmed to accept the user defined time intervals which will improve flexibility of the dashboard.

At the first load of the webpage, all components are set to the default values. API request then start calling the backend Django server that retrieves the data from the database and React received it in the form of API response. Once received, data are structured into JSON format, separated for each of the React components and component element is updated.

This process then repeats indefinitely as long as the webpage is loaded into web browser.

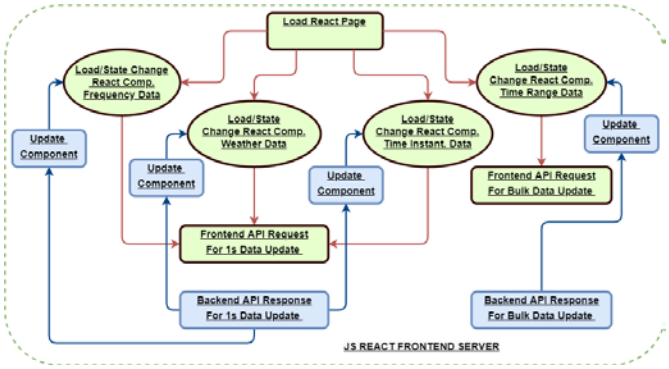

Fig. 5 *Schematic of the frontend sub-system*

4. CONCLUSION

Noise monitoring process is expensive and to be able to performing it on a large scale throughout the city, large number of the high-end equipment is required. This, in most cases, is not financially viable. There are several attempts to create the low-cost solutions that would increase the monitoring locations, decreasing the cost and improving the resolution of the measured data. This paper proposes a system that contains the design of the low-cost monitoring station based on the RPi and a web server to handle the data storage and graphical representation. In that context, data streaming server based on Python, backend server based on Python Django, Postgree database server and frontend server based on JavaScript React have been realized.

Frontend framework is implemented on the same PC machine as the backend, streaming and database servers. For the purpose of the proof of concept, all of these servers work seamlessly. In reality, if the system is deployed as a complete bug proof solution, these servers should run on separate machines, preferably on a rented cloud servers that have enough processing power to serve thousands of requests per second. Besides that, there are modern technologies and frameworks such as Docker and Kubernetes that operates through subscription plan and enables scaling of the system, so if the number of request increases, other clones and machines takes over the request load.

Future plan of the work is to increase the dashboard capability by adding advance statistics and noise prediction sections. This will include writing more complex React components, user interaction with the graphs, complex API request, but also corresponding backend routines to handle all of the frontend demands. Data streaming sub-system will be enhanced to serve the multiple monitoring stations and perform the adequate fast data handling. All of the servers will be moved on the rented cloud-based machines that can handle large number of requests.

ACKNOWLEDGEMENT

The authors acknowledge the support of Ministry of Education, Science and Technology Development of Republic of Serbia to its institution through grant No. 451-03-68/2022-14/200148.

REFERENCES

[1] C. Asensio, "Acoustic in smart cities", *in Proc. Applied Acoustic, Volume 117, Part B*, February 2017, pp. 191-192

[2] P. Belluci, L. Peruzzi, and G. Zambon, "Life dyna map project: The case study of Rome", *in Proc. Applied Acoustic, Volume 117, Part B*, February 2017, pp. 193-206.

[3] C. Mydlarz, J. Salamon, and J.P. Bello, "The implementation of low-cost urban acoustic monitoring devices", *in Proc. Applied Acoustic, Volume 117, Part B*, February 2017, pp. 207-218.

[4] M. Ličanin, M. Praščević, D. Mihajlov, "Realization of the low-cost noise measurement monitoring station using MEMS microphone technology and micro PC", *in Proc. of 26th International Conference: Noise and Vibration, pp. 133-136, Faculty of occupational safety*, Niš, December 06-07 2018,

[5] https://www.raspberrypi.com/products/raspberry-pi-4-model-b/specifications/

[6] https://invensense.tdk.com/products/digital/inmp441/

[7] https://www.arduino.cc/

[8] https://www.djangoproject.com/

[9] D. Mihajlov, M. Praščević M. "Permanent and Semi-permanent Road Traffic Noise Monitoring in the City of Nis (Serbia)", *Journal of Low Frequency Noise, Vibration and Active Control 34(3): 251-268.* 2015.

[10] https://reactjs.org/

University of Nis
Faculty of Occupational Safety
„Politechnica“ University of Timisoara
Faculty of Mechanical Engineering
27th International Conference
NOISE AND VIBRATION
Niš, 20 - 21. 10. 2022.

THE EFFECT OF NOISE AND TEMPERATURE ON THE STRESS OF AGRICULTURAL TRACTOR OPERATORS

Mihaela Picu[1]

[1] "Dunarea de Jos" University of Galati, Romania, mihaela.picu@ugal.ro

Abstract - *This paper studies the effect of noise on tractor operators. Two tractors were used in the experiments: one from 1993 (U650) and one from 2013. The noise level was measured with the Blue Solo sound level meter (01dB-Metravib). Noise analysis was done by two methods. Method I: With «Noise exposure ready-reckoners» that allow to estimate the daily or weekly noise exposure. Method II: Noise was analyzed with dBTRAIT, a powerful software dedicated to post-processing sound data. The analysis consists in obtaining sonograms that are graphical representations of a complex sound over a certain period of time. In the case of subjects operating the old tractor, the average of Daily noise exposure is 98 dB, higher than the lower exposure action value by 18dB and higher than the upper exposure action value by 13 dB, and the average of Exposure points is 2144.667 (62 times as high as the lower exposure action value). In the case of subjects driving the new tractor, the average of Daily noise exposure is 79 dB, lower than the lower exposure action value by 1 dB and higher than the upper exposure action value by 1 dB, and the average of Exposure points is 23.666 (lower than the lower exposure action value by 8.333 points). The reaction of the subjects to the noise pollution caused by the operation of the tractors was also analyzed using the Likert scale.*

1. INTRODUCTION

Maintaining the health of workers, but also increasing productivity are only possible in an environment that ensures the best working conditions.

The stressors that frequently intervene in a difficult workplace, exposing workers to a high degree of danger to their safety are: environment with very high temperature, environment with very loud noise, environment with high vibrations, etc. [1]. These can lead to reduced power of concentration, failure to achieve work-related tasks at optimal parameters and can even cause work accidents.

Hancock in 1989 [2] created a model of how stress influences the physiological and psychological abilities of workers (Fig. 1).

Psychologists Robert M. Yerkes and John D. Dodson [4] discovered an empirical relation between pressure and performance: performance increases in proportion to physiological or mental arousal, but only up to a point. When the excitation levels become too high, the performance decreases (Fig. 2). The process is represented by a bell-shaped curve that exhibits an upper trend, followed by a downward one, corresponding to higher levels of excitation.

It has been found that the human brain can "introduce inherent limitations in information processing." There are “a number of suboptimal neurocognitive states of deteriorated performance that are predictive, such as: inattention, decreased effort and perseverance, blindness, and deafness caused by inattention (Fig. 3).

Commitment to a task is defined as a cognitive effort to serve the goals of the task [6-8], while arousal is a state of physiological readiness to respond to tasks [9].

A paper in 1992 [11] studies the effect of noise on tractor operators: studies on human sensitivity to noise [L_{eq} = 55 dB(A) and 75dB(A)] were conducted in the laboratory on 45 subjects in which the following were analyzed: psychological functions: Short-Term Memory, Search and Memory (vigilance), Hidden Figures (spatial reasoning) and Mental Arithmetic (parallel processing).

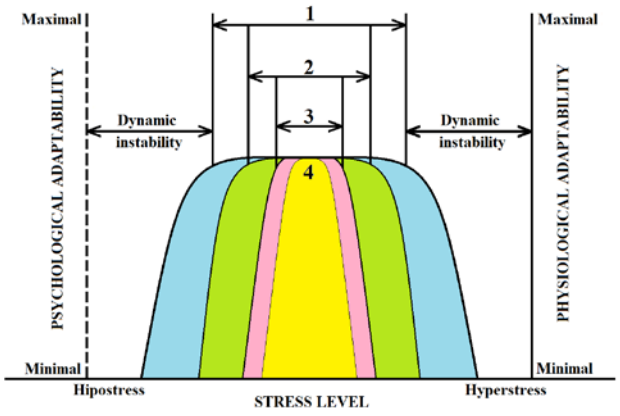

Fig. 1 *Physiological adaptation capacity (solid lines) and psychological adaptation capacity (outer dashed lines: equated with attentional resources capacity) as functions of the stress level. Embedded in these zones is a region (3-pink) of comfort sought by the active operator. A central normative zone (4-yellow) describes a region in which compensatory action is minimized, as environmental input is insufficient to elicit appreciable dynamic response. In areas of maximum adaptability (2-green-zone of maximum psychological adaptability and 1-blue-zone of maximum physiological adaptability), negative feedback predominates. Beyond the stable limits, positive feedback induces a dynamic instability that leads to the breakdown of the adaptive response and, ultimately, to functional failure. According to Hancock and Warm [3]*

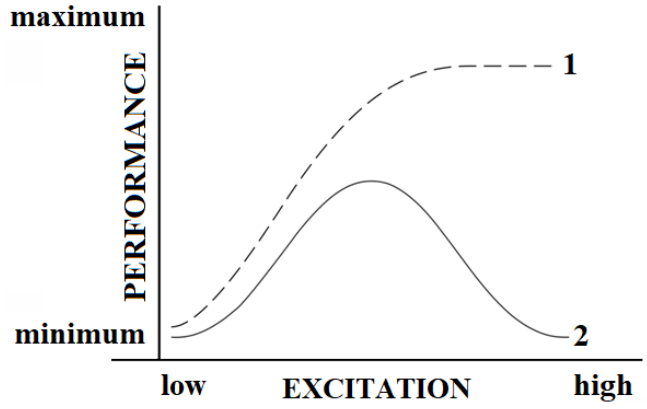

a) Yerkes-Dodson's original law [5]: 1) Simple task; focused attention, flash memory, fear conditioning; 2) Difficult task Impairing divided attention, working memory, decision making and multitasking

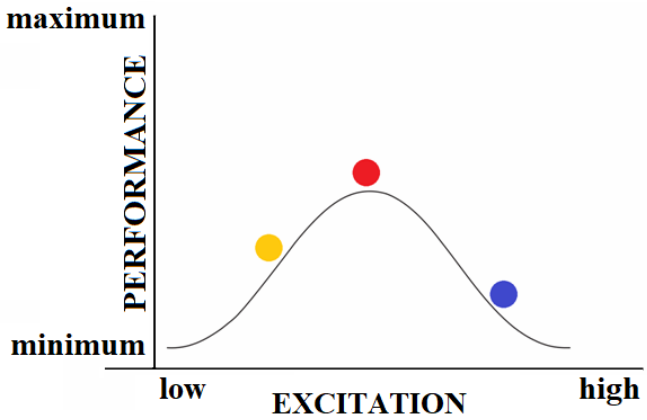

b) Yerkes-Dodson bell curve: (●) - Increasing attention and interest; (●) - Maximum excitation and performance; (●) - Performance impairment caused by maximum anxiety

Fig. 2 *Yerkes-Dodson law (According to Yerkes–Dodson law wikipedia [5])*

The results showed that the performance of solving the tests was lower in a noisy environment. A number of deviations in behavior could also be noticed (some of the subjects showed frustration or even anger).

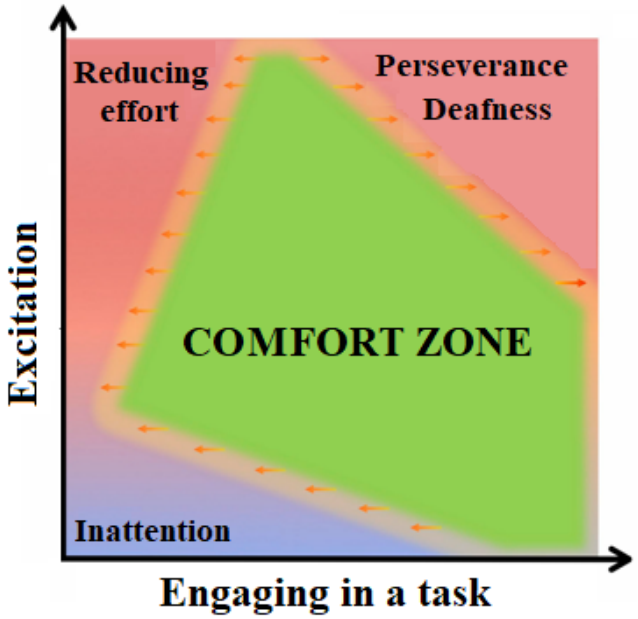

Fig. 3 *Performance, excitation and involvement in the task: the green area conceptually describes the "comfort zone" of the operator where the performance is optimal. Deteriorated mental states are represented by a "task involvement" axis and an "arousal" axis. Interestingly, this view makes it possible to link the notion of deteriorated commitment and behavior in a straightforward way. (According to Dehais et al. 2020 [10])*

Waye K. Persson et al., in 1997 [12] studied the effect of low-frequency noise from two ventilators on subjects undergoing cognitive tests. The results led to the conclusion that the subjects displayed a lower social orientation than they would if there was no noise; in addition, the response time to the questionnaires was longer in the case of exposure to low frequency noise.

Noise is also a factor that negatively affects the quality of the workers' activity; it alters people's performance in carrying out complex tasks, changes social behavior, and causes irritation [13]. Studies of people exposed to noise at work and in the environment also suggest an association with high blood pressure [14].

Noise, although overlapping with other sources of stress, has multiple specific effects on people in the occupational environment. Researchers Szalma and Hancock [15] conducted specific tests to quantify these effects, and the results were consistent with the theory of maximum adaptability, which postulates that, in order to avoid this stress, additional mental resources were consumed. At the same time, the quality of the performance visibly decreased. The effects of noise have been intensively studied by Picu M., Picu L. and Rusu E. in 2019 [16]; they are a psychological trigger for those on therapy: sleep disturbance, decreased heart rate, changes in the immune system, anxiety, discontentment, mood swings, increased cortisol production, hypertension, myocardial infarction, vasoconstriction, increased blood pressure, increased adrenalin levels .

In addition to this stressor, tractor operators are also subject to:

→ vibrations; The negative effect of vibrations transmitted by moving equipment on operators has been studied by many researchers [17-28].

→ humidity; the air quality in a work environment is particularly important. In addition to the ambient temperature, humidity is a decisive factor responsible for the work performance of workers. A number of studies have been conducted, showing that there is a marked decrease in subjects' attention, memory, reaction time, and comfort associated with increasing humidity [29-32].

→ dust; in agriculture, "the physical, physico-chemical and chemical properties of dust largely determine the nature of its toxic, irritating and fibrogenic effects on the human body. The main role in the nature of the general toxic and specific action of dust is played not only by its concentration in the working area air or atmospheric air, but also by the density and shape of dust particles, its adsorption properties, dust solubility and electrocharge [33].

→ extreme temperatures; In this regard, Ramsey et al., [34] analyzed the behavior of workers in two industrial plants over a period of 14 months. It was found that temperatures lower or higher than normal for most people had a negative impact on worker safety behavior, ie several unsafe patterns of behavior were observed at work. Extreme temperatures affect: the nervous system (migraines, altered consciousness, convulsions, coma); heart rate (increased heart rate, nosebleeds, high risk of heart attack); renal system (lack of blood and oxygen flow to the kidneys, poor urination, kidney blockage); intestine (nausea, vomiting, damage to certain sections of the intestine); skin (stopping perspiration, skin hot to the touch); circulatory system (small blood clots form in vessels, oxygenated blood no longer reaches the vital organs); muscle system (cramps caused by dehydration), involuntary spasms, deteriorated overall function).

The effects of noise on human health and productivity, as well as on the levels of stress experienced by agricultural tractor operators have been studied extensively [11, 14-16, 20-27, 35-47].

2. MATERIALS AND METHODS

The determinations took place in the Brăila Plain (Fig. 4) which is located N-E of the Bărăgan Plain in southeastern Romania; it is a plain known for its black soil, rich in humus content, as well as for the steppe vegetation, typical of its particularly harsh climate: hot and dry summers; very cold winters with strong winds. It is part of the Romanian Plain, being its eastern sector.

Fig. 4 *The area where the determinations were made*

In the Brăila area there are:

- old tractors (≈30% of the total). Some have been made in Romania since the late 1980s, others were manufactured abroad, and have in excess of 10000h of operation, and

- new tractors (≈70%); they have less than 2000 hours of operation. Once they exceed 2000 hours of operation , they lose their warranty. Purchasing new tractors is difficult because of the prices, which may amount to hundreds of thousands of euros.

Fig. 5 *Tractor since 1993 (U650)*

Fig. 6 *Tractor since 2013*

Fig. 7 *Noise measurement on the old tractor*

Fig. 8 *Noise measurement on the new tractor*

A tractor driver works 10-12 h/day. In summer, they work more efficiently at night. When it rains, they cannot work in the field because the soil becomes impassable. The determinations took place in the autumn, during the treatment operations (tractors pull other machines that provide plant treatments). The characteristics of the tractor drivers who agreed to participate in the experiments are described in Table 1.

Two tractors were used in the experiments: one from 1993 (U650) and one from 2013 (Fig. 5 and Fig. 6).

The noise level was measured with the Blue Solo sound level meter (01dB-Metravib) (Fig. 7 and Fig. 8).

Table 1 *Information about the subjects*

Tractor	Subject	BMI	Age (years)	Smoker	Drinker *	Seniority (years)	Graduated	Personal problems
Old	1	29.8	58	x	x	37	a	x
	2	25.6	51	-	x	34	b	x
	3	28.8	59	-	x	40	a	x
New	4	26.4	49	x	x	28	b	x
	5	25.1	47	x	x	29	b	x
	6	27.8	51	x	x	31	b	x

* More than 2 glasses of alcohol/day; a) middle school; b) high school

Noise analysis was done by two methods:

Method I: With *Noise exposure ready-reckoners* can be calculated: ”The noise exposure ready-reckoners allow you to estimate daily or weekly noise exposure. To use the daily exposure ready-reckoner you will need to know the levels of noise and durations of exposure which make up a person's working day. For weekly noise exposure, appropriate where somebody's noise exposure varies markedly from day to day, you will need to know the daily noise exposure for each day in the working week.” Noise at work limits are given in *Noise exposure ready-reckoners*:

- For ”Daily noise exposure”
  - Above upper exposure action value ($L_{EP,d}$ 85 dB(A)) is represented by 100 exposure points
  - Above lower exposure action value ($L_{EP,d}$ 80 dB(A)) is represented by 32 exposure points
  - Below lower exposure action value ($L_{EP,d}$ 80 dB(A)) is represented by 32 exposure points
- For ”Weekly Noise Exposure”
  - Above upper exposure action value ($L_{EP,d}$ 85 dB(A) or $L_{EP,W}$ 85 dB(A))
  - Above lower exposure action value ($L_{EP,d}$ 80 dB(A) or $L_{EP,W}$ 80 dB(A))
  - Below lower exposure action value ($L_{EP,d}$ 80 dB(A) or $L_{EP,W}$ 80 dB(A))” [48]

Method II: Noise was analyzed with dBTRAIT, a powerful software dedicated to post-processing sound data. The analysis consists in obtaining sonograms that are graphical representations of a complex sound over a certain period of time. They contain 3 parameters: sound level, frequency and time. In the top left corner, one can see the frequency spectrum at a given time. In the bottom right corner is the evolution of the sound level over time for a given frequency.

The reaction of the subjects to the noise pollution caused by the operation of the tractors was analyzed using the Likert scale. ”A Likert scale is a psychometric scale commonly involved in research that employs questionnaires. It is the most widely used approach to scaling responses in survey research, such that the term is often used interchangeably with *rating scale*.” [49]

Likert Scale	*Disturbing*
1	Very low
2	Low
3	Moderate
4	High
5	Very high

3. RESULTS AND DISCUSSIONS

Method I

Noise exposure ready-reckoners were first used to calculate “Daily noise exposure” ($L_{EP,\,d}$), where L_{Aeq} is Noise Level (dB) for each tractor driver (Fig. 9).

Noise exposure ready-reckoners also served to calculate "Weekly noise exposure" ($L_{EP,\,w}$), where $L_{EP,\,d}$ is Daily noise exposure (dB) for each tractor driver (Fig. 10).

	L_{Aeq} (dB)	**Exposure duration (hours)**	**Exposure points (task)**	**Exposure points per hour**
Task 1	99	1min 20s	418	314
Task 2	96	1min 35s	249	157
Task 3	98	50s	207	249
Task 4	98	20s	82	249
Task 5	95	1min 25s	176	125
Task 6	102	1min 10s	727	626
Task 7	97	55s	180	198
Task 8	99	30s	157	314
Total duration		8min 3s		
$L_{EP,d}$		**98 dB**	**2196 points**	

1

	L_{Aeq} (dB)	**Exposure duration (hours)**	**Exposure points (task)**	**Exposure points per hour**
Task 1	95	1min 55s	239	125
Task 2	96	35s	91	157
Task 3	101	30s	249	498
Task 4	98	1min	249	249
Task 5	99	1min 20s	418	314
Task 6	97	10s	32	198
Task 7	95	1min 30s	188	125
Task 8	98	1min	249	249
Total duration		7min 59s		
$L_{EP,d}$		**97 dB**	**1715 points**	

2

	L_{Aeq} (dB)	Exposure duration (hours)	Exposure points (task)	Exposure points per hour
Task 1	94	1min 10s	115	99
Task 2	102	1min	626	626
Task 3	99	1min	314	314
Task 4	96	35s	91	157
Task 5	98	1min 20s	332	249
Task 6	99	20s	104	314
Task 7	99	1min 25s	443	314
Task 8	101	1min	498	498
Total duration		7min 49s		
$L_{EP,d}$		**99 dB**	**2523 points**	

3

	L_{Aeq} (dB)	Exposure duration (hours)	Exposure points (task)	Exposure points per hour
Task 1	78	15s	1	2
Task 2	79	50s	3	3
Task 3	77	1min 15s	2	2
Task 4	78	1min 35s	4	2
Task 5	77	2min 10s	4	2
Task 6	80	1min	4	4
Task 7	81	55s	5	5
Task 8				
Total duration		7min 59s		
$L_{EP,d}$		**79 dB**	**23 points**	

4

	L_{Aeq} (dB)	Exposure duration (hours)	Exposure points (task)	Exposure points per hour
Task 1	79	50s	3	3
Task 2	78	1min 55s	5	2
Task 3	79	1min 30s	5	3
Task 4	77	1min 25s	3	2
Task 5	76	35s	1	2
Task 6	81	1min 10s	6	5
Task 7	80	5s	0	4
Task 8	78	15s	1	2
Total duration		7min 43s		
$L_{EP,d}$		**79 dB**	**24 points**	

5

	L_{Aeq} (dB)	Exposure duration (hours)	Exposure points (task)	Exposure points per hour
Task 1	77	25s	1	2
Task 2	74	1min 35s	2	1
Task 3	78	1min 20s	3	2
Task 4	79	20s	1	3
Task 5	81	1min	5	5
Task 6	80	2min	8	4
Task 7	79	1min 10s	4	3
Task 8				
Total duration		7min 49s		
$L_{EP,d}$		**79 dB**	**24 points**	

6

Fig. 9 *Calculation of "Daily noise exposure" (1; 2 & 3 - Subject on old tractor) and (4; 5 & 6 - Subject on new tractor) [48]*

	$L_{EP,d}$ dB
Day 1	98
Day 2	98
Day 3	101
Day 4	98
Day 5	99
Day 6	99
Day 7	
$L_{EP,w}$	**100 dB**

1

	$L_{EP,d}$ dB
Day 1	98
Day 2	99
Day 3	99
Day 4	97
Day 5	97
Day 6	96
Day 7	
$L_{EP,w}$	**99 dB**

2

	$L_{EP,d}$ dB
Day 1	99
Day 2	101
Day 3	99
Day 4	98
Day 5	101
Day 6	102
Day 7	
$L_{EP,w}$	**101 dB**

3

	$L_{EP,d}$ dB
Day 1	78
Day 2	77
Day 3	77
Day 4	79
Day 5	77
Day 6	76
Day 7	
$L_{EP,w}$	**78 dB**

4

	$L_{EP,d}$ dB
Day 1	79
Day 2	78
Day 3	78
Day 4	79
Day 5	79
Day 6	78
Day 7	
$L_{EP,w}$	**79 dB**

5

	$L_{EP,d}$ dB
Day 1	79
Day 2	80
Day 3	80
Day 4	81
Day 5	81
Day 6	79
Day 7	
$L_{EP,w}$	**81 dB**

6

Fig. 10 *Calculation of "Weekly Noise Exposure" (1, 2, 3 - Subject on old tractor) and (4, 5, 6 - Subject on new tractor) [48]*

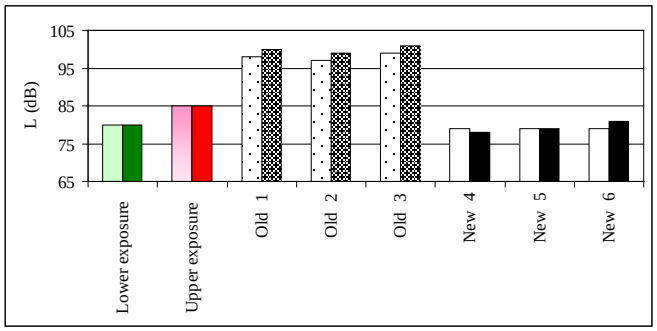

Fig. 11 *Comparison between the values obtained from the measurements and those given by Noise exposure ready-reckoners (■) - $L_{EP,d}$ for lower exposure; (■) - $L_{EP,W}$ for lower exposure; (■) - $L_{EP,d}$ for upper exposure; (■) - $L_{EP,W}$ for upper exposure; (▨) - $L_{EP,d}$ for old tractor; (▨) - $L_{EP,W}$ for old tractor; (□) $L_{EP,d}$ for new tractor; (■) - $L_{EP,W}$ for new tractor*

In the case of subjects operating the old tractor, the average of Daily noise exposure is 98dB, higher than the lower exposure action value by 18 dB and higher than the upper exposure action value by 13 dB, and the average of Exposure points is 2144,667 (62 times as high as the lower exposure action value).

In the case of subjects driving the new tractor, the average of Daily noise exposure is 79 dB, lower than the lower exposure action value by 1 dB and higher than the upper exposure action value by 1 dB, and the average of Exposure points is 23,666 (lower than the lower exposure action value by 8,333 points).

Method II

Figures 12 and 13 are the tables containing the results of the noise measurements, for the tractor, made in 2013. It is noticeable that the average Leq is much higher (99dB) for the old tractor, compared to the new tractor (79.3 dB) because there are differences between the engines, the anti-vibration supports and the degree of noise insulation.

061103_220127_124744000.CMG : Results table

D:\Lucru\EI PICU\Universitate\Doctorat\NAVE FLUVIALE\Masuratori\Burghila ian.'22\4\061103_220127_124744000.CMG

Name	ID	Family	Data type	Weighting	location	Information	Comments	Start	End	Duration	Value	Unit
	0	Leq	Leq	A				01/27/22 12:47:44	01/27/22 12:52:53	0:05:09	99.0	dB[2.000e-05 Pa]
	0	Leq	Max	A				01/27/22 12:47:44	01/27/22 12:52:53	0:05:09	103.9	dB[2.000e-05 Pa]
	0	Leq	Min	A				01/27/22 12:47:44	01/27/22 12:52:53	0:05:09	77.7	dB[2.000e-05 Pa]
	0	Leq	Sel	A				01/27/22 12:47:44	01/27/22 12:52:53	0:05:09	123.9	dB[2.000e-05 Pa]

Fig. 12 *Experimental data for the old tractor*

061103_220127_134856000.CMG : Results table

D:\Lucru\EI PICU\Universitate\Doctorat\NAVE FLUVIALE\Masuratori\Burghila ian.'22\8\061103_220127_134856000.CMG

Name	ID	Family	Data type	Weighting	location	Information	Comments	Start	End	Duration	Value	Unit
	0	Leq	Leq	A				01/27/22 13:48:56	01/27/22 13:54:42	0:05:46	79.3	dB[2.000e-05 Pa]
	0	Leq	Max	A				01/27/22 13:48:56	01/27/22 13:54:42	0:05:46	91.3	dB[2.000e-05 Pa]
	0	Leq	Min	A				01/27/22 13:48:56	01/27/22 13:54:42	0:05:46	44.3	dB[2.000e-05 Pa]
	0	Leq	Sel	A				01/27/22 13:48:56	01/27/22 13:54:42	0:05:46	104.7	dB[2.000e-05 Pa]

Fig. 13 *Experimental data for the new tractor*

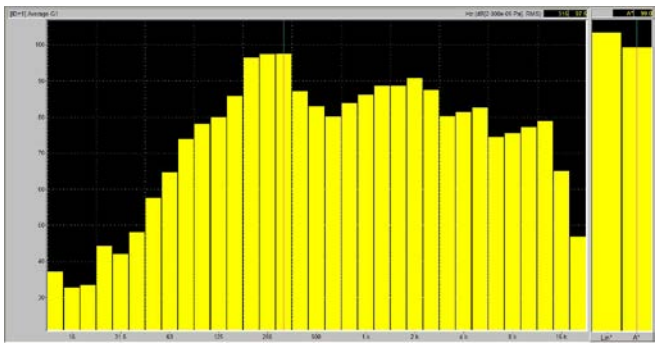

Fig. 14 *Frequency spectrum for the old tractor*

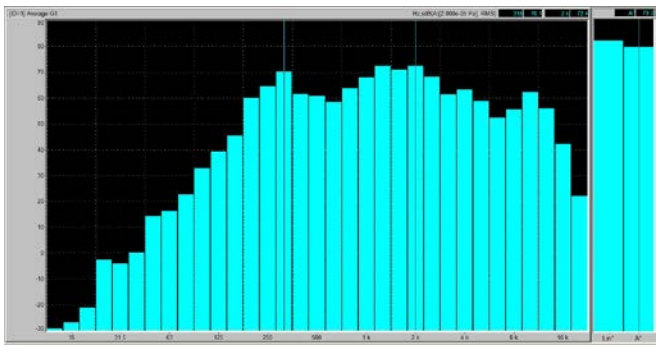

Fig. 15 *Frequency spectrum for the new tractor*

Figures 14 and 15 show the spectral levels per one third of an octave. It can be seen that, for the old tractor, the highest levels of noise are recorded at frequencies between 200 Hz and 315 Hz (Fig. 14). As for the new tractor, the noise is loudest at frequencies between 1250 Hz and 2 kHz (Fig. 15). There is also a maximum at 315 Hz, as with the old tractor, which means that this frequency is specific to these types of tractors.

Fig. 16 and Fig. 17 show the sonograms of the noise for the 2 tractors. These representations have the values of 99.1 dB(A) and 66.5 dB(A), respectively, at the intersection of cursors.

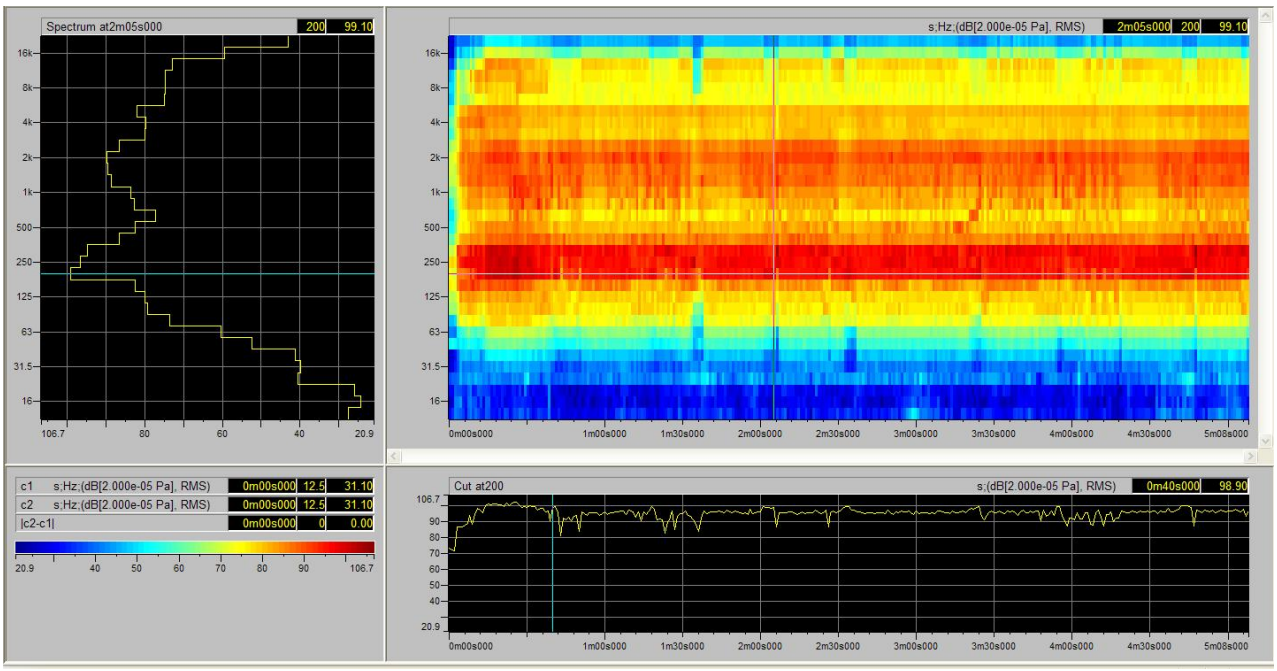

Fig. 16 *Sonogram for old tractor*

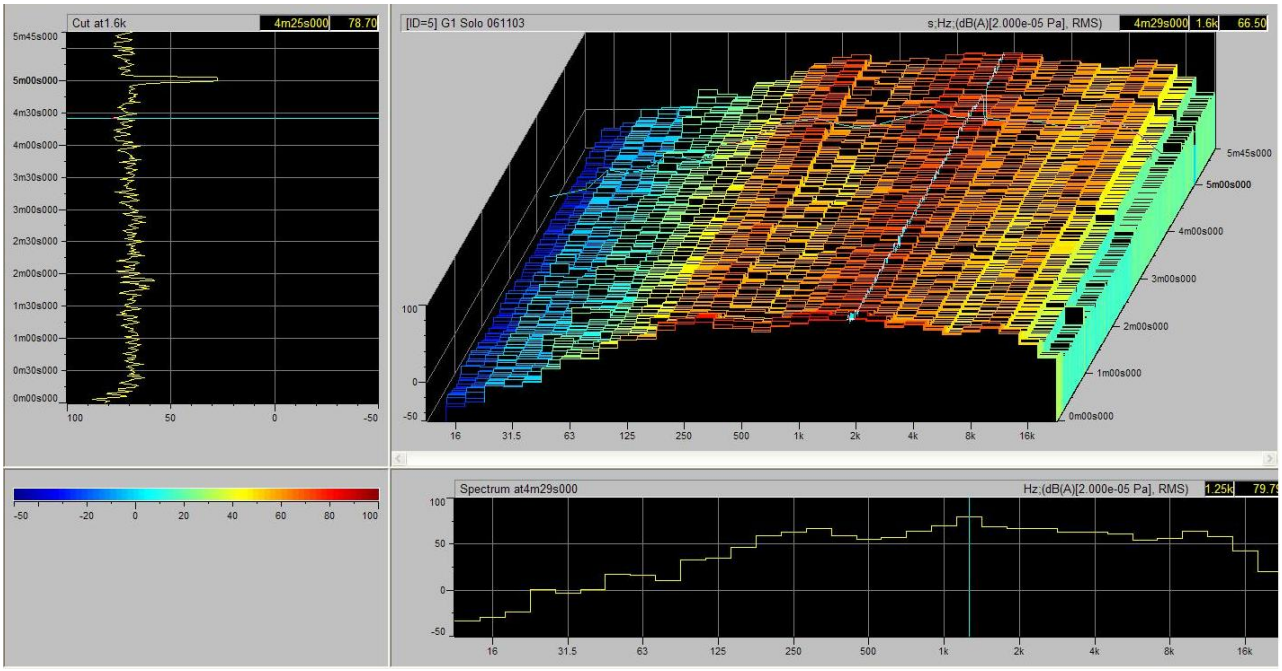

Fig. 17 *Sonogram for new tractor*

Fig. 16 represents the sonogram of the noise measured in the cabin of the old tractor (top right). The sliders are placed at 200 Hz and at 2 min and 5 sec. For the moment 2 min and 5 sec. the frequency spectrum diagram (top left) also shows a maximum of 99.1 dB(A) because it is also at 200 Hz. The sound level L_{eq} has a maximum of 98.9 dB(A), at the moment 40 sec. in the time history presentation (bottom right) for 200 Hz.

Fig. 17 illustrates the sonogram of the noise measured in the cabin of the new tractor (top right). We have the sliders placed at 1.6 kHz and at 4 min. and 29 sec. For the moment 4 min. and 29 sec. the frequency spectrum diagram (bottom right) shows a maximum of 79.79 dB(A) at 1.25 kHz. The L_{eq} sound level has a maximum of 78.7 dB(A), at the moment 4 min. and 25 sec. in the time history presentation (top left) for 1.6 kHz. Also here, more visible than in the sonogram, one can notice a moment of silence (after 5 min) corresponding to stopping-starting the tractor before closing the measurement.

4. CONCLUSIONS

The conclusions below derive from the analysis of the subjects' manifestations in response to the noise pollution to which they are subjected. (Fig. 18) clearly shows that the first 3 subjects are subjected to the highest noise, both in terms of "Daily noise exposure" and "Weekly noise exposure" (the difference in sound level is about 20 dB).

According to Table 1, it has been found that the workers operating the old tractor have a BMI ≥ 27.5, ie they fall into the category "Very overweight to obese" (High risk of

developing heart disease, high blood pressure, stroke, diabetes mellitus and Metabolic Syndrome), while those operating the new tractor have a BMI ∈ (23.0 - 27.4), being included in the category "Mild to moderate overweight" (Moderate risk of developing heart disease, high blood pressure, stroke, diabetes mellitus) (Fig. 19).

Another important aspect of the reaction of this category of workers to the noise caused by the tractor is the age and seniority of the workers. Fig. 20 shows that the age difference, as well as the difference in seniority is about 19 years.

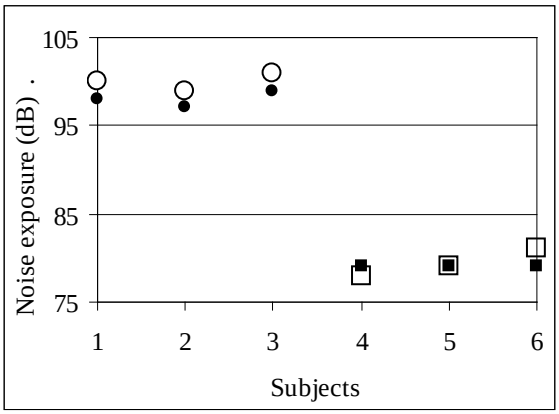

Fig. 18 ***S****ubject exposure to noise (●) – Daily noise exposure (old tractor); (■) – Daily noise exposure (new tractor); (o) – Weekly noise exposure (old tractor); (□) – Weekly noise exposure (new tractor)*

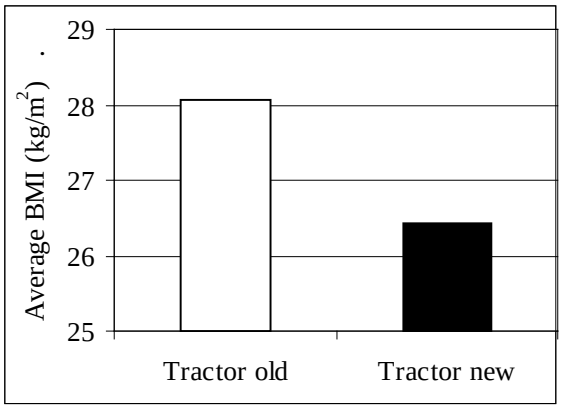

Fig. 19 *Average BMI of tractor drivers*

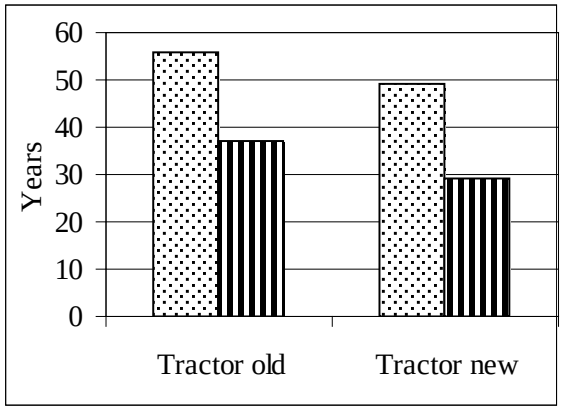

Fig. 20 *(▒) - Average age of tractor drivers (///) - Average seniority of tractor drivers*

In Fig. 21 the subjects' answers to the questionnaire items are presented: "How much do you mind the noise produced by tractors?" Using the Likert scale, it has been found that the subjects in the older group are much more resistant to noise pollution, their answers being as follows:

- for old tractor: 3 ÷ 3.8 (Moderate ÷ High)

- for new tractor: 1.5 ÷ 1.8 (Very low ÷ Low);

unlike subjects in the younger age group, for whom their answers are as follows:

- for old tractor: 4.3 ÷ 4.5 (High)

- for new tractor: 2.5 ÷ 3.1 (Low ÷ Moderate).

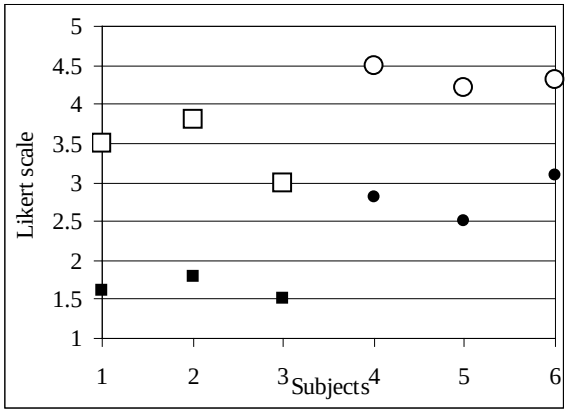

Fig. 21 *Subject assessments of tractor noise: (□) – Old tractor (Subjects 1, 2 and 3); (o) – Old tractor (Subjects 4, 5 and 6); (■) – New tractor (Subjects 1, 2 and 3); (●) – New tractor (Subjects 4, 5 and 6)*

The fact that older subjects have worked longer on this type of tractor (U650), which was and still is a good tractor, also contributes to this difference in the assessment of the discomfort caused by noise pollution. Also, these subjects are used to more physically-demanding work, as they have never had the opportunity to do lighter work – they only finished middle school.

Obviously, a renewal of the tractor fleet is needed, which would improve the drivers' working conditions (not only in terms of noise, but also in terms of vibration and air conditioning). This would mean implicitly, higher labor productivity.

REFERENCES

[1] P.A. Hancock, Sustained attention in human performance, *Ch.4 Environmental stressors*, Ed by J.S.Warm, John Wiley and Sons Ltd., 1984

[2] P.A. Hancock, „A Dynamic Model of Stress and Sustained Attention", *The Journal of the Human Factors and Ergonomics Society*, Vol. 31(5), pp. 519-537, 1989, http://hfs.sagepub.com/content/31/5/519.short

[3] P.A. Hancock, J.S. Warm, „A Dynamic Model of Stress and Sustained Attention", *Journal of Human Performance in Extreme Environments*, Vol. 7(1), 2003

[4] R.M. Yerkes, J.D. Dodson, „The relation of strength of stimulus to rapidity of habit-formation", *Journal of Comparative Neurology and Psychology*, Vol. 18, pp. 459-482, 1908

[5] Yerkes–Dodson law https://en.wikipedia.org/wiki/Yerkes%E2%80%93Dodson_law

[6] A.T. Pope, E.H. Bogart, & D.S. Bartolome, „Biocybernetic system evaluates indices of operator engagement in automated task", *Biol. Psychol.*, Vol. 40, pp. 187-195, 1995

[7] G. Matthews, et al., „Fundamental dimensions of subjective state in performance settings: task engagement, distress, and worry", *Emotion*, Vol. 2, pp. 315, 2002

[8] C. Stephens, et al., „Biocybernetic adaptation strategies: machine awareness of human engagement for improved operational performance", in *Proc. International Conference on Augmented Cognition*, Copenhagen, pp. 89-98, 2018

[9] K.H. Pribram & D. McGuinness, „Arousal, activation, and effort in the control of attention", *Psychol. Review*, Vol. 82, pp. 116, 1975

[10] F. Dehais, A. Lafont, R. Roy & S. Fairclough, „A Neuroergonomics Approach to Mental Workload, Engagement and Human Performance", *Frontiers in Neuroscience*, Vol. 14, pp. 1-17, 2020

[11] G. Belojević, E. Öhrström, R. Rylander, „Effects of noise on mental performance with regard to subjective noise sensitivity", *International Archives of Occupational and Environmental Health*, Vol. 64(4), pp 293-301, 1992

[12] K.P. Waye, R. Rylander, S. Benton, H.G. Leventhall, „Effects on performance and work quality due to low frequency ventilation noise", *Journal of Sound and Vibration*, Vol. 205(4), pp. 467-474, 1997

[13] M. Picu & S. Nastac, „Some Aspects Regarding Noise Exposure Dose Monitoring for Working Personnel", *Journal of Science and Arts*, Vol. 12(1)1, pp. 299-304, 2010

[14] S.A. Stansfeld, M.P. Matheson, „Noise pollution: non-auditory effects on health", *British Medical Bulletin*, Vol. 68(1), pp. 243-257, 2003

[15] J.L. Szalma, P.A. Hancock, „Noise effects on human performance: A meta-analytic synthesis", *Psychological Bulletin*, Vol. 137(4), pp. 682-707, 2011

[16] L. Picu, M. Picu & E.V.C. Rusu, "An Investigation into the Health Risks Associated with the Noise and Vibrations on Board of a Boat – A Case Study on the Danube River", *Journal of Marine Science and Engineering*, Vol. 7(8), pp. 1-16, 2019

[17] Bovenzi, M., Ronchese, F., Maurom M., A longitudinal study of peripheral sensory function in vibration-exposed workers, International archives of occupational Environmental Health, 84:325-334, 2011

[18] Dupuis, H., Zerlett, G., The Effects of Whole-Body Vibration, Springer-Verlag Berlin Heidelberg, 2012

[19] Paddan, G.S., Mansfield, N.J., Arrowsmith, C.I., Rimell, A.N., King, S.K., Holmes, S.R., The influence of seat backrest angle on perceived discomfort during exposure to vertical whole-body vibration, Volume 55, Issue 8, pages 923-936, 2012

[20] Picu, M., The Qualitative Assesment of Emerging Risks to Workers Exposed to HAV, Journal of Materials Science and Engineering A, 4 (9) pp.315-320, 2014

[21] Picu, M., A Dynamic Model of the Human Body in the Vertical Direction, Advanced Materials Research, Vol. 837, pp. 452-457, 2014

[22] Picu, M., Personality determination using vibrating movement parameters, Proceedings of Papers, pp. 209-216, 24th International Conference Noise and Vibration, 29-31 Oct, 2014, Nis, Serbia

[23] Picu, M., A Study of Vertical Vibration Transmissibility by the Human Body, Applied Mechanics and Materials (Vol. 325 - 326), pp. 152-157, 2013

[24] Picu, M., The Transmission of Vibration Through Car Seats, Acoustics and vibration of mechanical structures, 23-24 May 2013, International Journal of Modern Manufacturing Technologies ISSN 2067–3604, Vol. V, No. 1, pp. 87-90, 2013

[25] Picu, M., A comparative study of the disconfort induced by vehicles to driver, International Journal of Modern Manufacturing Technologies ISSN 2067–3604, Vol. IV, No. 2, pp. 61-66, 2012

[26] Picu, M., Nastac, S., A Study Concerning The Driver Comfort Improvement As Regards The Transmitted Vibrations By The Vehicle Running On Roads In Romania, Carpathian Journal of Earth and Environmental Sciences, Volume 6, Number 2, pp. 313-320, 2011

[27] Picu, M., Nastac, S., Some Aspects Regarding Noise Exposure Dose Monitoring for Working Personnel, Journal of Science and Arts, Volume 12, Number 1, pp. 299-304, 2010

[28] Village, J., Trask, C., Chow, Y., Morrison, J.B., Koehoorn, M., Teschke, K., Assessing whole body vibration exposure for use in epidemiological studies of back injuries: measurements, observations and self-reports, Ergonomics, Volume 55, Issue 4, pages 415-424, 2012

[29] Fang, L., Wyon, D. P., Clausen, G., Fanger, P.O., Impact of indoor air temperature and humidity in an office on perceived air quality, SBS symptoms and performance, Indoor Air, Volume 14, Issue Supplement s7, pages 74–81, August 2004

[30] Wyon, D.P., The effects of indoor air quality on performance and productivity, Indoor Air, Volume 14, Issue Supplement s7, pages 92–101, August 2004

[31] Wolkoff, P., Kjærgaard, S.K., The dichotomy of relative humidity on indoor air quality, Environment International, Volume 33, Issue 6, August 2007, Pages 850–857

[32] Picu, M., Multi-stress and human performance: a refutation of inverted-U hypothesis, Journal of Multidisciplinary Engineering Science and Technology (JMEST) ISSN: 3159-0040, Vol. 2, Issue 9, Sept, 2015,

[33] Lyovina I.V., The effect of dust in the air of the work area on the body and human health, Practical Conference "Science without borders and language

barriers", pp.71-73, N.V. Parakhina ", Ministry of Agriculture, Russian Federa-tion, April 18, 2018

[34] Ramsey J.D., Burford C.L., Beshir M.Y., Jensen R.C., Effects of workplace thermal conditions on safe work behavior, Journal of safety Research, 14(3), 105-114, 1983

[35] Behroozi Lar, M., Payandeh, M., Bagheri, J., Khodarahm Pour, Z., Comparison of noise level of tractors with cab and without in different gears on driver ear and bystander, African Journal of Agricultural Research, Vol.7(7), pp. 1150-1155, 2012

[36] Celen, I.H., Arin, S., Noise levels of agricultural tractors, Pakistan journal of biological sciences, Vol. 6(19), pp. 1706-1711, 2003

[37] Ehlers, J.J., Graydon, P.S., Noise-induced hearing loss in agriculture: Creating partnerships to overcome barriers and educate the community on prevention, Noise and Health, Vol. 13, Issue 51, pp. 142-146, 2011

[38] Ghotbi, M.R, Monazzam, M.R, Khanjani, N., Nadri, F., Fard, S.M.B., Driver exposure and environmental noise emission of Massey Ferguson 285 tractor during operations with different engine speeds and gears, African Journal of Agricultural Research, Vol.8(8), pp. 652-659, 2013

[39] Jahanbakhshi, A., Yousefi, M., Karami-Boozhani, S., Heidarbeigi, K., Abbaspour-Gilandeh, Y., The effect of combined resistance muffler on noise pollution and the allowable driver exposure in Massey-Ferguson tractors, Journal of the Saudi Society of Agricultural Sciences, Vol. 19 Issue 6, pp. 409-414, 2020

[40] Monazzam, M.R, Khanjani, N., Nadri, F., Nadri, H., Tractor drivers and bystanders noise exposure in different engine speeds and gears, Journal of Military Medicine. June, pp. 149-154, 2012

[41] Pochi,D., et al., Levels of noise and vibrations transmitted to the driver of a medium-high power agricultural tractor, under operative conditions, Ergonomics, Safety and Health, International Conference of Agricultural Engineering – CIGR-AgEng. 2012: Agriculture an Engineering for Healthier Life, Valencia, Spain, pp. P-1325 ref. 7, 8-12 July

[42] Sena, T.R.R., Dourado, S.S.F., Lima, L.V., Antoniolli, Â,R., The Hearing of Rural Workers Exposed to Noise and Pesticides, Noise Health, Vol. 20(92), pp. 23–26, 2018

[43] Stayner, R.M., Maximum permissible noise levels emitted by wheeled agricultural and forestry tractors in the Member States of the European Community, Applied Acoustics, Vol. 23, Issue 3, pp. 191-197, 1988

[44] Talamo, J.D.C., The perception of machinery indicator sounds, Ergonomics, Vol. 25, pp. 41-51, Published online: 27 Mar 2007

[45] Vallone, M., Bono, F., Quendler, E., Febo, P., Catania, P., Risk exposure to vibration and noise in the use of agricultural track-laying tractors, Annals of Agricultural and Environmental Medicine, Vol 23, No 4, pp. 591–597, 2016

[46] Persson Waye, K., Rylander, R., Benton, S., Leventhall, H.G., Effects on performance and work quality due to low frequency ventilation noise, Journal of Sound and Vibration, Volume 205, Issue 4, 28 August 1997, Pages 467–474]

[47] S. Booth, Loud Noises Aren't Just Annoying, They're Bad for Your Health,‖ Healthline. Found at: https://www.healthline.com/health-news/loud-noises-bad-for-your-health#Your-mood-darkens, 2018 (Online)

[48] https://www.hse.gov.uk/noise/calculator.htm

[49] https://en.wikipedia.org/wiki/Likert_scale

University of Nis
Faculty of Occupational Safety
„Politechnica“ University of Timisoara
Faculty of Mechanical Engineering
27th International Conference
NOISE AND VIBRATION
Niš, 20 - 21. 10. 2022.

INDUSTRIAL IMPULSIVE NOISE, PRACTICAL STUDY: FROM COMPARING THE EXISTING CRITERIA TO FORMING THE NOVEL EVALUATION MODEL

Jovan Miočinović [1], Biljana Beljić Durković [2]

[1] TEHPRO d.o.o., Serbia, jovan.miocinovic@tehpro.rs
[2] TEHPRO d.o.o., Serbia

Abstract - *Since the seventies of 20th century numerous studies indicate the possible additional damaging effect of impulsive noise on hearing. In this paper the existing impulsiveness evaluating criteria are to be compared to a distribution-based criterion founded both on recent physiological models and studies on exposed groups of industrial workers. Impulsive noise descriptors of a sample of 140 various noise exposures in industry where impulsive noise appearing measured in situ are being statisticaly treated. Further, an attempt is made to classify the noise types rated as impulsive based on the relation of kurtosis to existing impulsiveness descriptors criteria statisticaly found to be relevant.*

1. INTRODUCTION

As the number of investigations since the seventies of 20th century [1] have shown, the time-averaged sound pressure levels are not an adequate and only indicator of risk of hearing loss but also the impulsive character of the sound in addition to its time-averaged level has to be considered. Still there is no consent neither in the proper descriptor of the impulsiveness nor in the valid method to combine noise equivalent levels with eventual correction factor to it to compare with limit values [2]. Yet the novel researches considering both the impact of impulsive noise on industrial workers [3] and experimental studies on chincillas [4] modelling the human hearing loss have shown that the statistical measurements such as kurtosis hold promise for the quantitative prediction of hearing loss. A basic form for noise metrics is designed by combining the equivalent sound pressure level (SPL) and a temporal correction term defined as a function of kurtosis of the noise. Kurtosis is defined as the fourth standardized moment about the mean of the data:

$$\frac{E(x-m)^4}{s^4} \quad (1)$$

where s is the standard deviation of x, $E(x\text{-}m)$ represents the expected value of quantity, m is the mean of x. Kurtosis describes the peakedness of a distribution, which is independent of the overall level and was suggested as a metric of impulsiveness by Erdreich [5].

The indicators of impulsiveness were compared to kurtosis for a sample of 140 various noise exposures measured in situ in industry where impulsive noise appearing: in metal fabrication industry near machinery like angle grinders, metal working machines as punch presses and nailing machines, cutting saws, in hammering and banging on metal objects (sample of 98 measurements), construction materials industry (sample of 18 measurements), wood working industry (sample of 19 measurements), in glass industry near bottling machines (sample of 4 measurements) and beverage industry in filling barrels with beverages (one measurement).

2. INDICATORS OF IMPULSIVENESS

Impulsive noise is defined as noise consisting of a series of bursts of sound energy, each burst having a duration of less than approximately 1 s [6]. Impulsive noise is described by many parameters such as peak level, duration, rise- and fall times, impulse energy, inter-impulse interval, impulse rate and the background continuous noise level.

In the literature the following descriptors may be found [7]. The highest peak in the series of succesive peaks, peak level, a duration of of the first overpressure (zero level crossing) and the duration from the highest peak level to a point of time when the envelope of pressure fluctuation stays within 20 dB of the peak pressure level.

Impulsive noise is measured with sound level meter using exponential RMS integration for impulse exponential time constant, τ = 35 ms, that is AI-weighted equivalent continuous sound pressure level, L_{pAIeq} comparing to linear RMS integration for fast time constant, τ = 125 ms that is used for measuring A-weighted equivalent continuous sound pressure level, L_{pAeq}.

Also, there is a method based on the crest factor. The crest factor is defined as a difference between peak and RMS level of the noise, and is in relationship to the effective length and to the energy of a single impulse. The definition of impulse noise based to the effective length is:

$$I = L_{A_p} - L_{AS} \geq 15\ dB \quad (2)$$

where L_{Ap} is A-weighted peak level, L_{AS} is A weighted RMS level measured with slow time constant, τ=1000 ms, and I is impulsiveness.

The other quantity for evaluating impulsive noise is C-weighted peak sound pressure level.

Another descriptor would be the number of impulses that overpass the given peak pressure during the working day. For limiting the risk of hearing damage common approach is to limit the number of impulses at a given peak pressure over a workday.

2.1 Impulsiveness descriptors used

In this paper the following descriptors are being used: AI-weighted equivalent continuous sound pressure level, L_{pAIeq} (actually, K_I defined in (6)), C-weighted peak sound pressure level, $L_{p,Cpeak}$, and crest factor. The descriptors are compared to kurtosis, a metrics that takes into account temporal characteristics of noise exposure that is recently shown that discriminates the best the the risk of hearing demage for noise exposures with the same level and different temporal characteristics. For practical reasons here the crest factor is simplified to difference in A-weighted peak sound pressure level and equivalent sound pressure level measured with fast time constant:

$$CF = L_{p,A_{peak}} - L_{pAeqT_e} \quad (3)$$

The simplification is being introduced due to the available measured parameters.

2.2 Kurtosis

Kurtosis is calculated from the noise exposures measurements associated statistics.

2.2.1 Definition of kurtosis

For the data Y_1, Y_2, …, Y_N, the formula for kurtosis is:

$$kurtosis = \frac{\sum_{i=1}^{N}(Y_i-\bar{Y})^4/\mathrm{N}}{s^4} \quad (4)$$

Where $\bar{Y}$ is the mean, s is the standard deviation and N is the number of data points.

2.2.2 Noise exposures measurements associated statistics and kurtosis

Statistics logger provides the decibel levels noted during measurement period together with associeted time frequencies, i.e. the percentage of total measuring time each decibel level appeared. In Fig. 1 an example of statistics loger is presented.

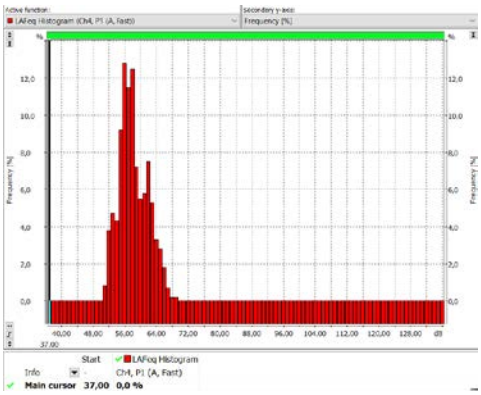

Fig. 1 *Example of graphical form of statistics logger from the measurement device*

Table form of logger may be easily transferred to Excel file to perform adequate calculations. The transformation of (4) to formula based on the these statistics data is straightforward:

$$kurtosis = \frac{\sum_{i=1}^{n}(f_i*Y_i-\bar{Y})^4/(\sum_{i=1}^{n}f_i)}{s^4} \quad (5)$$

where f_i is the frequency the Y_i decibel level occur. It may be seen that here $\bar{Y}$ is the equivalent sound pressure level for the total measurement duration.

3. DATA ANALYSIS

3.1 Statistical analysis

Data for the indicators of impulsiveness for the sample of 140 noise measurements are correlated to the kurtosis values calculated according to (5). Additionaly, the correlation is calculated separately for the subsamples of measurements in metal fabrication industry and for the subsamples rated as impulsive.

The criterion for impulsiveness is from DIN 45645-2 [8] (hereinafter the new criterion) and ISO 9612:1997 [9] (hereinafter the old criterion), the noise is considered to be impulsive if there are noticeable observed impulses and $K_I \geq$ 3 dB (according to the new criterion) and $K_I \geq 2$ dB (according to the new criterion), calculated according to (6):

$$K_I = L_{pAIeq} - L_{pAeq} \quad (6)$$

Here K_I is the impulsive adjustment for the impulsive noise determined as the difference between the AI-weighted sound pressure level and L_{pAeq}.

3.1.1 The sample

The sample constists of 140 various noise exposures measured in situ in industry where impulsive noise appearing. From those, 98 measurements in metal fabrication industry, 18 measurements in construction materials industry, 19 measurements in wood working industry, 4 in in glass industry and 1 in beverage industry. From the total sample, the subsample of 90 measurements from metal fabrication industry is thought to be heterogeneos, i.e. all the measurements made in situ are being included in the sample by chance. The other measurements in total sample are targeted picked up for the research to expand it to other industries where the impulsive noise occurs. In order to prevent the possible impact of this selection bias the analysis has been performed in addition for that subsample.

3.1.2 The analysis used

Hypothesis that there is a significant correlation between kurtosis and a descriptor of impulsiveness (here: K_I, crest factor, or peak level $L_{p,Cpeak}$) has been tested. The idea is that for the descriptor that turns out to be significantly correlated to kurtosis it might be said that both, kurtosis and the indicator under test in some way do describe the same property, assumedly impulsiveness.

From the calculated correlations for each sample the T-scores have been calculated and from those for each sample and sample's degree of freedom p value has been calculated. For the each pair of compared descriptors it than may be said that they correlate at the given significance level (0,01, 0,05 or 0,10) when the corresponding p value is found to be less than the given significance level.

The calculations of correlation coefficients (r) and corresponding test statistics (t) were performed in Excel and the calculations of p values in an online calculator [10].

Test statistics (t) are calculated according to formula [11]:

$$t = \frac{r\sqrt{n-2}}{\sqrt{1-r^2}} \quad (7)$$

where n is the number of measurements in the sample.

3.1.3 Statistical analysis results

For the total sample of 140 noise exposures measured in situ the results are given in Tables 1 (for K_I and kurtosis), 2 (for crest factor and kurtosis) and 3 (for peak level $L_{p,\mathrm{Cpeak}}$ and kurtosis).

Table 1 *Statistical analysis results for K_I and kurtosis*

sample	correlation coefficient	t-score	degrees of freedom	p value
total (140)	-0,223	-2,754	138	0,00334
impulsive (old) (78)	-0,180	-1,623	76	0,0544
impulsive (new) (50)	-0,222	-1,621	48	0,0559

It may be seen from the p values that the impulsive adjustment K_I and kurtosis are strongly correlated.

K_I correlates with kurtosis at the significance level of 0,01 (that is, there is 99 % of probability that measurands K_I and kurtosis are correlated, i.e. they do measure the same quality). For the subsamples of impulsive noise they less strongly correlate, the significance level is 0,1 (90 % of probability that they correlate).

Table 2 *Statistical analysis results for crest factor and kurtosis*

sample	correlation coefficient	t-score	degrees of freedom	p value
total (140)	-0,0576	-0,679	138	0,249
impulsive (old) (78)	0,0161	0,140	76	0,444
impulsive (new) (50)	0,0060	0,042	48	0,483

It may be seen from the p values that the crest factor and kurtosis are not significantly correlated, i.e. it is very probable that they do not measure same quality.

Table 3 *Statistical analysis results for peak level $L_{p,Cpeak}$ and kurtosis*

sample	correlation coefficient	t-score	degrees of freedom	p value
total (140)	-0,0900	-1,065	138	0,464
impulsive (old) (78)	-0,2240	-2,056	76	0,022
impulsive (new) (50)	-0,2987	-2,272	48	0,014

It may be seen from the p values that the peak level and kurtosis are not significantly correlated. However focusing on subsamples rated as impulsive it may be seen that they do correlate to kurtosis (at the significance level of 0,05). This may be due to definition of impulsiveness that is imposed to the subsamples and (by means of (6)) imports the quality for that it is already shown (Table 2) to correlate to kurtosis.

Table 4 *Statistical analysis results for K_I and kurtosis for the subsample from metal fabrication industry*

sample	correlation coefficient	t-score	degrees of freedom	p value
total (90)	-0,273	-2,764	88	0,00348
impulsive (old) (56)	-0,291	-1,800	54	0,0443
impulsive (new) (34)	-0,222	-1,621	32	0,0406

When focusing on the subsample of metal fabrication industry, the results are given in Tables 4 (for K_I and kurtosis), 5 (for crest factor and kurtosis) and 6 (for peak level $L_{p,\mathrm{Cpeak}}$ and kurtosis).

Here the results are similar to the analysis made on the total sample (Table 2). There is a strong correlation between the impulsive adjustment K_I and kurtosis and, here, the subsamples of impulsive noise correlate stronger than the ones of total sample (at the significance level of 0,05).

Table 5 *Statistical analysis results for crest factor and kurtosis for the subsample from metal fabrication industry*

sample	correlation coefficient	t-score	degrees of freedom	p value
total (90)	-0,0570	-0,536	88	0,296
impulsive (old) (56)	0,00788	0,583	54	0,281
impulsive (new) (34)	0,00316	0,179	32	0,429

Table 6 *Statistical analysis results for peak level $L_{p,Cpeak}$ and kurtosis for the subsample from metal fabrication industry*

sample	correlation coefficient	t-score	degrees of freedom	p value
total (90)	-0,1407	-1,346	88	0,091
impulsive (old) (56)	-0,1117	-0,832	54	0,204
impulsive (new) (34)	-0,2004	-1,181	32	0,123

In Table 5, as in analysis made on total sample (Table 2), it may be seen that the crest factor and kurtosis are not significantly correlated.

The results given in Table 6 show that here, on the total sample of metal fabrication industry noises, peak level and kurtosis correlate at the significance level 0,1, and, on the contrary to results from the analysis made on total sample of all industrial noises (Table 3) for the subsamples rated as impulsive peak level and kurtosis do not correlate significantly.

In Fig. 2, 3 and 4 the correlation plots from Excel calculator for the total sample of 140 measurements and the impulsive rated subsample of 50 measurements (according to the new criterion) are presented.

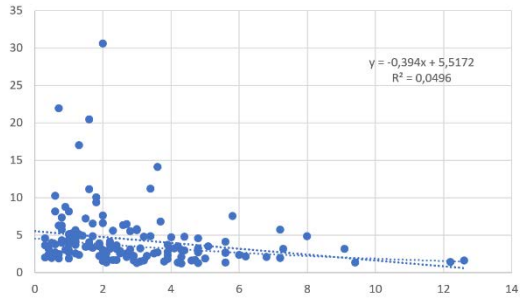

Fig. 2 *Correlation plot for K_I and kurtosis for the total sample of 140 measurements*

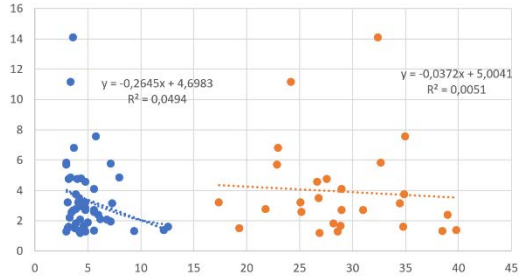

Fig. 3 *Correlation plot for K_I and kurtosis (left) and for the crest factor and kurtosis (right) for the sample of 50 noise measurements rated as impulsive*

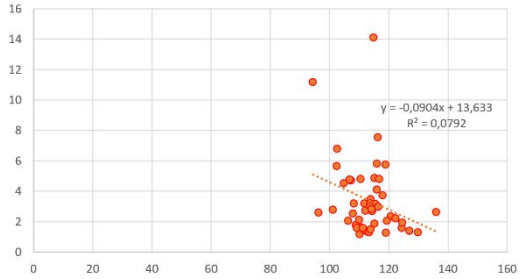

Fig. 4 *Correlation plot for peak level $L_{p,Cpeak}$ and kurtosis for the sample of 50 noise measurements rated as impulsive*

3.2 Descriptive analysis

Whilst the other descriptors of impulsiveness as hereby defined seem not to correlate with kurtosis, an attempt is to be made to classify the noise tipes rated as impulsive into classes based solely on the relation of impulsive adjustment K_I and kurtosis.

In Fig. 5 correlation plot for K_I and kurtosis is given classified into distinctive zones according to the rated significance.

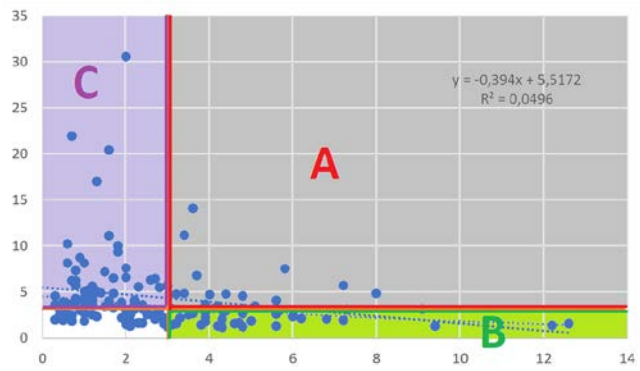

Fig. 5 *Correlation plot for K_I and kurtosis classified into zones according to the rated significance*

3.2.1 Significant K_I and significant kurtosis

Here, K_I is significant in the sense that is ≥ 3 dB, i.e. noise is rated as impulsive and based on up-to-date knowledge one should expects some correction factor for the impulsivity to the measured equivalent noise level to compare it to limit values to prevent the risk of hearing damage. In Table 7 and Fig. 6 and 7 an example is presented, noise of lathe machine and in Table 8 and Fig. 8 and 9 the other one, noise of bottling machine. These measurements may be classified to zone A in Fig. 5.

Table 7 *Measurement results for K_I and kurtosis for the example of noise of universal lathe machine*

Source	L_{pAIeq}	K_I	kurtosis
Universal lathe machine	79,4	3,9	2,8

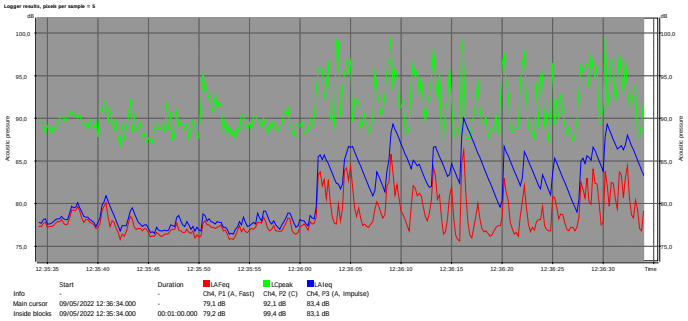

Fig. 6 *Example of noise measurement rated as impulsive with kurtosis of the similar level. In red is equivalent noise level, in blue AI-weighted sound pressure level and in green C-weighted peak sound pressure level.*

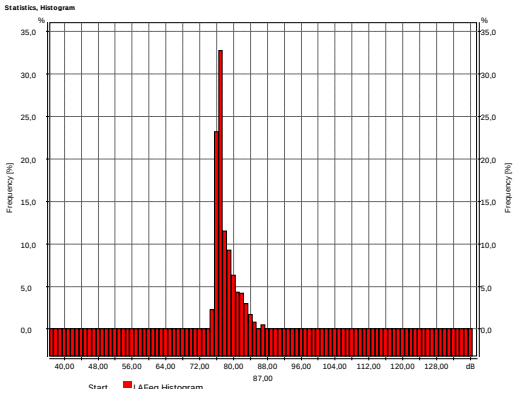

Fig. 7 *Example of graphical form of statistics logger associated to noise measurement rated as impulsive with kurtosis of the similar level*

Table 8 *Measurement results for K_I and kurtosis for the example of noise of bottling machine*

Source	L_{pAIeq}	K_I	kurtosis
Bottling machine	89,1	4,4	4,8

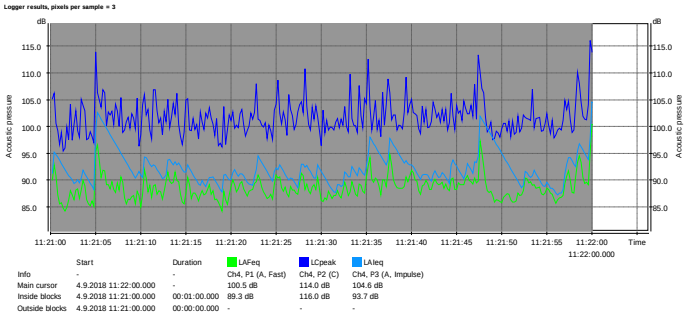

Fig. 8 *Example of noise measurement of bottling machine rated as impulsive with kurtosis of the similar level. In green is equivalent noise level, in light blue AI-weighted sound pressure level and in blue C-weighted peak sound pressure level.*

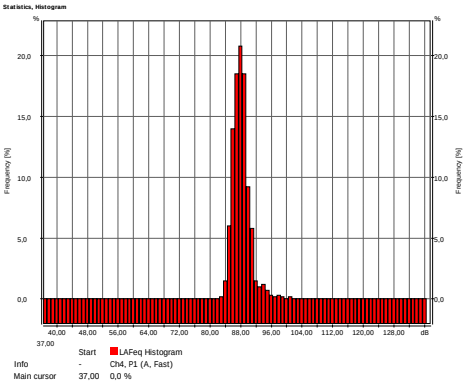

Fig. 9 *Example of graphical form of statistics logger associated to noise measurement of bottling machine rated as impulsive with kurtosis of the similar level*

3.2.2 Significant K_I and insignificant kurtosis

Here, K_I is significant in the sense that is ≥ 3 dB, i.e. noise is rated as impulsive but kurtosis is low. Following the recent research, one sholuld not expect the additional damaging effect of the impulsiveness of the noise adding to the measured equivalent noise level. In Table 9 and Fig. 10 and 11 an example is presented. This measurement may be classified to zone B in Fig. 5.

Table 9 *Measurement results for K_I and kurtosis for the example of noise of hammering*

Source	L_{pAIeq}	K_I	kurtosis
Hammering	87,2	12,2	1,4

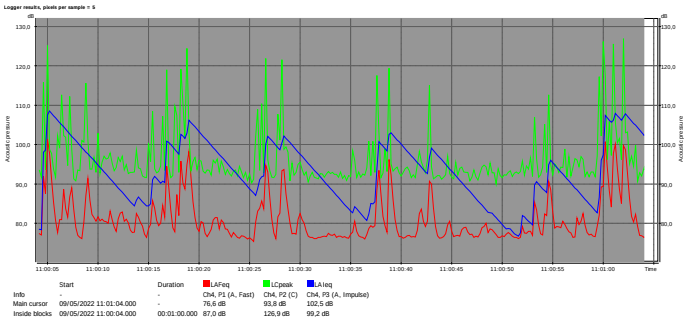

Fig. 10 *Example of noise measurement rated as impulsive with kurtosis of the low level. In red is equivalent noise level, in blue AI-weighted sound pressure level and in green C-weighted peak sound pressure level.*

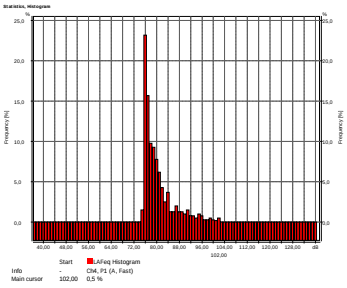

Fig. 11 *Example of graphical form of statistics logger associated to noise measurement rated as impulsive with kurtosis of the lower level*

3.2.3 Significant K_I and insignificant kurtosis, noise not rated as impulsive

The criterion for impulsiveness stated in 3.1 is that both there are noticeable observed impulses and $K_I \geq 3$ dB. Here, K_I is significant in the sense that is ≥ 3 dB, but the noticeable impulses are not present. Examples from the noise exposures measured in situ are common speech in the office and filling barrels with beer in brewery. In both examples kurtosis happen to be low. These measurements may also be classified to zone B in Fig. 5.

Table 10 *Measurement results for K_I and kurtosis for the example of noise of common speach*

source	L_{pAIeq}	K_I	kurtosis
Common speach	62,1	9,0	2,5

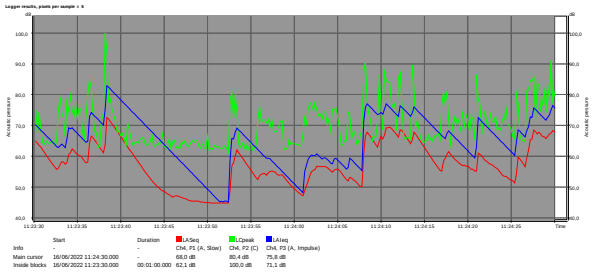

Fig. 12 *Example of noise measurement of common speach rated as not impulsive but with $K_I \geq 3$ dB, and kurtosis of the low level. In red is equivalent noise level, in blue AI-weighted sound pressure level and in green C-weighted peak sound pressure level.*

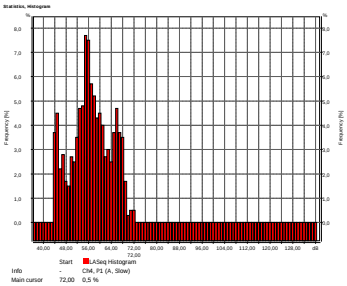

Fig. 13 *Example of graphical form of statistics logger associated to the noise measurement of common speech with kurtosis of low level.*

Table 11 *Measurement results for K_I and kurtosis for the example of noise of filling barrels with beer in brewery*

source	L_{pAIeq}	K_I	kurtosis
Filling barrels	87,8	6,8	2,1

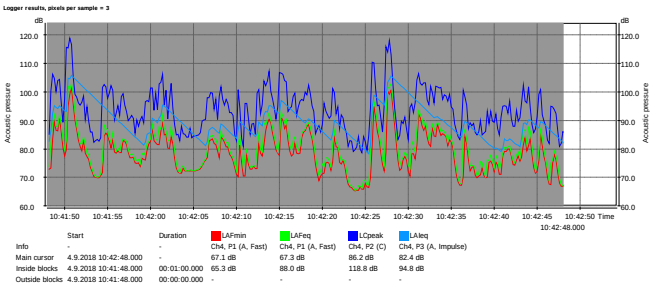

Fig. 14 *Example of noise measurement of filling barrels with beer in brewery rated as not impulsive but with $K_I \geq 3$ dB, and kurtosis of the low level. In red is equivalent noise level, in light blue AI-weighted sound pressure level and in blue C-weighted peak sound pressure level.*

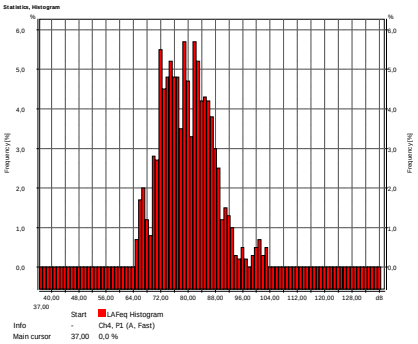

Fig. 15 *Example of graphical form of statistics logger associated to the noise measurement of filling barrels with beer in brewery with kurtosis of low level.*

3.2.4 Insignificant K_I and significant kurtosis

Here presented is the case of insignificant K_I for noise to be rated as impulsive and significant kurtosis. Examples from the noise exposures measured in situ are decorator and lacquer spray machine in metal working and processing industry, cement mill in construction materials industry and metalworking with hand tools. These measurements may be classified to zone C in Fig. 5.

Table 12 *Measurement results for K_I and kurtosis for the example of noise of lacquer spray machine in metal working industry*

source	L_{pAIeq}	K_I	kurtosis
Lacquer spray machine	93,3	0,6	10,3

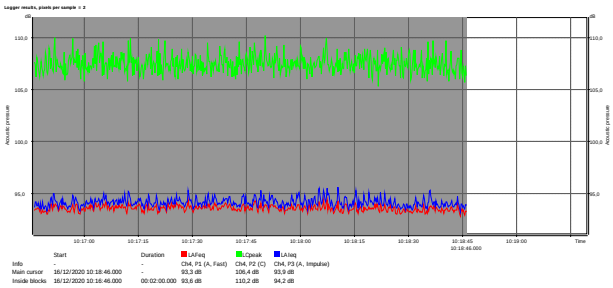

Fig. 16 *Example of noise measurement of noise of lacquer spray machine in metal working industry where K_I is low (quasi-impulsive noise) and kurtosis of the high level. In red is equivalent noise level, in blue AI-weighted sound pressure level and in green C-weighted peak sound pressure level.*

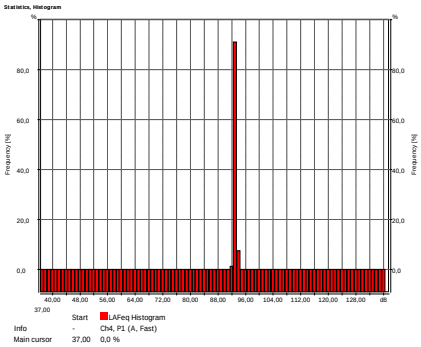

Fig. 17 *Example of graphical form of statistics logger associated to the noise measurement of lacquer spray machine in metal working industry.*

Table 13 *Measurement results for K_I and kurtosis for the example of noise of cement mill*

Source	L_{pAIeq}	K_I	kurtosis
Cement mill	90,1	0,7	10,3

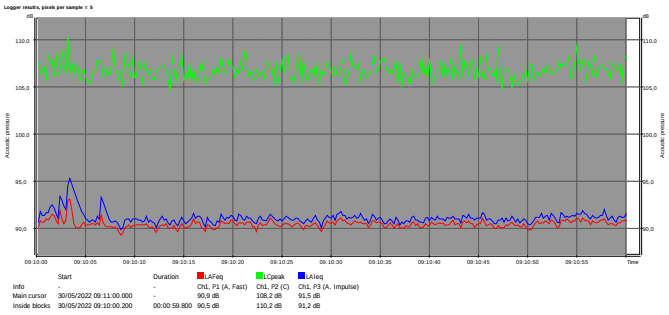

Fig. 18 *Example of noise measurement of noise of cement mill where K_I is low (quasi-impulsive noise) and kurtosis of the high level. In red is equivalent noise level, in blue AI-weighted sound pressure level and in green C-weighted peak sound pressure level. The impulses are random and audible yet masked by noise.*

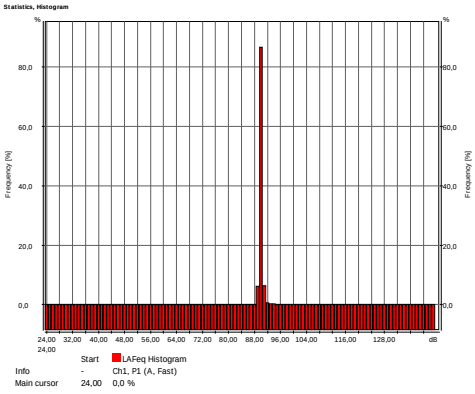

Fig. 19 *Example of graphical form of statistics logger associated to the noise measurement of noise of cement mill.*

Table 10 *Measurement results for K_I and kurtosis for the example of metalworking with hand tools.*

Source	L_{pAIeq}	K_I	kurtosis
Hand tools metalworking	89,5	0,8	6,3

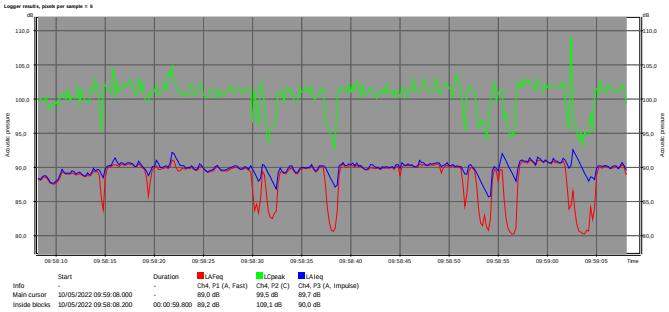

Fig. 20 *Example of noise measurement* of *noise of metalworking with hand tools where K_I is low (quasi-impulsive noise) and kurtosis of the high level. In red is equivalent noise level, in blue AI-weighted sound pressure level and in green C-weighted peak sound pressure level. One can see „negative peak“ noise pattern.*

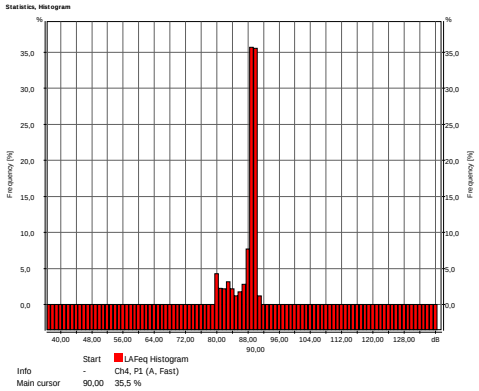

Fig. 21 *Example of graphical form of statistics logger associated to the noise measurement of noise of* metalworking with hand tools.

4. CONCLUSION

A sample of 140 various noise exposures measured in situ in industry where impulsive noise appearing were analysed and the common indicators of impulsiveness of the sample were compared and correlated to kurtosis, the indicator that seems to hold promise for the quantitative prediction of hearing loss in exposures to impulsive noise. The main finding is that the impulsive adjustment for the impulsive noise, K_I, strongly correlates to kurtosis, at the significance level of 0,01, whilst other indicators do not significantly. Some correlation to kurtosis for C-weighted peak sound pressure level is confirmed for some subsamples of noise at lower significance levels. However, this may partly be due to sample selection. This favors the assumption that both indicators, K_I and kurtosis, could be the adequate measures of the same property, impusiveness, and therefore according to the recent research, predictors of the risk of hearing damage by impusiveness in addition to the equivalent noise level. The other indicators as C-weighted peak sound pressure level and crest factor seem not to corelate to kurtosis significantly and therefore there is no evidence (at least by the results here reported and thus defined) that they correlate to the eventual additional risk.

Further, while waiting for the right metrics that is expected to be the function of kurtosis, some sugestions for the impulsive noise hearing damage hazards prevention may be made. The classification is suggested based on relation of the level of the impulsive adjustment for the impulsive noise, K_I, and corresponding kurtosis. Where both values are shown to be significant, it is it is strongly advisable to be taken into account the additional risk of hearing damage due to impulsiveness. Special attention needs to be paid in cases where K_I is neglectable and kurtosis large, that is, when it could be possible that potentional damaging effect of impulsive noise goes under the radar.

REFERENCES

[1] A. Lie et al. “Occupational noise exposure and hearing: a systematic review”, *Int Arch Occup Environ Health* 89:351–372, 2016.

[2] Starck J, Toppila E, Pyykko I. “Impulse noise and risk criteria”, *Noise Health* 5:63-73, 2003.

[3] Davis RI, Qiu W, Heyer NJ, Zhao Y, Qiuling Yang M S, Li N, Tao L, Zhu L, Zeng L, Yao D. “The use of the kurtosis metric in the evaluation of occupational hearing loss in workers in China: Implications for hearing risk assessment”, Noise Health 2012;14:330-42.

[4] R. P. Hamernik, W. Qiu and B. Davis “The effects of the amplitude distribution of equal energy exposures on noise-induced hearing loss: The kurtosis metric”, *J. Acoust. Soc. Am.* 114, 386–395, 2003.

[5] J. Erdreich “Distribution based definition of impulse noise,” *J. Acoust. Soc. Am.* 77, S19–S19, 1985.

[6] ISO 12001:1996, SRPS EN ISO 12001:2009 Acoustics -- Noise emitted by machinery and equipment -- Rules for the drafting and presentation of a noise test code

[7] Miočinović, J. and Beljić Durković, B. “Industrial impulsive noise and hearing: evaluation according to the regulations and applicable standards and possible additional risk on hearing comparing to the effect of steady noise”, *26th International Conference Noise and Vibration*, Niš, 2018.

[8] DIN 45645-2: 2012 Determination of rating levels from measurement data — Part 2: Determination of the noise rating level for occupational activities at the work place for the level range underneath the given risk of hearing damage.

[9] ISO 9612: 1997, SRPS ISO 9612:2008 Acoustics — Guidelines for the measurement and assessment of exposure to noise in a working environment.

[10] An online calculator, https://www.socscistatistics.com/pvalues/tdistribution.aspx.

[11] Chapter 12.5: Testing the Significance of the Correlation Coefficient, in: https://stats.libretexts.org/Bookshelves/Introductory_Statistics

LABORATORIJA ZA BUKU I VIBRACIJE

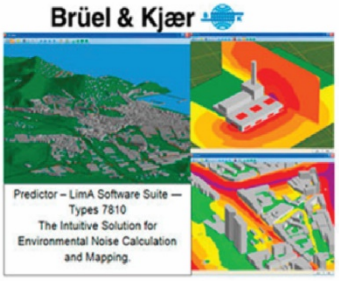

LABORATORY FOR NOISE AND VIBRATION

University of Nis
Faculty of Occupational Safety
„Politechnica“ University of Timisoara
Faculty of Mechanical Engineering
27th International Conference
NOISE AND VIBRATION
Niš, 20 - 21. 10. 2022.

ANALYSIS OF CRITERIA FOR DETERMINING THE RATING EQUIVALENT CONTINUOUS SOUND PRESSURE LEVEL

Darko Mihajlov[1], Momir Prascevic[1], Marko Licanin[1]

[1] University of Nis, Faculty of Occupational Safety, Serbia
e-mail: darko.mihajlov@znrfak.ni.ac.rs

Abstract - *Rating equivalent continuous sound pressure level is a noise indicator that is frequently used to describe and assess environmental noise. In order to identify the variety and significance of specific national criteria used to determine it, this paper provides a comparative analysis of the obtained results and highlights the outcome of various methodologies for calculating this size in Serbia, Croatia, and Great Britain.*

1. INTRODUCTION

Noise is associated with human response and is defined as unwanted sound, i.e. sound that is considered undesirable or disruptive when being engaged in typical human activities.

One of the global goals to address environmental noise issues in the European Union is a unique approach of all member countries through the joint application of appropriate ISO standards and the harmonization of national environmental noise regulations [1]. By doing this, the groundwork is laid for the development of a European strategy for noise pollution reduction, its incorporation into national regulations, and, ultimately, the implementation of adequate noise control measures.

Noise in the environment originates from individual noise sources or any combination thereof.

If the noise exhibits particular specific temporal and frequency characteristics, then the basic quantity for describing and evaluating noise must be Rating equivalent continuous sound pressure level (further: rating level, $L_{\mathrm{Req},T}$). Noise assessment is performed by comparing the calculated value of the rating level with the limit values of the environmental noise indicators [1].

The upper limits for environmental noise indicators are determined by competent national institutions based on their understanding of how noise affects human health, and social and economic factors. In this sense, the following factors are taken into account: the time of day, the intended use of the residential space (open and closed space), the type of noise source, different situations (such as construction works in settlements), etc. The limit values of the noise indicator for the same cases and acoustic zones may vary across countries due to differences in national regulations.

In a mathematical sense, the rating level represents the adjusted equivalent continuous sound pressure level and is calculated as follows [2]:

$$L_{\mathrm{Req},T} = L_{\mathrm{Aeq},T} + K\,, \tag{1}$$

where:

- T - measurement time interval (time interval during which measurements are conducted) [3];
- $L_{\mathrm{Aeq},T}$ - equivalent continuous sound pressure level;
- K - adjustment (quantity, positive or negative, constant or variable, that is added to a predicted or measured acoustical level to account for some sound character, the time of day, or the source type) [2].

For adjustments that relate to the character of the sound, these adjustments shall only be applied during the time that the specific character is present [2].

Different methodological approaches and the use of additional criteria to more accurately assess the state of noise in the environment and its impact on the exposed population yield different results while determining the rating level in individual countries.

Special consideration is given to the size of the *reference time interval* (time interval to which the sound rating is referred) as it has a significant impact on the value of the rating level. The reference time interval may be specified in national or international standards or by local authorities to cover typical human activities and variations in the operation of sound sources. Reference time intervals can be, for example, part of a day, the full day, or a full week [2].

2. RATING LEVELS AND NOISE ASSESSMENT METHODOLOGIES: EXAMPLES IN CERTAIN COUNTRIES

The paper discusses the methodologies for determining the rating level in three countries: the Republic of Serbia, which is an EU accession member, the Republic of Croatia, which is an EU member state, and Great Britain, which is a former EU member state and whose regulations in the subject area are based on ISO standards and regulations EU.

2.1 Methodology for determining the rating level and noise assessment in Serbia

The Regulation specifies environmental noise indicators, noise indicator limit values, and methods for determining noise indicators [4].

According to the Regulation, rating level is a noise indicator used for noise monitoring and noise originating from individual (specific) noise sources.

The national standards SRPS ISO 1996-1 [5] and SRPS ISO 1996-2 [6] determine rating levels and adjustments for sounds in the manner specified by the expression (1).

In the context of this regulation, a 24-hour period is divided into three *reference time intervals*: a day lasts 12 hours (from 6 am to 6 pm); *evening* lasts 4 hours (from 18:00 to 22:00); *night* lasts 8 hours (from 10 pm to 6 am).

If there is only one source of noise with only one mode of operation, and no tonal or impulse character to the noise, the following formula is used to determine the rating level for specific reference time intervals:

$$L_{\mathrm{Req},Td} = 10\log\left(\frac{t_{d,total}}{T_d}10^{L_{d,total}/10} + \frac{t_{d,res}}{T_d}10^{L_{d,res}/10}\right), \quad (2)$$

$$L_{\mathrm{Req},Te} = 10\log\left(\frac{t_{e,total}}{T_e}10^{L_{e,total}/10} + \frac{t_{e,res}}{T_e}10^{L_{e,res}/10}\right), \quad (3)$$

$$L_{\mathrm{Req},Tn} = 10\log\left(\frac{t_{n,total}}{T_n}10^{L_{n,total}/10} + \frac{t_{n,res}}{T_n}10^{L_{n,res}/10}\right), \quad (4)$$

gde su:

- $L_{\mathrm{Req},Td/e/n}$ - rating levels for reference time intervals *day*, *evening* and *night*, respectively;
- $L_{d/e/n,total}$ - equivalent continuous sound pressure level of total sound for reference time intervals *day*, *evening* and *night*, respectively [2];
- $L_{d/e/n,res}$ - equivalent continuous sound pressure level of residual sound for reference time intervals *day*, *evening* and *night*, respectively [2];
- T_d = 12 h - reference time interval *day*;
- T_e = 4 h - reference time interval *evening*;
- T_n = 8 h - reference time interval *night*;
- $t_{d/e/n,total}$ - duration of total noise during the day/evening/night;
- $t_{d/e/n,res}$ - duration of residual noise during the day/evening/night ($t_{d/e/n,res} = T_{d/e/n} - t_{d/e/n,total}$);

This approach to determining the rating level yields reliable results if all changes in the operation of all sound sources during the measurement are taken into account, that is, if the measurement time interval is as close to the reference time interval as possible. In practice, this procedure is very difficult to implement because it requires a lot of commitment and is dependent on the choice and duration of the measurement time interval.

The noise rating is a comparison between the calculated rating level values and the prescribed limit values of the rating level of total noise in an open space (for five acoustic zones) and in closed rooms used for various purposes [4].

2.2 Methodology for determining the Rating level and noise assessment in Croatia

The Regulation specifies the maximum permissible noise levels, taking into account the type of noise source, time, and place of origin [7].

The national standard HRN ISO 1996-1 [8] defines basic sizes, concepts and procedures for assessing noise in the sense of this Procedure, while the national standard HRN ISO 1996-2 [9] defines the methods for calculating sound pressure level.

The provisions of the Regulation apply to the time intervals *day*, *evening and night*, as well as to the all-day interval *day-evening-night*. The beginning, end, and duration of time intervals are determined by a special regulation in the field of noise protection.

Rating levels are determined in the same manner as in the Republic of Serbia, using time intervals *day*, *evening and night* as reference time intervals. The duration of individual measurements and the total number of measurements depend on the nature of specific and residual noise.

For each of the five acoustic zones, the limit values of the rating level for specific time intervals are defined. Limit values refer to the level of total noise originating from the combined emission of all currently existing and future noise sources.

The Regulation also prescribes the limit values of the rating levels for certain time intervals in closed residence rooms according to acoustic zones [7].

2.3 Methodology for determining the Rating level and noise assessment in Great Britain

British Standard 4142 [10] is one of the most widely used UK standards for the assessment of environmental noise.

The main concepts of BS 4142 are as follows:

- Make measurements of all noise at the assessment location, including the "problem" noise, in terms of L_{Aeq} - termed *the ambient noise level*;
- A measurement is then made of all the noise excluding the "problem" noise in terms of both L_{Aeq} and L_{A90}; these measurements are termed *the residual* and *background noise levels* respectively;
- The *residual* L_{Aeq} *measurement* is then subtracted (logarithmically) from *the ambient* L_{Aeq} *measurement* to produce the noise level produced by the "problem" noise alone - termed *the specific noise level*.

The duration of measurement or number of sample periods will depend on how stable the source and background noise is.

The *reference time interval* is the period over which a representative ambient and residual L_{Aeq} is to be estimated. The measurement time needn't be the same as the reference time interval.

A different reference time interval is defined for *day* and *night*:

- Day (7 am to 11 pm): 1 hour;
- Night (11 pm to 7 am): 15 mins.

This makes a difference to any "on-time" correction for sound sources that are intermittent and so are not on for the duration of the reference interval.

An extensive body of noise legislation exists governing statutory nuisance in Great Britain [11]: industrial noise, transport noise, etc. There are no legislated national limits, however, there are many guidance documents including national standards, and additional local procedures are in place [12,13,14].

3. ANALYSIS OF DIFFERENT NOISE ASSESSMENT APPROACHES

Due to the possibility of different noise ratings for the same operating conditions of the source, in terms of whether the rating level is lower or higher than the limit values, this paper determines the rating levels using the same methodology as in Serbia, and Croatia and Great Britain; afterward, the obtained values are compared with limit values of the rating levels in Serbia [4] and Croatia [7], and the evaluation is carried out.

The situation being observed is the effect of noise from machinery in a furniture workshop on nearby residential areas [15]. Measurements of $L_{\mathrm{Aeq},T}$ for residual noise and total/ambient noise, which includes residual noise and noise from specific machines in the workshop, were performed in the open space and in the residential space for testing purposes. Noise level measurements were repeated at least three times for each different way the noise source was operating, with a measurement time interval of T = 15 mins. Following this, the measured average noise levels were calculated.

Elements for calculating rating levels at receiver location 1 - open space, $L_{\mathrm{Req1,12h}}$, and receiver location 2 – residential space, $L_{\mathrm{Req2,12h}}$, according to requirements in Serbia and Croatia:

- Duration of reference time interval: T_{ref} = 12 h;
- Average estimated duration of the first production phase during working hours: t_1 = 2 h;
- Average equivalent level of total noise at the receiver location 1 during the first production phase: $L_{\mathrm{Aeq1,1}}$ = 51.3 dB;
- Average equivalent level of total noise at the receiver location 2 during the first production phase: $L_{\mathrm{Aeq2,1}}$ = 24.0 dB;
- Estimated average duration of the second stage of production during working hours: t_2 = 2 h;
- Average equivalent level of total noise at the receiver location 1 during the second stage of production: $L_{\mathrm{Aeq1,2}}$ = 49.9 dB;
- Average equivalent level of total noise at the receiver location 2 during the second stage of production: $L_{\mathrm{Aeq2,2}}$ = 24.9 dB;
- Estimated average duration of the third stage of production during working hours: t_3 = 2 h;
- Average equivalent level of total noise at the receiver location 1 during the third stage of production: $L_{\mathrm{Aeq1,3}}$ = 44.0 dB;
- Average equivalent level of residual noise at the receiver location 2 during the third stage of production: $L_{\mathrm{Aeq2,3}}$ = 19.4 dB;
- Estimated average time required for preparations prior to the start of each production phase, without the use of specific noise sources: t_{pa} = 1 h;
- Total duration of breaks during working hours: t_{p} = 1 h;
- Estimated average duration of residual noise during the reference time interval: t_{res} = 6 h;
- Average equivalent level of residual noise at the receiver location 1: $L_{\mathrm{Aeq1,res}}$ = 44.1 dB;
- Average equivalent level of residual noise at the receiver location 2: $L_{\mathrm{Aeq2,res}}$ = 19.6 dB;
- Equivalent noise level correction for tonal character: K_{T} = 5 dB.

Rating levels were calculated for receiver locations 1 and 2 in accordance with Serbian and Croatian regulations, taking into account the duration and nature of noise in specific circumstances:

$$L_{\mathrm{Req1,12h}} = 10\log\left(\begin{array}{l}\frac{t_1}{12}\cdot 10^{0.1\left(L_{\mathrm{Aeq1,1}}+K_{\mathrm{T}}\right)}+\\ +\frac{t_2}{12}\cdot 10^{0.1\left(L_{\mathrm{Aeq1,2}}\right)}+\\ +\frac{t_3}{12}\cdot 10^{0.1\left(L_{\mathrm{Aeq1,3}}\right)}+\\ +\frac{t_{res}}{12}\cdot 10^{0.1\left(L_{\mathrm{Aeq1,res}}\right)}\end{array}\right) = 50.2\,\mathrm{dB} \quad (5)$$

$$L_{\mathrm{Req2,12h}} = 10\log\left(\begin{array}{l}\frac{t_1}{12}\cdot 10^{0.1\left(L_{\mathrm{Aeq2,1}}\right)}+\\ +\frac{t_2}{12}\cdot 10^{0.1\left(L_{\mathrm{Aeq2,2}}\right)}+\\ +\frac{t_3}{12}\cdot 10^{0.1\left(L_{\mathrm{Aeq2,3}}\right)}+\\ +\frac{t_{res}}{12}\cdot 10^{0.1\left(L_{\mathrm{Aeq2,res}}\right)}\end{array}\right) = 21.9\,\mathrm{dB} \quad (6)$$

Since noise assessment in Great Briatin is based on data on the values of various noise levels, the following information is significant in the situation examined in this paper.

- The first stage of production requires the greatest number of machines, which typically operate simultaneously; Estimated average duration of the first stage of production during working hours: t_1 = 2 h;
- Reference time interval for *day*: T_{ref} = 1 h;
- Average equivalent level of ambient noise at the receiver location 1 (during the first stage of production): $L_{\mathrm{Aeq1,1}}$ = 51.3 dB;
- Average equivalent level of residual noise at the receiver location 1: $L_{\mathrm{Aeq1,res}}$ = 44.1 dB;
- Average equivalent level of background noise at the receiver location 1: $L_{\mathrm{A90,1}}$ = 39.6 dB;
- Average equivalent level of ambient noise at the receiver location 2 (during the first stage of production): $L_{\mathrm{Aeq2,2}}$ = 24.0 dB;

- Average equivalent level of residual noise at the receiver location 2: $L_{Aeq2,res}$ = 19.6 dB;
- Average equivalent level of background noise at the receiver location 2: $L_{A90,2}$ = 17.6 dB;

According to Croatian regulations [7], the area where the workshop and residential space are located is in the second acoustic zone, with a maximum daily rating level of 55 dB in the open space. According to Serbian regulations [4], the aforementioned area is classified as being in the third acoustic zone, which also set a daily limit of 55 dB for the rating level in open spaces. The limit value of the rating level in the residential space during the day is 35 dB for the given case in both Serbia and Croatia.

By comparing the calculated rating level values to the prescribed limit values in Serbia and Croatia, it is concluded that the total noise rating levels in the open space and the residential area do not exceed the prescribed limit values.

4. CONCLUSION

For the same purpose of residential space, different methodologies for determining the rating level and different limit values of the rating level in some countries can yield different conclusions regarding whether the rating level is lower or higher than the recommended limit values. If the limit values are exceeded, it is necessary to take measures to reduce the rating level. These measures can include changing the mode of operation of the source of specific noise, limiting the duration of specific noise operation, and, in the worst-case scenario, prohibiting its use. The aforementioned measures highlight the significance of establishing criteria for determining rating levels and threshold values. With the goal of providing equal protection to the population from environmental noise pollution, it is desirable to harmonize national regulations in this area and define a unique system of measures for the remediation of environmental noise pollution caused by specific sources. Preventive measures to stop environmental noise pollution include defining the circumstances under which specific noise sources can be used, including the type of source, the environment (use of space) in which they are located, the amount of time for the work during the day, the level of noise emission, and other factors.

ACKNOWLEDGEMENT

The authors acknowledge the support of Ministry of Education, Science and Technology Development of Republic of Serbia to its institution through grant No. 451-03-68/2022-14/200148.

REFERENCES

[1] EU, Directive 2002/49/EC of the European Parliament and of the Council of 25 June 2002 relating to the assessment and management of environmental noise (OJ L 189, 18.7.2002), 2002.

[2] International Organization for Standardization. (2016). *Acoustics - Description, measurement and assessment of environmental noise - Part 1: Basic quantities and assessment procedures* (ISO Standard No. 1996-1:2016).

[3] International Organization for Standardization. (2017). *Acoustics - Description, measurement and assessment of environmental noise - Part 2: Determination of sound pressure levels* (ISO Standard No. 1996-2:2017).

[4] Ministry of Environmental Protection of the Republic of Serbia. (2010). *Regulation on noise indicators, limit values, methods for rating noise indicators, disturbance and harmful effects of noise in the environment*. Official Gazette of the Republic of Serbia, No. 75/2010.

[5] Institute for Standardization of Serbia. (2019). *Acoustics - Description, measurement and assessment of environmental noise - Part 1: Basic quantities and assessment procedures* (SRPS ISO Standard No. 1996-1:2019).

[6] Institute for Standardization of Serbia. (2019). *Acoustics - Description, measurement and assessment of environmental noise - Part 2: Determination of sound pressure levels* (SRPS ISO Standard No. 1996-2:2019).

[7] Ministry of Health of the Republic of Croatia. (2021). *Rulebook on the highest permissible noise levels with regard to the type of noise source, time and place of occurrence*. NN 143/2021.

[8] Croatian Institute for Standards. (2016). *Acoustics - Description, measurement and assessment of environmental noise - Part 1: Basic quantities and assessment procedures* (HRN ISO Standard No. 1996-1:2016).

[9] Croatian Institute for Standards. (2017). *Acoustics - Description, measurement and assessment of environmental noise - Part 2: Determination of sound pressure levels* (HRN ISO Standard No. 1996-2:2017).

[10] The British Standards Institution. (2019). *Methods for rating and assessing industrial and commercial sound* (BS Standard No. 4142:2014+A1:2019).

[11] European Network of the Heads of Environment Protection Agencies (EPA Network), EPA Network Interest Group on Noise Abatement (IGNA). (2019). *Overview of critical noise values in the European Region*. Report No. M+P.BAFU.18.01.1

[12] See https://www.gov.uk/government/publications/noisepolicy-statement-for-england

[13] See http://www.legislation.gov.uk/uksi/2006/2238/contents/made

[14] See https://www.gov.uk/government/publications/resistance-to-sound-approved-document-e

[15] University of Nis, Faculty of Occupational Safety, Report No. 01/03-31/18, 2019.

University of Nis
Faculty of Occupational Safety
„Politechnica“ University of Timisoara
Faculty of Mechanical Engineering
27th International Conference
NOISE AND VIBRATION
Niš, 20 - 21. 10. 2022.

ENVIRONMENTAL NOISE IN THE CITY STREETS ZONE IN NOVI SAD BEFORE AND DURING THE STATE OF EMERGENCY DUE TO COVID-19

Emil Živadinović[2], Marija Jevtić[1,2], Sanja Bijelović[1,2], Nataša Dragić[1,2], Maja Lazović[2], Siniša Milošević[2], Živojin Lalović[2]

[1] University of Novi Sad, Faculty of Medicine, Novi Sad, Serbia
[2] Public Health Institute of Vojvodina, Novi Sad, Serbia, emil.zivadinovic@izjzv.org.rs, +381641720433

Abstract - *Noise is a physical hazard to the environment, and it causes adverse effects on human health. Noise ranks third among all environmental risk factors. Since 2011, the experts from the Public Health Institute of Vojvodina (PHIV) have conducted 24-hour outdoor environmental noise measurements and directly determined the values of basic noise indicators (L_{day}, $L_{evening}$, L_{night}, L_{den}), and also the value of L_{90}, a parameter recognized in the literature as residual or background noise level. During the state of emergency caused by the COVID-19 epidemic (15.03 - 06.05.2020), a few 24-hour noise measurements in the City of Novi Sad were conducted in March, in conditions of reduced traffic and normal human activities, in impossible situations to have on regular occasions. During the state of emergency, there were lower values of basic noise indicators. The background noise level (L_{90}) and the total noise indicator (L_{den}) decreased by 27%, i.e., 4%, in March 2020 compared to average values for the previous ten months. The significantly higher decline of the background noise level concerning the total noise recognizes traffic as the dominant noise source in the city. It recognizes the importance of managing local noise sources (sirens, for example) in urban areas. The results acknowledge the importance of monitoring both the temporal and frequency characteristics of noise to understand the exposure of the population and the health impacts.*

1. INTRODUCTION

Environmental noise is unwanted / harmful outdoor sound created by human activities, including noise emitted by means of transport, road traffic, rail traffic, air traffic, and from sites of industrial activity, and also cause adverse effect to human health [1,2,3]. The effects could be on the hearing system - the auditory effect of noise and on other organs and organic systems - the extraaudititive noise effect. It is known that environmental noise has effects on sleep, annoyance, cognitive impairment, cardiovascular disease, hearing impairment, tinnitus, adverse birth outcomes and mental health and wellbeing [4]. World Health Organization (WHO) indicates that more than one million healthy years of life are lost every year from road traffic-related noise in the west Europe [5]. Also, noise pollution is a major environmental health problem in Europe, road traffic is the most dominant source of environmental noise with an estimated 125 million people affected by noise levels greater than 55 dB L_{den} [6].

In one Serbian cross sectional interview study, it is showed that highly noise disturbed adult male residents were under increased risk of arterial hypertension and myocardial infarction, compared to subjects slightly annoyed, or not annoyed by noise [7]. During 2006, the average daytime noise of 69 dB in the City of Novi Sad was a contributing factor to the burden of ischemic heart diseases in 14% of cases [8]. Another study has identified the presence of public transport at daytime and at night as a significant and independent predictor of high noise annoyance [9].

Recent studies on long term noise exposure, especially night noise ≥55 dB, have reported relationship with pathogenesis of male infertility. Large epidemiological studies on community noisehave reported its relationship with breast cancer, stroke, type 2 diabetes, and obesity [10]. Further research is needed to examine coping strategies and possible health consequences of adaptation to noise [11].

The aim of this paper was to determine if the traffic changed during the time period 15. 03 - 06. 05. 2020, i.e. during the state of emergency („lockdown“) due to the COVID-19 pandemic in the City of Novi Sad, affected the level of total (L_{den}), i.e. the level of background (L_{90}) noise indicators.

The limitation of this research because, in that period, *PHIV* performed only one measurement at representative points in the city center zone and city roads, residential area and industrial zone.

2. METHODOLOGY

The national legal basis defines the allowed environmental noise level, noise measurement methods, conditions for noise measurement organizations and content of noise sources documents.

PHIV as authorized and accredited institution (SRPS ISO/IEC 17025:2017, SRPS ISO 9001:2015, SRPS ISO 14001:2015) performed environmental noise monitoring in the city according to standardized methodology [12,13] and due to legal and proffesional basis [14,15,16,17,18,19]. Since 2011, PHIV determined the basic noise indicators - indicators of daily, evening, night and overall noise (L_{day}, L_{den}, $L_{evening}$, L_{night}) (an indicator is a physical value that describes environmental noise, which is associated with adverse influence on human health) and also background noise, i.e. the noise that is always present, recognized in the literature as L_{90} [20].

The City of Novi Sad is the largest city in the AP Vojvodina, Serbia. The City is administrative, cultural, scientific, medical, university and political center center, almost 400.000 of people is exposed to the environmental noise levels shown in this paper.

Fig. 1 *The City of Novi Sad*

The measuring system that PHIV used in environmental noise monitoring is: Brüel&Kjær (BK) type 2250, BK type 3535-A (all weather suitcase), BK Outdoor Microphone type 4952, BZ 5503 Utility Software, Noise Explorer Type 7815 and KIMO AMI 300 for microclimate measurements.

3. RESULTS

In this paper were discussed the results of environmental noise measurements at representative measuring points in the City of Novi Sad during the period April / May 2019 - March 2020, in the city center and city streets zone ("Corner of Bulevar oslobodenja and Futoška Street"), residential area ("Narodnog fronta 42, Liman IV, "Maslačak") and the industrial zone ("Near Nylon Market, Temerinski put 1") (Tables 1 - 3).

It should be noted that a few noise measurements during the time period 15. 03 - 06. 05. 2020, i.e. „lockdown“ due to the COVID-19 pandemic, were made in conditions of traffic restriction from the afternoon until the early hours of the morning, i.e. in conditions of significantly reduced night traffic.

Table 1 *Data for city center and city streets zone ("Corner of Bulevar oslobodenja and Futoška Street"), May 2019 – March 2020*

Date of measurement	L_{90}	L_{den}
May 2019	47,7	70,5
June 2019	48,9	68,2
July 2019	45,8	69,6
August 2019	55,1	74,3
September 2019	53,4	74,2
October 2019	59,3	74,5
November 2019	58,2	73,2
December 2019	55,8	76,8
January 2020	55,3	74,6
February 2020	57,7	72,9
19.3.2020	39,0	70,2
Average value / May 2019 - February 2020	53,7	72,9
Value / March 2020	39,0	70,2
Percentage reduction	**27,40%**	**3,68%**

Table 2 *Data for residential area ("Narodnog fronta 42, Liman IV, "Maslačak"), April 2019 – March 2020*

Date of measurement	L_{90}	L_{den}
April 2019	43,7	62,3
May 2019	43,4	62,3
June 2019	43,0	62,0
July 2019	44,7	61,0
August 2019	44,0	59,8
September 2019	43,0	65,4
October 2019	43,3	61,5
November 2019	41,9	61,6
December 2019	41,8	63,3
January 2020	44,6	61,5
February 2020	41,7	64,2
31.3.2020	30,7	50,8
Average value / april 2019 - february 2020	43,2	62,3
Value / Mach 2020	30,7	50,8
Percentage reduction	**28,92%**	**18,41%**

Table 3 *Data for industrial zone ("Near Nylon Market, Temerinski put 1"), April 2019 – March 2020*

Date of measurement	L_{90}	L_{den}
April 2019	43,5	64,7
May 2019	43,9	65,7
June 2019	45,9	65,4
July 2019	41,7	64,3
August 2019	49,2	65,6
September 2019	46,6	66,4
October 2019	46,0	67,3
November 2019	45,2	67,3
December 2019	48,2	68,6
January 2020	44,0	69,8
February 2020	46,5	66,6
21.3.2020	33,5	65,0
Average value / april 2019 - february 2020	45,5	66,5
Value / March 2020	33,5	65,0
Percentage reduction	**26,40%**	**2,28%**

The percentage reduction of background noise (L_{90}) during the state of emergency in 2020, compared to the previous one-year period, was 27.40% in the city center and city streets zone, 28.92% in the residential area and 26.40% in the industrial zone.

The percentage reduction of the total noise indicator (L_{den}) during the state of emergency in 2020, compared to the previous one-year period, was 3.68% in the city center and city streets zone, 18.41% in the residential area and 2.28% in the industrial zone.

4. CONCLUSION

The reduction of traffic and usual human activities in the City of Novi Sad during the state of emergency („lockdown“) in 2020 due to the COVID-19 pandemic affected the reduction of environmental noise, especially the level of background noise, i.e. the noise that is always present, recognized in the literature as L_{90}.

Based on a few noise measurements in the conditions of „lockdown“, at a time of reduced normal human activities, it can be concluded that the background noise level was reduced by a third.

The reduction of background noise level originating mainly from traffic (which was present during the daytime period in the conditions of „lockdown“) indicates the significant contribution of night noise in the City of Novi Sad.

AKNOWEGDMENTS

This paper was supported by the Ministry of Education and Science of the Republic of Serbia throught the Project "Biosensing Technologies and Global System for Continues Research and Integrated Management" No. 43002

REFERENCES

[1] The European Parliament and The Council, "Directive 2002/49/EC" (Official Journal of the European Communities, 2002).

[2] E. Zivadinovic, S. Bijelovic, N. Dragic, M. Popovic, S. Milosevic, Z.Lalovic, "Highly Annoyed People With Noise in The city of Novi Sad" (14th DKMT Euroregional Conference on Environment and Health, Abstract of papers and posters in electronic form) (M34) (Szeged, Hungary, May 18-19, 2012).

[3] E. Zivadinovic, S. Bijelovic, N. Dragic, M. Popovic, S. Milosevic, Z. Lalovic, "Environmental Noise As The Hazard In The Environment of The City Of Novi Sad", (23rd National Conference & 4th International Conference Noise And Vibration) (Niš, Serbia, October 17-19, 2012).

[4] WHO Environmental noise guidelines for the European Region. Copyright©(2015) by EAA-NAG-ABAV, ISSN 2226-5147. Available on http://www.na-paw.org/WHO-noise-guidelines-Euronoise-2015.pdf

[5] World Health Organization, Regional Office for Europe and JRC European Commission, "Burden of disease from environmental noise". Quantification of healthy life years lost in Europe. (WHO, Geneva, 2011). Available on http://www.euro.who.int/__data/assets/pdf_file/0008/136466/e94888.pdf

[6] Noise in Europe 2014. © European Environment Agency, 2014 (EEA). ISBN 978-92-9213-505-8. ISSN 1977-8449

[7] Belojević G, Sarić-Tanasković M. Prevalence of Arterial Hypertension and Myocardial Infarction in Relation to SubjectiveRatings of Traffic Noise Exposure. Noise Health. 2002;4(16):33-37.

[8] Bijelović S. Činioci životne sredine kao pokazatelji uticaja na zdravlje ljudi. Doktorska disertacija. Medicinski fakultet Univerziteta u Novom Sadu, 2011.

[9] Paunović K, Belojević G, Jakovljević B. Noise annoyance is related to the presence of urban public transport. Sci total environ. 2014 may 15;481:479-87. Doi: 10.1016/j.scitotenv.2014.02.092. Epub 2014 mar 12.

[10] Belojević G, Paunović K. Recent Advances In Research On Non-Auditory Effects Of Community Noise. Srp Arh Celok Lek. 2016 JAN-FEB;144(1-2):94-8.

[11] Stansfeld SA, Matheson MP. Noise pollution: non-auditory effects on health. Br Med Bull. 2003;68:243-57.

[12] SRPS ISO 1996-1:2019 "Acoustics – Description, measurement and estimation of noise in environment – Part 1: Basic units and estimation methods" (Institute for Standardization of Serbia, Belgrade, 2010).

[13] SRPS ISO 1996-2:2019, "Acoustics – Description, measurement and estimation of noise in environment – Part 2: Determination of the noise level in environment" (Institute for Standardization of Serbia, Belgrade, 2010).

[14] National Assemby of the Republic of Serbia, "Law on environmental care" (Official Gazette of RS No 135/04 and 36/09, 2009).

[15] National Assemby of the Republic of Serbia, "Law on environmental noise protection" (Official Gazette of RS", no. 36/2009 and 88/10, 2010).

[16] National Assemby of the Republic of Serbia, "Law on public health" (Official Gazette of RS RS No 72/09, 2009).

[17] Serbian Government, "Regulation on noise indicators, limit values, assessment methods for indicators of noise, disturbance and harmful effects of noise in the environment" (Official Gazette of RS, no. 75/2010, 2010).

[18] Republic of Serbia, Ministry of Environmental Protection and Sppatial Planing, "Rulebook on the methodology for action plans development" (Official Gazette of RS, no. 72/2010, 2010).

[19] Republic of Serbia, Ministry of Environmental Protection and Sppatial Planing, "Rulebook on noise measurement methods, contents and scope of noise measurement reports" (Official Gazette of RS, no. 72/2010, 2010).

[20] Abiodun, & O.T., Oyelola & Popoola, Oluseun & Babatunde, & Technology, Yaba & Yaba, & Akoka, & Lagos,. (2011). Assessing noise levels in a commercial and industrial centres of Lagos Metropolis. Continental J. Water, Air and Soil Pollution. 2. 1-11.

Акредитационо тело Србије **01965**
Accreditation Body of Serbia

Београд
Belgrade

додељује
awards

СЕРТИФИКАТ О АКРЕДИТАЦИЈИ
Accreditation Certificate

којим се потврђује да тело за оцењивање усаглашености
confirming that Conformity Assessment Body

Универзитет у Нишу
Факултет заштите на раду у Нишу
Центар за техничка испитивања
Ниш

акредитациони број
accreditation number

01-393

задовољава захтеве стандарда
fulfils the requirements of

SRPS ISO/IEC 17025:2017
(ISO/IEC 17025:2017)

те је компетентно за обављање послова испитивања
and is competent to perform testing activities

који су специфицирани у важећем издању Обима акредитације
as specified in the valid Scope of Accreditation

Важеће издање Обима акредитације доступно је на интернет адреси: www.ats.rs
Valid Scope of Accreditation can be found at: www.ats.rs

Акредитација додељена
Date of issue
21.05.2021.

Акредитација важи до
Date of expiry
20.05.2025.

ATC

ВД ДИРЕКТОРА
проф. др Ацо Јанићијевић

Acting Director
prof. Aco Janićijević, PhD

Акредитационо тело Србије је потписник Мултилатералног споразума о признавању еквивалентности система акредитације Европске организације за акредитацију (EA MLA) и ILAC MRA споразума у овој области. / ATS is a signatory of the EA MLA and ILAC MRA in this field.

University of Nis
Faculty of Occupational Safety
„Politechnica“ University of Timisoara
Faculty of Mechanical Engineering
27th International Conference
NOISE AND VIBRATION
Niš, 20 - 21. 10. 2022.

IMPACT OF THE COVID-19 PANDEMIC ON POPULATION NOISE EXPOSURE IN THE VICINITY OF SARAJEVO AIRPORT

Nermin Zijadić[1], *Emir Ganić*[2]

[1] International Airport Sarajevo, Kurta Schorka 36, Sarajevo, Bosnia and Herzegovina, nermin.zijadic@gmail.com
[2] University of Belgrade, Faculty of Transport and Traffic Engineering, Vojvde Stepe 305, Belgrade, Serbia, e.ganic@sf.bg.ac.rs

Abstract - *Air traffic noise is one of the primary environmental issues confronting modern airports, and it is likely to remain a limiting factor in airport development in the future. Air traffic has been severely disrupted since the COVID-19 pandemic began in 2020. Nonetheless, airport authorities continue to address the negative impact of aircraft noise on the environment and the population despite the temporary reduction in noise exposure. The aim of this paper is to evaluate how much the COVID-19 pandemic has influenced the exposure of the population to aircraft noise in the vicinity of Sarajevo Airport. The number of highly annoyed and highly sleep-disturbed people during 2020 is compared to the same indicators from 2019 when the air traffic was not affected by the COVID-19 pandemic. The results indicated that the decrease in the number of take-off and landing operations of 64.3% lead to a reduction of the estimated number of people highly annoyed by aircraft noise by 57% in 2020 compared to 2019, while the estimated number of people highly sleep disturbed decreased by 63%.*

1. INTRODUCTION

Airports and air traffic in general have a negative impact on the environment as a result of aircraft pollutants, such as exhaust gases and noise. Nevertheless, along with the abovementioned externalities, there are numerous benefits of air traffic to the society. The aviation sector not only contributes significantly to the socio-economic development of the world, but it also plays a critical role in economic growth by fostering direct and indirect employment, promoting travel and local enterprises, and fostering foreign investment and trade. Air transport is intricately linked to many other aviation-related sectors and is a major driver of many economic activities across numerous industries.

In December 2019, the coronavirus pandemic, also known as COVID-19, caused enormous damage to the global economy, trade and liquidity in addition to the human suffering. Due to the COVID-19 restrictions, the demand for air transport of passengers has fallen sharply, threatening the viability of many companies in the aviation sector and other sectors of the aviation industry. This worldwide pandemic has forced airport closures, which has reduced traveler numbers and income across all geographies. Although many nations began gradually opening up various economic sectors, which has a direct impact on air traffic, regrettably some of them were forced to deal with multiple waves of infection, and many nations chose to reintroduce partial or full quarantines.

Although the aviation industry is frequently the subject of government policy, the COVID-19 issue has resulted in a number of new loans, wage subsidies, and capital infusions, raising questions about competition and the effective use of public funds [1]. In order to safeguard the welfare, health, and safety of both passengers and employees, airports have implemented a number of connected measures.

One of the rare COVID-19's beneficial effects is a reduction in noise exposure of population as a result of fewer air traffic movements. This study aims to analyse COVID-19's effects on population noise exposure using noise maps generated by the EUROCONTROL Integrated Aircraft Noise and Emissions Modelling web-based Application (IMPACT). Based on a comparison of the population noise exposure for 2019 and 2020, the analysis was conducted.

The next chapter explains the impact of the COVID-19 outbreak on air traffic. The third chapter, which goes into greater detail on the process of aircraft noise modelling, provides the methodology of this research. The fourth chapter outlines the elements of the Sarajevo Airport case study. The fifth chapter, which presents the statistically processed results, examines the impact of the COVID-19 pandemic on the population's exposure to noise near Sarajevo Airport. The sixth and last chapter provides concluding remarks.

2. IMPACT OF THE COVID-19 PANDEMIC ON AIR TRAFFIC

2.1. Air traffic in 2019

The year 2019 was the busiest year for air traffic ever before to the COVID-19 pandemic. The total number of passengers that travelled by air in the European Union, as reported by EUROSTAT , was 1.034 million, a rise of 3.8% from the previous year 2018. In the region that EUROCONTROL monitors, there is an upward trend in the number of flights, up 0.8% in 2019 over 2018. This was not a significant rise compared to the annual growth in recent years, as the overall growth since the start of the increase in air travel passengers in 2013 was 15.4%.

It is crucial to take note of other air traffic growth factors in addition to the rise in flight numbers. For instance, the average aircraft size grew by 1.7% in 2019 compared to 2018, and the

distance travelled increased by 1.7% as well. As a result, even though there were 0.8% more flights, there were 3.2% more passengers flying in 2019 than there were in 2018, according to EUROCONTROL [2]. The fact that there were a record 225,000 flights on July 24, 2019 [3], further supports the assertion that 2019 was the busiest year in aviation.

2.2. Air traffic during the COVID-19 pandemic

A sharp decline in air traffic demand in 2020 has been brought on by modifications in air passenger behaviour due to the COVID-19 crisis, travel bans and restrictions, and ultimately the global economic crisis. The International Air Transport Association (IATA) reported a 90% decrease in Revenue Passenger Kilometres (RPK) in April 2020 over the course of a year. According to ACI [1], the reported decrease in August 2020 was also very large compared to 2019, specifically 75% higher.

There has been a loss of one billion air passengers as compared to the baseline prediction for 2020 produced before to the coronavirus pandemic. In other terms, actual passenger traffic was 64.6% lower than anticipated for 2020. According to the OECD [4], the actual number of passengers achieved in 2020 compared to 2019 shows a decline of 63.3% overall.

Statistical data on the number of passengers transported at international airports in Bosnia and Herzegovina is shown in **Table 1**. The largest percentage of drop in the number of passengers is evident at Mostar Airport, i.e. -95.8%. The second largest drop was recorded for Sarajevo Airport, which in 2019 had 1,143,680 passengers, and in 2020 only 249,642 passengers. The smallest drop in the number of passengers is recorded at Tuzla Airport.

Table 1 *Passenger statistics for international airports in Bosnia and Herzegovina*

Airport	Number of passengers		% of change
	2019	2020	
Sarajevo Airport	1,143,680	249,642	-78.2%
Tuzla Airport	593,050	228,899	-61.4%
Banja Luka Airport	149,996	43,904	-70.7%
Mostar Airport	32,866	1,394	-95.8%

source: Bosnia and Herzegovina Directorate of Civil Aviation

3. METHODOLOGY

The analysis of the impact of the COVID-19 pandemic on the noise exposure of the population was conducted using the findings of modelling aircraft noise and the number of residents living close to the airport. The first step was to collect all the necessary input data for aircraft noise modelling. Data about the airport, runway, topography, meteorology, population, fleet mix, departure and arrival routes, and distribution of flight operations were all collected for this research.

Aircraft noise modelling and noise map generation was done using EUROCONTROL Integrated Aircraft Noise and Emissions Modelling web-based Application (IMPACT). Noise contours were calculated for average days for 2019 (the year before the onset of COVID-19) and 2020 (during COVID-19) separately.

The most widely used noise indicators in Europe, namely L_{den} and L_{night} as established by the European Commission [5], were used for this study to evaluate the noise at each location. These indicators are yearly averaged noise values intended to depict the exposure to environmental noise from various industrial and transportation sources. The default state values for the time periods used to determine L_{den} and L_{night} in Bosnia and Herzegovina are as follows: daytime hours are from 06:00 to 18:00, evening hours are from 18:00 to 22:00, and night-time hours are from 22:00 to 06:00, all in local time.

The next step is to estimate the population exposed to the calculated L_{den} and L_{night} noise levels at each site in order to assess the cumulative noise impact. Noise exposure analysis is performed by combining the calculated noise levels with the population data. Estimation of annoyance and sleep-disturbance was conducted through dose-effect relations, as explained in Commission Directive (EU) amending Annex III to Directive 2002/49/EC [6].

For the calculation of absolute risk of a harmful effect of high annoyance (AR_{HA}) the following dose-effect relation [6] has been used:

$$AR_{HA} = \left(-50.9693 + 1.0168 \cdot L_{den} + 0.0072 \cdot {L_{den}}^2\right)/100 \quad (1)$$

This value was combined with the number of people living in each location for which the L_{den} was calculated to estimate the total number of people highly annoyed by aircraft noise.

For the calculation of absolute risk of a harmful effect of high sleep disturbance (AR_{HSD}) the following dose-effect relation [6] has been used:

$$AR_{HSD} = \left(16.7885 - 0.9293 \cdot L_{night} + 0.0198 \cdot {L_{night}}^2\right)/100 \quad (2)$$

Similarly, this value was combined with the number of people living in each location for which the L_{night} was calculated to estimate the total number of people highly sleep disturbed by aircraft noise.

4. CASE STUDY FOR SARAJEVO AIRPORT

Sarajevo Airport is the main international airport in Bosnia and Herzegovina, and serves the City of Sarajevo (population: 413,593) from which it is located 7 km. The airport has joint civil and military operations, with one runway 2,600 m long and 45 m wide. The declared capacity of the passenger terminal per year is one million passengers. The record year in terms of number of passengers in the airport's history was 2019 (1,143,680 passengers), while in 2020 this number was reduced by 78.2% (249,642 passengers) due to COVID-19. The current number of passengers in the first eight months of 2022 is 20.8% higher than for the same period in 2019, indicating full recovery from COVID-19 and even growth.

Table 2 shows the number of movements per aircraft type and time of day for 2019 and 2020, which has been used for this research. The fleet mix in 2019 consisted of 122 different aircraft types, while in 2020 this number was 46. **Table 2** shows statistics for eleven aircraft types that accounted for 90.4% of all movements in 2019, while the others were presented jointly.

As representatives of the routes used for modelling, four departure routes and one arrival route from eAIP were chosen.

The one selected approach route (ILSs 198KIS) is assigned to runway 11, while three departure routes (BOSNA1A, BOSNA4W, KUTAK1A, MITNO1D) are assigned to runway 29. All flights were assigned to these five routes.

The data on population density in the airport's vicinity that were used and presented in this study were freely obtained from the European Commission's Joint Research Centre (JRC) [7], while the Iowa State University provided the meteorological data required for noise modelling [8].

5. RESULTS

The analysis of the effects of the COVID-19 on noise exposure of population is based on the obtained noise contours and a comparison of population and area exposed to different noise levels, for two observed years. **Fig. 1** shows Sarajevo Airport L_{den} noise contours for the years 2019 (**Fig. 1a**) and 2020 (**Fig. 1b**), while **Fig. 2** shows L_{night} noise contours for the years 2019 (**Fig. 2a**) and 2020 (**Fig. 2b**). These two figures clearly illustrate the significant decrease in area and population exposed to noise. This decrease is further quantitatively described in more details, by comparing population exposed to different noise levels (**Table 3**) and area exposed to different noise levels (**Table 4**) for L_{den} and L_{night} for 2019 and 2020. **Table 3** shows that in 2020, less population is exposed to noise compared to the values from 2019, for each 5 dB noise band, both for L_{den} and L_{night}. When comparing the population exposed to noise levels above 55 dB L_{den}, **Table 3** shows that there was a decrease of 69.2%, from 11,029 in 2019 to 3,395 in 2020. Even higher decrease of 91.6% (from 9,806 in 2019 to 823 in 2020) was estimated for the population exposed to noise levels above 45 dB L_{night}.

Table 4 shows that there was a 70.6% of reduction in the area exposed to noise levels above 55 dB by comparing L_{den} noise contours for 2019 and 2020, and 78.3% of reduction when comparing L_{night} noise contours for noise levels above 45 dB.

Furthermore, based on the calculated L_{den} and L_{night} noise levels, population data and the assessment methods for harmful effects provided in **Eq. (1)** and **Eq. (2)** [6], expected annoyance and sleep disturbance have been estimated for 2019 and 2020. **Table 5** shows that the estimated number of people highly annoyed by aircraft noise was reduced by 57% in 2020 compared to 2019, while the estimated number of people highly sleep disturbed decreased by 63%.

Table 2 *Number of movements per aircraft type and time of day for 2019 and 2020*

ICAO aircraft type code	Day		Evening		Night	
	2019	2020	2019	2020	2019	2020
B738	2357	598	236	54	111	1
A320	2003	611	325	112	136	10
A319	1376	274	270	72	217	8
DH84	678	386	339	157	329	35
L410	1102	1306	2	6	86	19
A321	410	213	438	95	28	4
AT72	611	297	/	1	11	0
E195	340	250	56	53	/	23
C208	234	0	10	0	12	0
CRJ9	246	0	/	0	/	0
C525	117	0	16	0	3	0
Others	1190	170	67	12	27	5
Total	10664	4105	1759	562	960	105

Table 3 *Population exposed to different noise levels for L_{den} and L_{night} for 2019 and 2020*

Population exposed		Noise levels (dBA)									
		35 - 40	40 - 45	45 - 50	50 - 55	55 - 60	60 - 65	65 - 70	70 - 75	75 - 80	>80
L_{den}	2019	/	57,581	28,109	12,835	7,134	3,209	595	91	0	0
	2020	/	24,166	13,099	8,120	3,327	68	0	0	0	0
L_{night}	2019	23,357	10,652	6,316	2,852	520	118	0	0	0	0
	2020	9,800	7,474	793	30	0	0	0	0	0	0

Table 4 *Area exposed to different noise levels for L_{den} and L_{night} for 2019 and 2020*

Area (km^2) exposed to noise	L_{den}					L_{night}				
	> 35	> 45	> 55	> 65	> 75	> 35	> 45	> 55	> 65	> 75
2019	/	48.24	6.03	0.21	0.00	41.66	5.09	0.18	0.00	0.00
2020	/	10.97	1.77	0.19	0.00	8.13	1.11	0.08	0.00	0.00
% of change	/	-77.3%	-70.6%	-12.3%	0.0%	-80.5%	-78.3%	-53.8%	0.0%	0.0%

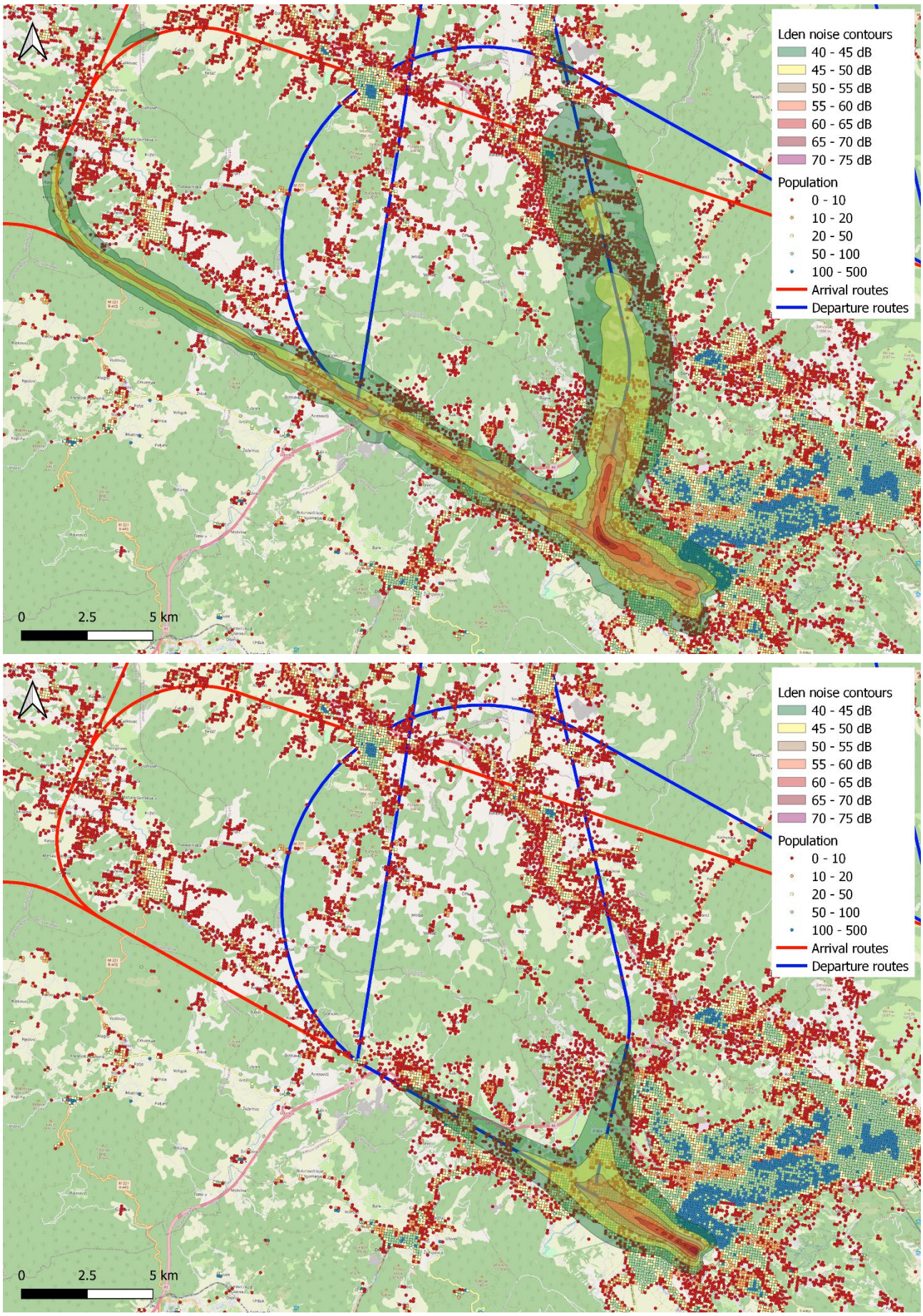

Fig. 1 *Sarajevo Airport noise contours (a) L_{den} 2019, (b) L_{den} 2020*

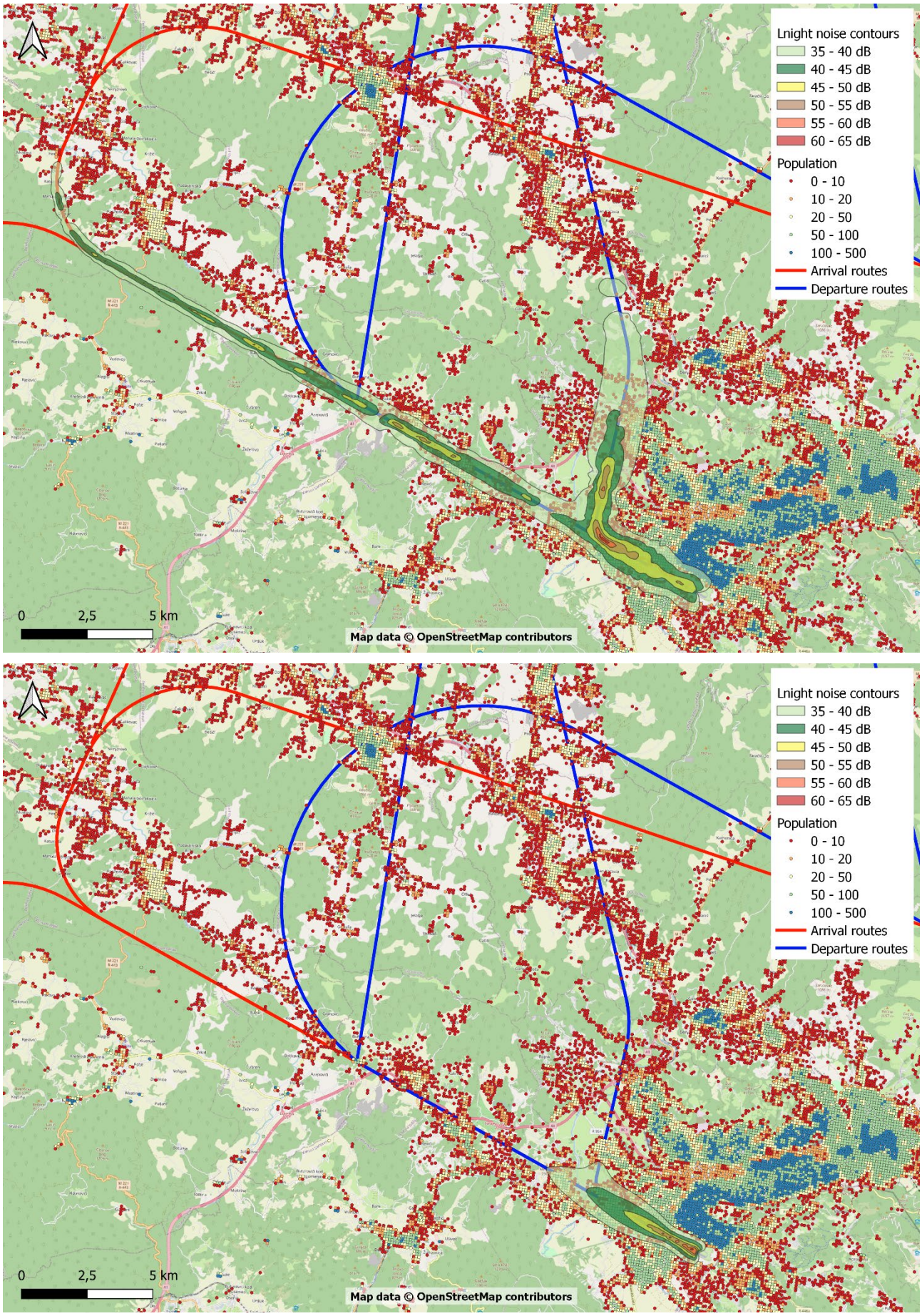

Fig. 2 *Sarajevo Airport noise contours (a) Lnight 2019, (b) Lnight 2020*

Table 5 *Expected annoyance and sleep disturbance for 2019 and 2020*

Year	NPHA	NPHSD
2019	13,009	5,515
2020	5,600	2,041
% of change	-57.0%	-63.0%

6. CONCLUSION

This research aimed at estimating the overall effect of COVID-19 on the reduction of noise exposure on the population living close to Sarajevo Airport. Among various negative effects of the coronavirus pandemic, the noise reduction could be seen as one of its benefits. In order to assess the magnitude of this impact, noise contours for the year 2019 when the COVID-19 had no effect, were compared to the ones developed for the year 2020 during the pandemic. The results for Sarajevo Airport revealed the decrease of 69.2% in the population exposed to noise levels above 55 dB L_{den}, while decrease of 91.6% was estimated for the population exposed to noise levels above 45 dB L_{night}. Furthermore, the estimated number of people highly annoyed by aircraft noise was reduced by 57% in 2020 compared to 2019, while the estimated number of people highly sleep disturbed decreased by 63%.

Traffic figures for the year 2022 for Sarajevo Airport show that air traffic is recovering faster than expected, with the 20.8% increase compared to the previous year. This means that the population's noise exposure will soon be at pre-COVID-19 levels, with further increases expected. Although the results currently demonstrate the significant reduction in terms of the number of people exposed to aircraft noise, this is only a temporary effect that will be quickly reversed. As a conclusion, noise abatement measures that were in place prior to COVID-19 or that were planned but delayed due to a decrease in aircraft operations should be maintained in order to alleviate future adverse effects of air traffic operations on the population near the airport.

ACKNOWLEDGEMENTS

This research was supported by the Ministry of Education, Science, and Technological Development of the Republic of Serbia. The authors would like to thank the EUROCONTROL for providing the Integrated Aircraft Noise and Emissions Modelling web-based Application (IMPACT) for noise exposure calculations.

REFERENCES

[1] Airports Council International, "ACI Advisory Bulletins. The impact of COVID-19 on the airport business and the path to recovery," 25-Mar-2021. [Online]. Available: https://aci.aero/news/2021/03/25/the-impact-of-covid-19-on-the-airport-business-and-the-path-to-recovery/. [Accessed: 08-July-2022].

[2] Performance Review Commission, "Performance Review Report. An Assessment of Air Traffic Management in Europe during the Calendar Year 2019," Brussels, Belgium, June. 2020.

[3] D. Slotnick, "Wednesday was one of the busiest recorded days in aviation history — and it's going to keep getting busier," *Insider*, 25-Jul-2019. [Online]. Available: https://www.businessinsider.com/most-flights-ever-225000-flightradar24-flight-tracking-2019-7.

[4] OECD, "COVID-19 and the aviation industry: Impact and policy responses," *Tackling coronavirus (COVID-19): Contributing to a global effort*, 15-Oct-2020. [Online]. Available: https://www.oecd.org/coronavirus/policy-responses/covid-19-and-the-aviation-industry-impact-and-policy-responses-26d521c1/.

[5] EC, "Directive 2002/49/EC of the European parliament and the Council of 25 June 2002 relating to the assessment and management of environmental noise," *Official Journal of the European Communities*, vol. 189, no. 12. pp. 12–25, 2002.

[6] European Commission, "COMMISSION DIRECTIVE (EU) 2020/367 of 4 March 2020 amending Annex III to Directive 2002/49/EC of the European Parliament and of the Council as regards the establishment of assessment methods for harmful effects of environmental noise," *Official Journal of the European Union L 67/132*, 2020.

[7] S. Freire, M. Halkia, and M. Pesaresi, "GHS Population Grid, Derived from EUROSTAT Census Data (2011) and ESM R2016", European Commission, Joint Research Centre: Ispra, Italy, 2016

[8] Iowa State University, "Iowa Environmental Mesonet," 2022. [Online]. Available: https://mesonet.agron.iastate.edu/request/download.phtml?network=RS__ASOS.

University of Nis
Faculty of Occupational Safety

„Politechnica“ University of Timisoara
Faculty of Mechanical Engineering

27th International Conference

NOISE AND VIBRATION

Niš, 20 - 21. 10. 2022.

ACOUSTICS

University of Nis
Faculty of Occupational Safety
„Politechnica“ University of Timisoara
Faculty of Mechanical Engineering
27th International Conference
NOISE AND VIBRATION
Niš, 20 - 21. 10. 2022.

SPATIAL ALIASING AND FALSE DETECTION OF STANDING WAVES IN EXPERIMENTAL DETERMINATION OF DISPERSION RELATIONSHIP BY CORRELATION METHOD

Vladimir Sinđelić, Snežana Ćirić Kostić, Branko Radičević and Zlatan Šoškić[1]

[1] University of Kragujevac, The Faculty of Mechanical and Civil Engineering in Kraljevo, Serbia
sindjelic.v@mfkv.kg.ac.rs

Abstract - *The experimental determination of a dispersion relation by measurements of wave properties in different points in space meets various challenges due to the spatial aliasing, which is a consequence of description of a continuous wave by a discrete set of measurement points. The paper presents an analysis of the phenomenon of false detection of standing waves during experimental determination of dispersion relationship of flexural waves in beams by correlation method. The false detection of standing waves, manifested as zero group velocity of the waves that does not correspond to a real resonance, is a consequence of equidistant spacing of measurement points in experimental setup, and may be avoided by different positioning of measurement points in space. The results of the analysis are verified by comparison between the results of experimental setups with equidistant measurement points and measurement points with distances to excitation point proportional to prime numbers.*

1. INTRODUCTION

One of key elements of any definition of waves is that a wave is propagation of a disturbance through a medium. The disturbed part of the medium is the wavefield, and the border of a wavefield is a wavefront, which expands with propagation of a wave. Many complex theoretical and practical problems of wave propagation are solved by application of the Huygens principle, which describes the wave propagation by interference of spherical waves that are expanding with constant velocity c around all points of a wavefront. The velocity of propagation of the disturbance by spherical waves c is called "the phase velocity" of the wave, while the velocity of propagation of energy (or mass in the case of mechanical waves) by a wave (which does not have to be equal to phase velocity) is called "the group velocity" of the wave v. The knowledge of the phase velocity of a wave in a medium, therefore, is the key to the applications of the Huygens principle. An important property of wave motion is that the phase velocity c and the group velocity v of a harmonic wave, in general, depend on the frequency f of the harmonic wave. Since any wave may be represented as a sum of harmonic waves using the Fourier transformation, different frequency components of a wave propagate with different velocities, which leads to an effect of decomposition of waves that is called "dispersion". For that reason, the all-important relationship between the phase velocity and the frequency of a wave, $c(f)$, is called "the dispersion relationship" (abbreviated as "DR" in the following text). Since the phase velocity c, frequency f, angular frequency $\omega = 2\pi/f$, wavelength λ, and the wavenumber $k = 2\pi/\lambda$ of a harmonic wave are related by the equations $\lambda = c/f$ and $\omega = c/k$, the DR is most often expressed in the analytical form $F(\omega,k) = 0$ or $\omega = \omega(k)$, because it enables simple calculation of both phase velocity (as $c = \omega/k$) and the group velocity (as $v = d\omega/dk$).

Theoretical calculation of the DR is possible only in a limited number of cases with high symmetry and simple structure of the medium, and the alternative for the other cases is the experimental determination of DR [1]. Even in the cases when it is possible to determine the DR by theory, experimental determination of DR is used for characterization of materials [2][3]. The main concept for experimental determination of the DR consists in measurement, in multiple points of a structure, of the response (usually acceleration) to an excitation (usually impulse or harmonic). The responses at these points at a particular excitation frequency (obtained by direct measurement or spectral decomposition) are then used to construct the "optimal" wavefield, with a known wavenumber, that has minimal deviation from the measured responses. Different approaches to construction of the wavefield lead to different methods for experimental determination of the DR [4]. The subject of this paper is the correlation method [5], which, in suitable structures, uses harmonic progressive waves to construct the test wavefields, and the simple sequential search of wavenumber space to find the wavenumber of optimal wavefield. It has been already shown that a straightforward application of the correlation method is limited to a low-frequency range due to the spatial aliasing [4], but the research presented in this article warns that even that frequency range is reduced in the case of equidistant measurement points due to the false detection of standing waves. Fortunately, the research shows that the false detection of standing waves may be avoided by non-equidistant positioning of measurement points.

2.THEORY

For the sake of simplicity, the present paper will consider propagation of flexural waves over a thin homogenous beam, which is a well-studied case in theory [6]. The flexural waves are suitable for experimental studies because they are simple for excitation and detection. The DR of flexural waves that propagate over a thin homogenous beam is given by the expression:

$$\omega = \sqrt{\frac{EI}{\rho A}} k^2 \qquad (1)$$

with ρ standing for density, E for Young's modulus of the material, while I represents the area moment of inertia, and A the area, of the cross-section of the beam.

Let a harmonic progressive flexural wave, with the angular frequency ω and the wavenumber k related by the DR (1), be excited in a homogenous thin beam by the action of harmonic transversal force $\underline{F}(t) = \underline{F}_\omega \cdot \exp(-i\omega t)$. If the x-axis is oriented along the longitudinal axis of the beam, and if one end of the beam is taken as the origin of the axis, then the transversal accelerations of the beam points will have values $\underline{a}(x,t) = \underline{a}_\omega \cdot [i \cdot \exp(kx - \omega t)]$, and the response to the excitation of the beam to the excitation, the accelerances $\underline{w}(x,t) = \underline{a}_t(x,t)/F(t)$ will have values $\underline{w}(x,\omega) = \underline{w}_\omega \cdot \exp(ikx)$, independent of t. Due to the orthogonality of harmonic functions, the correlation between the accelerance $w_t(x,\omega)$ of any harmonic wavefield, with the angular frequency ω and the wavenumber k_t, and the accelerance of the wavefield of the excited harmonic wave $\underline{w}(x,\omega)$, defined as

$$\underline{W}_\omega(k_t) = \int_{-\infty}^{+\infty} \underline{w}(x,\omega)\, \underline{w}_t^*(x,\omega)\, dx \qquad (2)$$

will be equal to zero unless the wavenumber of the harmonic wavefield is equal to the wavenumber of the excited wave, $k_t = k$, when the correlation tends to infinity. This property of the correlation is the basis for correlation method for experimental determination of DR. The method uses measurements of accelerations in a finite number of points L, with the coordinates x_l ($l = 1, 2, \ldots, L$), which are, in the case of thin homogenous beam placed along the beam. The measured accelerations and excitation force are used to obtain the accelerances in the measurement points $w_l(\omega) = w(x=x_l, \omega)$, which are then used for calculations of the sums that are estimations $\underline{\hat{W}}_\omega(k_t)$ of correlation between the measured wavefield at angular frequency ω and different harmonic progressive waves with wavenumbers k_t and accelerances $\underline{w}_t(x,\omega) = \underline{w}_\omega \cdot \exp(ik_t x)$.

$$\underline{\hat{W}}_\omega(k_t) = \underline{w}_{t\omega}^* \sum_{l=1}^{L} \underline{w}(x_l,\omega) e^{-ik_t x_l} \Delta x_l = \underline{w}_{t\omega}^* \sum_{l=1}^{L} \underline{w}_{l\omega} e^{-ik_t x_l} \Delta x_l \qquad (3)$$

where Δx_l represents the space interval around the point x_l. Since $\underline{\hat{W}}_\omega(k_t)$ is only an estimation of the correlation $\underline{W}_\omega(k_t)$, it is not equal to zero for $k \neq k_t$ and not infinite for $k = k_t$, but it should, anyway, have maximal value in the latter case. Using that property of $\underline{\hat{W}}_\omega(k_t)$, correlation method selects value for wavenumber of the measured wavefield to be equal to the test value k_t which has maximal value of estimated correlation (3), and that is the value that maximizes the correlation function $Y_\omega(k_t)$, given by the expression:

$$Y_\omega(k_t) = \left| \sum_{l=1}^{L} \underline{w}_{l\omega} \exp(-ik_t x_l) \Delta x_l \right| \qquad (4)$$

As explained, the correlation method uses progressive waves to construct the test wavefields, which implies that the method is applicable to the wavefields that consist of progressive waves. However, in all real structures, due to their finite dimensions and reflections from the boundaries, exist standing waves with the corresponding natural frequencies of the structures. While the standing waves may be considered as a superposition of progressive waves moving in opposite directions (therefore having wave vectors with equal intensity, but opposite signs), they do not transfer energy and their group velocities are zero. Since the group velocity is derivative of DR, the DR obtained by correlation method has inflexion point at resonant frequencies of the structure, which is different from DR of progressive waves that the correlation method intends to reveal. Therefore, it may be concluded that the existence of standing waves prevents the application correlation method. This paper focuses on the phenomenon of false detection of standing waves that arises when experimental determination of DR is performed by correlation method with data obtained using equidistant measurement points (abbreviated as DR-CM-ED). This phenomenon, which will be shown to be avoidable, further reduces applicability of correlation method for determination of DR.

The measurement points are most frequently taken to be equidistant, $x_l = l \cdot d$, where d is the distance between adjacent measurement points. There are several reasons for such approach, and one of dominant is application of the most popular signal processing technique, FFT (Fast Fourier Transformation), which requires measurement from equidistant input points. In such a case, the correlation function has the form:

$$Y_\omega = \left| \sum_{l=1}^{L} \underline{w}_{l\omega} \exp(-i \cdot l \cdot d \cdot k_t) \right|. \qquad (5)$$

It has been shown [4] that the correlation function in the case of equidistant measurement point is periodic in wavenumber space with the period $2\pi/d$, $Y_\omega(k+2\pi/d) = Y_\omega(k)$, as illustrated in Fig. 1. Since it means that the maxima of the correlation function are also periodic, the periodicity of the correlation function has a consequence that the DR obtained DR-CM-ED is also periodic with the same period, $2\pi/d$, $\omega(k+2\pi/d) = \omega(k)$, as Fig. 2 illustrates. Such a periodicity is a well-known consequence of the equidistant selection of measurement points, and it occurs in general in all cases of propagation of waves through periodic structures [7]. The basic period in the wavenumber space, $-\pi/d < k < \pi/d$, is called "the Brillouin zone" (BZ) or "the first Brillouin zone". If the limits of the first Brillouin are denoted as $\pm\pi/d = \pm k_{BZ}$, and the corresponding values of angular frequency and frequency as ω_{BZ} and f_{BZ}, then the period of a DR-CM-ED may be written as $2k_{BZ}$.

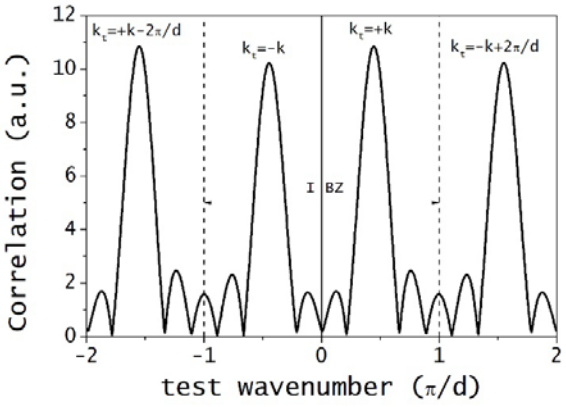

Fig. 1 *Correlation function of a DR-CM-ED*

For physical reasons, any DR is even function, $\omega(-k) = \omega(k)$, because the reversed sign of k means only change of direction of propagation, which does not affect phase velocity due to the

symmetry properties of space and matter. Due to the periodicity and even parity of a DR-CM-ED, its derivative has to be periodic with the same period,

$$\left.\frac{d\omega}{dk}\right|_{k+\frac{2\pi}{d}} = \left.\frac{d\omega}{dk}\right|_{k} \tag{6}$$

and has to have odd parity

$$\left.\frac{d\omega}{dk}\right|_{-k} = -\left.\frac{d\omega}{dk}\right|_{k}. \tag{7}$$

Furthermore, since the derivative of a DR, $d\omega/dk$, is the group velocity of a wave, it has to be a continuous function of k, because any physical quantity in classical mechanics has a single value. The continuity of the first derivative for any wavenumber $k = k_0$ may be expressed as

$$\lim_{k\to k_o}\left(\frac{d\omega}{dk}\right) = \left.\frac{d\omega}{dk}\right|_{k_0}, \tag{8}$$

which means that the left and the right limit of the derivative of DR have to be equal for any wavenumber $k = k_0$

$$\left.\frac{d\omega}{dk}\right|_{k_o^-} = \left.\frac{d\omega}{dk}\right|_{k_o^+}. \tag{9}$$

Since the equations (7) and (9) hold for all wavenumbers, they have to hold also for $k = 0$. From (7) follows that the first derivatives of the DR on the left side and right side of zero have opposite signs

$$\left.\frac{d\omega}{dk}\right|_{0^-} = -\left.\frac{d\omega}{dk}\right|_{0^+}, \tag{10}$$

and from (9) it follows that they have to have the same sign

$$\left.\frac{d\omega}{dk}\right|_{0^-} = \left.\frac{d\omega}{dk}\right|_{0^+}. \tag{11}$$

Both (10) and (11) may hold only if the derivative of the DR for $k = 0$ is zero. Due to the periodicity, the first derivative of a DR-CM-ED also has to be equal to zero for all points $k = \pm z\cdot 2k_{BZ} = \pm m\cdot k_{BZ}$, where z is an integer, and $m = 2z$ is an even number.

On the other hand, the equations (6) , (7) and (9) have also to hold for all wavenumbers, and therefore also for the border of the Brillouin zone, $k = +k_{BZ}$. However, due to the continuity (9) the first derivatives of the DR-CM-ED on the left side and right side of $+k_{BZ}$ have to have the same signs

$$\left.\frac{d\omega}{dk}\right|_{k_{BZ}^-} = \left.\frac{d\omega}{dk}\right|_{k_{BZ}^+}, \tag{12}$$

and, at the same time, due to the combination of the requirements for periodicity (6) and odd parity (7), they have to have opposite signs

$$\left.\frac{d\omega}{dk}\right|_{k_{BZ}^-} \overset{(7)}{=} -\left.\frac{d\omega}{dk}\right|_{-k_{BZ}^-} \overset{(6)}{=} -\left.\frac{d\omega}{dk}\right|_{-k_{BZ}^- + 2k_{BZ}} = -\left.\frac{d\omega}{dk}\right|_{k_{BZ}^+} \tag{13}$$

which is, again, only possible if the derivative of the DR for $k = \pm k_{BZ}$ is zero. Due to the periodicity, the first derivative of a DR-CM-ED also has to be equal to zero for all points $k = k_{BZ} \pm z\cdot 2k_{BZ} = \pm m\cdot k_{BZ}$, where z is an integer, and $m = (2z+1)$ is an odd number.

In conclusion, the physical requirements for even parity and continuity of DR and the mathematical requirement for periodicity of DR-CM-ED mean that the first derivative of the DR-CM-ED has to be equal for all wavenumbers satisfying conditions $k = \pm m\cdot k_{BZ}$ with m being an integer.

$$\left.\frac{d\omega}{dk}\right|_{k=m\cdot k_{BZ}} = 0, \tag{14}$$

On the other hand, the equation (1) shows that the first derivative of the DR of flexural waves a thin homogenous beam is equal to zero only for k=0, which means that the DR-CM-ED cannot be a good description of the DR for wavenumbers satisfying conditions $k = \pm m\cdot k_{BZ}$ (in other word, in centres and borders of Brillouin zones).

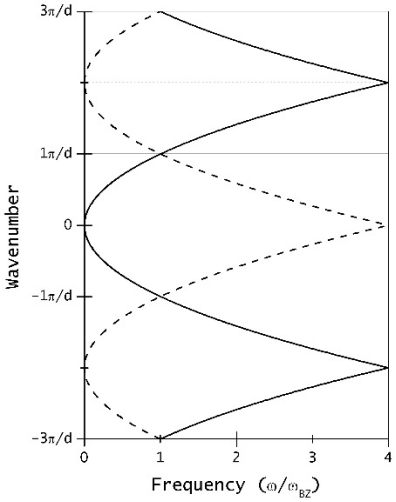

Fig. 2 *Theoretical prediction of DR-CM-ED (solid line – centres in even BZ, dashed line – centres in even BZ)*

The reason for the observed failure of DR-CM-ED is periodicity of the array of measurement points, which is caused by their equidistant positions. It is well-known fact from studies of waves in periodic structures [7] that waves with $k = \pm m\cdot k_{BZ}$ in discrete periodic structures (e.g. crystals) degenerate into oscillations for even values of m, while for odd values of m they represent standing waves. It is easy to demonstrate because in all points of a periodic discrete structure with period d, $x_l = l\cdot d$, a wave with $k = \pm m\cdot k_{BZ}$ for even m=2z has phase factors $\exp(ikx_l) = \exp(i\cdot z\cdot l\cdot 2\pi) = 1$, which means that phases of the wave are equal in the same points, implicating that the wave degenerates into whole-body (or rigid-body) oscillations. On the other hand, if m=2z+1 is odd, then the phase factors have values $\exp(ikx_l) = \exp(i\cdot(2z+1)\cdot l\cdot\pi) = (-1)^l$, which means that the adjacent points have opposite phases, implicating that the wave is a standing wave. The same relationships hold for the accelerations of a progressive wave with $k = \pm m\cdot k_{BZ}$ taken in an array of equidistant points, which means that such a progressive wave will be falsely detected as standing wave or whole-body oscillation.

At first glance, the effect of false detection of standing waves and whole-body oscillations may be easily avoided by selecting non-periodic positioning of measurement points. However, the Fourier theorem shows that any finite non-periodic array may be decomposed in an infinite sum of periodic arrays with the period equal to the least common denominator of differences between the members of array (the distances between the measurement points). Since, by definition, irrational distances cannot be measured, the longest practical

period of a set of distances between the measurement points is obtained if the positions of the measurement points x_l are proportional to prime numbers.

3.EXPERIMENT

The experiment was carried with the aim to apply correlation method for determination of DR of flexural waves on a free homogenous thin beam using a set of equidistant measurement points and a set of measurement points with distances proportional to prime numbers. The complete experiment is described in the reference [4], and here will be repeated just the part about the test object and positioning of the measurement points, which are the most relevant for further discussion of the obtained results.

The beam was a steel rod with length $D \approx 1{,}65$ m, and roughly square cross-section with side $b \approx 1$ cm. The end parts of the rod, with the length of around 25 cm, were resting on soft sponges, with the aim to emulate a beam with free ends. The measurements were organized in three series, with different positions of measurement points.

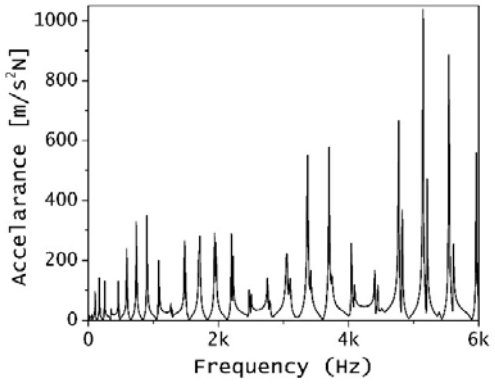

Fig. 3 *Accelerance of the beam measured at the point x=90 cm from the beginning of the rod*

In the first series, the measurement points were uniformly distributed at 10 equidistant positions with distances $d \approx 15$ cm, with the first measurement point being at the distance d from the beginning of the rod and the last being at the distance d from the end of the rod. Therefore, the arrangement of the measurement points was symmetric with respect to the centre of the rod.

In the second series, 10 measurement points were selected to have the distances to the beginning of the rod (the excited end) being proportional to prime numbers sequence 5, 7, 11, 13, 17, 19, 23, 29, 31 and 37. The selected set of measurement points covered the part of the rod between 20 cm and 148 cm.

In the third series, 31 measurement points were selected to have the distances to the beginning of the rod (the excited end) being proportional to prime numbers sequence 2, 3, 5, 7, 11, 13, 17, 19, 23, 29, 31, 37, 41, 43, 47, 53, 59, 61, 67, 71, 73, 79, 83, 89, 97,101, 103, 107, 109, 113 and 127. The selected set of measurement points covered the part of the rod between 7.5 cm and 157.5 cm.

4. RESULTS AND DISCUSSION

The accelerance amplitude spectra for all cases revealed the expected resonant behaviour, as Fig. 3 illustrates. The resonant peaks at low frequencies (14 Hz – 590 Hz) are singlets, while at higher frequencies the resonant peaks appear to be doublets, with the frequency split of the doublets increasing with resonant frequency.

The frequencies are detected at frequencies close to the natural frequencies predicted by theory for flexural vibrations of a thin homogenous beam with free ends:

$$f_m = (2m)^2 \left(\frac{1}{2\pi} \sqrt{\frac{EI}{A\rho}} \left(\frac{\pi}{2D} \right)^2 \right), \; m = 0,1,2... \qquad (15)$$

and these are the frequencies of the standing waves that form at the beam.

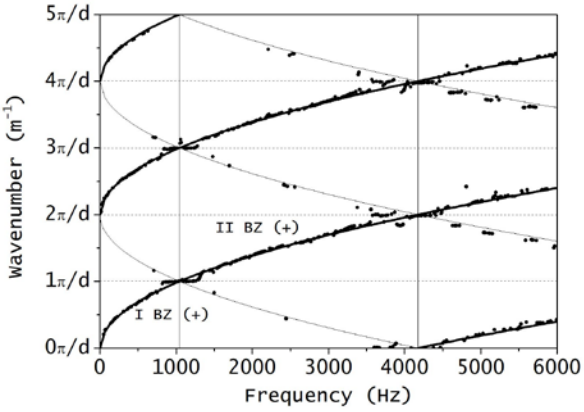

Fig. 4 *DR-CM-ED obtained in the experiment (dots-experimental data, lines-theory)*

As explained in the theoretical analysis, in the case of the equidistant measurement points the obtained DR (it is the DR-CM-ED), presented by points in the Fig. 4, is periodic function of wavenumber k, with the period $2k_{BZ} = (2\pi/d) \approx 42\text{m}^{-1}$, so that the frequency $f_{BZ} \approx 1044$ Hz corresponds to the end of the first Brillouin zone ($k_{BZ} = \pi/d$), and the frequency $4 \cdot f_{BZ} \approx 4176$ Hz corresponds to the center of the next Brillouin zone ($2 \cdot k_{BZ}$). Even in such a large-scale view (0-6000 Hz) it is clear that at frequencies corresponding to wavenumber values $k = m \cdot k_{BZ}$ the obtained DR departs both from the monotonously increasing trend within Brillouin zones and from the predictions of theory, presented by solid lines in Fig. 4.

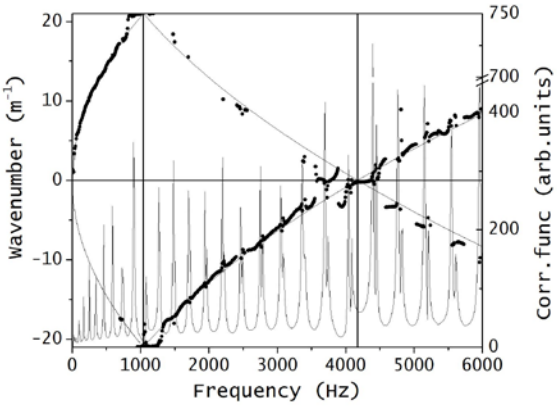

Fig. 5 *Restricted DR-CM-ED and correlation function obtained in the experiment (dots-experimental data, thick lines-theoretical DR, thin line-correlation function)*

In order to increase visibility and use the periodicity of the obtained results, the DR-CM-ED is frequently presented confined to the first Brillouin zone, as shown in the Fig. 5. The DR-CM-ED is presented in the figure by the points, while the thin line presents the correlation function, which indicates resonances. The figure clearly presents the influence of the

standing waves to the experimental determination of DR in general: close to the natural frequencies of the beam, correlation method is unable to distinguish the incident (the monotonously increasing branches) and reflected (the monotonously increasing branches) progressive waves. Furthermore, the figure also shows that the DR-CM-ED contains ranges of false standing waves at the ends of Brillouin zones (flat DR-CM-ED near $f_{BZ} \approx 1044$ Hz) and false oscillations (flat DR-CM-ED near $f_{BZ} \approx 4176$ Hz). Finally, Fig. 5 also indicates that there is interaction between real and false standing waves detection, observable in the range 3500-4500 Hz.

With the aim to clearly show the effect of false standing wave detection, Fig. 6 shows the part of DR-CM-ED containing the first Brillouin zone and the range close to its boundary $k = k_{BZ}$. The figure also shows the theoretical predictions for DR of incident (solid line) and reflected (dashed line) progressive waves. It is clear that the DR-CM-ED is flat, indicating detection of standing waves, in the area range where the values of wavenumbers of incident and reflected waves coincide due to periodicity artificially induced by positioning of measurement points.

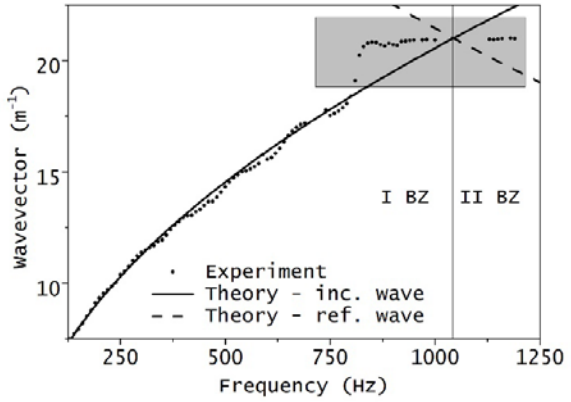

Fig. 6 *DR-CM-ED within the I BZ and close to the boundary between the I BZ and II BZ*

In order to test the effects of different positions of measurement points, three sets of measurement points were formed for application of correlation method for determination of DR:

- "equidistant" set of data obtained in 10 equidistant measurement points during the first series of measurements,
- "mixed" set, containing data obtained in 10 equidistant measurement points during the first series of measurements and the data obtained in 10 non-equidistant measurement points during the second series of measurements,
- "primed" set, containing data obtained in 31 non-equidistant measurement points during the third series of measurements.

Fig. 7 shows that the periodicity of the measurement points is indeed the sole reason for the false detection of standing waves near the boundary of Brillouin zone. The false detection occurs not only when the measurement points are equidistant, but also when there is a subset of equidistant points within the measurement points set. When all the positions of the measurement points are proportional to prime numbers, the detection of false standing waves disappears, and the DR in the region follows theoretical predictions, shown by the solid line.

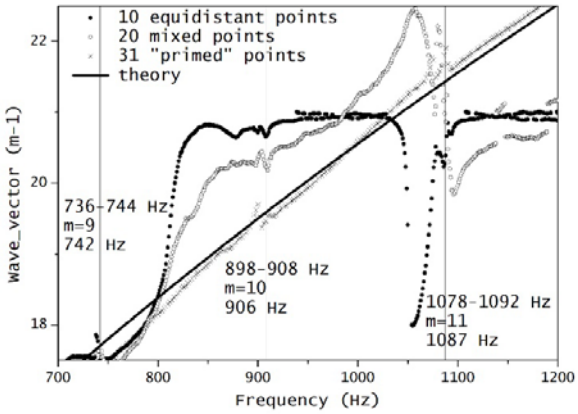

Fig. 7 *DR-CM-ED obtained using three different sets of measurements points*

Fig. 7 also shows that the detection of real standing waves, that arise at natural frequencies of the structure, as expected, does not depend on positions of measurement points. The natural frequencies of the beam in the observed range correspond to resonant frequencies (15) for values $m = 9$, $m = 10$ and $m = 11$.

5. CONCLUSIONS

This article presents research of false detection of standing waves during experimental determination of dispersion relationship using by correlation method and equidistant measurement points.

The theoretical analysis revealed that a progressive wave with wavenumber k, discretized in an equidistant set of measurement points with distance d between them, cannot be distinguished from a standing wave when $k = (2z+1)\pi/d$ (ends of Brillouin zones) and from whole-body oscillation when $k = (2z)\pi/d$ (centers of Brillouin zones). Since standing waves and whole-body oscillations do not transfer energy, the false detection causes false inflection points ("flat ranges") in the dispersion relationships detected by correlation method. This theoretical analysis shows that the false detection of standing waves is an artifact of equidistant measurement points and the simplest way to avoid it is by positioning measurement points so that their distances to excitation point are proportional to prime numbers.

The experiment that was designed to verify the theoretical considerations confirmed the presented conclusions. Furthermore, the experiment revealed that even the application of correlation method to experimental data obtained using non-equidistant set of points are sensitive to false standing waves detection if the set contains a subset with equidistant points.

Due to their finite dimensions, in all real structures exist real standing waves, which are also detected by correlation method and cause inflection points in DR. Since they are real, their detection, and the corresponding deviation of experimental DR from the true values, cannot be avoided by positioning of measurement points. Therefore, the correlation method is not applicable in vicinity of resonant frequencies of structures.

ACKNOWLEDGEMENT

The authors acknowledge the support of Ministry of Education, Science and Technology Development of Republic of Serbia to its institution through grant No. 451-03-68/2022-14/200108.

REFERENCES

[1] E.B. Groth., T. G. R.Clarke, G. Schumacher da Silva, I. Iturrioz and G. Lacidogna, "The elastic wave propagation in rectangular waveguide structure: Determination of dispersion curves and their application in nondestructive techniques", *Applied Sciences*, 10(12), p.4401, 2020

[2] J.G. McDaniel, P. Dupont, L. Salvino, "A wave approach to estimating frequency-dependent damping under transient loading", *Journal of Sound and Vibration*, Vol. 231(2), 433-449, 2000

[3] J.G. McDaniel and W.S. Shepard Jr, "Estimation of structural wave numbers from spatially sparse response measurements", *The Journal of the Acoustical Society of America*, Vol. 108(4), 1674-1682, 2000

[4] V. Sindjelic, S. Ciric-Kostic, A Nikolic, Z. Soskic, "Extension of the frequency range for experimental determination of dispersion relationship of flexural waves in beams by correlation method", *IMK-14 – Research & Development in Heavy Machinery*, Vol. 26(4), pp. 95-107, 2020

[5] N.S. Ferguson, C.R. Halkyard, B.R. Mace, and K.H. Heron, "The estimation of wavenumbers in two-dimensional structures", *Proceedings of ISMA2002: International Conference on Noise and Vibration Engineering, Leuven (Belgium) 16-18 Sep 2002*. pp.799-806, 2002

[6] C.F. Beard, *Structural Vibrations – Analysis and Damping*, Elsevier, Oxford, (UK), 1996

[7] L. Brillouin, *Wave propagation in periodic structures: electric filters and crystal lattices*, Dover publications; 1953.

University of Nis
Faculty of Occupational Safety
„Politechnica“ University of Timisoara
Faculty of Mechanical Engineering
27th International Conference
NOISE AND VIBRATION
Niš, 20 - 21. 10. 2022.

ACOUSTIC ARRANGEMENT OF A VIBRATION TESTING LABORATORY

Vasile Bacria[1], *Sebastian Capotescu*[2], *Nicolae Herisanu*[1]

[1] Politehnica University of Timisoara, Faculty of Mechanical Engineering, nicolae.herisanu@upt.ro
[2] GreenForest Furniture & Fit Out, Timișoara, Romania

Abstract - *There are many situations of closed spaces in which noisy equipment generate such a noise that exceeds admissible limits, which is very detrimental for workers. This is the case of a shaker used for vibration tests, which is placed along with auxiliary equipments in a closed space of a vibration testing laboratory. The generated noise having a very high level determined the owner to search for reduction solutions. In this respect, measurements were organised to evaluate the characteristic parameters of the noise in the vibration laboratory and neighbourhood. Based on the obtained results an appropriate solution for acoustic arrangement is proposed. The efficiency of the applied solution will be investigated by a new round of measurements. In the paper are presented the investigations on the described situation.*

1. INTRODUCTION

In many industrial units there is often the situation of having closed spaces in which installations operate that generate a noise whose level exceeds the allowed limits, affecting the personnel working in these spaces and in the neighboring spaces.

This is the case for an industrial unit that has a vibration test shaker and ancillary equipment located between an enclosed space located on the ground floor of the building intended for a vibration test laboratory.

In order to determine the degree to which the general noise of this shaker exceeds the permissible limits and how it affects persons working in the vibration test laboratory and in the surrounding areas, measurements were made by which the characteristic parameters of the noise were determined at the working point near the shaker, in the surveillance room and also in the upstairs meeting room.

After the measurements, the values obtained for the noise characteristic parameters were compared with the permissible limit values for the three mentioned rooms.

This comparison showed that the values obtained by measurements exceed the permissible limit values, proving that the noise generated by the shaker affects the personnel working in the space intended for it and in the neighboring ones.

From here it was identified the need to reduce the noise level by applying appropriate measures.

In this sense, because it is not possible to act directly on the shaker to reduce the noise level in the room in which it operates, one must act on its propagation path.

After implementation, performing new measurements will allow the evaluation of the effectiveness of the applied solution.

2. INVESTIGATION OF THE EXISTING SITUATION

To characterize the noise climate of noise exposure in the vibration test laboratory, in the meeting room, as well as to establish the noise reduction solution, the existing situation was investigated by performing measurements of noise characteristics in the enclosed spaces mentioned above.

The vibration test laboratory comprises the test enclosure and an adjoining surveillance control room (fig.1).

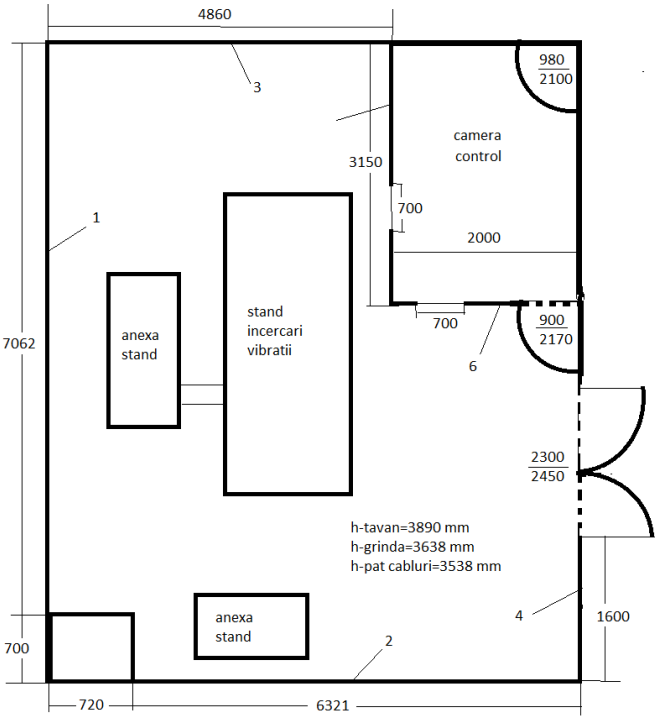

Fig. 1 *The vibration test laboratory*

A shaker for vibration testing and auxiliary equipment is located inside the laboratory. The test chamber is a closed enclosure where multiple reflections of acoustic waves occur due to the walls of the hall which are strongly reflected so that the test enclosure is characterized by a complex acoustic field.

The surveillance/control room is separated from the laboratory enclosure by an insulating wall so that two distinct

areas of acoustic field are well delimited. The meeting room is located upstairs above the laboratory.

The measurements were performed during the vibration test process under normal operating conditions of the equipment. Two positions specific to the test laboratory were investigated, the first in the control room and the second in the test room, the microphone being located at 0.1m ± 0.01 m from the entrance to the external auditory canal that receives the highest exposure value.

In addition, measurements were performed in the meeting room located above the test laboratory where the structural transmissibility makes the noise present.

Before and after performing the series of measurements, a check of the calibration status of the entire measuring system was performed by applying an acoustic calibrator with a 94 dB calibrated signal at the frequency of 1000 Hz.

The automatic measurement mode was used and after the measurement time elapsed the recorded data was saved. These were transferred to the computer and then listed. The validity of the equipment calibration certificates was also verified.

The method for determining the noise characteristic parameters according to [5] and the complementary documents such as PS-01 "Determination of the noise characteristic parameters" and IL-01 "Instructions for determining the noise characteristic parameters", as well as [6], [7] were used.

Given the general noise that is maintained regularly throughout the operation, five samples were taken for each station using sampling according to Art.11 from [7].

The duration of a sample was set at five minutes in agreement with [5] to cover all characteristic phases of noise manifestation, for each point being measured five samples.

A load-based measurement strategy was applied according to [5], Chapter 9.

The tests were performed using the noise analyzer Bruel&Kjaer type 2250 class 1 with windscreen, acoustic calibrator Bruel & Kjaer type 4231 and anemometer Testo 410-2.

During the measurements in the area of the investigated workplace, there were normal environmental conditions.
In parallel with the recording of noise parameters, the speed of air currents, relative humidity and temperature were monitored, which did not influence the propagation conditions of sound waves.

There were no other noise sources affecting the measurement result.

The measurements were performed by the acoustics and vibration laboratory from the Polytechnic University of Timișoara, accredited by RENAR.

The characteristic parameters of the noise were determined by the variation of the noise level over time as well as the spectral and statistical distribution of the noise at the working point next to the shaker, in the surveillance/control room and in the upstairs meeting room.

The summary of the final results regarding the noise exposure of the operator is presented in Table 1, in which LCpeak is the maximum weighted peak noise level and LEx8h is the daily noise exposure level for a nominal working day of 8 hours calculated according to [5].

Table 1 *Noise exposure parameters*

No	Working point	LCpeak [dB(C)]	Lex8h [dB(A)]
1	Near sheaker	118.93	100.11
2	Control room	102.55	79.44
3	Meeting room	98.34	59.59

The values of sound pressure levels in dB in octave bands corresponding to the Cz noise curves measured at the three working points are shown in Table 2.

Table 2 *Sound pressure levels in octave bands*

	31.5Hz	63Hz	125Hz	250Hz	500Hz	1kHz	2kHz	4kHz
1	77.1	84.9	93.2	97.1	95.3	96.3	94.3	74.9
2	66.9	69.9	82.6	79.9	75.6	74.0	73.8	53.7
3	60.5	59.6	58.8	57.1	60.6	52.5	46.6	37.7

The following are diagrams of the variation of the noise level over time, of the spectral distribution of the noise in frequency bands and the statistical distribution of noise levels for the investigated jobs.

a) Near shaker.

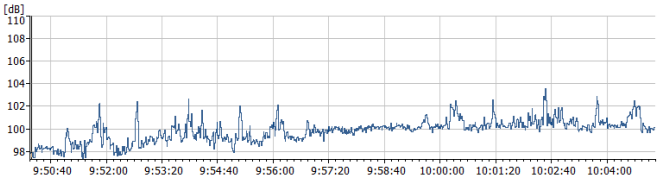

Fig. 2 *Time history of the noise near the shaker*

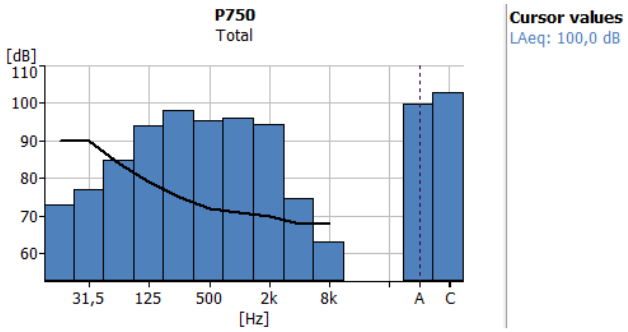

Fig. 3 *Spectral distribution of the noise near the shaker*

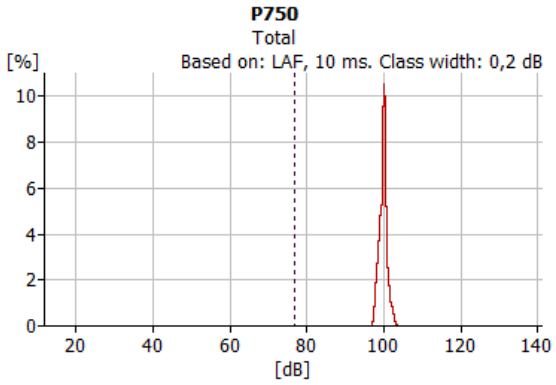

Fig. 4 *Statistical distribution of the noise near the shaker*

b) Control room

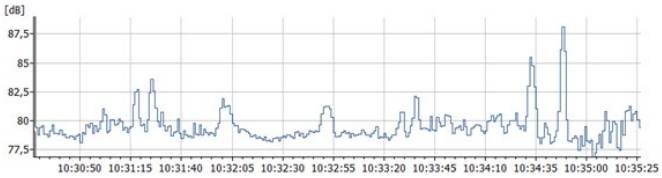

Fig. 5 *Time history of the noise in the control room*

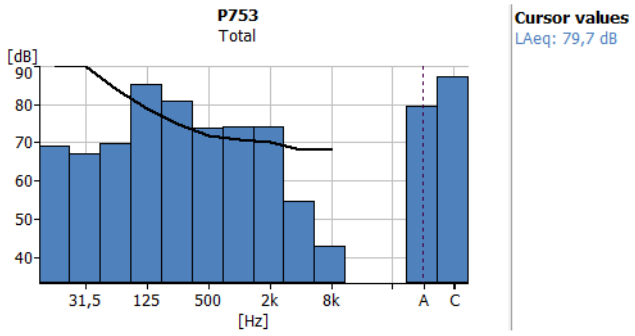

Fig. 6 *Spectral distribution of the noise in the control room*

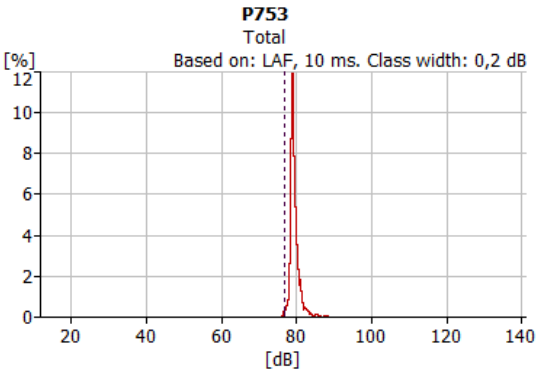

Fig. 7 *Statistical distribution of the noise in the control room*

c) Meeting room

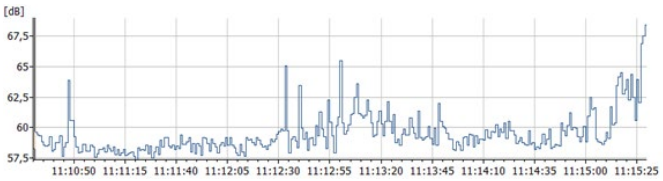

Fig. 8 *Time history of the noise in the meeting room*

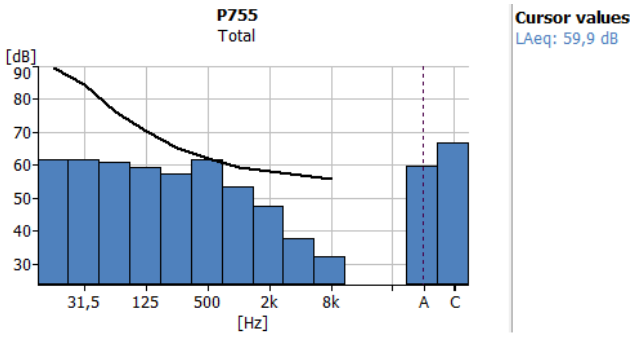

Fig. 9 *Spectral distribution of the noise in the meeting room*

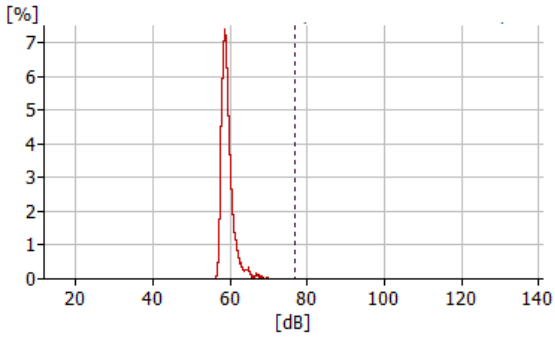

Fig. 10 *Statistical distribution in the meeting room*

Having the values of the measurements performed, it is necessary to compare them with the limit values allowed by the regulations in force.

In accordance with HG 493/2006 on the minimum safety and health requirements for exposure to noise risks, the maximum permitted limit is 87 dB.

The daily personal exposure to noise of an employee is expressed using relation [5]:

$$L_{EX,8h} = L_{p,A,eq,Te} + 10\lg\left[\frac{T_e}{T_0}\right] \quad dB \qquad (1)$$

where

$$L_{p,A,eq,Te} = 10\lg\left[\frac{\frac{1}{T}\int_{t_1}^{t_2} p_A^2(t)dt}{p_0^2}\right] \qquad (2)$$

in which $L_{p,A}$ is the weighted continuous equivalent sound pressure level a for T_e duration, T_e is the effective duration in hours of a working day, T_0 is the reference duration (8 hours), p(t) is the A-weighted instantaneous pressure to which it is exposed in the air at atmospheric pressure an employee, p_0=20 μPa is the reference sound pressure.

The weekly noise exposure level is defined as the time-weighted average of the daily noise exposure levels between a nominal week of 5 working days.

Having a daily noise exposure level of 100,11 dB(A), this exceeds the maximum value allowed in the vibration test chamber with 13.1 dB. In the same time, using the Eq. (1) it is established that the presence of the operator in the vibration test chamber for maximum 0.077 hours would provide a daily exposure level of 79.9 dB, i.e. the lower exposure value from which the action of the employer is triggered according to [7], while the presence in the test chamber for a maximum of 0.39 hours (23 minutes) would ensure a daily exposure level of 86,9 dB, i.e. below the higher exposure value allowed with the wearing of protective equipment.

Any duration longer than those specified shall lead to exceeding the permitted limits of [7].

Also according to [9] the maximum permissible values of the continuous noise level equivalent in the annex rooms of the production halls are:
- in the control room 75 dB and the Cz 70 noise curve
- in the sitting room 40 dB and the noise curve Cz 35
Table 3 shows the allowable values corresponding to the two mentioned Cz curves.

Table 3 *Allowable values corresponding to Cz curves*

C_z	31.5Hz	63Hz	125Hz	250Hz	500Hz	1kHz	2kHz	4kHz
70	103.1	90.8	89.9	77.1	73.0	70	67.5	65.7
35	79.2	63.1	52.4	44.5	38.9	35	32.0	29.8

Comparing the measured noise levels presented in table 1 and 2 with the limit values allowed according to the regulations in force [7], [9], it is found that they are exceeded as follows.

a) in the case of the working point in the vibration test chamber near the shaker the overrun is as mentioned by 13.11 dB(A).

b) in the surveillance control room the excess is 4.4 dB(A)

c) in the upstairs meeting room the excess is 19.99 dB(A)

d) the exceedances of the sound pressure level in dB in octave bands corresponding to the noise curves in the surveillance/control room and in the meeting room are presented in table 4.

Table 4 *Exceedances of the sound pressure level in dB in octave bands (1-control room; 2-meeting room)*

C_z	63Hz	125Hz	250Hz	500Hz	1kHz	2kHz	4kHz	8kHz
1	-	-	2.77	1.6	4.03	6.26	-	-
2	-	6.44	0.67	21.7	17.5	14.36	7.37	3.52

From the analysis of the values presented in table 4 it is found that in the surveillance control room the exceedances are 1.6-6.26 dB(A) in the frequency bands of 1/1 octave with the centered frequencies of the bands 250-2000 Hz and in the case of the meeting room the exceedances are of 3.50-21.7 dB(A) for centered frequency bands of 125-8000 Hz.

In this case the most significant exceedances are in the centered frequency bands of 500, 1000 and 2000 Hz.
solution.

3. THE PROPOSED ACOUSTIC ARRANGEMENT SOLUTION

Knowing the conclusions regarding the exceedances of the global noise level and the levels in different frequency bands, one can identify the need to reduce the noise level and apply an appropriate insulation.

In this regard, because it is not possible to act directly on the shaker to reduce the noise level in the room in which it is located and implicitly in the working point, it will act on the propagation path.

Because the noise level at one point of the acoustic field is the result of overlapping the effects of direct waves and reflected ones, the reduction of the latter contribution is done by treating the walls and ceiling of the closed space where the shaker is located with sound-absorbing materials.

The reduction of the noise level in the surveillance control room and in the meeting room located upstairs is achieved both by reducing the noise in the room where the vibration test shaker is located and on the transmission path between it and the two adjacent rooms.

Taking into consideration all these, the acoustic arrangement solution consists in:

a) the two metal sheet walls (1 and 2 from Fig.1) which constitute vibrating and reflective plates are stiffened by fixing them on double layer plasterboard, an acoustic board and an additional standard plasterboard which are phonic insulators.

These tiles are covered with sound-absorbing decorative tiles Basotect 615 x 615 x 60 mm..

b) covering the two rigid walls (3 and 4 from Fig.1) with sound-absorbing decorative plates Basotect 615 x 615 x 60 mm.

c) the separating walls between the laboratory room (the vibration test chamber) and the surveillance control cabin are arranged acoustically by mounting on them a layer of insulating material Blocktec 70 of 3.5 mm (7.5 kg/m2), a double layer of drywall, an acoustic board with an additional standard drywall, and on the outside the application of decorative sound-absorbing boards Basotect 615 x 615 x 60 mm.

d) the glass in the control cabin is replaced with triple-glazed glass which achieves an insulation of 40 dB.

e) the passage door from the laboratory to the control room is replaced with one that achieves an increased sound insulation

f) the passage from the laboratory to the optional production hall can be replaced with one that achieves a higher sound insulation

g) the acoustic arrangement of the ceiling comprises the application of a sound and vibration insulation membrane

made of Blocktec 70 at the level of the ceiling, realization of an apparent plasterboard acoustic plate and the application of sound-absorbing decorative plates Basotect 615 x 615 x 60 mm on the apparent ceiling.

The materials indicated for the execution of the work is characterized by very good sound-insulating and sound-absorbing properties.

Thus, the phonic and anti-vibration Blocktec 70 insulation material has a high degree of sound insulation, the values of which, depending on the frequency, are given in table 5.

Table 5 *Sound insulation degree - blocktec 70 insulation material*

Dimension [mm]	Frequency [Hz]					
	100	315	630	1250	2500	5000
3.5	18.1	20.9	25.0	30.0	34.5	38.9

As can be seen from Table 5, this very high degree of isolation is manifested in the frequency range of the noise generated by the shaker.

This feature is also valid for decorative melamine foam boards Basotect.

It should also be noted that due to the fact that the Blocktec 70 membrane has high density, it allows the addition of mass on the construction system without taking up space at all.

It is easy to apply thanks to the self-adhesive foil.

It significantly reduces points with weaker insulation due to the resonance frequency and the frequency of coincidence typical for traditional construction structures.

In combination with sound-absorbing materials the membrane generates some products with high performance sound insulation.

Gypsum boards make a contribution to increasing the degree of sound insulation by surface mass that they add to the mass of existing structures and in combination with sound-absorbing and sound-insulating materials.

In addition, this plasterboard with a thickness of 12.5 mm is used, which is particularly good for improving the acoustic performance of existing walls.

Expected performance is obtained in combination with ordinary plasterboard.

The laminated sound insulation glass of 8.7 mm that replaces the old one will achieve a 46 dB reduction of the noise level that will be transmitted in the control room, which will lead to a noise level within the allowed limits.

The material from which the passage door from the vibration test chamber to the control chamber is made ensures a sound insulation of 42 dB and the passage door from the laboratory to the production hall ensures a sound insulation of 41 dB.

Based on the proposed design solution taking into account the insulating and sound-absorbing characteristics of the materials and evaluations of the surfaces of the partitions of the vibration test laboratory, the necessary materials were determined and then implemented.

In order to evaluate the efficiency of the implemented solution, new measurements will performed, the result of which will be analysed and presented in a future paper.

REFERENCES

[1] M. Grumăzescu, A. Stan, N. Wegener, *Combaterea zgomotului şi vibraţiilor*, Bucureşti: Ed. Tehnică, 1975.

[2] E. Ia. Iudin, *Izolarea împotriva zgomotului*, Bucureşti: Ed. Tehnică, 1968.

[3] M. Gafiţanu, V. Focşa, V. Merticaru, L. Biborotsch, *Vibraţii şi zgomote*, Iaşi: Ed. JUnimea, 1980.

[4] A. Darabont, D. Văiteanu, *Combaterea poluării sonore şi a vibraţiilor*, Bucureşti: Ed. Tehnică, 1975.

[5] *** SR ISO 9612:2009, Acustică. Determinarea expunerii la zgomot în mediul de muncă. Metodă tehnică.

[6] *** Directive 2003/10/EC of the European Parliament and of the Council on the minimum health and safety requirements regarding the exposure of workers to the risks arising from physical agents (noise)

[7] *** H.G.493/12.04.2006 privind cerinţele minime de Securitate şî sănătate referitoare la expunerea lucrătorilor la riscurile generate de zgomot.

[8] V. Bacria, N. Herişanu, "Noise control in an industrial hall", *Applied Mechanics and Materials*, vol. 430, pp. 251-256, 2013.

[9] *** SR 6156:2020, Acustica în construcții. Protecția împotriva zgomotului în construcții civile și social-culturale. Limite admisibile și parametri de izolare acustică

BRÜEL & KJÆR
SOUND & VIBRATION
MEASUREMENTS

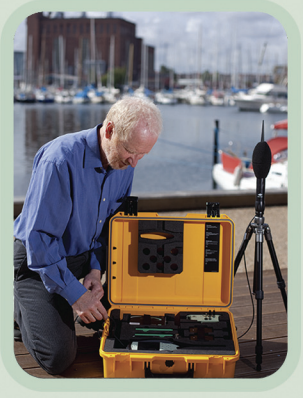

We help our partners and customers
measure and manage
the quality of sound and vibration
in products and enviroment

With more than 90 sales offices or local agents,
we provide immediate and comprehensive
customer support

Contact your local
sales representative:

RMS d.o.o.
Partizanske avijacije 12/3
11070 Novi Beograd, Srbija
Tel.: +381(0)11 2280 951
Fax: +381(0)11 2280 751
www.rms.rs

Brüel & Kjær
an HBK company

University of Nis
Faculty of Occupational Safety
„Politechnica“ University of Timisoara
Faculty of Mechanical Engineering
27th International Conference
NOISE AND VIBRATION
Niš, 20 - 21. 10. 2022.

IDENTIFICATION OF RESONANCE FREQUENCIES OF TONE WOOD USED FOR MUSICAL INSTRUMENTS

Mariana Domnica Stanciu[1], Silviu Marian Nastac[1,2], Camelia Cosereanu[1], Vasile Ghiorghe Gliga[1,3], Florin Dinulică[1], Roxana Gall[1], Eugenia Filimon[1]

[1] Transilvania University of Brasov, Faculty of Mechanical Engineering, Romania, mariana.stanciu@unitbv.ro
[2] “Dunarea de Jos” University of Galati, Faculty of Engineering and Agronomy, Braila, Romania
[3]S.C. Gliga Musical Instruments S.A., Reghin, Romania

Abstract - *In the analysis of the vibration modes of violins, "signature modes" are generally evaluated, which represent the frequency response of the violin body due to the structure of the materials used in their construction and the geometry of the violin body. This paper presents the experimental results made on rectangular boards made of spruce and maple wood, with different macroscopic anatomical structures. The modal analysis of the boards was achieved by exciting them with the impact hammer at different points on the board surface, the response in time and frequency being evaluated based on the signals of the three accelerometers fixed on the board. The results highlighted the influence of the material structure on the resonance frequencies and the frequency spectrum.*

1. INTRODUCTION

In Romania, a wide and varied range of chordophone musical instruments is manufactured, in terms of dimensions, materials and structural form, wood being the basic material for their construction, both in terms of acoustic quality (resonance wood-spruce resonance) as well as from an aesthetic point of view (mahogany, ebony, rosewood, curly palatine - appreciated for texture, design and color), as well as from the point of view of viability and resistance to wear (acacia, ebony, walnut). Resonance wood means wood material with a very fine structure, respectively with physical properties suitable for the construction of stringed musical instruments. Regardless of the field of applicability of wood, knowing the elastic properties is necessary for the design of structures, for the predictability of their behavior over time, for the possibility of the optimal choice of the material. Moreover, in stringed musical instruments, the elastic, acoustic and dynamic properties correlated with the anatomical and physical descriptors of the wood provide the scientific argument for the acoustic quality of the musical instrument and last but not least the economic argument for the price of the finished product [2; 4].

The most important elastic, mechanical, acoustic and dynamic properties of the soundboard studied in the literature can be divided into fundamental (basic) properties and secondary properties (calculated on the basis of the primary ones). Among these, the following can be mentioned: the propagation speed of sound waves in wood in the longitudinal and radial direction; longitudinal and radial modulus of elasticity; resonance frequency; specific modulus of elasticity; the dynamic module; specific acoustic resistance (impedance); acoustic radiation; logarithmic decrement; the quality factor [5,6].

In this sense, the study presents the research carried out on spruce and maple wood boards with different anatomical structures, grouped into two quality classes A and D. Thus, the paper presents the modal analysis carried out on the wood boards, being identified for each species and the quality class, the values of the natural frequencies and the frequencies spectrum.

2. METHODOLOGY

2.1 Materials

Four categories of wood samples were analyzed in the study: two categories belong to the spruce species coded M, the difference consists in the anatomical structure of the wood (the width of the annual rings, the proportion of early wood and that of late wood, these being grouped in class A and D), respectively samples from the maple wood species coded P, divided into class A and D (in class A, maple with wavy fiber, and in class D - maple with straight fiber) (Fig. 1).

Fig. 1a *The studied samples - spruce (Picea Abies L.) from A and D quality class*

b)

Fig. 1b *The studied samples - maple (Acer Pseudoplatanus L.) from A and D quality class*

From a geometric point of view, the samples are plates with the dimensions of 240 mm (length) x 80 mm (width) and the thickness of 4 mm.

Table 1 *Physical featuters of samples*

Samples (No. of plates)	Average values		
	Mass (g)	Annual ring width (mm)	The pitch of the curly fiber (mm)
MAUV (3)	36.54	1.045	-
MDUV (3)	33.11	1.985	-
PAUV (3)	53.36	1.249	5.448
PDUV (3)	47.43	0.987	-

2.2 Methods

2.2.1 Experimental set-up

The experimental set-up consists of the system shown in Fig. 2. Sample (1) is suspended elastically. The signals produced by means of the impact hammer (2) are received by the uniaxial accelerometers (3) located on the plate and transmitted to the acquisition plate (4). Visualization of the signals and their processing was carried out in a program developed in MatLab on a PC (5) (Fig. 2a). Each wooden plate was excited in the three points A9; B8; C7 according to the scheme in Fig. 2b, the signals being acquired with the accelerometers positioned at points A2; B3; C4. A similar method was applied by [7–11].

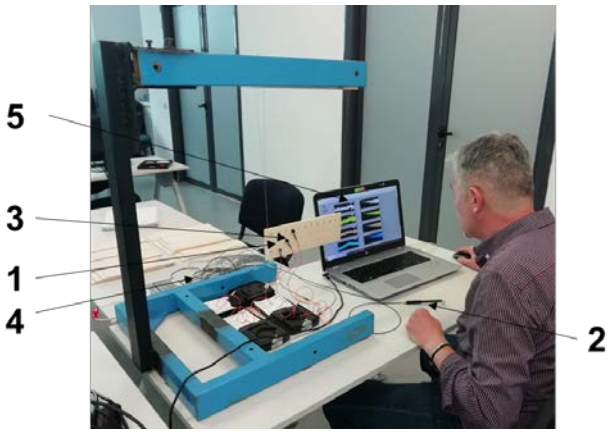

Fig. 2a *Experimental set-up - sample testing method*

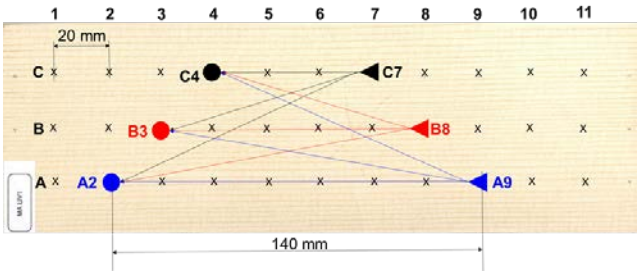

Fig. 2b *Experimental set-up - the variants of signals acquired by hitting the three points A9; B8; C7 and and receiving the signals in the points A2; B3; C4*

2.2.2 Processing signals

The processing of the signals consisted in the time and frequency analysis of the signals for each plate, obtaining both the spectrum of the resonance frequencies and their values. In the next stage of signal processing, these results were correlated with the anatomical descriptors of the wood for each individual category. In Fig. 3 shown the time analysis of signals for each accelerometer denoted A2, B3 and C3 and the force variation due to impact excitation.

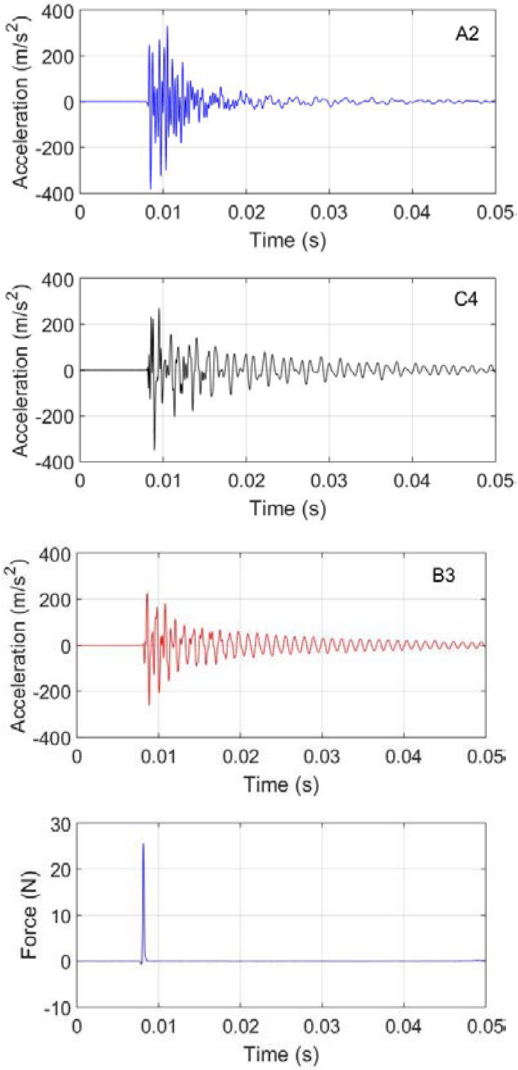

Fig. 3 *Time analysis of recorded acoustic signals*

3. RESULTS AND DISCUSSIONS

3.3. The frequencies spectrum

In Fig. 3 shows the frequency spectra for the four categories of wooden boards tested. Thus, it can be observed that the resonance frequency values differ from one species to another, for spruce wood boards, the dominant frequency is recorded around 1040 Hz, compared to maple wood for which the value of 880 Hz is recorded.

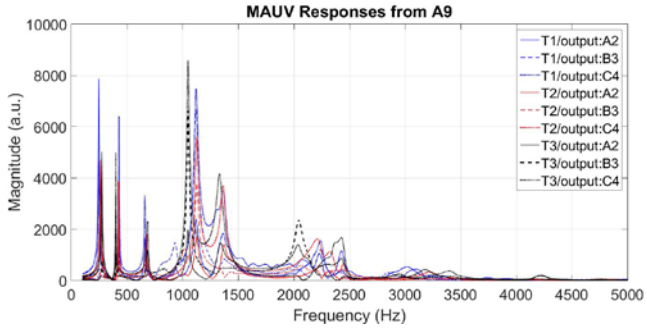

a)

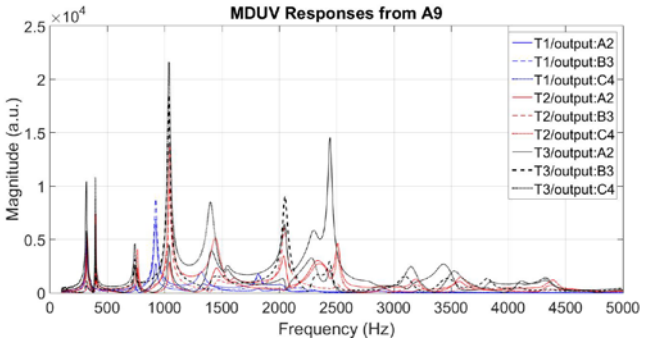

b)

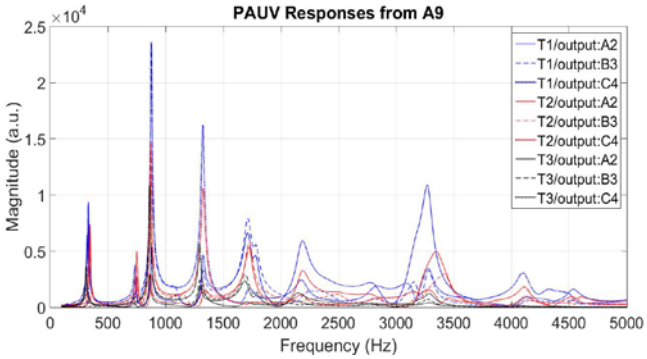

c)

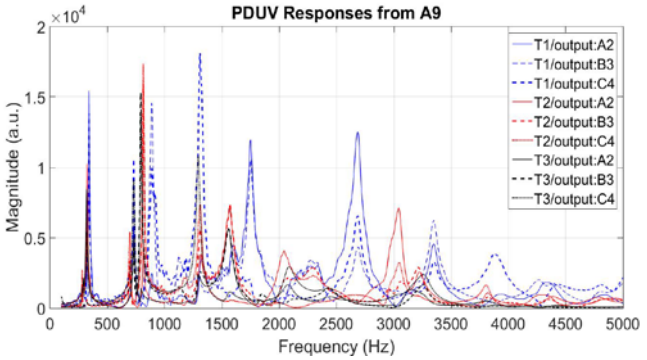

d)

Fig. 4 *The frequencies spectrum: a) spruce plates class A; b) spruce plates class D; c) maple plates class A; d) maple plates class D*

It is also observed that the anatomical and morphological structure of the wood, which differs within the same species, influences the frequency response of the tested boards. The values are presented in Table 2.

Table 2 *The first resonance frequencies*

Samples	Resonant frequencies (Hz)				
	f_1	f_2	f_3	f_4	f_5
MAUV 1	246	428	661	1122	
MAUV 2	262	423	676	1126	
MAUV 3	274	399	685	1048	
MDUV 1	323	360	750	921	
MDUV 2	326	399	763	1045	
MDUV 3	318	396	742	1038	
PAUV 1	-	342	730	887	1310
PAUV 2	282	324	699	813	1310
PAUV 3	292	318	732	795	1299
PDUV 1	-	330	735	877	1328
PDUV 2	317	344	751	872	1326
PDUV 3	314	333	730	862	1296

Both in Fig. 4 as well as Fig. 5 the convergence of the signals for the three measurement points can be observed. The correspondence between the modal frequencies and the measurement points for the studied plates is observed. Thus, in the low frequency range (10-500 Hz), experimentally identified modal frequencies are found for most measurement points (Figure 5).

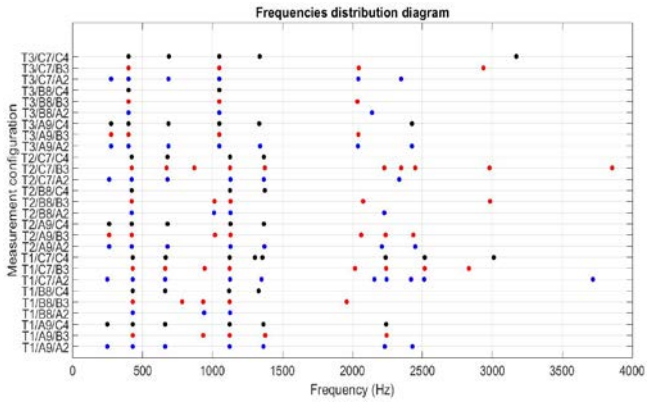

Fig. 5a *Frequency distribution diagrams - spruce plates class A*

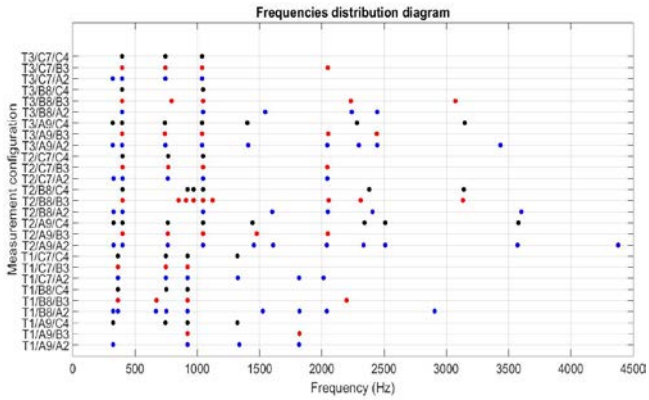

Fig. 5b *Frequency distribution diagrams - b) spruce plates class D*

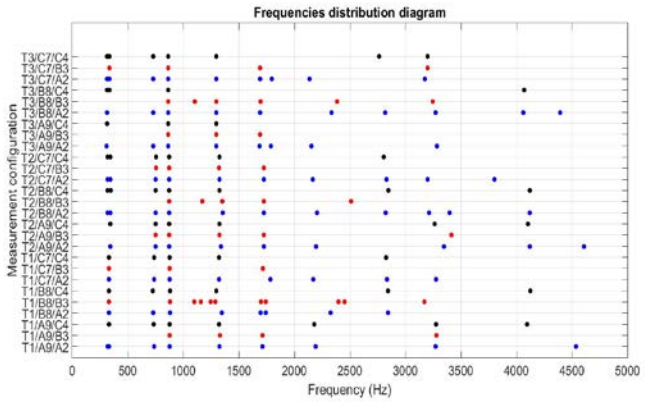

Fig. 5c *Frequency distribution diagrams - c) maple plates class A*

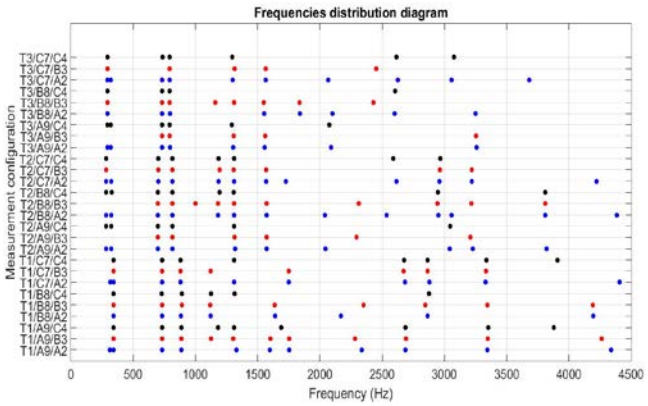

d)

Fig. 5d *Frequency distribution diagrams - maple plates class D*

An interesting aspect to mention is the fact that both class A spruce and class A maple samples show the best convergence of signals, as a result of a more homogeneous anatomical structure of the wood than in the case of quality class D. Although the dominant frequencies differ from one board to another, they are found in the frequency spectrum of the category they belong to (Fig. 4).

Maple wood boards present a richer spectrum of frequencies than spruce wood boards. It is known that the paltin wood is characterized by a complex structure, with distinct annual rings, with a regular outline, without a pronounced difference between the early and the late wood. From the point of view of microstructure, it presents pores uniformly scattered, small, invisible to the naked eye, visible with a magnifying glass, relatively rare (30 – 50/mm^2), single or in radial rows (2 – 5), with the opening almost equal throughout the width of the annual ring, and their membranes (longitudinal walls) show helical thickenings and large intervascular punctuations, with a diameter of about 18μm and arranged in a honeycomb (Fig. 6). Anatomically, spruce wood is a non-porous wood with a fine and uniform structure, with invisible pith rays on transverse and tangential sections, without wood parenchyma [5, 10, 11]. With increasing frequency, their spectrum differs from one plate to another both between species and between classes of anatomical and structural quality. The anisotropy of wood comes both from the way its biological structure is organized and from its main components: cellulose, lignin and hemicelluloses. Thus, the cell wall of wood has a composition in which crystalline cellulose fibers are embedded in substances with an amorphous matrix [12–15].

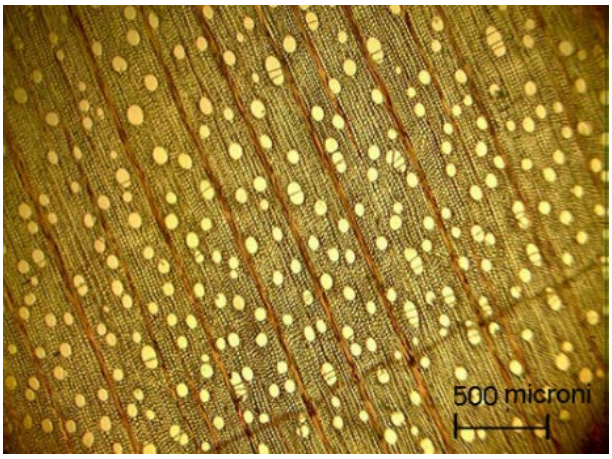

a)

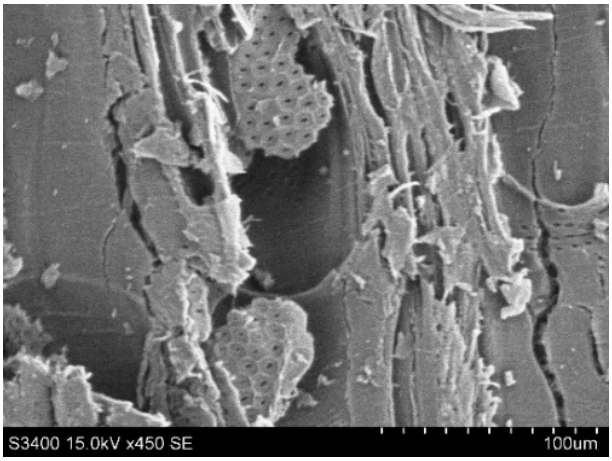

b)

Fig. 6 *Anatomical structure of maple wood: a) cross section; b) SEM analysis detail*

It can be seen in Fig. 7, as the position of the excitation point quantitatively and qualitatively influences the convergence diagram: the excitation from point A9 (located at the greatest distance from the measurement points) returns modes and eigenvalues much better outlined and with a wider spectrum of frequencies, compared to the other points B8 and C7. The frequency analyzes in Fig. 7 are for class D maple board. A similar trend was observed for the other boards tested.

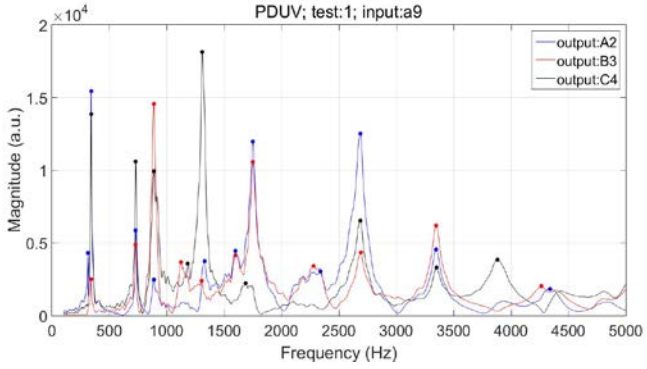

Fig. 7a *The signals generated in different excitation points in case of maple plates, class D - excitation point A9*

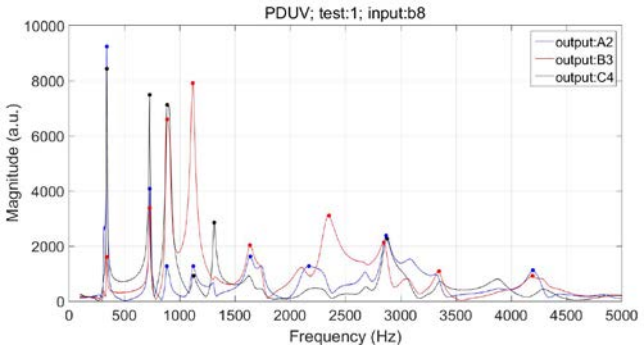

Fig. 7b *The signals generated in different excitation points in case of maple plates, class D - excitation point B8*

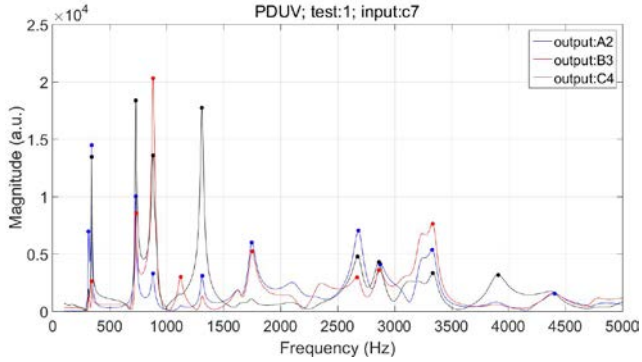

c)

Fig. 7c *The signals generated in different excitation points in case of maple plates, class D - excitation point C7*

Fig. 8 presents the statistical analyzes regarding the variation amplitude of the standard deviation for the resonance frequencies specific to each category of boards. For boards with a uniform and quasi-homogeneous structure, it can be observed that the deviations between the resonance frequencies of the signals recorded on the three boards at different measurement points are reduced at low frequencies, than in the case of class D boards (spruce and maple). As the frequency bands increase, the variability increases from one plate to another, from one species to another. The biggest deviations are observed for class D boards, both for those made of spruce wood and for those made of poplar wood (approximately +/-6 Hz). The main differences among species are located in the 200–2000 Hz band, accordance with [9].

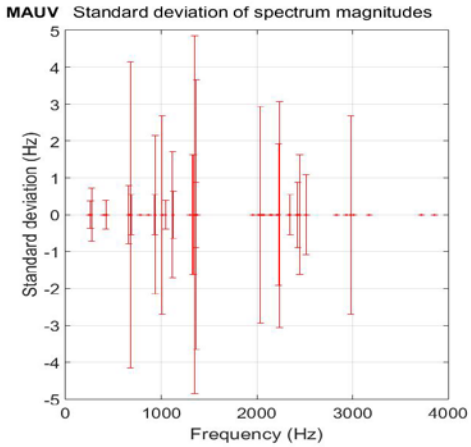

Fig. 8a *Statistical analysis regarding the standard deviation of resonance frequency values - spruce plates class A*

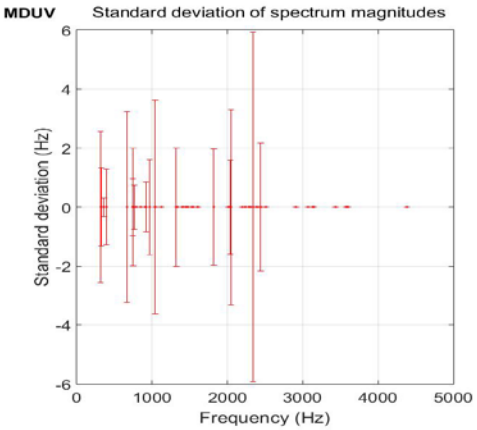

Fig. 8b *Statistical analysis regarding the standard deviation of resonance frequency values - spruce plates class D*

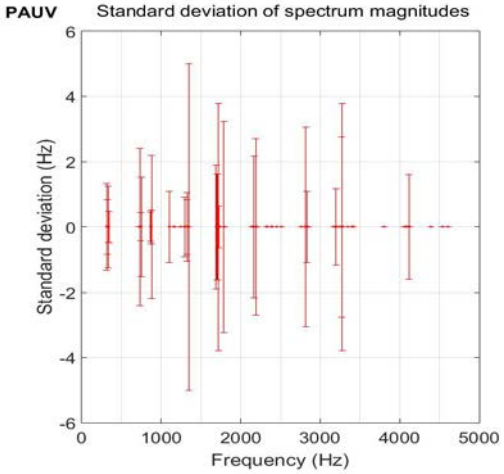

Fig. 8c *Statistical analysis regarding the standard deviation of resonance frequency values - maple plates class A*

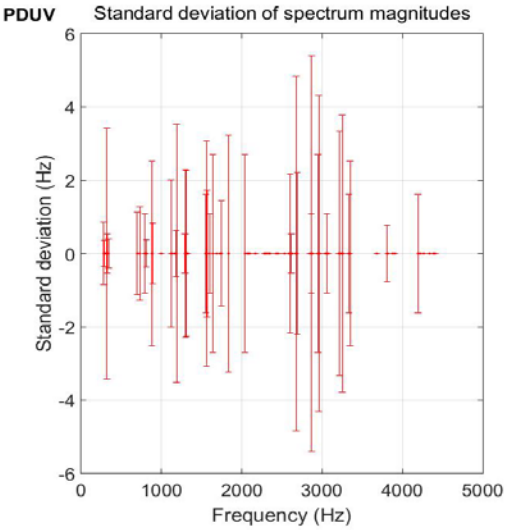

d)

Fig. 8d *Statistical analysis regarding the standard deviation of resonance frequency values - maple plates class D*

Regarding the spruce plates, similarly frequencies for second mode were reported by [16].

From an application point of view, the obtained results confirm the fact that each individual musical instrument has its own frequency spectrum and specific timbre, independent of the geometric shape and auxiliary elements. The wooden material, through its structure and the way it responds to excitations, gives the chordophone musical instrument its specific timbre and series of more or less rich harmonics.

4. CONCLUSION

The research presented in the paper aimed to highlight the modal frequencies of spruce and maple boards used in the construction of stringed musical instruments. Since the timbre of violins and their acoustic quality is closely related to the wood species used, the identification of resonance frequencies helps to understand the formation of signature modes, as well as to evaluate the connection between the structure of the material, the anatomical quality class and the acoustic quality class of the musical instrument.

ACKNOWLEDGMENTS

This research was supported by a grant of the Ministry of Research, Innovation and Digitization, CNCS/CCCDI – UEFISCDI, project number PN-III-P4-PCE2021-0885, ACADIA – Qualitative, dynamic and acoustic analysis of anisotropic systems with modified interfaces, PCE61/2022.

REFERENCES

[1] J.C. Schelleng, “Acoustical effects of violin varnish”. *J. Acoust. Soc. Am.*, vol. 44, pp. 1175–1183, 1968.

[2] C.K. Su, et al. “Materials Engineering of Violin Soundboards by Stradivari and Guarneri”, *Angew. Chem.* vol. 133, pp. 19293 – 19303, 2021.

[3] N. Harris, R. Sheldon, J. Johnston, ,, A Recreation of the Particulate Ground Varnish Layer Used on Many Violins Made before 1750”, *J. Violin Soc. Am.: VSA Papers*, Vol. XXI, No. 1, pp. 1 – 15, 2007.

[4] M.D. Stanciu, F. Dinulica, V. Bucur, G.V. Gliga, S.M. Nastac, M. Campean, “Changing the Vibrational Behavior of the Wooden Thin Arched Plates – the Maestro Violins Experimental Study Case”, *Thin Walled Structures*, vol. 174, 109042, 2022. https://doi.org/10.1016/j.tws.2022.109042

[5] F. Dinulică, M.D. Stanciu, A. Savin, “Correlation between anatomical grading and acoustic–elastic properties of resonant spruce wood used for musical instruments” *Forests*, vol. 12, 1122, 2021, https://doi.org/10.3390/f12081122.

[6] U.G.K. Wegst, (2006) “Wood for sound”, *Am. J. Bot.* Vol. 93, pp. 1439–1448, 2006.

[7] A. Savin, N. Iftimie, S.M. Nastac, M.D. Stanciu, “Structural health monitoring of critical zones of small wind turbine blades for domestic users”, IManEE 2019 IOP Conf. Series: Materials Science and Engineering 564 (2019) 012067 IOP Publishing doi:10.1088/1757-899X/564/1/012067

[8] M.V. Munteanu, M D Stanciu, S M Năstac, A Savin, Modal analysis of small turbine blade made from glass fibres composites The 8th International Conference on Advanced Concepts in Mechanical Engineering - ACME 2018, June 07 - 08, 2018, http://iopscience.iop.org/issue/1757-899X/444/6

[9] J.A.M. Rojas, J. Alpuente, D. Postigo, I.M. Rojas, S. Vignote, “Wood species identification using stress-wave analysis in the audible range”, *Appl. Acous.* Vol. 72, pp. 934 – 942, 2011.

[10] M. Mihălcică, M.D. Stanciu, S.M. Nastac, F. Dinulică, A.M. Nauncef, I.C. Roșca, A. Savin, “Signature Modes of Old and New Violins with Symmetric Anatomical Wood Structure”. *Appl. Sci*., Vol. 11, 11297, 2021.

[11] M.D. Stanciu, C. Cosereanu, F. Dinulică, V. Bucur, “Effect of wood species on vibration modes of violins plates”. *Eur. J. Wood Prod*. Vol. 78, 785–799, 2020.

[12] R. Jordan, F. Feeney, N. Nesbitt, J.A. Evertsen “Classification of wood species by neural network analysis of ultrasonic signals”. *Ultrasonics*; Vol. 36, pp. 219–22, 1998

[13] V. Bucur, P. Lanceleur,B. Roge ”Acoustic properties of wood in tridimensional representation of slowness surfaces”, *Ultrasonics*; Vol. 40, pp. 537–41, 2002.

[14] E. Obataya, “Effects of natural and artificial ageing on the physical and acoustic properties of wood in musical instruments”, *Journal of Cultural Heritage*, Vol. 27S pp. S63–S69, 2017.

[15]O. Dünisch, “Frequencies in vibrating wood – Does cell organization matter?” *International Association of Wood Anatomists*, vol. 40 (1) , pp. 124 – 142, 2019.

[16] P.Dumond, N. Baddour, “Experimental investigation of the mechanical properties and natural frequencies of simply supported Sitka spruce plates”, *Wood Sci Technol* Vol. 49, pp. 1137–1155, 2015.

University of Nis
Faculty of Occupational Safety
„Politechnica“ University of Timisoara
Faculty of Mechanical Engineering
27th International Conference
NOISE AND VIBRATION
Niš, 20 - 21. 10. 2022.

THE SPECTRAL ACOUSTIC EVOLUTION OF VIOLINS BEFORE AND AFTER VARNISHING

Mariana Domnica Stanciu[1], Silviu Marian Nastac[2], Adriana Savin[1,3]

[1] Transilvania University of Brasov, Faculty of Mechanical Engineering, Romania, mariana.stanciu@unitbv.ro
[2] “Dunarea de Jos” University of Galati, Faculty of Engineering and Agronomy, Braila, Romania
[3]National Institute of Research and Development for Technical Physics, Iași, Romania

Abstract - *There are numerous factors that influence the acoustic quality of violins during the manufacturing stage. Thus, the quality of the resonating wood from the point of view of the macroscopic anatomical structure, the physical, mechanical and acoustic properties of the wood, the geometry of the resonating body, the surface coverings of the violin, respectively the varnish. The aim of this study was the comparative analysis of the spectral evolution of a violin before and after varnishing.*

1. INTRODUCTION

The concerns of luthiers in making the best quality violins revolve around the optimal choice of varnish that will lead to the prolongation of the life of the violins, protecting them from humidity variations, to a special aesthetic appearance and last but not least not to damage the acoustic quality of the violins [1–3]. There are studies that argue that the secret of famous violins is attributed to the way the wood is processed and, in particular, to the technological grinding operation, which corrects all the irregularities of the previous processing, giving the surface a quality corresponding to the finishing operations [4–8]. One of the most important Romanian luthiers from the 60s - 80s, specialized in the repair and construction of musical instruments, Roman Boianciuc, in his publication, believes that the secret of famous violins is attributed to the varnish used, supporting the hypothesis that the type of varnish used is the great secret of violins. Some studies highlight the fact that the two wood species used to make the violin body, spruce and poplar, react differently from an acoustic point of view, to the varnish treatment [2; 4].

Thus, the changes observed by [9–10] on spruce wood were much more pronounced than in the case of poplar wood. Regarding the influence of varnish on the dynamic response of violins, [11–14] found that violins coated with oil-based varnish were rated as having a better acoustic quality than those varnished with spirit-based varnish. In the case of violins varnished with oil-based varnish, the frequency of the B1+ mode recorded lower values than for the violin varnished with spirit varnish.

The objective of the study was the comparative acoustic analysis of the violins before varnishing and after varnishing in order to identify how the varnish film influences the spectrum of frequencies emitted by the violin.

2. METHODOLOGY

2.1 Materials

The violin under study was made by a famous musical instrument factory in Romania, belonging to the category of maestro instruments. The wood used for this violin comes from the Gurghiu region (Romania) and presents the following anatomical characteristics: spruce wood - the average value of the width of the annual rings 0.716 mm; Earlywood proportion of 74.97%; Latewood proportion of 25.02%; density 438 kg/m^3; paltin wood - Annual ring width of 1.249 mm; the pitch of the corrugated fiber is 5.448 mm; density of 570 kg/m^3 [15]. The wood used for these violins was stored for natural drying for about 10 years, knowing that for musical instruments, the natural drying of wood is very important. A kiln-drying of the resonant wood immediately after harvesting can lead to the destruction of the cell walls by the appearance of tensions and pressure variations at the microcellular level. Varnishing the violin consisted of applying 12 successive layers of oil-based varnish (Fig. 1).

Fig. 1 *The studied violin: before and after varnishing*

The analyzed violin is part of the Maestro quality class. The analyzed violin is part of the Maestro quality class. During its realization, the modal analysis of the boards used in the construction of the violin, of the body without a neck and then with a neck, results that were presented in [16]. In Fig. 2 shows a cross-section of the violin before varnishing, taken with a computer tomograph. It can see both the arched shape of the top and back plates, as well as the small thickness of the plates compared to the surface bordered by them.

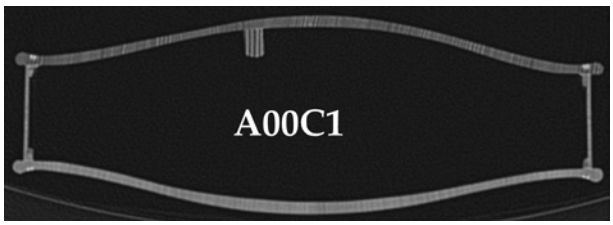

Fig. 2 *Transverse section through the violin*

2.2 Methods

2.2.1 Signals recording

The acoustic signals selected for the excitation of the violin in the three successive stages, consisted of three sequences: the excitation of the free strings; string excitation in Pizzicato style and string excitation with two musical sequences - an excerpt from Max Bruch - Concerto no.1 in G minor op. 26, PI (first cadence of the solo violin) and an excerpt from Jules Massenet - Meditation for violin and orchestra from the Opera Thaïs.

The acoustic sequences were produced by the direct interpretation by an experienced violinist, in all three study stages (unfinished violin, varnished violin after 1 month, varnished violin after 1 year). The recordings were made under the same conditions, in the concert hall of the Brasov Philharmonic. The position of the microphone in relation to the tested violin is represented in Fig. 3.

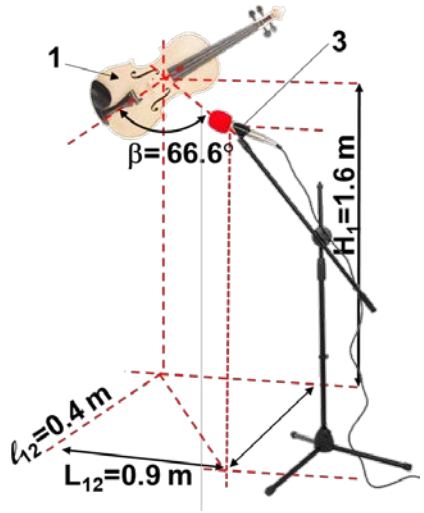

Fig. 3 *Source-receiver scheme used for recording acoustic signals*

2.2.2 Processing signals

The processing of the signals consisted of two stages: the preparation of the recorded acoustic samples, redundant recordings being eliminated and the sizing of the sample, and the second stage consisted of the time and frequency analysis of the signals applying the Fast Fourier Transform (FFT) analysis. This analysis was applied both globally, to the entire acoustic sample, and to the three recorded sequences: free strings, Pizzicato, the musical part (Fig. 4). Applying the Short Time Fourier Transform (STFT) analysis, the histograms of the frequencies of occurrence of the acoustic frequencies in 1/1 and 1/3 octave bands were obtained. The analyzes of the signals as a relationship between magnitude - time and frequency were highlighted by means of spectrograms. The values of the fundamental frequencies and the specific signature modes were extracted from the frequency analysis and compared.

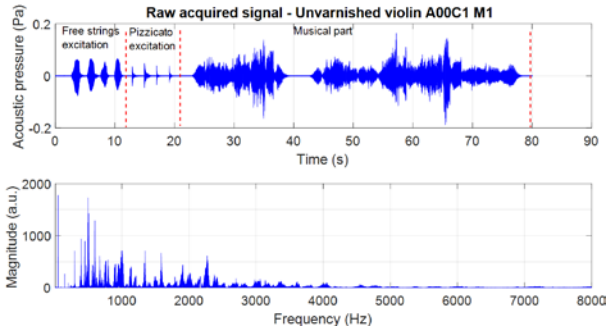

a)

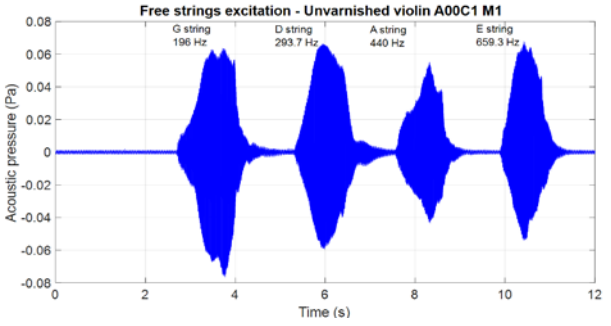

b)

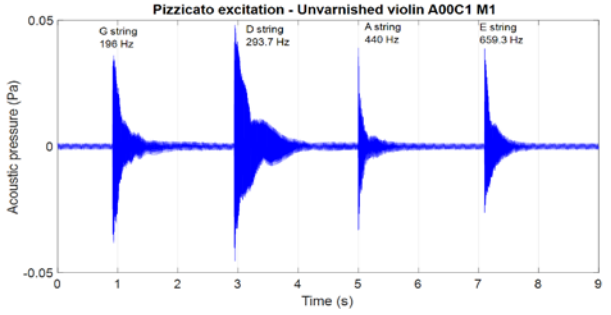

c)

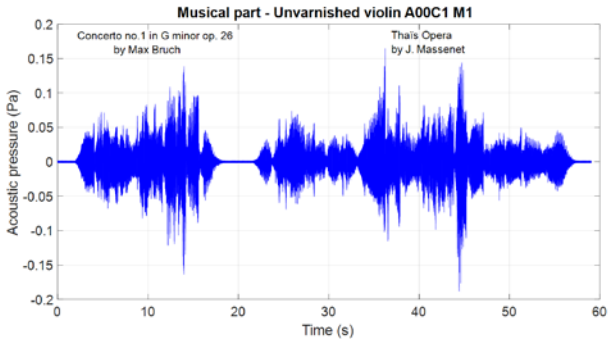

d)

Fig. 4 *Time analysis of recorded acoustic signals*

3. RESULTS AND DISCUSSIONS

Figure 5 shows the spectrograms of the acoustic signals in the three analyzed situations. This analysis separates frequencies and amplitudes into their components, they are visualized, with different degrees of amplitude (represented by the color map displayed on the right), at different frequencies (on the

horizontal axis) as a function of time (vertical). It can be seen that up to 4000 Hz, the fundamental frequencies and formants can be well located in time and have a good resolution, above 4000 Hz, the amplitude is lower. It is also observed that the application of varnish changes the response of the violin: the power of the fundamental frequencies and the first harmonics remains high for a few seconds in the one-year varnished violin, compared to the unvarnished violin, and in addition, other harmonics are also evident. The frequency analysis for the signals emitted by open strings (called in this study free strings excitation) is presented in Figure 6, where the range of 0 - 2000 Hz was selected for the analysis of the frequency spectrum for the three cases.

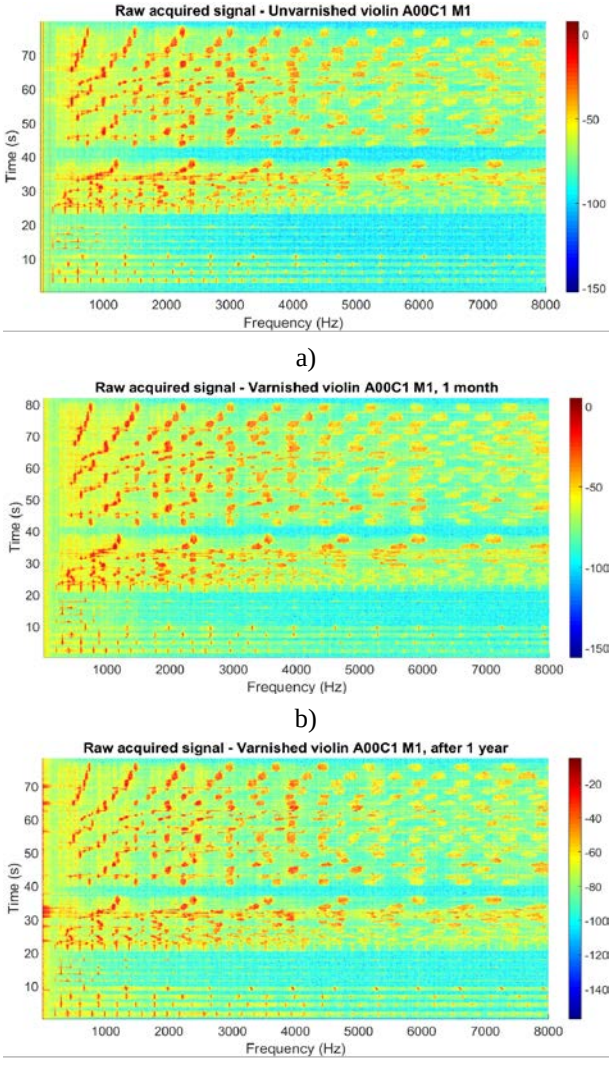

Fig. 5 *The musical signals spectrograms: a) unvarnished violin; b) after one month from varnishing; c) after one year from varnishing*

It can be seen that the resonance frequency spectrum is similar in all three stages of the violin (Fig. 6). There are differences of 3 - 6 Hz between the values of the specific modes, but according to [9–11] a tolerance of 4-5 Hz can be accepted. However, between the three stages, the appearance or disappearance of some vibration modes is noted, especially in the low frequency range (below 700 Hz). As a trend, it is observed that after one month after applying the varnish, most of the resonance frequencies tend to decrease compared to those recorded with the unvarnished violin. After one year after varnishing, a slight increase of 2 – 4 Hz is observed compared to the signals recorded after one month after varnishing the violin, but the values of these frequencies are still lower than in the case of the violin in white.

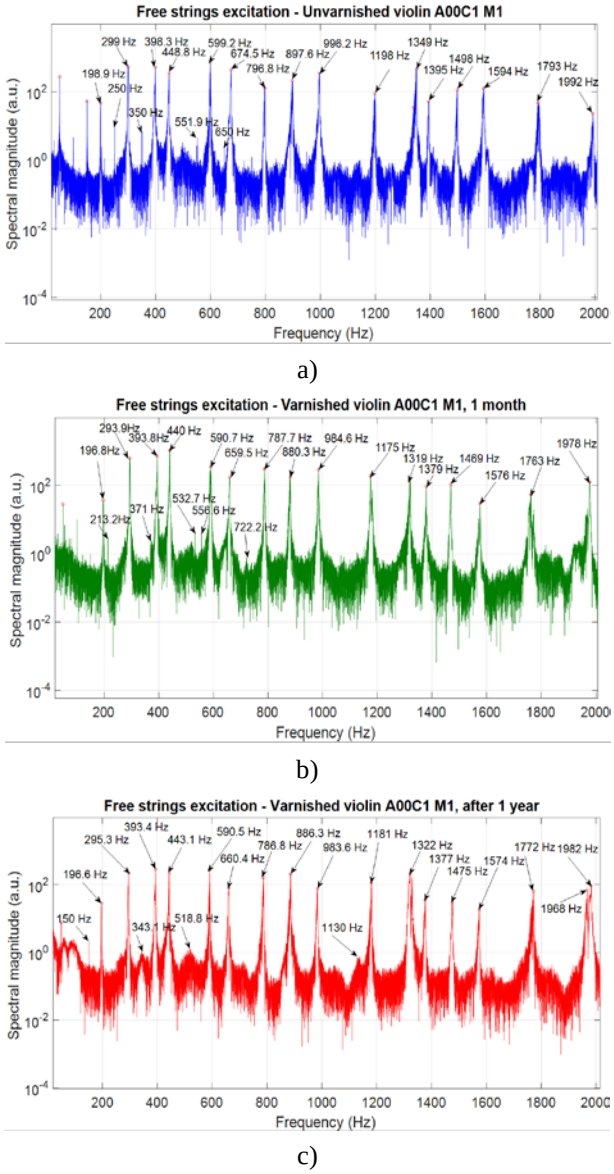

Fig. 6 *The analysis of frequency domain, in range of 0 – 2000 Hz, for open strings excitation: a) unvarnished violin; b) after one month from varnishing; c) after one year from varnishing*

In the case of the acoustic signals generated by plucking the strings in Pizzicato style, they show a similar envelope for unvarnished and varnished violins after one month, compared to the signals recorded after one year of varnishing (Fig. 7). The unvarnished and the varnished violin, recorded after one year (Fig. 7 a and c), show well-defined, distinct resonance frequencies, unlike the signals recorded after one month of varnishing (Fig. 7b).

The effect of varnish application and its curing time on the acoustics of the violin is highlighted in Fig. 8 where the values of the spectrum of frequencies emitted by the studied violin in the three different postures are represented: thus, in the case of open strings, the widest spectrum of frequencies is

recorded for the varnished violin and recorded after one year (represented in green) (Fig. 8a).

The same trend is observed for the acoustic signals corresponding to the musical parts (Fig. 8c). In the case of the signals obtained by plucking the strings, although the varnished violin and recorded after one year presents a lower spectrum of frequencies, their height is slightly higher than in the other two cases.

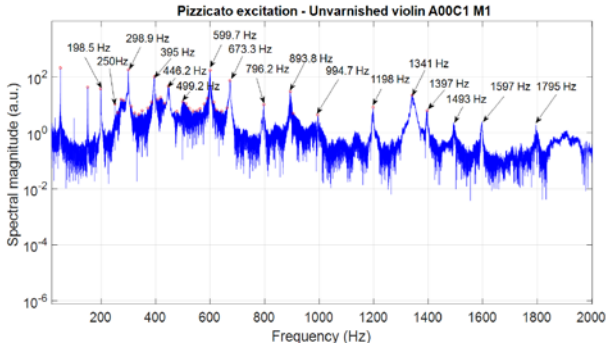

a)

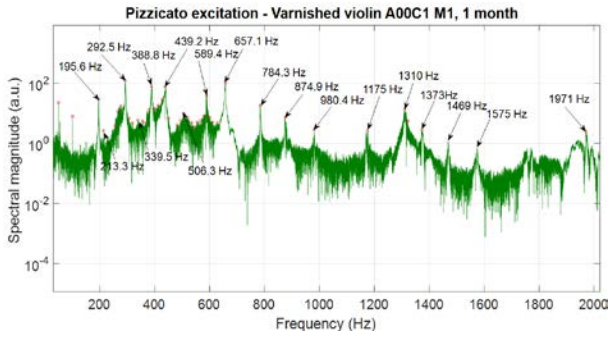

b)

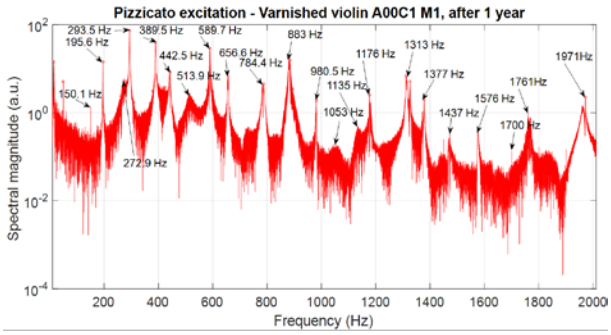

c)

Fig. 7 *The analysis of frequency domain in range of 0 – 2000 Hz, for Pizzicato excitation: a) unvarnished violin; b) after one month from varnishing; c) after one year from varnishing*

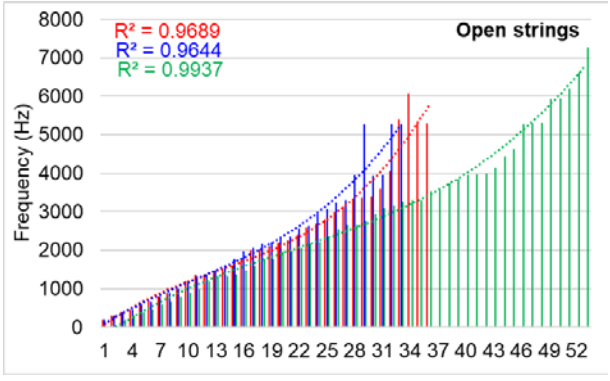

Fig. 8a *The analysis of frequency spectrum - free strings excitation*

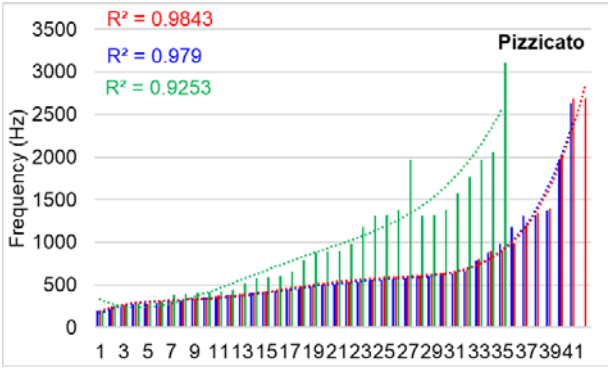

Fig. 8b *The analysis of frequency spectrum - Pizzicato excitation*

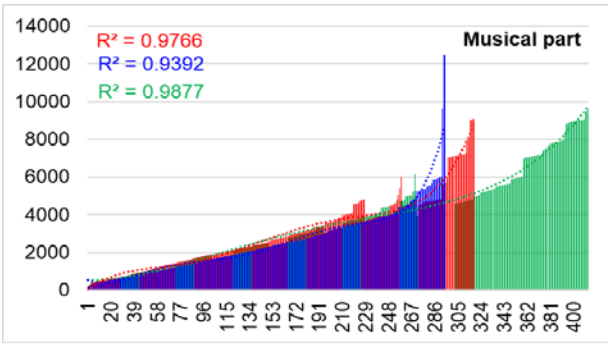

c)

Fig. 8c *The analysis of frequency spectrum - musical part*

The unvarnished violin presents a richer spectrum of frequencies than the varnished violin and recorded after one month, this fact highlighting that the application of the varnish leads to the decrease of the acoustic quality of the violin, in a first stage, the aging of the varnish subsequently leading to the improvement of the acoustic quality [17–20]. The statistical analysis followed the identification of the number of occurrences of the frequencies in the spectra on intervals of 100 Hz, between 0 and 8000 Hz. Thus, the resonance frequencies identified by peaks of amplitude of min 2% of the max amplitude of the respective spectrum and were analyzed statistically, obtaining the histograms for 1/1 octave band and 1/3 octave band (Fig. 9 and 10). It can be seen that the histograms of the signals recorded with an unvarnished and then varnished violin, after one month, are similar, for the free strings, compared to the histogram determined on the signals recorded after one year after the varnishing. Thus, the mode frequency is located in the octave band 1/1 of 353.6 - 707.1 Hz both for the unlacquered violin and for the one recorded after one month of varnishing, while for the violin registered after one year of varnishing, the mode frequency appears in range 1414.2 - 2828.4 Hz.

In 1/3 octave band analysis, the differences between the three stages of the violin are much more clearly highlighted from the point of view of the frequency of occurrence of the frequencies. It can be assumed that the hardening of the varnish after 1 year modifies the dynamic response of the violin body, favoring the emission of high frequencies.

In the case of the musical sequence, the acoustic response is closer between the three stages analyzed, but the tendency of

increasing the value of the frequencies with the highest occurrence is observed in the case of the violin played after one year of varnishing. (Fig. 10)

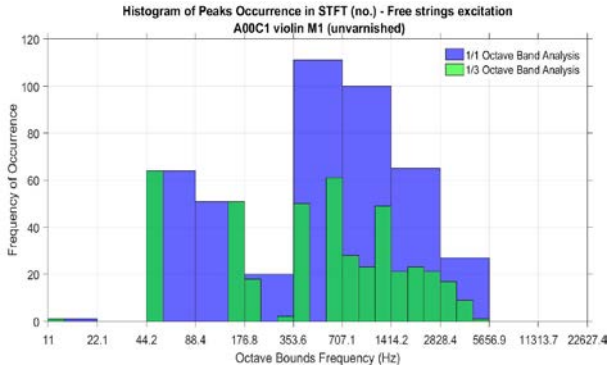

a)

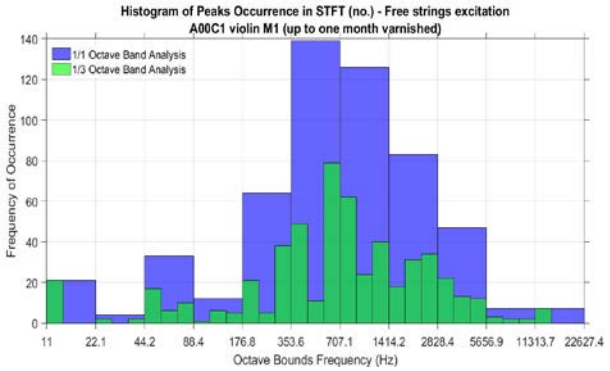

b)

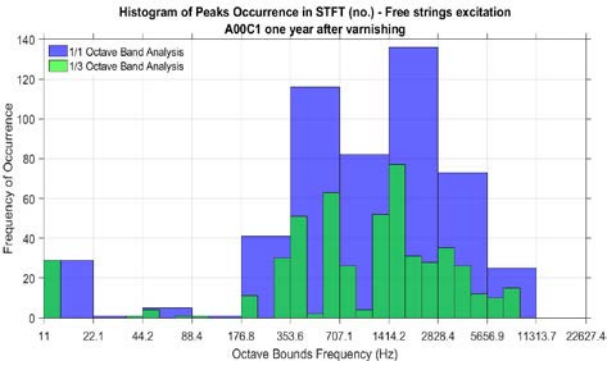

c)

Fig. 9 *The histograms of mode frequency – free strings excitation: a) unvarnished violin; b) after one month from varnishing; c) after one year from varnishing*

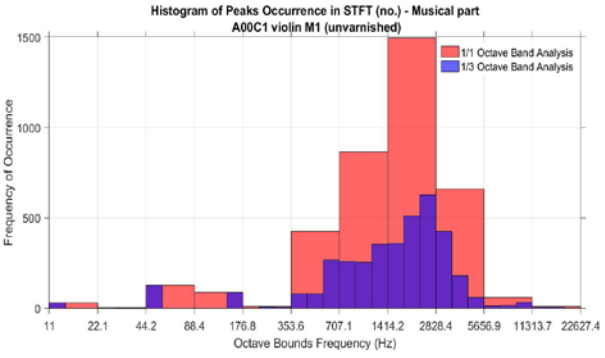

Fig. 10a *The histograms of mode frequency – musical part: unvarnished violin*

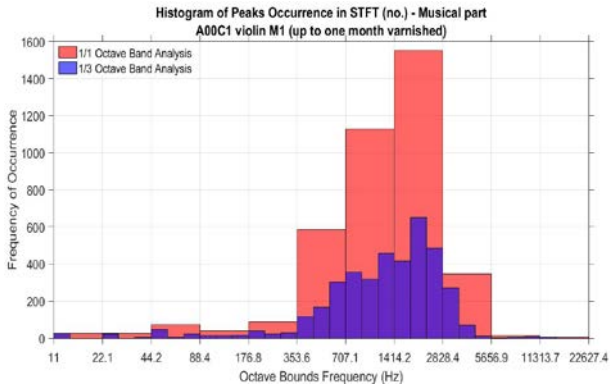

Fig. 10b *The histograms of mode frequency – musical part: after one month from varnishing*

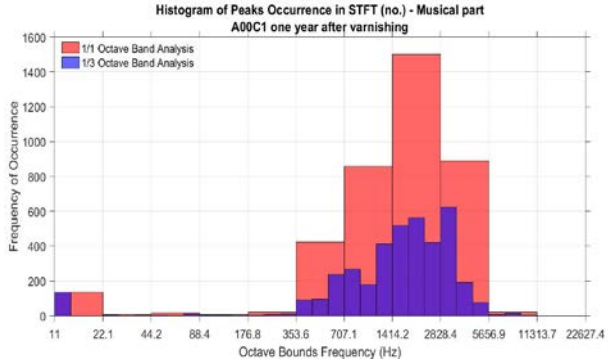

c)

Fig. 10c *The histograms of mode frequency – musical part: after one year from varnishing*

4. CONCLUSION

The paper presents a comparative acoustic analysis of the same violin in different stages of varnishing: before varnishing, after one month of varnishing and after one year of varnishing. The sequences performed on the violin were the same and produced by the same violinist.

Although the variations are relatively small in terms of the frequency spectrum (time and frequency analyses), there are still significant differences in terms of mode frequency, especially in the 1/3 octave band. Moreover, the acoustic perception of sounds by musicians differs from one stage to another, but this aspect is not the object of study in the current paper.

ACKNOWLEDGMENTS

This research was supported by a grant of the Ministry of Research, Innovation and Digitization, CNCS/CCCDI – UEFISCDI, project number PN-III-P4-PCE2021-0885, ACADIA – Qualitative, dynamic and acoustic analysis of anisotropic systems with modified interfaces.

We thank Nauncef Alina maria, instrumental artist from the Brașov Philharmonic for the support offered, as well as the company AP Studio Brașov for the professional recording of the violin.

REFERENCES

[1] J.C. Schelleng, "Acoustical effects of violin varnish". *J. Acoust. Soc. Am.*, vol. 44, pp. 1175–1183, 1968.

[2] AI Toth "The influence of the primer on the sound quality of the violins", *Revista Padurilor – Industria Lemnului – Celuloza si hartie, Industria Lemnului*, (in Romanian Language), vol. 30(1), pp. 33 – 45, 1979.

[3] M. Schleske, "On the acoustical properties of violin varnish". *Catgut Acoust. Soc. J.*, vol. 3, pp. 27–43, 1998.

[4] Tr Penciuc "Contributions to the acoustic study of the violin", *Revista Padurilor – Industria Lemnului – Celuloza si hartie, Industria Lemnului*, (in Romanian Language) vol. 31(4), pp. 184 – 187, 1980.

[5] M. Schleske, "Contemporary violin making. Analysis of design, materials, varnish and normal modes". *Catgut Acoust. Soc. J.*, vol. 4, pp. 50–65, 2002.

[6] H-C. Tai, Y.P. Shen, J.H. Lin, D.T. Chung, "Acoustic evolution of old Italian violins from Amati to Stradivari". *Proc. Natl. Acad. Sci. USA*, vol. 115, pp. 5926–5931, 2018, doi:10.1073/pnas.1800666115

[7] C.K. Su, et al. "Materials Engineering of Violin Soundboards by Stradivari and Guarneri", *Angew. Chem.* vol. 133, pp. 19293 – 19303, 2021.

[8] N. Harris, R. Sheldon, J. Johnston, ,, A Recreation of the Particulate Ground Varnish Layer Used on Many Violins Made before 1750", *J. Violin Soc. Am.: VSA Papers*, Vol. XXI, No. 1, pp. 1 – 15, 2007.

[9] S.L. Lämmlein, T. Künniger, M. Rüggeberg, F. W.M.R. Schwarze, D. Mannes, I. Burgert, "Frequency dependent mechanical properties of violin varnishes and their impact on vibro-mechanical tonewood properties", *Results in Materials*, vol. 9, 100137, 2021, https://doi.org/10.1016/j.rinma.2020.100137.

[10] S.L. Lämmlein, B. Van Damme, D. Mannes, F.W.M.R. Schwarze, I. Burgert, "Violin Varnish Induced Changes in the Vibro-Mechanical Properties of Spruce and Maple Wood", *Holzforschung*, Vol. 74(8), pp. 765–776, 2020.

[11] E.B. Skrodzka, B.B. Linde, A. Krupa, "Modal parameters of two violins with different varnish layers and subjective evaluation of their sound quality", *Arch. Acoust. Q., vol.* 38, pp. 75–81, 2013

[12] M.D. Stanciu, F. Dinulica, V. Bucur, G.V. Gliga, S.M. Nastac, M. Campean, "Changing the Vibrational Behavior of the Wooden Thin Arched Plates – the Maestro Violins Experimental Study Case", *Thin Walled Structures*, vol. 174, 109042, 2022. https://doi.org/10.1016/j.tws.2022.109042

[13] L. Trapasso "Feature-based Analysis of the Violin Tone Quality", Master thesis. Politecnico di Milano, 2013.

[14] C.S. Pannila, A.S. Pannila, D.C. Jayarathna, J.R.P. Jayakody, "Evaluation of the Sound Quality of a Classical Violin by Physically Measurable Acoustical Properties", Proceedings of the Technical Sessions, Vol. 32, pp. 23-30, 2016 Institute of Physics – Sri Lanka.

[15] F. Dinulică, M.D. Stanciu, A. Savin, "Correlation between anatomical grading and acoustic–elastic properties of resonant spruce wood used for musical instruments" *Forests*, vol. 12, 1122, 2021, https://doi.org/10.3390/f12081122.

[16] M.D. Stanciu, M. Mihălcică, F. Dinulică, A.M. Nauncef, R. Purdoiu, R. Lăcătuș, G.V. Gliga, "X-ray Imaging and Computed Tomography for the Identification of Geometry and Construction Elements in the Structure of Old Violins". *Materials*, vol. 14, 5926, 2021, doi:10.3390/ma14205926.

[17] R. Malvermi, S. Gonzalez, F. Antonacci, A. Sarti, R.A. Corradi, "A Statistical Approach to Violin Evaluation". *Appl. Sci.* vol. 12, 7313, 2022, https://doi.org/10.3390/app12147313.

[18] W. Cai; H.C. Tai "String Theories: Chemical Secrets of Italian Violins and Chinese Guqins", *Asia Chem*, vol. 11, pp. 10 – 17; 2020, https://doi.org/10.51167/acm00006.

[19] G. Bissinger, "Structural Acoustics of Good and Bad Violins", *J. Acoust. Soc. Am.*, vol. 124, pp. 1764–1773, 2008.

[20] C. Gough, Acoustic characterization of string instruments by internal cavity measurements. *J. Acoust. Soc. Am.*, vol. 150, 1922, 2021, doi: 10.1121/10.0006205.

University of Nis
Faculty of Occupational Safety
„Politechnica“ University of Timisoara
Faculty of Mechanical Engineering
27th International Conference
NOISE AND VIBRATION
Niš, 20 - 21. 10. 2022.

SOFTWARE MODELING OF OCEAN SOUND FIELD

Alexander Andonov [1], *Tihomir Trifonov* [2]

[1] St. Cyril and St. Methodius University of Veliko Tarnovo, Faculty of Mathematics and Informatics, №2 "Teodosi Tarnovski" street, 5003, Veliko Tarnovo, Bulgaria, apal@abv.bg
[2] Vasil Levski National Military University, Department of Communication and Information Systems, 76 Bulgaria bul., Veliko Tarnovo, 5000, Bulgaria, TihomirTrifonov@ieee.org

Abstract - *Two software models of sound ray propagation in aquatic media are created and developed in the form of two sets of programs. The first one calculates the transmission loss of sound intensity from source to receiver, time delay and length of different paths of rays. The other one reflects the path of rays in environments with known sound speed profiles. Mathematical models are depictured. The results of concrete model calculations are presented graphically. Easy to use interface is set between the programs and input and output data files and thus the software can easily be used for further studies.*

1. INTRODUCTION

The sea and its borders form a complex environment for the propagation of sound. This medium has an internal structure and its upper and lower limits influence the propagation of the signals of the underwater emitter. It is expressed in a number of effects.

The speed of sound is an oceanographic characteristic of the environment, determining many features of the propagation of signals at sea. Generally it depends on the depth, the time of year, the geographical area and the time of day.

$$c = \sqrt{\frac{æ}{\rho_0}}\ [m/s] \qquad (1)$$

where æ is the elastic modulus of longitudinal waves (longitudinal modulus) [MPa].

The literature describes in detail the different types of underwater sound channels that are formed under the influence of these factors [1-11]. The purpose of this article is to create software that takes into account the features of two models of sound propagation in the ocean, which are interesting for practice.

2. SHALLOW WATER SOUND CHANNEL

The basic model developed by Ethem Mutlu Sözer from Massachusetts Institute of Technology – MIT Sea Grant College Program in [1] will be used for the shallow water sound channel model (SWSC). The software model is developed by the authors, and consists of a set of C++ classes, which are easy to combine in computer programs solving a set of problems by modeling the sound propagation in water environments. For example the RangeFr.exe program is compiled to solve the Freq-range-loss problem described further in this article.

2.1 Model description

The shallow water sound channel is considered with the multipath ray tracing model of propagation of sound.

In the shallow water channel, the acoustic waves move along the direct path ray, and alternatively after bouncing off the surface and the bottom reach the sound receiver. We can roughly calculate the propagation of acoustic signals of individual rays by simplifying the parameters of the medium. Assuming the following simplifications:

- the speed of sound is almost constant
- the surface and the bottom are smooth
- the depth does not vary significantly in the considered range

we can calculate geometrically the expected paths (rays) of motion of acoustic waves.

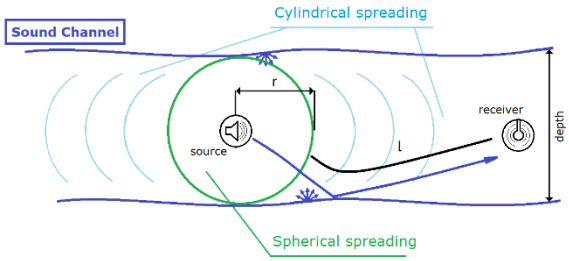

Fig. 1 *Shallow water sound channel*

2.2 Model variables

The measured or calculated quantities describe the channel, the sound and the instruments.

Once we have determined the ray tracing paths, we can estimate the received signal power, taking into account the transmitted signal power and the locations of the source and the receiver. This type of sound movement model with multiple rays reaching a receiver is called multipath propagation.

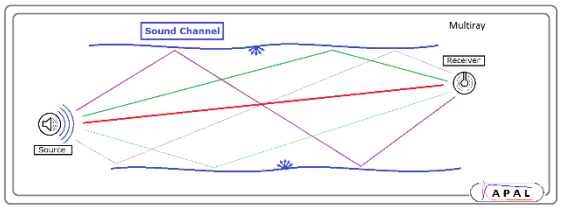

Fig. 2 *Multipath propagation*

For every sound ray (path) distance traveled, elapsed time and propagation loss (*PL*) are calculated.

Reflection losses for every reflection are considered constant (in [dB]), and are contained in two constants (one for surface and one for bottom reflection), which are part of the channel characteristics.

Sound-transmitting transducers and receiving hydrophones, convert electrical signal into sound, and vice versa. The values of variables depend on instrument characteristics – *OCRR*(Open Circuit Receiving Response), *TVR*(Transmitting Voltage Response), preamplifier and postamplifier.

Example list of considered variables:

- *Vin* – input voltage [V]
- *SILs* – Sound Intensity Level at the sound source [dB]
- *di* – source-receiver distance for ray i [m]
- *ti* – travel time for ray i [s]
- *RL* – Reflection loss [dB]
- *PL* – Propagation loss [dB]
- *TL* – Transmission loss [dB]
- *SILr* – Sound Intensity Level receiver [dB]
- *Vout* – output voltage [V]

2.3 Solved problems

Direct problem: A signal with power *SILs* is emitted at the source. What is the strength of the received signal at the receiver - *SILr*? What is the breakdown of the strength of the sound signal by rays, and what is the time delay?

Inverse problem: The channel (with its variables) and locations (of sound source and receiver) are given, a signal with intesity *SILr* is received via direct path; what is the strength of the transmitted signal *SILs*?

Range problem: For a given channel (*Swch*), at what distance will the transmitted signal with a given frequency (*freq*) attenuate by 20 [dB]? At what distance will the signal attenuate by 40 [dB]? At what distance will the signal attenuate by 60 [dB]? What is the dependency of the distance [m] on the losses *TL* [dB], at a given frequency (*freq*)? Same question for a frequency spectrum (*freq_min ... Freq_max*); Same question for a range of losses (*TL_min ... TL_max*);

Frequency problem: For given channel characteristics, at what frequency will the transmitted signal lose certain TL decibels at a given distance (*dist*)?

Freq-range-loss problem: For a given channel, given two of the quantities (frequency, distance range, losses) to determine the third. With the help of computer software the same issue can be solved for a given range of values of variables, not just a quantity. The data can be presented graphically – for example in fig 3 a range of *TL* losses (20--100 dB) are calculated for a range of frequences (4--20 kHz) and a range of distances (5--45 km) with the RangeFr.exe program.

2.4 Mathematical model

The range of audible communication is determined by sound energy lost with distance.

2.4.1 Attenuation and losses

Attenuation is the gradual loss of flow intensity with the movement through a medium. Sound energy decreases with distance from source.

$$TL = PL + RL \ [dB] \tag{2}$$

Here *TL* are Transmission losses (total), *PL* are Propagation losses and *RL* are Reflection losses.

$$PL = 10.\lg\left(\frac{A(d,f)}{A_0}\right) \ [dB] \tag{3}$$

Here *A(d,f)* is the Attenuation factor [dB], which is dimensionless. This is the ratio of the sound volume at the source and at the receiver. It depends on the sound frequency and the distance traveled.

$$A(d,f) = \frac{P_{source}}{P_{receiver}} \ [dB] \tag{4}$$

In the literature ([2], [3], [4]) the estimation of the attenuation factor is done by the following formula:

$$A(d,f) = A_0.d^k.a^d \ [dB] \tag{5}$$

which, if converted to decibels, yields:

$$PL = k.10.\lg(d) + d.10.\lg(a(f)) \ [dB] \tag{6}$$

Here:

k.10.lg(d) is the Spreading Loss [dB];

d.10.lg(a(f)) is the Absorption Loss [dB];

k is the spreading factor;

d is the path distance in [km];

a(f) is the absorption coef in [dB], which depends on the frequency of the sound wave;

A_0 is the unit-normalizing constant; When the frequency is in [kHz] and the distance is converted in [km], then A_0 = 1;

When estimating the propagation losses *PL*, the value of the spreading factor *k* (or power expansion factor) is used. This is a dimensionless quantity [--] that reflects the geometric model of sound propagation. It is used in the calculation of geometric attenuation (Spreading Loss). In the literature ([2], [5], [6]) the spreading factor *k* is estimated as follows:

$$k = \begin{cases} 2 & spherical\ spreading \\ 1.5 & practical\ spreading \\ 1 & cylindrical\ spreading \end{cases} \tag{7}$$

In case of combined geometry of sound propagation (in part of the distance the propagation is by spherical law, and in another part - cylindrical), which is the most common case in practice, a factor *k* = 1.5 is accepted. But this is a very inaccurate estimate, which is not taking into account what part of the way one model is valid, and in what part the other is valid. An example setting is shown in fig. 1.

The reflection loss *RL* could be constant for every reflection (in decibels), or could depend on the angle of incidence and/or on the frequency. In this model reflection losses are 2 different constants – one for surface reflection, and one for bottom reflection.

2.5 Software C++ class design

Data and variables are organized in several classes:

- class Swch – physical data of the channel - depth, reflection losses, speed of sound;
- class SpAllocation – space positions and location data; depth of the sound source, depth of the receiver, horizontal distance between them;
- class RayTravel – specific ray data - distance traveled, time, propagation losses PL;
- class RayProp – specific ray data - frequency, number of reflections on the path;
- class RayPath – summerized ray data – sound intensity (volume) at the source and at the receiver, RayTravel, RayProp;
- class MultiPathRay – data for multipath (multiray) calculations for a group of rays with one source;
- class SigTravel – complete study - integrates all classes from above;

Class implementation example – SpAllocation:

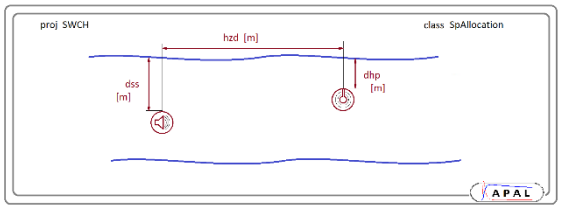

Fig. 3 *Variables of SpAllocation*

Code (header file only) of SpAllocation:

```
==========================================

// SpAllocation.h
/*****************************************/
/* class SpAllocation for hydroacoustics */
/* helper class for SWCH - Plitkov Zvukov Kanal */
/* library.Apal.fisica                   */
/*****************************************/

#ifndef _lib_apal_fisica_hydroacoustics_SpAllocation_zn00105_INCLUDED_
#define _lib_apal_fisica_hydroacoustics_SpAllocation_zn00105_INCLUDED_
// includes
#include <iostream>
#include <fstream>

namespace fisica
{
class SpAllocation
{
private:
  // member variables
  double dss;      // depth of Sound Source [m]
  double dhp;      // depth of Hydrophone [m]
  double hzd;      // horizontal distance [m]
public:
  // constructors
  SpAllocation();
  SpAllocation(const SpAllocation& donor): dss(donor.dss),
        dhp(donor.dhp), hzd(donor.hzd) {  }
  SpAllocation(const double zss, const double zhp, const double dist): dss(zss),
        dhp(zhp), hzd(dist) {  }
  ~SpAllocation() {}
  // operators
  SpAllocation& operator=(const SpAllocation& rhs); // assign func
  friend std::ostream& operator<<(std::ostream &stream, const SpAllocation &mrs); // inserter function
  friend std::ifstream &operator>>(std::ifstream &infile, SpAllocation &mrs);
// extractor function
      // relational operators
  friend bool operator==(const SpAllocation &lhs, const SpAllocation &rhs);
  inline bool operator<(const SpAllocation& rhs);
  // access funcs
  inline void setDepthSS(double depth) { dss = depth;}
  inline void setDepthHp(double depth) { dhp = depth;}
  inline void setDistHor(double dist) { hzd = dist;}

  inline double getDepthSS() const { return dss;}
  inline double getDepthHp() const { return dhp;}
  inline double getDistH() const { return hzd;}

  // member methods
  double directDistance() const ;
  inline void print() { std::cout << "directDist = " << directDistance() << ";\n" << *this;}
  bool readRaw(std::ifstream &ifile);
};//class SpAllocation
} // namespace fisica
#endif // _lib_apal_fisica_hydroacoustics_SpAllocation_zn00105_INCLUDED_

==========================================
```

2.6 Program I/O

The developed classes read input data and write output data to files. The chosen method for data storage is in text files (and not binary). The program works with files with the extension ".swch", and these files can be created and edited with any text editor, including Microsoft Notepad. The data from the file can be copied to the buffer, and pasted into any other files or applications. The ".swch" files themselves can be converted to ".txt" or any other type.

Comments can be written in the files. When they do not affect the data, the programs will read the input and ignore the comments. This allows visualization of results, submitting notes and other ways of presentation. Thus, these files are suitable for manipulation by people, by computer programs, and for data storage at the same time.

Contents of a human-edited file – vhodRange.swch:

```
----------------------------------------------------------------
{ freq ; range };
{ [Hz] ; [m]   };
{ 500.3 ; 391365 };
{ 2625.26 ; 96844 };    // left value
{ 4750.23 ; 54617 };
{ 6875.19 ; 34270 };    // right value
{ 9000.15 ; 23394 };
{ 11125.1 ; 17030 };
// input data
{40.0}; // criterion [dB] == maxTL
Spec{ 500.3; 17500; 8 };  // Frequency [Hz]
SWCH{ 110.2; 1499.7; 1.1; 3.1; 0.7}; // ZKanal
SpL{ 15.2; 33.3; 312.7}; // space
----------------------------------------------------------------
```

2.7 Calculations and results

Example of range problem solved with RangeFr.exe program

Input data – vhod.01.swch:

{40.0}; // criterion [dB] == maxTL
Spec{ 500.3; 17500; 8 }; // Frequency [Hz]
SWCH{ 110.2; 1499.7; 1.1; 3.1; 0.7}; // ZKanal
SpL{ 15.2; 33.3; 312.7}; // space

Output data – izhod.01.swch:

{ freq ; range };
{ [Hz] ; [m] };
{ 500.3 ; 391365 };
{ 2625.26 ; 96844 };
{ 4750.23 ; 54617 };
{ 6875.19 ; 34270 };
{ 9000.15 ; 23394 };
{ 11125.1 ; 17030 };
{ 13250.1 ; 13014 };
{ 15375 ; 10325 };

With this problem we obtain the distance as a function of the frequency and the maximum allowed transmission losses *maxTL*. The results of seven test runs of the program are combined and presented in fig. 4:

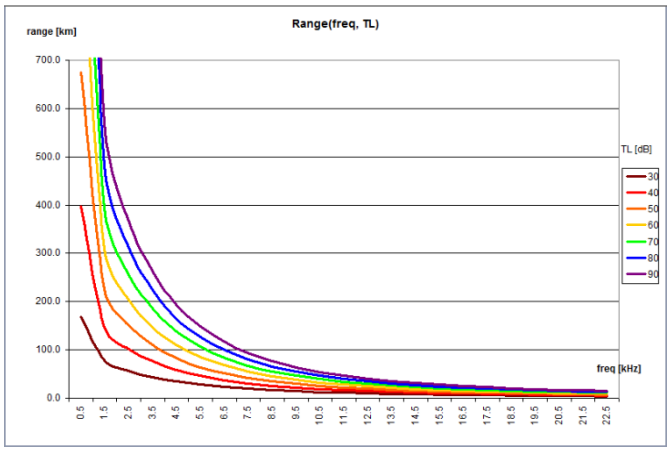

Fig. 4 *Distance as a function of frequency and TL*

An example of aggregated data of Freq-range-loss problem solved with RangeFr.exe program is shown below, presented graphically in fig. 5.

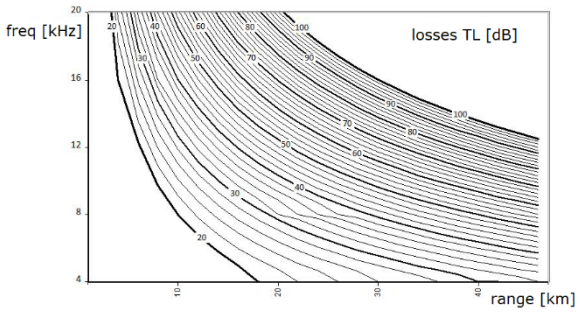

Fig. 5 *Data from shallow water sound channel model calculations. Source depth 50[m]; Receiver depth 50[m]; Bottom depth 100[m];*

How well does the calculating model and the calculated data fit the actual marine environment? For comparison, the following are graphs of data from studies conducted on losses in shallow water - from source [3].

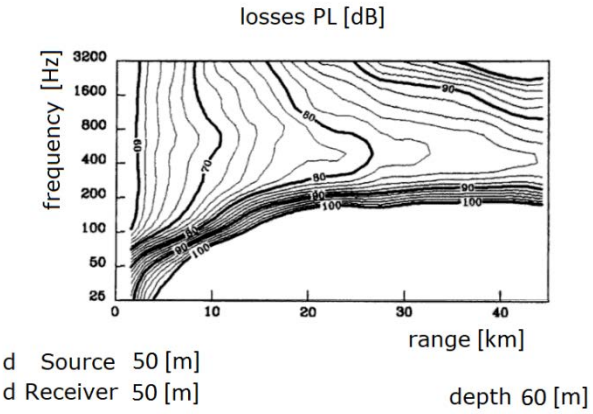

Fig. 6 *Data from Barents sea sound PL study*

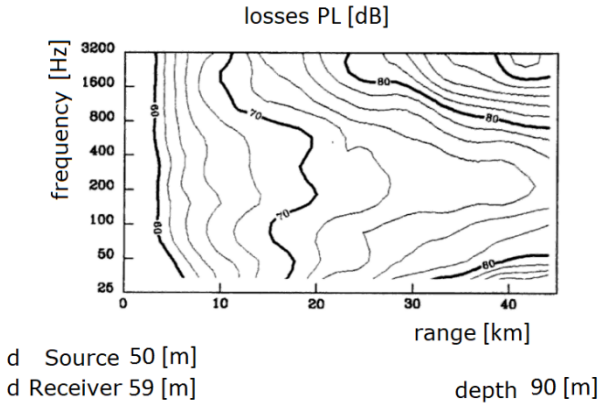

Fig. 7 *Data from La Manche sound PL study*

2.8 Model development

The modeling process includes the following stages:

- -1- choosing a model; simplification of the model;
- -2- selection of considered parameters / variables;
- -3- software implementation of the model; coding of classes (data types) representing the parameters of the environment and the sound channel; compiling classes into working programs;
- -4- model testing; carrying out specific research or studies - calculations made by the developed programs;
- -5- analysis of the obtained results; setting parameters; modifying the model in order to improve it or to perform specific simulations;
- -6- return to {-4- and -5-} or to {-3-, -4- and -5-};

3. TIPICAL OCEAN CHANNEL

The SOFAR (Sound Fixing And Ranging Channel) or Deepwater Sound Channel (DSC) is a horizontal layer of water in the ocean where the speed of sound is minimal. Based on this channel, LOFAR (LOw Frequency Analysis and Ranging) and SOSUS (Sound SUrveillance System) systems have been developed - networks of eavesdropping devices. Very few extraneous sounds are detected in this deep-water channel, except by submarines or whales that use it to communicate over great distances in the oceans.

The source of fig. 8 is [7].

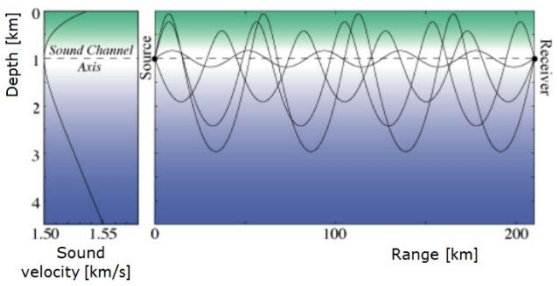

Fig. 8 *Ocean deepwater sound channel*

3.1 Mathematical model

Usually the sound speed in the ocean is a function of temperature, salinity, and ambient pressure. But the ambient pressure depends on depth, so it is customary to express the sound speed *c* in [m/s] as an empirical function of temperature *T* in [°C], salinity *S* in [‰] and depth *z* in [m]. One of the many such formulas is sourced from [8]:

$$c = 1444.92 + 4.6T - 0.055T^2 + 0.00029T^3 + (1.34 - 0.01T).(S - 35) + 0.016z \ [m/s] \quad (8)$$

The change of sound speed with regard to depth is called sound velocity profile – *c = c(z)*. Velocity profile example is shown on fig. 8.

3.1.1 Model assumptions

The sea environment is heterogeneous with respect to temperature and salinity for many reasons. But the big changes are almost entirely in the vertical direction. The same is even more true for pressure. So the basic model accepted assumes these variables are constant within a thin horizontal layer (stratum) and pressure changes linearly with depth. Thus the sound speed *c* horizontally is the same everywhere in this layer and in vertical direction changes linearly. The mathematical model below is based on the research of Prof. M. Karnovskiy [11].

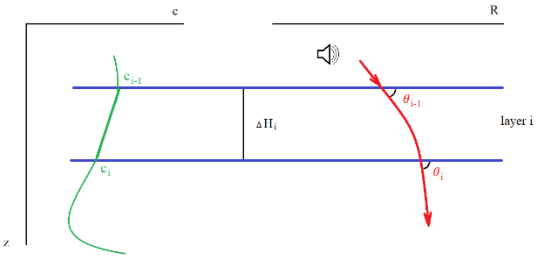

Fig. 9 *Horizontal layer*

3.1.2 One layer geometry

To examine a ray passing through a thin layer, we slice the region in horizontal layers and take a look at layer *i* – fig. 9.

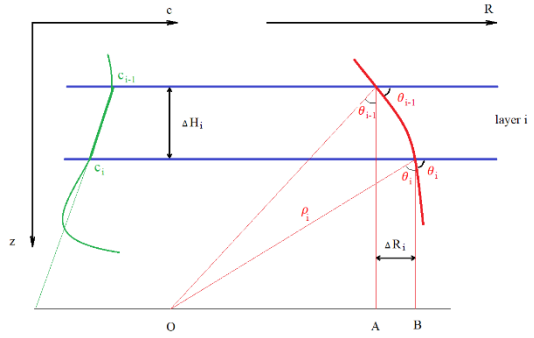

Fig. 10 *Horizontal layer geometric breakdown*

We enter the following notations

$$g_c = \frac{c_i - c_{i-1}}{\Delta H_i} \quad (9)$$

$$\Delta R_i = \rho_i |\sin\theta_i - \sin\theta_{i-1}| \quad (10)$$

These formulas can be summarized as follows

$$\Delta R_i = -\frac{c.\rho}{g_{ci}}(\sin\theta_i - \sin\theta_{i-1}) \quad (11)$$

$$\Delta R_i = \frac{\Delta H_i}{tg\frac{\theta_i + \theta_{i-1}}{2}} \quad (12)$$

The propagation anomaly can be defined as follows

$$A_p = \frac{J_0(\vec{r})}{J_k(\vec{r})} \quad (13)$$

Where

$$J_k = \frac{P}{4\pi r^2} \quad (14)$$

$$J_0(\vec{r}) = J_k(\vec{r}).A_p = \frac{P}{4\pi r^2}.A_p \quad (15)$$

Where P is acoustical power. In the general case for a layered inhomogeneous medium

$$A_p(\theta_n, R) = \frac{R.cos^2\theta_n}{\sin\theta_n.\ \sin\theta_{n+n}\ .\sum_{i=1}^{n}\frac{\Delta R_i}{\sin\theta_{n+i}.\sin\theta_{n+i-1}}} \quad (16)$$

Where

$$R = \sum_{i=1}^{n}\Delta R_i \quad (17)$$

4. CONCLUSION

In this paper two mathematical models of sound propagation in ocean were created and presented. A software implementation was also presented.

Initial testing of the programs shows good results, except with low frequencies at long distances. Comparisons between calculations and measurements show that at low frequencies the model does not reflects sound propagation appropriatelly. The main reason, according to the authors, is that the multiray theory, which is the basis of the model, is more suitable for short distances and high signal frequencies. Additionally, some of the main assumptions could be violated – the surface and the bottom were not so smooth or the depth could vary significantly. Or small objects in the water created diffusion.

In the future it is planned to improve and expand this software. Additional features can be added to improve the current software package. This is easy to achieve as the classes are convenient for editing, processing and updating. With regard to I/O communication, it is suitable to add a controllable writing offset to the output functions. An additional setprecision setting can be made to improve the output of the results. It will be appropriate to develop Transducer and Hydrophone classes, connecting acoustic communication with input and output electrical signals.

REFERENCES

[1] Ethem Mutlu Sözer, "Underwater Acoustics. A Brief Introduction", MIT Sea Grant College Program.

[2] Chengsheng Pan,Liangchen Jia, Ruiyan Cai, Yuanming Ding; "Modeling and Simulation of Channel for Underwater Communication Network"; in *"International Journal of Innovative Computing, Information and Control"* Volume 8, Number 3(B), March, 2012.

[3] Jensen F.B., Kuperman W.A., Porter M.B., Schmidt H., "Computational Ocean Acoustics", Springer, New York, 2000.

[4] Gerstoft Peter, "Introduction to Hydroacoustics", International Data Centre, Comprehensive Nuclear-Test-Ban Treaty Organization.

[5] Suhail Al-Dharrab, Murat Uysal, Tolga M. Duman, "Cooperative Underwater Acoustic Communications", *IEEE Communications Magazine*, 51(7), pp 146-153, 2013.

[6] Stojanovic Milica, "On the Relationship Between Capacity and Distance in an Underwater Acoustic Communication Channel", Massachusetts Institute of Technology, Cambridge, USA, 2007.

[7] https://dosits.org/tutorials/ ;

[8] Kuperman W.A., "Ocean Acoustic Environment", in *Encyclopedia of Ocean Sciences (Third Edition)*, Volume 5, pp 296-307, 2019.

[9] Urick R.J., "Principles of Underwater Sound", McGraw Hill, 1975.

[10] Evtutov A.P., V.B. Mitko, "Ingenernie razcheti v gidroakustike", Leningrad, Sudostroenie, 1988. In Russian language.

[11] M. I. Karnovskiy, "Asimptoticheskie metodyi v akustike" [Asymptotic methods in acoustics], Kyiv, USSR: KPI, 1982. In Russian language.

University of Nis
Faculty of Occupational Safety
„Politechnica“ University of Timisoara
Faculty of Mechanical Engineering
27th International Conference
NOISE AND VIBRATION
Niš, 20 - 21. 10. 2022.

STRUCTURAL SIMILARITY OF DC MOTOR SOUNDS AFTER MAPPING INTO MEL-SPECTROGRAM

Dejan Ćirić[1], Zoran Perić[1], Nikola Vučić[1]

[1] University of Niš, Faculty of Electronic Engineering, Serbia, dejan.ciric@elfak.ni.ac.rs

Abstract – *Health condition of machines that includes presence of malfunctions or faults can be obtained by applying various approaches. One of them known as sound signature is based on sound that machines generate during regular operations. This sound carries important information about the source, a target machine in this case. The information can be extracted in different ways. Here potentials of the structural similarity of spectrogram like images created from the sound samples of the direct current (DC) motors are investigated. Sound samples of these motors from own database are converted into mel-spectrogram images, which are further used for the comparison. Samples are divided into 8 classes, where the intraclass (within the same class) and interclass (between two classes) similarity is analysed. Statistical parameters are calculated and graphical representation is also given. The obtained results are discussed showing which classes have the highest and lowest similarity both at intraclass and interclass level.*

1. INTRODUCTION

Detection of machine malfunctions or faults represent one of the essential tasks in industry. The most recent developments in sensor technology, signal processing and artificial intelligence (AI) have enabled going into direction of automation of machine malfunction detection. This task can be realized by using different alternative approaches, where one of them is based on using sound, also known as a sound signature approach [1]. Here, the hypothesis that is proven in practice is that current state of a monitored machine is imprinted in sound or noise it generates. The phrase “current state” is related to “health” condition, that is, presence of malfunctions or faults of a particular machine, than mode of operation, etc. The sound signature has found diverse applications like those in detecting the mechanical faults – e.g., bearing faults, rotor and wing faults (unbalanced or broken component), etc. [1].

A number of examples can be found both in literature and practice where sound is used for machine current state detection or monitoring. Two broad fields of application include product quality control and predictive maintenance. Thus, fault detection and health monitoring can be done by using sound/noise generated by rotating blades as presented in [2]. Correlation between structural and acoustical phenomena of a three-phase alternate current induction motor is investigated in [2]. Fault diagnosis of industrial purpose robots is carried out using acoustic signals and condition based monitoring, while railroad wheel-bearing faults are identified from audible acoustic signals [1]. The sound signature analysis is used to define any potential failure or error of an induction motor that may lead to a failure [3]. Monitoring system for an online periodic surveillance of machine diagnosis that performs an automated sound analysis in industrial environment is presented in [4]. This system uses the blind source separation technique to isolate the sound of the monitored machine from other sounds. Machine fault detection using sound signature of the rotating machine at different loading and misalignment conditions is discussed in [5]. Anomaly detection in the domain of stationary valves and slide rails by using the acoustic data is improved in [6].

In sound signature analysis, diverse signal processing methods can be applied including common Fourier or wavelet transform, extraction of relevant parameters or mapping of sound into images. The latter one enables applying the performance boost from the field of image processing especially related to AI-based image processing. The sound mapping into images can be done in different ways resulting in different images. Some of them are spectrogram, mel-spectrogram, gammatonegram, constant Q transform image, etc. [7]. Spectrogram is a well-known representation of sound in combined time and frequency domain, while mel-spectrogram represents one of the most used alternatives especially when machine and deep learning models are to be applied on sound datasets.

Spectrograms can be used as such in recognition tasks, but also some features can first be extracted from spectrograms and applied in those tasks. For example, parametric statistical indexes are extracted from the raw spectrograms, one dimenasional (1D) projection of the spectrograms on the time and frequency axis and the numerical first derivatives of the spectrogram are used in [8], such as the mean pixel power, the second, third, and fourth moments of the pixel value distribution, the entropy measure, etc.

Somewhat better results for pattern-matching are obtained by applying first an affine transformation to the spectrograms, which discards the translational, rotational, scale and phase dependent information, and then calculating the cross-correlation coefficient between the observed spectrograms [8]. The correlation measure obtained in such a way has much larger predictive power for distinguishing different classes of unknown signals.

Apart from using machine and deep learning models applied to image datasets, certain tasks can be realized by developing

parametric classifiers. Such an alternative can be realized by using the image similarity in order to estimate how far is the analyzed image (sound) from the reference one. For that purpose, various image similarity measures can be exploited. They include some basic point-to-point measures such as peak signal-to-noise ratio (PSNR) or Euclidean distance (ED), measures based on correlation such as Pearson correlation coefficient or measures based on image structural similarity such as structural similarity (SSIM) index.

The SSIM index is a measure that demonstrated a good agreement with subjective evaluations in tasks with reference images [9, 10]. This is measure is chosen here to be used for evaluating image similarity in order to investigate the similarity between the sounds of machines, that is, direct current (DC) motors. The dataset used for the described purpose is the one containing sounds of a particular type of DC motor - a car window lifter. Sounds are classified into eight classes in reference to the presence of malfunctions or faults, direction of rotation and motor type. The SSIM is calculated for all combinations of images (sounds or motors) belonging to the same class, and this represents the intraclass similarity. The same is done for all combinations of images where the first one belongs to one class, while the second one belongs to another class resulting in the interclass similarity.

2. STRUCTURAL SIMILARITY AS A MEASURE OF IMAGE SIMILARITY

2.1 Image similarity measures

Image quality or similarity can be assessed by objective and subjective methods. The latter one provides the most accurate results, but it is expensive and too slow [11]. Objective methods are mainly based on relevant computational models, and have advantageous characteristics such as simple, low cost, easy to apply and embed [12]. Different objective measures are available for image quality or similarity assessment.

Simpler or low-complexity measures include those such as PSNR or mean square error/difference (MSE). These two measures are used for evaluation of image quality/similarity on a point-to-point basis [9]. On the other hand, there are measures based on human vision system meaning that their result will be similar to subjective evaluation, but they are typically rather complex for calculation [11]. Certain measures use the low-level models of human perception implemented in the sub-band/wavelet domain [9].

Some of those measures are more reliable for certain applications, and the right question is how to choose the most reliable measure for a particular task. Examples of using the image simailarity measures in illustrative applications are stated here. Thus, PSNR and SSIM are used for estimation of image similarity in image prediction [13-15]. SSIM is used for comparing the image quality in halftoning [16], Euclidean distance (ED) of the image intensity is used for comparing the object state [17], while multiscale SSIM (MSSSIM), squared Euclidean (L2) distance and mean absolute error (MAE), that is L1 distance are used as a loss function in image synthesis [10]. In addition, image similarity can be calculated by means of statistical values like mean, variance and standard deviation (STD) [18]. In image registration, mutual information (MI) is used as a primary similarity measures in a number of applications like medical imaging, stereo processing and object tracking [19].

Significant interest in literature has been shown to image quality/similarity measures. Thus, an extract of 27 measures are presented in [20] used for assessing the fused images either in an absolute or comparative sense. These measures have different performance depending on a particular task and conditions such as presence of noise. In [18], it is stated that Pearson correlation coefficient and cosine correlation outperforms some other measures like Tanimoto and angular similarity at low signal-to-noise ratio (SNR).

Generally speaking, it is worth mentioning that the image similarity measures typically evaluate the similarity between images and not the image quality. Nevertheless, in many studies, some of these measures, e.g., SSIM, are used for image quality assessment.

2.2 Structural similarity index

MSE can only measure distance between corresponding spectro-temporal points, and it has well-known inherit shortcomings, especially in case of perceptually important signals such as speech or images [21]. For measuring similarity of image structure, a much better performance is expected from SSIM being one of the most popular measures for image quality and similarity assessment in general. The SSIM is three components measure taking into account illumination, contrast and structure of the local patch (window) of an analyzed image. Such an approach is more similar to the one used in human visual system than the pixel-based evaluation found in point-to-point measures such as PSNR or ED.

As spectrogram of machine sound has some unique properties, and it is different from a natural image, it is worth considering the option of adapting SSIM measure to spectrograms or spectrogram-family images. It is interesting to note that in case of appying the SSIM to spectrograms, the spectral magnitude can be seen as the luminance, while the structural information is contained in the harmonics [21].

In developing deep neural network (DNN) models based on spectrograms, the error between the estimated (X_i) and target spectrogram (Y_i) is often estimated by MSE, that can be calculated as:

$$MSE = \frac{1}{N}\sum_{i=1}^{N}\left(X_i - Y_i\right)^2 \tag{1}$$

where N is the number of points in each of the compared spectrograms (images).

Let two patches of the above mentioned spectrogram images X_i and Y_i be x_i and y_i, then the mentioned three components of the SSIM (illumination, contrast and structure) are calculated from these patches as:

$$l(x,y) = \frac{2\mu_x\mu_y + C_1}{\mu_x^2 + \mu_y^2 + C_1} \tag{2}$$

$$c(x,y) = \frac{2\sigma_x\sigma_y + C_2}{\sigma_x^2 + \sigma_y^2 + C_2} \tag{3}$$

$$s(x,y)=\frac{\sigma_{xy}+C_3}{\sigma_x\sigma_y+C_3} \quad (4)$$

where μ_x and μ_y are the mean of the spectral magnitude while σ_x and σ_y are the STD of the spectral magnitue of the spectrogram patches x_i and y_i, respectively, σ_{xy} is the covariance coefficient of these patches, and C_1, C_2 and C_3 are the constants that are added to avoid instability when the denominators in the previous equations are close to zero. The mentioned three constants are typically calculated as:

$$C_1=(K_1L)^2 \quad C_2=(K_2L)^2 \quad C_3=(K_3L)^2 \quad (5)$$

using L as a dynamic range of image pixel values (the most often it is equal to 255) and three small constants K_1, K_2 and K_3. The SSIM in patches is obtained by combining the three terms from Equations (2) to (4) as:

$$SSIM(x,y)=[l(x,y)]^{\alpha}[c(x,y)]^{\beta}[c(x,y)]^{\gamma} \quad (6)$$

where the variables α, β and γ represent the parameters defining the relative importance of each component. The simplified version of the previos equation can be obtained by setting the variables α, β and γ to 1 as well as C_2 to $C_3/2$

$$SSIM(x,y)=\frac{2\mu_x\mu_y+C_1}{\mu_x^2+\mu_y^2+C_1}\frac{2\sigma_{xy}+C_2}{\sigma_x^2+\sigma_y^2+C_2} \quad (7)$$

One of the main differences of the point-to-point measures and SSIM is related to the local statistics given through the mean, STD and covariance values of local patches that are present in the SSIM calculation.

By moving the local patches throughout the images, a map of SSIM values are calculated. These values can be arranged in a matrix form. The overall SSIM measure is typically calculated by taking the mean value of this matrix containing the SSIM values of local patches. Larger value of the overall SSIM shows that the two compared images are more similar to each other. Since the SSIM is three components measure, contributions of each of these components can also be analyzed separately.

Some adjustments or customization of the SSIM calculation can be done in case of spectrograms [21]. For example, they can be related to the representations of values in spectrograms, either they are only positive or both positive and negative when they are obtained after applying the logarithm to the spectrum magnitude. Then, values of the small constants K_1, K_2 and K_3 as well as L can be chosen in such a way to be appropriate for spectrogram images. One more adjustment is related to the size of the local patches. In natural images, this size is often 11 × 11, but in case of spectrogram images it is better to set the patch size according to the content of the spectrogram. Thus, the size of patches is set to 3 × 3 in [21].

3. METHOD OF INVESTIGATION

For this research, the sounds of DC motors from the dataset created within the project „Advanced Methods of Quantization, Compression and Learning in Artificial Intelligence" are used, as it was the case with studies presented in [22, 23]. The sounds of DC motors of type A and type B are taken from the dataset. Each motor has two directions of rotation here denoted as direction 1 and direction 2. Besides, for each of the mentioned motor types, the motors are split into two classes, where the first one has the motors without any malfunctions or faults, denoted as class of OK motors, and the second one has motors with certain faults, denoted as class of NOK motors. Based on those three criteria, sound signals are classified into eight classes in the following way:

- Class 1 contains 281 signals of OK motor of type A with direction of rotation 1;
- Class 2 contains 281 signals of OK motor of type A with direction of rotation 2;
- Class 3 contains 387 signals of NOK motor of type A, direction of rotation 1;
- Class 4 contains 387 signals of NOK motor of type A, direction of rotation 2;
- Class 5 contains 282 signals of OK motor of type B, direction of rotation 1;
- Class 6 contains 282 signals of OK motor of type B, direction of rotation 2;
- Class 7 contains 174 signals of NOK motor of type B, direction of rotation 1;
- Class 8 contains 174 signals of NOK motor of type B, direction of rotation 2.

Motor sounds were recorded within the production line of the motor manufacturer, in a semi-anechoic chamber. The created audio files have a sampling frequency of 16 kHz, and they contain sound of a particular DC motor rotating first in one direction, and then rotating in opposite direction. Duration of the audio recording is about 18 s in total, meaning that useful signal for each direction of rotation is about 8 s. The middle part of 5 s of each audio signal segment for each direction of rotation is extracted first.

These extracted parts of audio signals in the time domain are then mapped into mel-spectrogram images. Here, the mel-spectrogram is chosen as a relevant image representation since it is used in a number of studies and practical applications. For sound mapping into mel-spectrogram, the time domain signal is segmented into frames of size of 1024 samples with the overlap size of 256 samples, and then transformed into mel-spectrum domain. The whole processing is carried out in the Python programming language.

The generated mel-spectrogram images are used as an input for calculating the SSIM indexes. They are determined for all images within a particular class, but also for all combinations of images between two classes. When SSIM is calculated within a class representing the intraclass similarity, both mel-spectrogram images belong to the same class. The order of images is not important. On the other hand, for calculating the SSIM measure between the classes representing the interclass similarity, the first image is taken from one class while the second image is taken from another class. Again, the order of images is not important. The SSIM index is calculated for all combinations without permutations of pair of images either within the same class or between the classes. The obtained SSIM values are placed in appropraite matrices for both intraclass and interclass similarities. They are used for calculating the statistical quantities including mean,

minimum, maximum, median and STD. These quantities as well as the obtained matrices are exploited for visualizing the results and for further analysis.

4. OBTAINED INTRACLASS AND INTERCLASS SSIM VALUES

The analysis of SSIM indexes for the intraclass comparison within the defined classes is made, whereby samples from one class are compared with all the samples from the same class. For each intraclass comparison, a square matrix is created, whereby size of the square matrix represents the number of the signals within the class as previously defined. The statistical parameters (average value, minimal value, maximal value, median value and STD) calculated from the values belonging to each of the obtained intraclass matrices are shown in Table 1.

Table 1 *Statistical parameters of SSIM indexes for intraclass comparison (samples within the defined class)*

Class	Class 1	Class 2	Class 3	Class 4
Average	0.465	0.4563	0.48	0.4749
Minimal	0.216	0.2033	0.2236	0.2046
Maximal	1.0	1.0	1.0	1.0
Median	0.4651	0.455	0.483	0.4788
STD	0.064	0.06	0.0646	0.062
Class	Class 5	Class 6	Class 7	Class 8
Average	0.4167	0.4165	0.4462	0.4394
Minimal	0.1814	0.1685	0.2141	0.197
Maximal	1.0	1.0	1.0	1.0
Median	0.4186	0.4178	0.4461	0.4415
STD	0.0777	0.0715	0.0753	0.0744

In order to give a visual representation, we have plotted heat maps for each intraclass comparison, that is, for SSIM values within the same class. Higher values of SSIM are shown with lighter colours and the lower values with the darker colours. These heatmaps are presented in Figure 1. It could be observed that all heatmaps from Figure 1 are simetrical regarding the main diagonal, which is a consequence of irrelevance of the order of samples in SSIM calculation. The SSIM value is the same if sample *X* is compared with sample *Y* and sample *Y* is compared with sample *X*. As a result, the similarity matrix has two simetrical halves. The main diagonal represents self-comparison, i.e. comparison of sample with itself (e.g. sample *X* with sample *X*). The SSIM index for self-comparison is always equal to 1. From this reason main diagonal is white line for all intraclass heatmaps.

From Table 1, we could see that classes 1 to 4, which are samples of type A motor, have higher intraclass similarity than classes 5 to 8, which are the samples of type B motor. Namely, the average, median, maximal and minimal values are higher, while having lower STD within the classes 1 to 4 than within the classes 5 to 8. Therefore, we can conclude that the samples of type A motor are more consistent (similar to each other) than the samples of type B motor.

As expected, the average SSIM values for intraclass comparison of classes with only different rotation directions are very similar. The motor rotates in both directions creating very similar sounds, more similar than comparing OK and NOK motors.

On the other hand, the average intraclass SSIM values for motors with failures are higher than the motors of the same type but without failures, which is an interesting result worth more detailed consideration.

The highest average value of the SSIM index, equal to 0.48, is achieved within the Class 3, and the lowest one, equal to 0.4165, is obtained for the Class 6, see Table 1. As explained, the maximal SSIM value refers to the self-comparison and is always equal to 1. The minimal SSIM parameter is the highiest for Class 3 (equal to 0.2236), and lowest for Class 6 (equal to 0.1685). The median value is also highiest for Class 3 (equal to 0.483), and the lowest for Class 6 (equal to 0.4178). Therefore, we could conclude that regarding the statistical SSIM parameters, Class 3 has the highest intraclass similarity and Class 6 has the lowest intraclass similarity.

In order to perform a more detailed analysis of structural similarity of the observed DC motor samples, we have made an interclass comparison. Here. it is not easy to observe differences when more than one criteria for splitting into classes (motor type, presence of failures and direction of rotation) is changed. So, we have decided to analyse the (interclass) structural similarity between classes that have only one different criteria.

Table 2 *Statistical parameters of SSIM indexes for interclass comparison between the samples from the defined classes*

Between classes	1 - 2	3 - 4	5 - 6	7 - 8
Average	0.4171	0.4418	0.412	0.4356
Minimal	0.191	0.2103	0.1711	0.1967
Maximal	0.605	0.6236	0.6683	0.6237
Median	0.4177	0.4453	0.4181	0.4402
STD	0.0443	0.0482	0.0603	0.0564
Between classes	1 - 3	2 - 4	5 - 7	6 - 8
Average	0.4592	0.4527	0.423	0.4176
Minimal	0.2269	0.1898	0.1828	0.1557
Maximal	0.646	0.6141	0.6324	0.602
Median	0.4619	0.4562	0.4265	0.423
STD	0.0542	0.0495	0.062	0.0599
Between classes	1 - 5	2 - 6	3 - 7	4 - 8
Average	0.4026	0.3994	0.4182	0.4073
Minimal	0.1821	0.1699	0.1713	0.1812
Maximal	0.6178	0.6131	0.5988	0.5663
Median	0.405	0.4028	0.4214	0.4124
STD	0.0558	0.05	0.054	0.0497

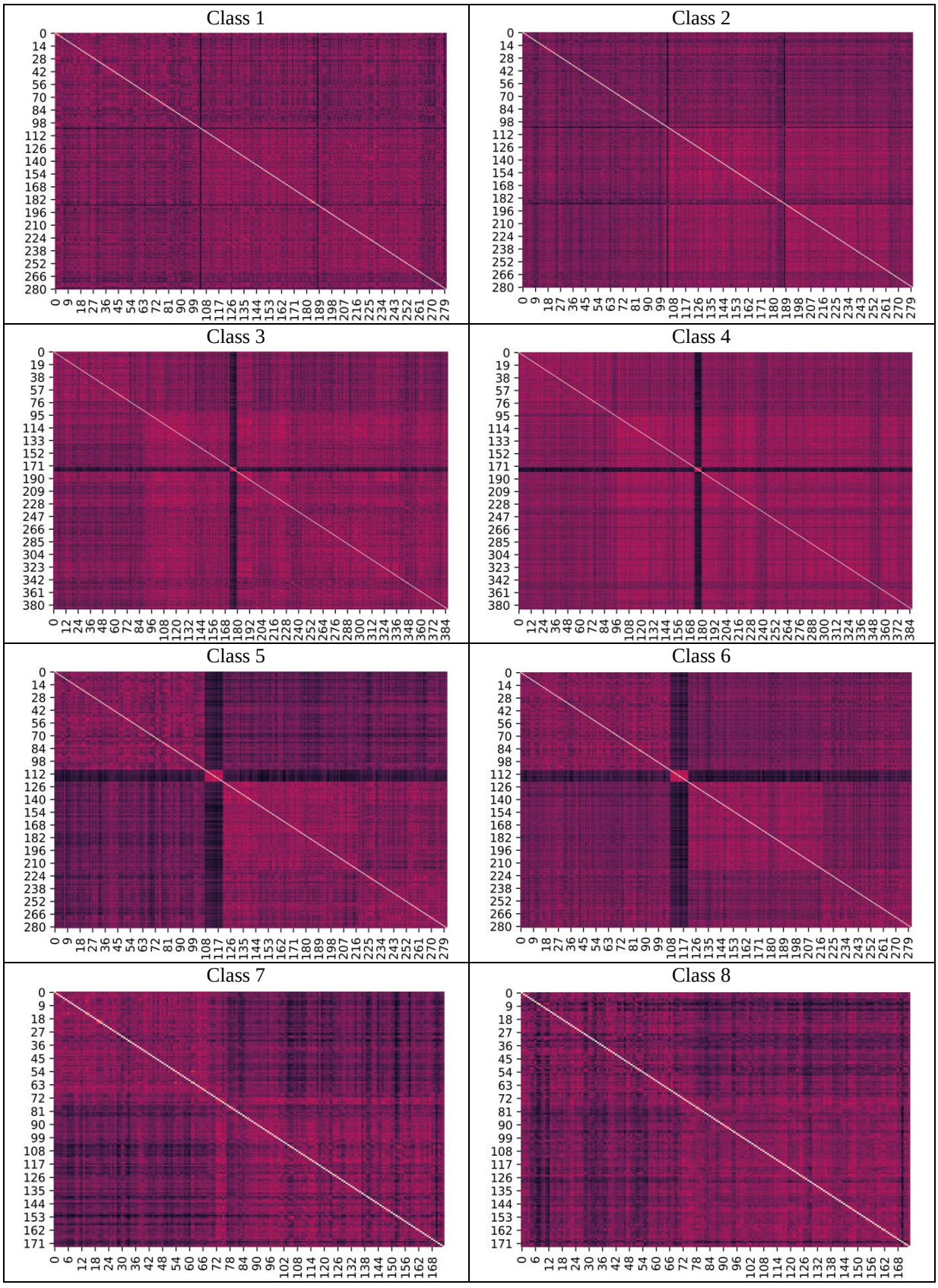

Fig. 1 *Heatmaps illustrating SSIM indexes for intraclass comparisons*

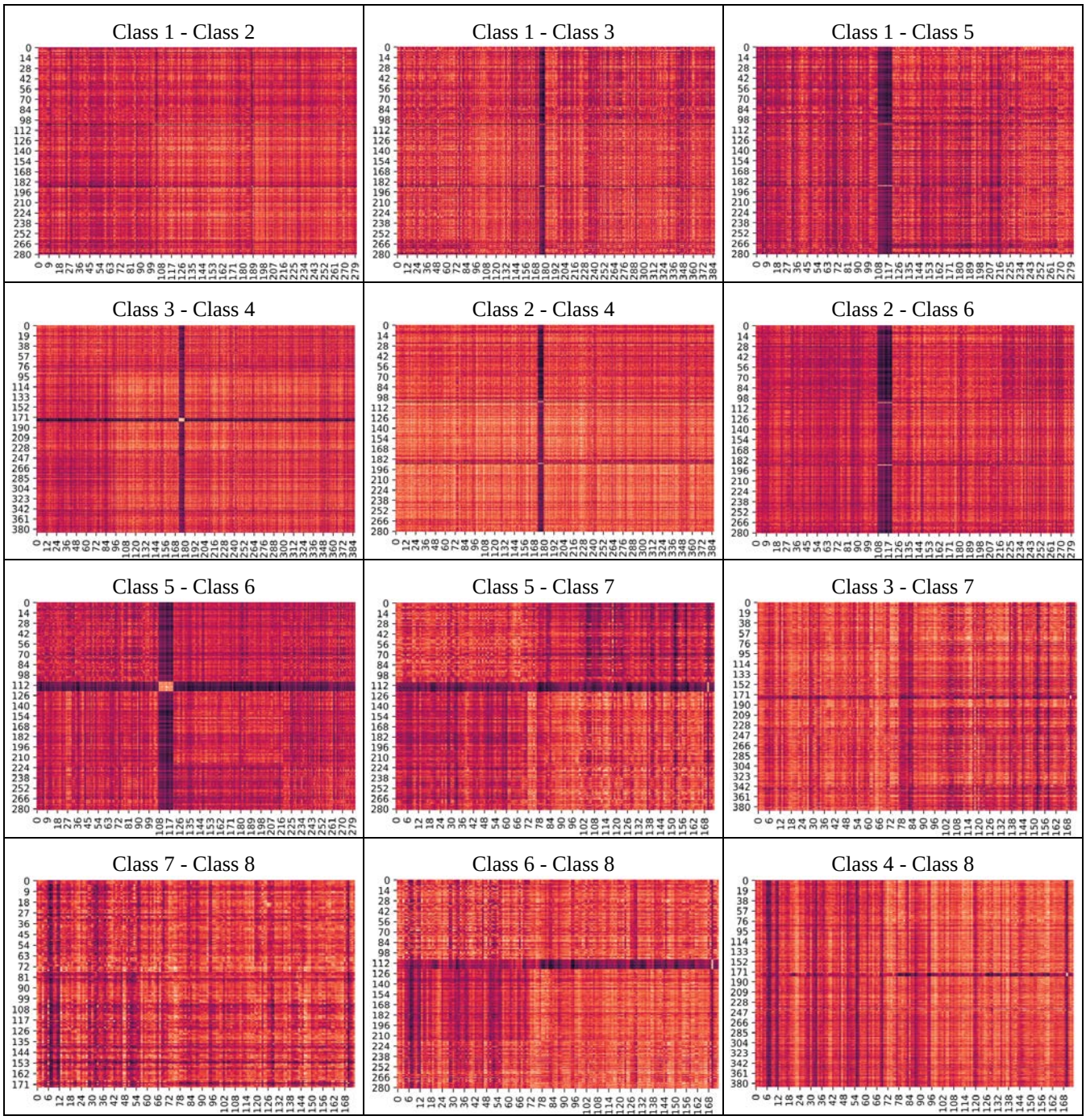

Fig. 2 *Heatmaps illustrating SSIM indexes for interclass comparisons between given classes*

To compare classes with only different direction of rotation we have made comparison of the following classes: 1 – 2, 3 – 4, 5 – 6 and 7 – 8; in order to compare classes with only different existence of failures (OK or NOK), the following pairs of classes are analysed: 1 – 3, 2 – 4, 5 – 7 and 6 – 8; to compare classes with only different type of motor (A or B), the following pairs of classes are analysed: 1 – 5, 2 – 6, 3 – 7 and 4 – 8. The SSIM indexes are calculated for all the mentioned interclass comparisons, and the rectangular matrices are obtained. Here, the sizes of matrices are different and they are equal to the number of samples of compared classes, as defined previously in the article. The mentioned statistical parameters (average value, minimal value, maximal value, median value and STD) are calculated from each of these interclass matrices, and they are shown in Table 2.

As a graphical illustration, we have plotted heatmapts for all the interclass comparisons. They are given in Figure 2. The first column in this figure gives the heatmaps of the samples with only different direction of rotation, the second column shows difference regarding the existence of failures (OK or NOK) and the third column illustrates comparisons if the classes with only different type of motor (A or B). Lighter coluours mean the higher values of the SSIM index and darker colours the lower values.

For all observed interclass comparisons, the SSIM values are lower than those for the intraclass comparisons of the analyzed classes. As expected, the samples are more similar to the other samples of the same class than with the samples from different classes. This enables the further research in the field of classification, which is of our particular interest.

In order to summarize the interclass analysis, it can be said that the highest similarity exists between Classes 1 and 3, as they have the largest average value, equal to 0.4592,and median value, equal to 0.4619. This is a comparison of type A motors rotating in direction 1 having the only difference regarding the existence of failures. Therefore, we can conclude that the registered failures within this type of motor make less different sounds than the different direction of rotation. On the other hand, the lowest similarity is observed between Classes 2 and 6, as they have the lowest average value, equal to 0.3994,and median value, equal to 0.4028. This is a comparison of two different motor types that both rotate in the same direction and do not have failures. As expected, if we compare two different motor types we are going to get the most different sounds.

Both figures with heatmaps (Figure 1 and 2) show some dark horizontal or vertical lines. These lines represent few sound samples from its class that are more different from other compared samples either from the same or from different classes. It is interesting to note that crossings of these dark lines are britgher than the rest of the heatmap, both at intraclass and interclass analysis. This indicates that the mentioned samples could be extracted into a subclass and further inspected, as they are labeled like the other sounds from its class but have different caracterstics.

5. CONCLUSIONS

In this article we have given the overview of structural similiraty of the images and in particular the SSIM index. We have investigated sound samples of DC motors from our own database from the point of view of their structural similarity when they are converted into mel spectrograms. The sounds samples are divided into 8 classes, based on the type of motor (A or B), the direction of rotation (1 or 2) and the existence of failures (OK or NOK). The intraclass comparison is made for all classes, i.e. comparison of one class' samples with other samples from the same class. On the other hand, the interclass comparison, i.e. comparison of the samples from one class with the samples from another class, is made for 12 cases, as we wanted to compare classes that have only one different criterion (characteristic). For all performed analyses, the statistical parameters are calculated and heatmaps are plotted, providing numerical and graphical overview of the results.

Summing the both intraclass and interclass analysis, we have elaborated which classes have the highest and lowest similarity. Regarding the intraclass similarity, Class 3 has the highest and Class 6 has the lowest similarity. For the interclass similarity, the most similar are Classes 1 and 3 and the least similar are Classes 2 and 6.

Generally, the samples from one class give higher SSIM inexes for the intraclass than for the interclass analysis. That would enable making further research in this field in order to make a classification of the DC motor sound samples using image processing approach.

ACKNOWLEDGMENT

This work has been supported by the Ministry of Education, Science and Technological Development of the Republic of Serbia, contract no. 451-03-68/2022-14/200102.

REFERENCES

[1] P. Sharma, N. Saraswat, "Diagnosis of motor faults using sound signature analysis", *Int. J. Inov. Res. Electr. Electron. Instrum. Control Eng.*, vol. 3, no. 5, pp. 80-83, May, 2015.

[2] A. Krishnasarma, S.J. Mostafavi Yazdi, A. Taylor, D. Ludwigsen, J. Baqersad, "Acoustic signature analysis and sound source localization for a three-phase AC induction motor", *Energies*, vol. 14, pp. 7182-7193, 2021.

[3] E. Awada, A. Al-Qaisi, E. Radwan, M. Nour, "Motor fault detection using sound signature and wavelet transform", *Int. J. Power Electron. Drive Syst.*, vol. 13, no. 1, pp. 2839-2847, March, 2022.

[4] R. Vilela, J.C. Metrolho, J.C. Cardoso, "Machine and industrial monitorization system by analysis of acoustic signatures", in *Proc. 12th IEEE Mediterranean Electrotechnical Conf.*, 2004, pp. 277-279.

[5] B. Rubhini, P. V. Ranjan, "Machine condition monitoring using audio signature analysis", in *Proc. 4th Int. Conf. Sig. Proc. Com. Networking*, 2017, pp. 1-6.

[6] Y. Tagawa, R. Maskeliunas, R. Damaševičius, "Acoustic anomaly detection of mechanical failures in noisy real-life factory environments", *Electronics*, vol. 10, pp. 2329-2351, 2021.

[7] D. Ćirić, Z. Perić, J. Nikolić, N. Vučić, “Audio signal mapping into spectrogram-based images for deep learning applications”, in *Proc. 20th Int. Symp. Infoteh-Jahorina*, 2021, pp. 1-6.

[8] G.R. Harp, J. Richards, S. Shostak, S.J. Tarter, G. Mackintosh, J.D. Scargle, C. Henze, B. Nelson, G.A. Cox, S. Egly, V.J. Voien, "Machine vision and deep learning for classification of radio SETI signals", *arXiv:1902.02426*, 2019.

[9] J. Zujovic, T.N. Pappas, D.L. Neuhoff, "Structural texture similarity metrics for image analysis and retrieval", *IEEE Trans. Image Process.*, vol. 22, pp. 2545-2558, 2013.

[10] J. Snell, K. Ridgeway, R. Liao, B.D. Roads, M.C. Mozer, R.S. Zemel, “Learning to generate images with perceptual similarity metrics”, in *Proc. IEEE Int. Conf. Image Proc.*, 2017, pp. 4277-4281.

[11] A. Zaric, M. Loncaric, D. Tralic, M. Brzica, E. Dumic, S. Grgic, “Image quality assessment - comparison of objective measures with results of subjective test”, in *Proc. 52nd Int. Symp. ELMAR-2010*, 2010, pp. 113-118.

[12] W. Lu, C. Li, Y. Shi, X. Sun, “Image quality assessment based on SIFT and SSIM”, in *Proc. Chinese Conf. Image Graphics Tech. – Com. Comp. Inf. Science*, 2014.

[13] G. Batchuluun, J.H. Koo, Y.H. Kim, K.R. Park, "Image region prediction from thermal videos based on image prediction generative adversarial network", *Mathematics*, vol. 9, pp. 1053-1072, 2021.

[14] Q. Liu, N. Li, H. Jia, Q. Qi, L. Abualigah, "Modified remora optimization algorithm for global optimization and multilevel thresholding image segmentation", *Mathematics*, vol. 10, pp. 1014-1055, 2022.

[15] G. Batchuluun, N.R. Baek, K.R. Park, "Enlargement of the field of view based on image region prediction using thermal videos", *Mathematics*, vol. 9, pp. 2379-2407, 2021.

[16] N. Ortega-Sánchez, D. Oliva, E. Cuevas, M. Pérez-Cisneros, A.A. Juan, "An evolutionary approach to improve the halftoning process", *Mathematics*, vol. 8, pp. 1636-1658, 2020.

[17] H. Yang, J. Wang, Y. Miao, Y. Yang, Z. Zhao, Z. Wang, Q. Sun, D.O. Wu, "Combining spatio-temporal context and Kalman filtering for visual tracking", *Mathematics*, vol. 7, pp. 1059-1072, 2019.

[18] Z.H. Almahdawie, Z.M. Hussain, "Performance of signal similarity measures under 1/f noise", *J. Theor. Appl. Inf. Technol.*, vol. 96, pp. 8399-8409, 2018.

[19] M.M. Valero, S. Verstockt, C. Mata, D. Jimenez, L. Queen, O. Rios, E. Pastor, E. Planas, "Image similarity metrics suitable for infrared video stabilization during active wildfire monitoring: A comparative analysis", *Remote Sens.*, vol. 12, pp. 540-563, 2020.

[20] S. Li, Z. Li, J. Gong, "Multivariate statistical analysis of measures for assessing the quality of image fusion", *Int. J. Image Data Fusion*, vol. 1, pp. 47-66, 2010.

[21] P. Arun, S. Abraham Lincon, N. Prabhakaran, "An automated method for the analysis of bearing vibration based on spectrogram pattern matching", *J. Appl. Research Tech.*, vol. 17, pp. 126-136, 2019.

[22] D. Ćirić, Z. Perić, J. Nikolić, N. Vučić, “Intra-class and inter-class differences in mel-spectrogram images of DC motor sounds”, in *Proc. 15th Int. Conf. Adv. Tech. Sys. Services Telecom.*, 2021, pp. 189-192.

[23] D.G. Ćirić, Z.H. Perić, M. Milenković, N.J. Vučić, "Evaluating similarity of spectrogram-like images of DC motor sounds by Pearson correlation coefficient", *Elektronika Ir Elektrotechnika*, vol. 28, no. 3, pp. 37-44, 2022.

[24] V.I. Utkin, "Variable structure control systems with sliding modes", *IEEE Trans. Automat. Control*, vol. AC-22, pp. 210-222, April, 1977.

[25] A.E. Bryson and Y. C. Ho, *Applied Optimal Control*, New York:Wiley, 1975.

[26] B.K. Bose, “Sliding mode control of induction motor”, in *Proc. IEEE Ind. Appl. Soc. Annu*. Meeting, 1995, pp. 479-486

University of Nis
Faculty of Occupational Safety
„Politechnica“ University of Timisoara
Faculty of Mechanical Engineering
27th International Conference
NOISE AND VIBRATION
Niš, 20 - 21. 10. 2022.

THE ESTIMATION AND COMPARISON OF SUBJECTIVE SPEECH INTELLIGIBILITY IN THE FUNCTION OF THE PHYSICAL PARAMETER REVERBERATION TIME FOR THE SERBIAN ORTHODOX CHURCH

Violeta Stojanović[1], Zoran Milivojević[2]

[1] The Academy of Applied Technical and Preschool Studies - Department Nis, Serbia, e-mail: violeta.stojanovic@akademijanis.edu.rs
[2] The Academy of Applied Technical and Preschool Studies - Department Nis, Serbia, e-mail: zoran.milivojevic@akademijanis.edu.rs

Abstract - *This paper presents an estimation and comparison of the subjective speech intelligibility in the a function of the physical parameter of reverberation time for the unoccupied and occupied Serbian Orthodox church "St. George" in Žitni Potok. The first part of the paper includes a describes of the experiment, tabularly and graphically presented results of the calculated values of the reverberation time RT_{30}, the objective index of speech transmission STI and the corresponding values of the subjective intelligibility of speech given by the Standard for an unoccupied church, as well as the estimated values of the analyzed acoustic parameters for the occupied church. In the second part of the paper a comparative analysis of the results is presented and a conclusion was given.*

Keywords – *Reverberation time RT_{30}, objective speech transmission index STI, subjective speech intelligibility, Standard IEC 60268 -16, Correlation and regression.*

1. INTRODUCTION

Since 1922 when Wallace Sabine introduced the reverberation time, RT, as a measure of acoustic conditions in rooms, this physical quantity has been used as the main acoustic parameter for the assessment of acoustic quality and church interiors [1]. According to the Sabine's pattern, the reverberation time decreases if the sound absorption in the room increases. This practically means that the reverberation time of an unoccupied church is the highest, while the the reverberation time reduces with the entrance of believers. Church acoustics implies a high reverberation, up to about 4 s; however, it may be even higher in extremely large churches. The objective speech intelligibility depends on the reverberation time. The longer the reverberation time, the lower the speech intelligibility, due to the fact that certain syllables overlap. Reverberation is also important for the subjective experience of loudness, but it primarily has an aesthetic function. because it is one of the basic elements of responsiveness from the aspect of influence on the overall subjective experience of sound. The correlation among the objective acoustic parameter, speech transmission index *STI* and subjective speech intelligibility of sentences SI_{sent}, PB words SI_{PBw} and CVC logatoms SI_{CVC} is given by Standard IEC 60268 - 16 [2].

This paper presents an estimation and comparison of the subjective speech intelligibility in the function of the physical parameter of reverberation time for the unoccupied and occupied Serbian Orthodox church "St. George" in Žitni Potok. The values of the objective acoustic parameters, the reverberation time RT_{30} and the speech transmission index *STI*, were determined on the basis of the measurement of acoustic impulse responses and the ARTA software package. First a connection was established between the measured values of RT_{30} at the central frequency f_c = 2 kHz and the values of the objective acoustic parameters of *STI*. Next, using the Standard IEC 60268 - 16, the percentage values, and therefore the quality, of the subjective speech intelligibility of sentences SI_{sent}, PB words, SI_{PBw} and CVC logatoms SI_{CVC} were determined. Using the Matlab software package, the connection between subjective speech intelligibility and reverberation time was determined by correlation and regression analysis.

The paper is organised as follows: Section II includes the explanation of the method used to determine the value of acoustic parameters for the unoccupied and occupied church, Section III presensts the experimental results and analysis and Section IV presents the conclusion.

2. METHODOLOGY

The experiment was carried out in the church of "St. George" in Žitni Potok (Serbia). This church has a volummae of V = 2163 m^3 and inner area is S = 167 m^2. The interior walls and the ceilings in the churches covered with plaster (the coefficient of absorption α = 0.02). The floors with the ceramic tiles (the coefficient of absorption α = 0.015). The church capacity of about 80 people.

The method used to calculate the $RT_{30unocc}$ and STI_{unocc} values of the unoccupied church is based on the measurement of acoustic impulse responses and the use of the ARTA software package. The procedure for recording and calculation of acoustic parameters was performed in accordance with ISO 3382 [3].

The equippment used for the experiment as follows: (a) an omnidirectional microphone (PCB 130D20), having a diaphragm diameter of 7mm; (b) a B&K omnidirectional sound source type 4295 (dodecahedron loudspeaker); (c) a B&K audio power amplifier, rated at 100W RMS, stereo, type

2716-C; (d) a laptop, incorporating a Soundmax Integrated Digital Audio sound card from Analog Devices.

Measuring of the impulse response is carried out using incentive log sweep signal with the duration of 5 s sampling frequency is f_S = 44.1 kHz. For the purposes of analysis in this work, acoustic impulse responses measured in MP = 9 measuring points of the church were taken, the layout of which is shown in Fig. 2. For each measurement point, 7 measurements were made, which makes a total of 63 files.

Based on the classification of the ratio of speech intelligibility and the *STI* parameter established by the Standard [2], the values of speech intelligibility were determined: $SI_{sent\text{-}unocc}$, $SI_{PBw\text{-}unocc}$ and SI_{CVC} for each MP measurement position in the unoccupied church.

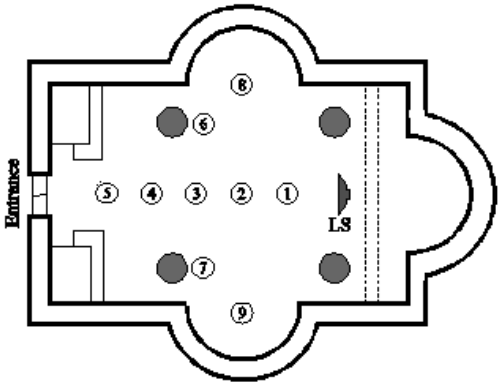

Fig. 1 *The position of measuring point MP and sound source LS in the church "St. George" in Žitni Potok during the recording impulse response.*

Then, the mean values and standard deviations of these quantities were calculated for all MP measurement positions in the unoccupied church. For the occupied church, for each MP measurement position, the following is calculated:

1) predicted reverberation time RT_{30occ} using the formula [4]:

$$RT_{30occ} = RT_{30unocc} - DT, \quad (1)$$

where *DT* is Schultz diffusion time and

2) estimation of speech transmission index parameter STI_{occ} by [5]:

$$STI_{occ} = STI_{unocc} + \Delta STI\,. \quad (2)$$

ΔSTI is a value calculated using the following formula:

$$\Delta STI = 0.45 \ln \frac{RT_{unocc}(2kHz)}{RT_{occ}(2kHz)} + 0.012\,. \quad (3)$$

Using the Standard [2], speech intelligibility values were determined: $SI_{sent\text{-}unocc}$, $SI_{PBw\text{-}unocc}$ and SI_{CVC} for each MP measurement position in the occupied church. Then, the mean values and standard deviations of these quantities were calculated for all MP measurement positions in the unoccupied church. The assessment of the quality of speech in the church was based on Standard [2].

The intensity of the connection between the objective parameters RT_{30} and *STI* and the acoustic parameters that qualify the subjective speech intelligibility :SI_{sent}, SI_{PBw} i SI_{CVC} for the unoccupied and occupied church, at 2 kHz, was determined by regression and correlation analysis.

3. RESULTS OF THE EXPERIMENT AND ANALYSIS

3.1 Results of the experiment

Table 1 shows the values of the following acoustic quantities at the central frequency *f* = 2kHz: 1) $RT_{30unocc}$, STI_{unocc}, $SI_{sent\text{-}unocc}$, $SI_{PBw\text{-}unocc}$ and $SI_{CVC\text{-}unocc}$ for each MP measurement position as well as the mean values and standard deviations of these quantities for all MP measurement positions in the unoccupied church and 2) RT_{30occ}, STI_{occ}, $SI_{sent\text{-}occ}$, $SI_{PBw\text{-}occ}$ and $SI_{CVC\text{-}occ}$ for each MP measurement position as well as the mean values and standard deviations of these quantities for all MP measurement positions in the occupied church.

Figs. 2. show regression lines for measures: a) STI_{unocc} and $RT_{30unocc}$ for the unoccupied church and b) STI_{occ} *and* RT_{30occ} for the occupied church at 2kHz . Figs. 3. -5. show regression lines for measures: $SI_{sent\text{-}unocc}$ and $RT_{30unocc}$, $SI_{PBw\text{-}unocc}$ and $RT_{30unocc}$ and $SI_{CVC\text{-}unocc}$ and $RT_{30unocc}$ at central frequency f_c = 2 kHz for unoccupied church. Figs. 6. -8. show regression lines for measures: $SI_{sent\text{-}occ}$ and RT_{30occ}, $SI_{PBw\text{-}occ}$ and RT_{30occ} and $SI_{CVC\text{-}occ}$ and RT_{30occ} at central frequency f_c = 2 kHz for occupied church.

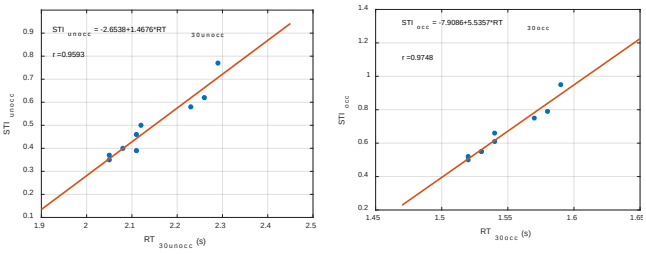

a) b)

Fig. 2. *The regression line for: a) STI_{unocc} and $RT_{30unocc}$ for the unoccupied church and b) STI_{occ} and RT_{30occ} for the occupied church at 2kHz*

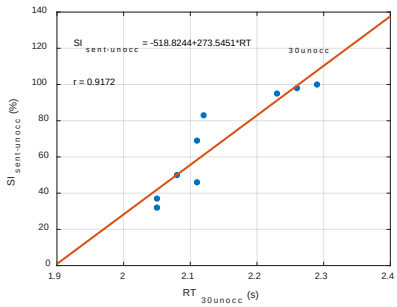

Fig. 3. *The regression line for $SI_{sent\text{-}unocc}$ and $RT_{30unocc}$ at 2kHz for the unoccupied church*

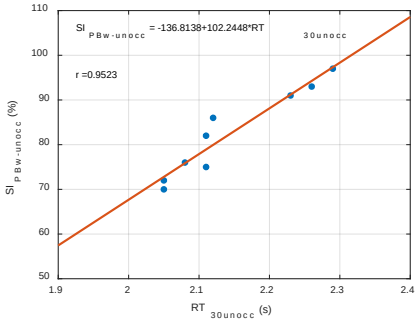

Fig. 4. *The regression line for $SI_{PBw\text{-}unocc}$ and $RT_{30unocc}$ at 2kHz for the unoccupied church*

Table 1 *Values of reverberation time RT_{30}, objective speech transmission index STI, subjective speech intelligibility SI (sentence, PB words and CVC logatoms), their mean values, standard deviations and speech quality for the unoccupied and the occupied church.*

MP	$RT_{30unocc}$ (2 kHz) (s)	STI_{unocc}	$SI_{sent\text{-}unocc}$ (%)	$SI_{PBw\text{-}unocc}$ (%)	$SI_{CVC\text{-}unocc}$ (%)	RT_{30occ} (2 kHz) (s)	STI_{occ}	$SI_{sent\text{-}occ}$ (%)	$SI_{PBw\text{-}occ}$ (%)	$SI_{CVC\text{-}occ}$ (%)
1	2.29	0.77	100	97	83	1.59	0.95	100	98	95
2	2.26	0.62	98	93	70	1.58	0.79	100	97	83
3	2.12	0.5	83	86	59	1.54	0.66	99	95	74
4	2.11	0.46	69	82	53	1.54	0.61	97	93	70
5	2.08	0.4	50	76	46	1.53	0.55	92	90	64
6	2.05	0.37	37	72	41	1.52	0.52	85	87	60
7	2.05	0.35	32	70	39	1.52	0.5	83	86	59
8	2.11	0.39	46	75	45	1.53	0.55	92	90	64
9	2.23	0.58	95	91	67	1.57	0.75	100	96	81
$\overline{RT_{30unocc,MP}}$ (2 kHz) (s)	$\overline{STI_{unocc}}$	$\overline{SI_{sent-unocc}}$ (%)	$\overline{SI_{CVC-unocc}}$ (%)	$\overline{SI_{PBw-unocc}}$ (%)	$\overline{RT_{30occ,MP}}$ (2 kHz)(s)	$\overline{STI_{occ}}$	$\overline{SI_{sen-occ}}$ (%)	$\overline{SI_{PBw-occ}}$ (%)	$\overline{SI_{CVC-occ}}$ (%)	
2.14	0.49	67.78	82.44	55.89	1.55	0.65	94.22	92.44	72.22	
$\sigma_{\overline{RT_{30unocc,MP}}}$ (2 kHz) (s)	$\sigma_{\overline{STI_{unocc}}}$	$\sigma_{\overline{SI_{sent-unocc}}}$ (%)	$\sigma_{\overline{SI_{PBw-unocc}}}$ (%)	$\sigma_{\overline{SI_{CVC-unocc}}}$ (%)	$\sigma_{\overline{RT_{30occ,MP}}}$ (2 kHz)(s)	$\sigma_{\overline{STI_{occ}}}$	$\sigma_{\overline{SI_{sent-occ}}}$ (%)	$\sigma_{\overline{SI_{PBw-occ}}}$ (%)	$\sigma_{\overline{SI_{CVC-occ}}}$ (%)	
0.09	0.14	27.26	9.81	15	0.03	0.15	6.63	4.39	12.14	
Rating										
-	poor fair	bad good	poor good	poor good	-	fair excell.	bad excellent	good excellent	fair good	

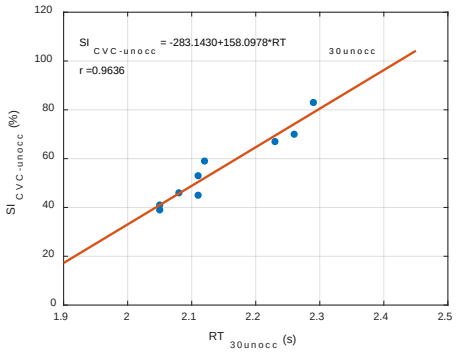

Fig. 5. *The regression line for $SI_{CVC\text{-}unocc}$ and $RT_{30unocc}$ at 2kHz for the unoccupied church*

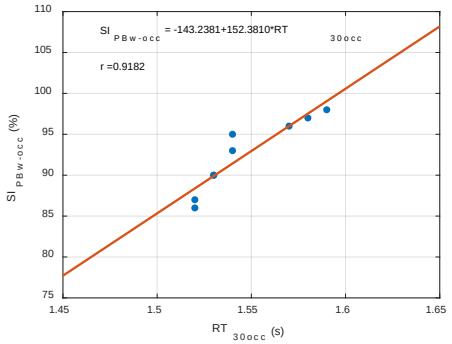

Fig. 7. *The regression line for $SI_{PBw\text{-}occ}$ and RT_{30occ} at 2kHz for the occupied church*

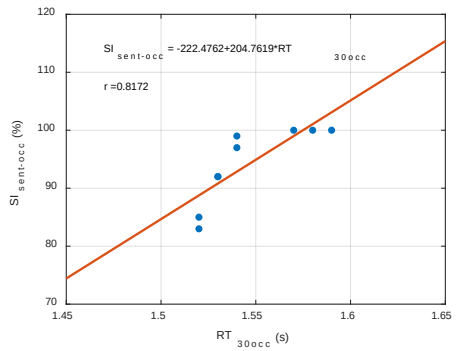

Fig. 6. *The regression line for $SI_{sent\text{-}occ}$ and RT_{30occ} at 2kHz for the occupied church*

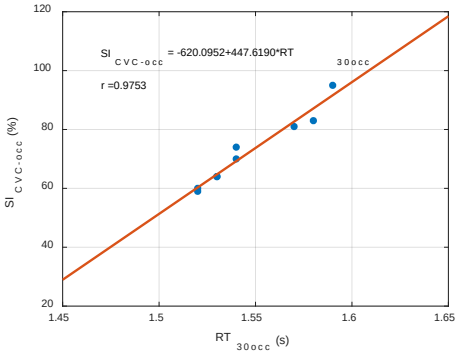

Fig. 8. *The regression line for $SI_{CVC\text{-}occ}$ and RT_{30occ} at 2kHz for the occupied church*

3.2 Analysis of experiment results

Based on the results shown in the Table 1 and the Figs 2. – 9. the following can be concluded:

1) for an unoccupied church is: a) the mean value of the reverberation time $\overline{RT_{30unocc,MP}}$=2.14 ± 0.09 s =2.05 ÷ 2.23 s; b) the mean of the speech transfer index $\overline{STI_{unocc}}$ = 0.49 ± 0.14 = 0.35 ÷ 0.63 classifies speech intelligibility from poor to fair; c) the mean value $\overline{SI_{sent-unocc}}$ = 67.78 ± 27.26 % = 40.52 ÷ 95.04 % classifies the subjective intelligibility of sentences from bad to good; d) the mean value $\overline{SI_{PBw-unocc}}$ = 82.44 ± 9.81 % = 72.63 ÷ 92.25 % classifies the subjective intelligibility of PB words from poor to good and e) the mean value $\overline{SI_{CVC-unocc}}$ = 55.89 ± 15 % = 40.89 ÷ 70.89 % classifies the subjective intelligibility of CVC logatom from poor to good. **2)** for an unoccupied church the correlation and regression analysis gave the following connection of subjective speech intelligibility and reverberation time with the corresponding Pearson coefficients at f = 2 kHz:

STI_{unocc} = -2.6538 + 1.4676 $RT_{30unocc}$, r = 0.9593;

$SI_{sent\text{-}unocc}$ = -518.8244 + 273.5451 $RT_{30unocc}$, r = 0.9172;

$SI_{PBw\text{-}unocc}$ = -136.8138 + 102.2448 $RT_{30unocc}$, r = 0.9523 i

$SI_{CVC\text{-}unocc}$ = -283.143+158. 0978 $RT_{30unocc}$, r = 0.9636.

This analysis shows that for an unoccupied church there is a statistically positive, strong linear connection between the subjective speech intelligibility: $SI_{sent\text{-}unocc}$, $SI_{PBw\text{-}unocc}$ and $SI_{CVC\text{-}unocc}$ and the reverberation time $RT_{30unocc}$. **3)** for an unoccupied church is: a) the mean value of the reverberation time $\overline{RT_{30occ,MP}}$ = 1.55 ± 0.03 s = 1.52 ÷ 1.58 s; b) the mean of the speech transfer index $\overline{STI_{occ}}$ = 0.65 ± 0.15 = 0.5 ÷ 0.8 classifies speech intelligibility from fair to excellent; c) the mean value $\overline{SI_{sent-occ}}$ = 94.22 ± 6.63 % = 87.59 ÷ 100.85 % classifies the subjective intelligibility of sentences from bad to excellent; d) the mean value $\overline{SI_{PBw-occ}}$ = 92.44 ± 4.39 % = 88.05 ÷ 96.83 % classifies the subjective intelligibility of PB words from good to excellent and e) the mean value $\overline{SI_{CVC-occ}}$ = 72.22 ± 12.14 % = 60.08 ÷ 84.36 % classifies the subjective intelligibility of CVC logatom from fair to good. **4)** for an occupied church the correlation and regression analysis gave the following connection of subjective speech intelligibility and reverberation time with the corresponding Pearson coefficients at f = 2 kHz:

STI_{occ} = -7.9086 + 5.5357 RT_{30occ}, r = 0.9748;

$SI_{sent\text{-}occ}$ = -222.4762 + 204.7619 RT_{30occ}, r = 0.8172;

$SI_{PBw\text{-}occ}$ = -143.2381 + 152.381 RT_{30occ}, r = 0.9182 i

$SI_{CVC\text{-}occ}$ = -620.0952+447.619 RT_{30occ}, r = 0.9753.

This analysis shows that and for an occupied church there is a statistically positive, strong linear connection between the subjective speech intelligibility: $SI_{sent\text{-}occ}$, $SI_{PBw\text{-}occ}$ i $SI_{CVC\text{-}occ}$ and the reverberation time RT_{30occ}.

4. CONCLUSION

In this paper, the an estimation and comparison of subjective speech intelligibility in the a function of the physical parameter of reverberation time for the unoccupied and occupied Serbian Orthodox church "St. George" in Žitni Potok and the correlation and regression analysis confirmed an strong correlation between these parameters.

The mean value of the reverberation time for the unoccupied church belongs to the range of values: $\overline{RT_{30unocc,MP}}$ = 2.05 ÷ 2.23 s. As believers enter the church, due to increased sound absorption, the values of this acoustic parameter decrease [1]. Namely, for the occupied church, the mean value of the reverberation time belongs to the range of values: $\overline{RT_{30occ,MP}}$ = 1.52 ÷ 1.58 s. Due to the reduction of reverberation time, the objective and subjective intelligibility of speech increases. The mean value of the speech transmission index belongs to the range of values: a) for the unoccupied church: $\overline{STI_{unocc}}$ = 0.35 ÷ 0.63 and classifies speech intelligibility from poor to faire, while b) for the occupied church: $\overline{STI_{occ}}$ = 0.5 ÷ 0.8 and classifies intelligibility speech from faire to excellent. Subjective intelligibility of speech (analyzed through subjective intelligibility of sentences, PB words and CVC logatoms determined by Standard IEC 60268-16), also significantly improves for the case of the occupied church. The mean value of the subjective intelligibility of sentences belongs to the range of values: a) for the unoccupied church: $\overline{SI_{sent-unocc}}$ = 40.52 ÷ 95.04 % and classifies speech intelligibility from bad to good and b) for the occupied church: $\overline{SI_{sent-occ}}$ = 87.59 ÷ 100.85 % and classifies speech intelligibility from bad to excellent. The mean value of the subjective intelligibility PB words belongs to the range of values: a) for the unoccupied church: $\overline{SI_{PBw-unocc}}$ = 72.63 ÷ 92.25 % and classifies speech intelligibility from poor to good. and b) for the occupied church: $\overline{SI_{PBw-occ}}$ = 88.05 ÷ 96.83 % and classifies speech intelligibility from good to excellent.

The mean value of the subjective intelligibility CVC logatoms belongs to the range of values: a) for the unoccupied church: $\overline{SI_{CVC-unocc}}$ = 40.89 ÷ 70.89 % and classifies speech intelligibility from poor to good and b) for the occupied church: $\overline{SI_{CVC-occ}}$ = 60.08 ÷ 84.36 % and classifies speech intelligibility from faire to good.

A statistically positive and strong linear correlation (r > 0.7) between subjective speech intelligibility and reverberation time for the acoustically analyzed Serbian Orthodox church was confirmed by correlation and regression analysis.

REFERENCES

[1] H. Kuttruff, "Room Acoustics", E&FN Spon, London, 2000.

[2] International Electrotechnical Commission IEC 60268-16 – International Standard, "Sound system equipment – Part 16: Objective rating of speech intelligibility by speech transmission index", Switzerland: IEC, 2011.

[3] ISO 3382: Measurement of the Reverberation Time of Rooms with Reference to Other Acoustical Parameters.

[4] M. Topa, N. Toma, B. Kirei, I. Saracut and A. Farina, *Experimental Acoustic Evaluation of an Auditorium*, Hindawi Publishing Corporation Advances in Acoustics and Vibration, Volume 2012.

[5] V. Desarnaulds, A. P. O. Carvalho , G. Monay, *The effect of occupancy in the speech intelligibility in churches*, The 2001 International Congress and Exhibition on Noise Control Engineering The Hague, The Netherlands, 2001.

University of Nis
Faculty of Occupational Safety
„Politechnica“ University of Timisoara
Faculty of Mechanical Engineering
27th International Conference
NOISE AND VIBRATION
Niš, 20 - 21. 10. 2022.

DECAY TIME MEASUREMENTS USING STOCKWELL TRANSFORM

Luka Čurović[1], Jure Murovec[1], Jurij Prezelj[1]

[1] University of Ljubljana, Faculty of Mechanical Engineering, Slovenia, jure.murovec@fs.uni-lj.si

Abstract - *Low-frequency noise issues can be exacerbated in living spaces by inadequate sound insulation and the modal behaviour of rooms, that can be characterised by various reverberation parameters. In the low frequency region, the reverberation of a room should be characterised by the decay time or modal reverberation time, which can be determined experimentally using different methods. In order to obtain robust and repeatable measurements of decay time application of time-frequency Stockwell transform is proposed.*
The time - frequency method methods were applied in a small test room under different test conditions. It has been shown that the choice of measurement method, sampling frequency, excitation duration and microphone position have an important effect on the estimation of the decay time and its modal frequency. The time - frequency impulse response method was also applied in low frequency sound absorption measurements and compared with standard method based on broadband filtering. The time - frequency impulse response method was found to be the more robust method. The use of specific methods to characterise low-frequency sound could improve our understanding of the effects of low-frequency sound in the living environment.

1. INTRODUCTION

The room impulse response observed in a room is determined by the acoustic and geometric properties of the room, the measurement setup, boundary conditions, and environmental factors. The room impulse response can be used to determine the decay of sound. The duration of the sound decay can be quantified by various values, the most commonly used being the reverberation time and the decay time.

The reverberation time is defined under the assumption of the diffuse sound field [1] and is determined using standardized measurement procedures [2,3,4]. At low frequencies, the size of the enclosure is of the same order of magnitude as the wavelength of the acoustic waves in question [5]. The acoustic response of such rooms is strongly shaped by individual room modes [6 - 9]. Low modal density and differences between individual decay rates result in acoustic responses characterised by nonlinear decays. Therefore, well below the Schroeder frequency, decay time can be used over reverberation time, and low-frequency decays must be analysed in terms of room mode characteristics, including modal frequency, number of modes, and modal amplitude. Unlike reverberation time measurements, decay time measurements are currently outside the scope of current standards.

An important step in the evaluation of decay time is the filtering process. Time response of standard broadband filters (third-octave and octave bandpass) [10 - 13] and the leakage of energy from adjacent frequency bands [14, 15] can affect the energy decay. The room modes must be studied individually in the time [9, 13], frequency [6, 16] or time-frequency domains. Time-frequency analysis is particularly useful for signals containing oscillatory components with time-varying amplitudes, as is often the case with measured sound decay signals. The evaluation of the sound decay at low frequencies is not limited to room acoustics only. Reverberation parameters directly influence the values of other acoustic quantities, such as the absorption coefficient, sound reduction index, sound power level, etc.

In this paper, we investigate the use of a window-width optimized S-transform (WWOST) [17 - 19] to determine the decay time of individual modes in a room impulse response signal. The S-transform has been successfully applied in various research areas, e.g., in the analysis of acoustic emission signals [20].

This paper is organised as follows. In Section 2, the theoretical background of the Stockwell transform is presented, including a method for estimating the decay time from an impulse response. Section 3 presents the experiments performed with numerical test signals. Section 4 describes the measurements performed in a small reverberation chamber. Finally, Section 5 contains the conclusion.

2. DETERMINATION OF DECAY TIME USING STOCKWELL TRANSFORM

The Stockwell transform (ST) can be viewed as a short-time Fourier transform of a signal h(t) with a Gaussian time window function. The time window is wide at low frequencies and becomes narrower as the frequency increases. Therefore, for low frequencies, good localization is expected in the frequency domain. The Gaussian window of the S-transform can be further fitted to the measured signal using the scaling parameter γ [21]. In this work, the Stockwell transform of a signal is defined as:

$$ST = \int_{-\infty}^{\infty} h(t) \frac{|f|}{\gamma\sqrt{2\pi}} \exp\left(\frac{-f^2(t-\tau)^2}{2\gamma^2}\right) \exp(-i2\pi f\tau) \mathrm{d}\tau \quad (1)$$

The scaling parameter is found based on the strategy proposed by Sejdic et al. [18] where the optimal γ maximizes the energy concentration measure CM [19]:

$$CM(\gamma) = \left(\int_{-\infty}^{\infty} \int_{-\infty}^{\infty} \left| \frac{ST}{\sqrt{\int_{-\infty}^{\infty} \int_{-\infty}^{\infty} |ST|^2 \, \mathrm{d}t\mathrm{d}f}} \right| \mathrm{d}t\mathrm{d}f \right)^{-1} \quad (2)$$

The identification of the sound decay with the window width optimised Stockwell transform (WWOST) is done in several steps. First, the impulse response with the optimal value of the parameter γ is projected onto a time-frequency plane. Then, the time-dependent energy decay function E_f is determined. E_f is calculated for each centre frequency f using Schroeder integration [22]:

$$E_f(t) = 2 \int_t^{\infty} |ST(t,f)|^2 \mathrm{d}t \quad (3)$$

where $ST(t,f)$ is the window-width optimized Stockwell time-frequency transform of the room impulse response. The decay function is normalized and converted to the decibel scale and decay function in the range of at least 5 dB below the initial level is used to determine the slope (k_n) by least squares fitting. In the last step, the decay time (T_n) is calculated for each frequency bin:

$$T_\mathrm{n} = -\frac{60 \text{ dB}}{k_\mathrm{n}} \quad (4)$$

A graphical representation of the procedure can be seen in Fig. 1.

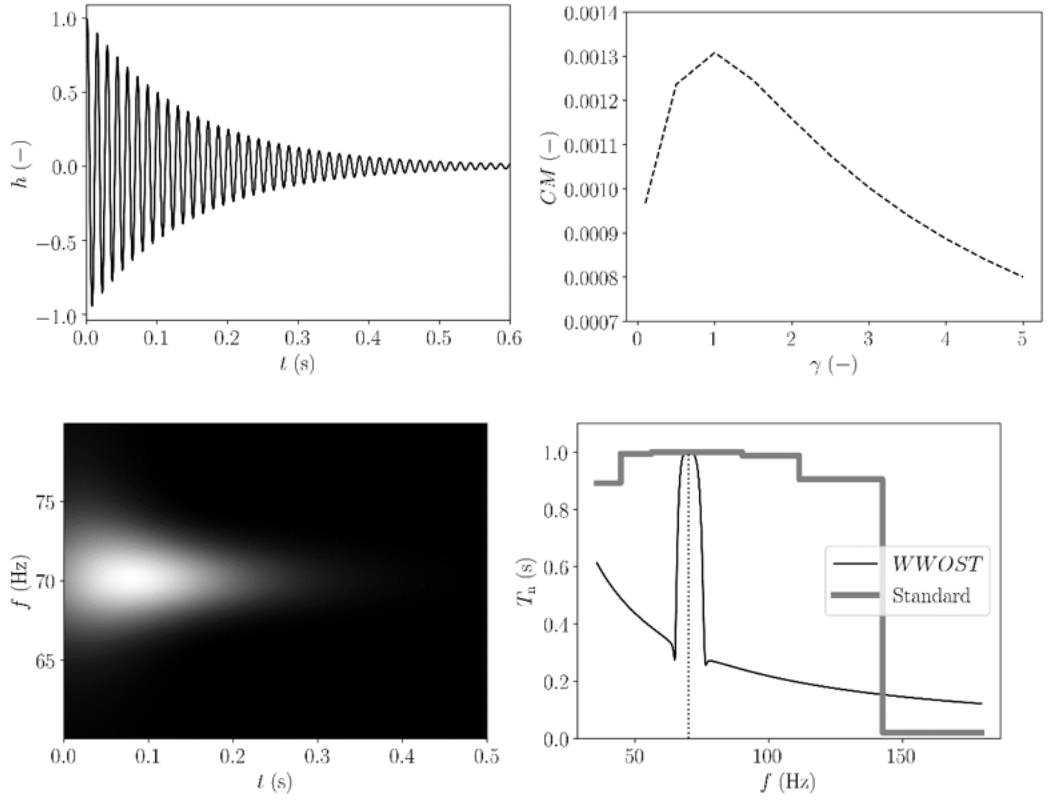

Fig. 1 *Test signal (t): (a) impulse response signal; (b) $CM(\gamma)$; (c) S-transform time-frequency analysis for $\gamma = 1$; (d) Decay time using WWOST and one - third octave band analysis using the standard method.*

3. ANALYSIS OF NUMERICAL EXPERIMENTS

Single decaying mode

In this section we used a Prony test signal [23] to model a decaying mode:

$$h_1(t) = A_1 \cos(2\pi f_1 t + \varphi_1) \exp\left(-\frac{3\log(10)t}{T_1}\right) \quad (5)$$

where A_1 is the amplitude of the signal and φ_1 is a phase of the signal relative to the initial time (t = 0 s). Decay time T_1 in Eq. (17) is the time it takes for the sound pressure level associated with modal frequency f_1 to decay by 60 dB from the initial value [7,9]. In such way, T_1 becomes comparable to the reverberation time of an enclosure [9] and is related to the damping constant [24].

In this experiment, the following values were chosen: T_1 = 1.0 s, $\varphi_1 = \pi/3$, $f_1 = 70$ Hz. The signal was calculated in the time interval between 0 and 4 s ($0 \leq t \leq 4$) with the sampling frequency (f_S) equal to 44100 Hz. The signal (h_1) in the time domain is shown in Fig. 1 a. For each value of γ, the concentration measure was calculated using Eq. (2). Fig. 1 b shows the variation of the $CM(\gamma)$ as a function of the parameter γ. The parameter γ, which corresponds to the highest value of the CM, is selected as optimal. For the presented signal h_1, the optimal value of γ is 1, which is used to calculate decay times. Fig. 1 c shows the *S*-transform in the frequency range from 60 Hz to 80 Hz using $\gamma = 1$. Fig. 1 d shows the decay time (T_1) in seconds as a function of frequency in Hz. The frequency scale ranges from 35 Hz to

180 Hz, which corresponds to 40 Hz, 50 Hz, 63 Hz, 80 Hz, 100 Hz, 125 Hz and 160 Hz one-third octave bands. The black line shows the results obtained with the proposed method using the optimal *S*-transform γ = 1). The thick grey line shows the decay times calculated with a class one one-third octave bandpass filter. Both methods correctly evaluate the decay time in the 63 Hz octave band. The frequency range from 35 Hz to 180 Hz is shown to present the effects of energy leakage. As a result, the standard method yields incorrect values in the neighbouring frequency bands, which is consistent with the results obtained by Marbjerg et al. [15] for higher frequency bands. The result of the time-frequency method is a set of frequency-dependent decay times. The Gaussian-shaped peak of the black curve is at 70 Hz and has a height of 1 s, which is the expected value. Energy leakage to adjacent frequencies is still present, but neighbouring frequencies are characterized by low numerical values of the decay times, which are easy to identify when displayed in a decay time vs. frequency diagram.

Influence of decay in neighbouring bands

In the next experiment, tests were performed on a Prony signal, which contained two decaying modes with the following characteristics: $A_1 = 1$, T_1 = 1.0 s, $\varphi_1 = \pi/2$, $f_1 = 63$ Hz, $A_2 = 2$, T_2 = 2.0 s, $\varphi_2 = \pi/3$, $f_2 = 80$ Hz.

The signal (h) was generated in time interval between 0 and 4 s, the sampling frequency f_S was 44100 Hz. Ideally, there should be no influence of the decay of the mode at 80 Hz at the output of the 63 Hz octave band. The signal was examined and the decay time in the frequency range from 44 Hz to 180 Hz was calculated using an optimized *S*-transform and the class 1 one-third octave band filter. The results are shown in Fig. 2a. The standard approach provides the correct value for the 80 Hz one-third octave band, while the estimated reverberation time for the 63 Hz octave band is 1.5 s and not 1.0 s as expected. The standard method is clearly affected by the 80 Hz resonance in the 63 Hz octave band (see [7]). The time-frequency method is able to recognize both modes and correctly estimate the expected value for the decay times at 63 Hz and 80 Hz.

The energy from the frequency band with a short decay time can distort the slower decay in the adjacent band. Fig. 2b shows the analysis of a signal with the following parameters: f_1 = 80 Hz, A_1 = 1, T_1 = 2 s, $\varphi_1 = \pi/2$, f_2 = 92 Hz, A_2 = 4, T_2 = 1 s, $\varphi_2 = \pi/3$. When using the standard method, the result for the 80 Hz band is lower than expected due to the fast-decaying mode with higher amplitude. Both decay times were correctly evaluated using the time-frequency method.

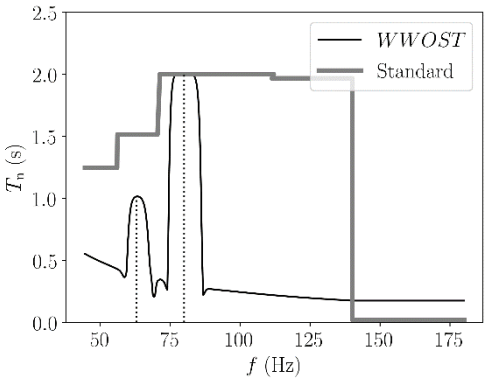

Fig. 2a. *Decay time calculated from the impulse response by standard and time-frequency methods*

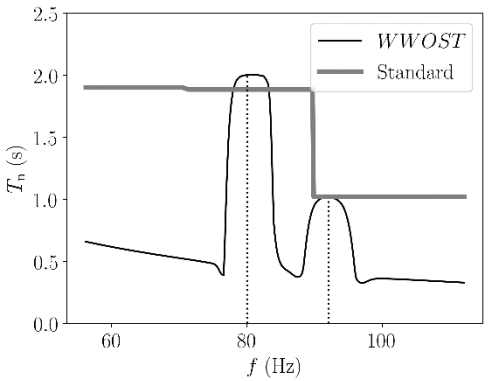

Fig. 2b. *T 60 calculated from the impulse response by standard and time-frequency methods.*

4. MEASUREMENTS IN A SMALL REVERBERATION ROOM

The time-frequency technique using *ST* was tested on signals recorded in a small alpha chamber ($V = 6.4\,\mathrm{m}^3$) with non-parallel surfaces at the Faculty for Mechanical Engineering in Ljubljana. Excitation signals were generated using NI LabVIEW software, sent to the sound card (Behringer U-Phoria UMC404), and played by the speaker (Yamaha HS8 with 8'' cone woofer and 38 Hz–30 kHz frequency response) located in the lower corner of the room. The response signals were measured using half inch microphone (BK type 4145, sensitivity 50 mV/Pa, dynamic range 10.2 to 146 dB, frequency range 2.6 Hz to 18 kHz). The microphone signals were amplified by a measuring amplifier (BK type 2636). The AC output of the amplifier was connected to the sound card (Behringer U-Phoria UMC404HD), which was connected to a PC. Acquisition was performed using the NI Sound and Vibration acquisition module. Signal processing was performed in the Python programming language.

The first ten modal frequencies (75.9 Hz, 92.6 Hz, 110.0 Hz, 121.4 Hz, 134.1 Hz, 145.0 Hz, 154.1 Hz, 163.4, 180.1, 188.3 Hz) were previously determined using the finite element method. The impulse response was determined in an empty enclosure with a sweep signal between 40 Hz and 20000 Hz. A microphone positioned in the upper corner of the room while the speaker was placed in the opposite corner.

The WWOST was able to identify the first 10 modal frequencies determined by the numerical method. The calculated decay times of modal frequencies are listed in Table 1. The decay times in one-third octave bands calculated by the standard method are shown in Table 2. Decay time in the 63 Hz band, calculated with the standard method, is 1.8 s. Such a result actually comes from the resonance at 75.9 Hz from the adjacent 80 Hz octave band.

The decay time in the 80 Hz band, calculated with the standard method, is shorter than 2 s, as evaluated by the *S*-transform method. Due to the strong resonance in the 100 Hz band, the decay function of the 80 Hz band is distorted despite a longer decay time. In the 100 Hz band, both methods provide comparable values for decay time. The two resonances in the 100 Hz band have similar decay times and were not affected by the modes in adjacent bands. The result of the standard method, however, is evidently equal to the value of the resonance with a lower frequency and higher amplitude. The results of standard analysis in the 125 Hz band were falsified by energy leakage.

Table 1 *Identified modal frequencies (f_i) and their decay times (T_n) using WWOST.*

f_i (Hz)	76	93	110	121	134	145	154	163	180	188
T_n (s)	2,03	1,51	1,33	0,62	0,9	1,09	0,71	1,03	0,54	0,51

Table 2 *Reverberation time measurements (one-third octave bands).*

f_i (Hz)	63	80	100	125	160	200
T_n (s)	1,80	1,40	1,21	1,16	0,90	0,52

In the end decay time using ST was evaluated at twenty microphone positions. One position was a corner position, the others were randomly distributed over the room volume. All signals were recorded with a half-inch microphone and a sampling frequency of 96000 Hz. The duration of the sweep and tone excitation signals was 10 s. The time - frequency impulse response method provided the consistent results with small deviations.

5. CONCLUSION

In many real applications, e.g., in low-frequency bands, where the sound field is considered to be non-diffuse multi-slope decay functions are observed. In such cases, traditional calculation models which apply one-third octave band filtering and describe the decay process with a single reverberation time should be avoided and modal analysis [9] should be performed. This paper investigates the use of time-frequency analysis to calculate the decay time, which makes bandpass filtering of the impulse response unnecessary. An optimized *S*-transform was used, which frequency filters the signal using a Gaussian function which favourably increases the frequency resolution at low frequencies using a single parameter γ.

The experiments performed on test signals demonstrated the applicability of the method to signals where modal behaviour is present. The algorithm was compared with the one-third octave method to clearly show the limitations of the standard methods, which are often misused as such. The decay function of the observed frequency band calculated with the traditional one- third octave method was shown to be influenced by slowly decaying neighbouring modes, which is consistent with the results presented in the literature [7,15]

In addition, the decay at the observed frequency band was shown to be altered by a standard filtering process even when the neighbouring mode decays rapidly, especially when having higher amplitude. Both effects were also observed in the actually measured impulse response in a small test room, thus confirming the conclusions derived from numerical examples.

Experiments were also conducted in the test chamber representing a real small room. The time – frequency method was able to identify all modes in a test chamber that were identified by the numerical FEM method and showed consistency in the estimated decay times. The method was not significantly affected by the selection of the microphone position.

REFERENCES

[1] W.C. Sabine, Collected papers on acoustics, Harvard University Press Cambridge, MA, 1927.

[2] ISO 3382-2:2008. Acoustics - Measurement of room acoustic parameters - Part 2: Reverberation time in ordinary rooms. Standard, International Organization for Standardization, Geneva, CH, 2008.

[3] ISO18233:2006. Acoustics –Application of new measurement methods in building and room acoustics. Standard, International Organization for Standardization, Geneva, CH, 2006.

[4] M. Schroeder, New method of measuring reverberation time, J. Acoust. Soc. Am. 37 (3) (1965) 409–412.

[5] M. Kleiner, J. Tichy, Acoustics of Small Rooms, CRC Press, 2014.

[6] A. Prato, F. Casassa, A. Schiavi, Reverberation time measurements in non-diffuse acoustic field by the modal reverberation time, Appl. Acoust. 110 (2016) 160–169.

[7] M.A.S. Seoane, D.P. Cabo, F.T. Agerkvist, Do wavelet filters provide more accurate estimates of reverberation times at low frequencies, in: 45th International Congress and Exposition on Noise Control Engineering, INTER-NOISE 2016, German Acoustical Society (DEGA), 2016, pp. 1088–1096.

[8] M. Meissner, Acoustics of small rectangular rooms: analytical and numerical determination of reverberation parameters, Appl. Acoust. 120 (2017) 111–119.

[9] D. Beaton, N. Xiang, Room acoustic modal analysis using Bayesian inference, J. Acoust. Soc. Am. 141 (6) (2017) 4 480–4 493.

[10] F. Jacobsen, A note on acoustic decay measurements, J. Sound Vib. 115 (1) (1987) 163–170.

[11] F. Jacobsen, J.H. Rindel, Time reversed decay measurements, J. Sound Vib. 117 (1987) 187–190.

[12] M. Kob, M. Vorländer, Band filters and short reverberation times, Acta Acust. United Acust. 86 (2) (20 0 0) 350–357.

[13] S.-K. Lee, An acoustic decay measurement based on time-frequency analysis using wavelet transform, J. Sound Vib. 252 (1) (2002) 141–153.

[14] M.A.S. Seoane, D.P. Cabo, F.T. Agerkvist, Do wavelet filters provide more accurate estimates of reverberation times at low frequencies, in: 45th International Congress and Exposition on Noise Control Engineering, INTER-NOISE 2016, German Acoustical Society (DEGA), 2016, pp. 1088–1096.

[15] G. Marbjerg, J. Brunskog, C.-H. Jeong, V. Zapata-Rodríguez, The influence of overlapping band filters on octave band decay curves, Acta Acust. United Acust. 104 (6) (2018) 943–946.

[16] F. Mo, Reverberation decay functions for narrow bands obtained from filtered time-windowed room impulse responses, J. Acoust. Soc. Am. 137 (6) (2015) 3555–3558.

[17] R.G. Stockwell, L. Mansinha, R.P. Lowe, Localization of the complex spectrum: the S transform, IEEE Trans. Signal Process. 44 (4) (1996) 998–1001.

[18] E. Sejdic, I. Djurovic, J. Jiang, A window width optimized S-transform, EURASIP J. Adv. Signal Process. 2008 (2008) 59.

[19] L. Stankovic, A measure of some time-frequency distributions concentration, Signal Process. 81 (3) (2001) 621–631.

[20] K. He, S. Xiao, X. Li, Time-frequency characteristics of acoustic emission signal for monitoring of welding structural state using Stockwell transform, J. Acoust. Soc. Am. 145 (1) (2019) 469–479.

[21] L. Mansinha, R.G. Stockwell, R.P. Lowe, M. Eramian, R.A. Schincariol, Local S-spectrum analysis of 1-D and 2-D data, Phys. Earth Planet. Inter. 103 (3-4) (1997) 329–336.

[22] M. Schroeder, New method of measuring reverberation time, J. Acoust. Soc. Am. 37 (3) (1965) 409–412.

[23] G.R.B. de Prony, Essai expérimentale et analytique, J. Ecole Polytech. 1 (22) (1795) 24–76.

[24] F. Jacobsen, P.M. Juhl, Fundamentals of General Linear Acoustics, John Wiley & Sons, 2013.

LABORATORIJA ZA BUKU I VIBRACIJE

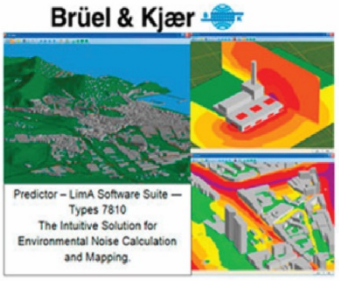

LABORATORY FOR NOISE AND VIBRATION

University of Nis
Faculty of Occupational Safety
„Politechnica“ University of Timisoara
Faculty of Mechanical Engineering
27th International Conference
NOISE AND VIBRATION
Niš, 20 - 21. 10. 2022.

TRANSMISSION LOSS AND ACOUSTIC ENERGY DISSIPATION OF GRANULAR MATERIALS IN A PULSE SEPARATION IMPEDANCE TUBE

Anže Železnik[1], Jure Murovec[1], Luka Čurović[1], Jurij Prezelj[1]

[1] University of Ljubljana, Faculty of Mechanical Engineering, Slovenia, anze.zeleznik@fs.uni-lj.si

Abstract - *There is great interest in the use of granular materials as sound absorption and insulation because they are relatively inexpensive compared to most acoustic materials. The objective of this study is to compare the transmission losses of different granular samples compared to other materials used for sound insulation to determine if the size distribution of the granules has a significant effect on the acoustic performance. In addition, the absorption in an impedance tube with an anechoic termination was compared for granular materials. For this study, a 4 m impedance tube using the pulse separation method was used because it is simple and robust. A set of laboratory test sieves was used to separate granular materials into different size fractions. Silica sand was used to compare the effect of particle size on acoustic properties. Granular materials were found to have good acoustic energy dissipation properties and high transmission loss values when enclosed in plastic film. The results show that multimodal granular mixtures have better acoustic properties than the individual size fractions used in the mixture.*

1. INTRODUCTION

The use of granules for sound absorption is a cost-effective alternative to foams and other purpose-made absorption materials because of their acoustic properties. The acoustic properties of granular materials have already been studied in terms of the influence of layer thickness [1, 2, 3, 4]. It was found that the thickness of the granular material affects the distribution of the sound absorption frequency spectra by shifting the position of the sound absorption peak in the frequency domain. The effect of grain size on the absorption coefficient has also been studied [1, 2, 5, 6], it was noted that some grain sizes have higher absorption coefficients, the peak frequency of absorption shifts for different grain sizes. Recycled granular materials such as rubber crumb [2], EPS beads [7], recycled plastic [5, 8, 9], and cork [10] were investigated for sound absorption properties. The sound absorption properties were improved by using multiple layers of granular materials with different diameters [11]. It was also found that the addition of polymer microparticles to polyurethane foam improved sound absorption [5]. The effect of the casing diameter on the absorption properties of granular materials has been studied [12], their measurement indicated that the first sound absorption peak shifts to a lower frequency as the casing diameter increases. A variety of models have been developed for the prediction of the absorption coefficient of porous and granular media [13, 14, 15, 16, 17, 18, 19]. These models mostly approximate granular materials as a stack of capillary tubes, empirical and semi-empirical models are commonly used that require different non-acoustic parameters to calculate the acoustic properties.

To measure the sound absorption of granular materials, an impedance tube using the pulse separation method [20, 21, 22] was used and compared with the standard two microphone transfer function method. The method is similar to the reflection (“Adrienne”) method introduced by Garai [23], but the measurement of the reflected impulse is performed in a closed tube. The method was further developed by Wei et al [24] to separate the pulses in a shorter tube by measuring the incident pulse at two different locations and subtracting it from the reflected pulse in the time domain.

Because there is no published work dealing with the absorption coefficient of different size fractions of granules mixed in different ratios, the objective of this study was to measure absorption coefficients of many size fractions of different granular materials and mixtures of these fractions. The transmission loss values of different size fractions were also compared because the influence of particle size on sound insulation properties has not yet been studied.

To investigate the mechanisms by which acoustic energy is dissipated inside granular materials, the absorption coefficient measurements (reflective termination) were compared with the absorption coefficient with an anechoic termination [25]. In this work, a new method for calculating the absorption coefficient in an anechoic impedance tube is proposed, which allows the comparison between the two absorption coefficients to better understand the differences between resonance effects and viscous losses in granular materials.

The pulse separation method was chosen to measure the sound absorption coefficient of granular materials for its ease of use because a large number of samples (over 100) needed to be evaluated. The 4 m long pulse separation impedance tube in a vertical configuration was also modified to measure the transmission and reflection coefficients and was used to compare the two sound absorption coefficients. This proposed variation of the pulse separation impedance tube can be used instead of the four-microphone transmission impedance tube. The granular materials were separated into different size fractions between 45 µm and 1 mm using laboratory test sieves and a shaker. In this paper, some of the more interesting findings considering the absorption coefficients and transmission loss values of granular materials are presented.

2. METHODOLOGY

Sound interacting with an absorption material can be divided into incident sound, reflected sound, transmitted sound, and absorbed sound. The most widely used methods use an impedance tube with a reflective termination to measure the incident sound and the sum of the sound reflected from the material surface and the transmitted sound to estimate the part of the sound energy that is lost in the material. The other type of impedance tube ideally has an anechoic termination behind the sample and is used primarily to measure the sound transmission loss of a sample. It is most useful for estimating the sound attenuation properties of materials. If an impedance tube with an anechoic termination is used to measure both reflected and transmitted sound, the results obtained with both impedance tubes on the same sample can be compared. The influence of the phase shift between the reflected and transmitted sound in the impedance tube with reflective termination can be evaluated. The influence of the placement of the sample depending on the positions of standing waves within the tube can also be evaluated (when the sample is placed against the reflective termination, the sound pressure on that surface of the sample is highest while the velocity is 0). The incident, reflected and transmitted sound for two different impedance tubes are shown in Fig. 1.

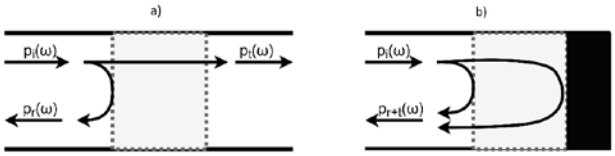

Fig. 1 *The incident, reflected and transmitted sound in impedance tubes with an anechoic termination (a) and a reflective termination (b).*

The reflection *R* and the transmission *T* are defined as the ratio between the sound pressure of the reflected (p_r) and transmitted wave (p_t) and the incident sound wave (p_i).

$$R = \frac{p_r(\omega)}{p_i(\omega)} \quad (1)$$

$$T = \frac{p_t(\omega)}{p_i(\omega)} \quad (2)$$

The reflected sound pressure wave in the reflective termination impedance tube is the sum of the surface reflection and the transmitted wave reflected from the reflective termination. Since ideal reflection by the reflective termination is assumed, the sample in the anechoic termination impedance tube needs to be twice as thick to compare the results from the two cases, since the sound passes through the material twice in the reflective termination case.

$$p_{r+t}(\omega) = p_r(\omega) + p_t(\omega) \quad (3)$$

The reflection in the reflective backing case R_{r+t} is therefore equal to the sum of the reflection and the transmission from the transmission tube case.

$$R_{r+t} = \frac{p_{r+t}(\omega)}{p_i(\omega)} = \frac{p_r(\omega)}{p_i(\omega)} + \frac{p_t(\omega)}{p_i(\omega)} = R + T \quad (4)$$

The absorption coefficient in the reflective termination impedance tube is:

$$\alpha = 1 - |R_{r+t}|^2 \quad (5)$$

And the absorption coefficient α_t in the anechoic termination impedance tube is equal to:

$$\alpha_t = 1 - |R + T|^2 \quad (6)$$

If there is no phase difference between *R* and *T* (the influence of the thickness of the sample and the speed of sound inside the sample), the following can be assumed:

$$\alpha_t = 1 - (|R| + |T|)^2 = 1 - |R|^2 - |T|^2 - 2|R||T| \quad (7)$$

A phase difference between *R* and *T* would cause the estimated α_t value to be higher than it really is, so Eq. (7) is used. Alternatively, the pulses in the pulse method can be aligned to achieve a phase match between *R* and *T*.

Previously proposed energy dissipation [25] is:

$$\alpha_t = 1 - |R|^2 - |T|^2 \quad (8)$$

The energy dissipation (absorption coefficient in an anechoic impedance tube) formula proposed by Feng [25] (Eq. (8)) gives different energy balances compared to the formula proposed in this paper (Eq. (7)). Using the equation proposed in this work, the absorption coefficient values are around 0 for frequencies close to 0 Hz. This enables the comparison between the two absorption coefficients.

2.1 The pulse separation method

The pulse separation method is used to calculate the absorption coefficient by separating the incident and reflected impulses in the time domain. Only one microphone is needed for this method and it does not require calibration. A variant of this method for measuring impedances of conical objects in a closed tube with a long duration source signal was introduced by Lefebvre [20]. The tube configuration for this method is shown in Fig. 2.

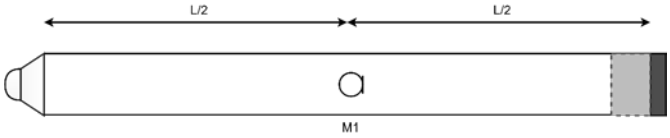

Fig. 2 *The pulse separation impedance tube.*

Since pink noise was used as the input signal for the speaker, the input signal $p_{in}(t)$ and the microphone signal $p_{mic}(t)$ are needed to calculate the impulse response in the time domain by deconvolving the recorded signals using spectral division.

$$ir(t) = IFFT\left(\frac{FFT(p_{mic}(t))}{FFT(p_{in}(t))}\right) \quad (9)$$

The combination of random noise and deconvolution using FFT can be used because of the properties of this particular system if the signals are filtered. *ISO 18233* states that this type of deconvolution can be used if some precautions are taken. The responses to harmonic components in the excitation that appear at negative times must be removed, the recorded signal must be much longer than the decay of the impulse response and the system must be linear or very close to linear to eliminate distortion. Because a high sampling frequency was used, the impulse response needs to be filtered using a band-pass filter in order to eliminate the errors caused in the spectral division by the noise in frequencies outside the frequency ranges of the speaker and microphone used. The use of random noise and spectral division drastically reduces the time needed for recording and the calculation of impulse responses. The comparison between the LMS algorithm and spectral division for deconvolution is shown in Fig. 3. Both impulse responses were filtered using a 6-th order band-pass filter (100-4000 Hz).

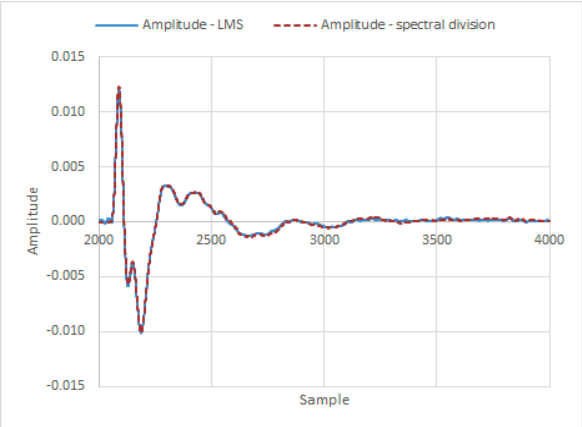

Fig. 3 *The impulse responses deconvolved using LMS and spectral division.*

Like with the transfer function method first introduced by Chung and Blaser [26, 27] and described in *EN ISO 10534-2:2001*, the reflection is calculated as the ratio of the incident and reflected sound power spectrum. The spectrums are calculated from the separated impulses.

Because some acoustic energy is lost on the reflective termination and inside the long tube, the reflection coefficient is calculated with the reflected pulse without the sample $p_{r,term}(t)$ and the reflected pulse with the sample $p_{r,sample}(t)$. If the incident pulse was used, the reflection coefficient would be underestimated. This way of calculation also compensates for the frequency characteristics of the loudspeaker and the microphone.

$$R_{r+t} = \frac{FFT\left(p_{r,sample}(t)\right)}{FFT\left(p_{r,term}(t)\right)} = \frac{p_{r,sample}(\omega)}{p_{r,term}(\omega)} \tag{10}$$

The normal incidence sound absorption coefficient α is calculated from the reflection the same as with the standard transfer function method (Eq. (5)).

The selected impulses from the reference measurement and the sample measurement are shown in Fig. 4. To compensate for the thickness of the sample, the pulse reflected from the sample is delayed according to the thickness of the sample. Since the sample causes the reflection to reach the microphone sooner, the impulse needs to be delayed so the reflection from the surface of the sample coincides with the reflection from the hard termination and there is no phase difference between the pulses.

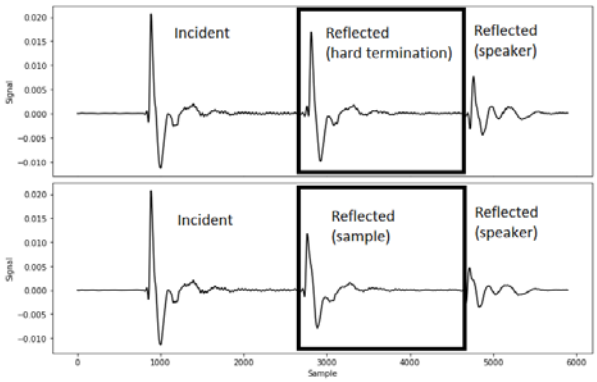

Fig. 4 *The impulses used for calculating absorption, the upper impulse response is without a sample inside the impedance tube and the lower impulse response is measured with a sample inserted into the impedance tube.*

The pulse separation method for measuring the absorption coefficient in an impedance tube is far more practical than the standard transfer function method because no microphone calibration or switching is required, the measurement process is fast and simple, and all measurements are made with a single microphone at a fixed position.

2.2 The pulse separation method for sound transmission

With a slight modification, the pulse separation method can also be used to replace the four -microphone impedance tube with an anechoic termination described in *ASTM E2611 – 19* to measure the transmission and reflection coefficients. The schematic for the pulse separation anechoic termination impedance tube is shown in Fig. 5. The same procedure as described for the one microphone method is used here to deconvolve the impulse responses for both microphones.

Fig. 5 *The pulse separation transmission impedance tube.*

In this method, a reference measurement must be made in the tube without a sample inserted. The ratio between the incident and the reflected impulse is saved as the reference reflection (the sample holder is assumed to reflect a small part of the incident wave). The impulse of the transmitted wave is also saved as a reference for the second microphone to compensate for the reflection of the sample holder and enabling this method to be used without calibrating the microphones.

The reflection and transmission coefficients can be expressed as ratios of Fourier transforms of the separated impulses. In the expressions below, indexes *s* (sample) and *e* (empty) represent the measurement with the sample or the reference measurement. Indexes *i*, *r* and *t* stand for the incident, the reflected and the transmitted wave (the incident and reflected wave are measured by microphone 1, the transmitted wave is measured by microphone 2).

$$T_a = \frac{p_{s,t}(\omega)}{p_{e,t}(\omega)} \tag{11}$$

The normal incidence transmission loss can be calculated as:

$$TLN = 10log_{10}\left(\frac{1}{T}\right) \tag{12}$$

The reference reflection is used to compensate for the imperfections of the sample holder and is subtracted from the ratio of the incident and reflected impulse of the sample measurement.

$$R_a = \frac{p_{e,r}(\omega)}{p_{e,i}(\omega)} - \frac{p_{s,r}(\omega)}{p_{s,i}(\omega)} \tag{13}$$

The absorption coefficient is calculated with *T* and *R* using Eq. (7).

Using this method, the speed of sound within the measured sample can be estimated by comparing the times at which the transmitted impulse reaches microphone 2 for the reference measurement and the measurement with a sample inside the impedance tube.

Since this method eliminates any other reflections off the tube termination and the reflections off the back surface of the sample by selecting only the first transmitted and reflected impulse, an anechoic termination is not required for the pulse separation method because all relevant reflections can be

selected and processed separately. If the termination of the four-microphone impedance tube (*ASTM E2611 – 19*) is not anechoic, the sound reflected from the termination can have a large impact on the measurements because it is reflected back from the back surface of the sample (increasing the measured transmitted sound) and is transmitted back through the sample (increasing the measured reflected sound).

The only disadvantage of the pulse separation method compared to the standard methods is the frequency resolution, which is determined by the length of the extracted impulses. For a 4 m long tube with a microphone in the middle, the frequency resolution is 86 Hz. The upper frequency limit of the tube is around 4 kHz, since the frequency limits according to *EN ISO 10534-2:2001* also apply to the pulse separation method. The lower frequency limit depends on the speaker and microphone used. This was a Miranda LSP 60/8 loudspeaker and two Panasonic electret condenser capsules. With this configuration, results above 100 Hz proved reliable as the signal to noise ratio is not sufficient at lower frequencies. To accurately measure the speed of sound within the samples, the sampling rate must be high enough to measure the delay caused by the sample material. The sampling rate that was used was 192 kHz.

The cups used for measuring absorption coefficients and energy dissipation values of granular materials were 3D printed. The cup used for measuring the absorption coefficient in the tube with a reflective termination was 40 mm deep and the cup in the anechoic impedance tube was 80 mm deep because with a reflective backing, sound passes through the sample twice. The deeper cup used for measuring the absorption coefficient in the anechoic impedance tube has a fabric bottom to reduce the influence the cup has on the measurements. For the transmission loss measurements, a 40 mm deep cup was used that could have either cloth or plastic foil for the top and bottom to compare the sound insulation provided by the granules that are enclosed in foil or open. All the material samples in the cups were lightly tapped to consolidate the particles.

The large silica sand particles needed to be slightly moistened to achieve mixing with the smaller sand. If no water is added, the finer sand will fall through the holes between the larger grains.

3. RESULTS

The measurement samples were prepared with a set of laboratory test sieves and a shaker. The materials were mixed by mass ratios.

The different absorption coefficients of the granular materials were measured with both variants of the pulse separation impedance tube. The material layer thickness is 40 mm in the reflective termination impedance tube and 80 mm for the anechoic termination impedance tube. The samples for the transmission loss comparison were 40 mm thick.

The shapes of the silica sand particles are quite close to spherical. The photos in Fig. 6 show different sizes of silica sand.

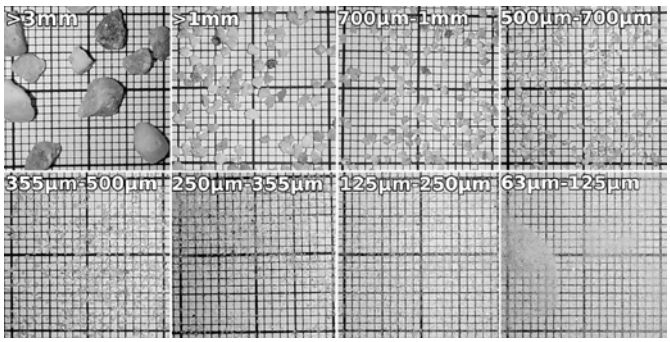

Fig. 6 *Different sizes of silica sand.*

Silica sand has very similar absorption coefficients for particle sizes below 250µm. The absorption peak becomes wider and lower as the particle size decreases to 355µm. The absorption coefficients for different grain sizes of silica sand are shown in Fig. 7.

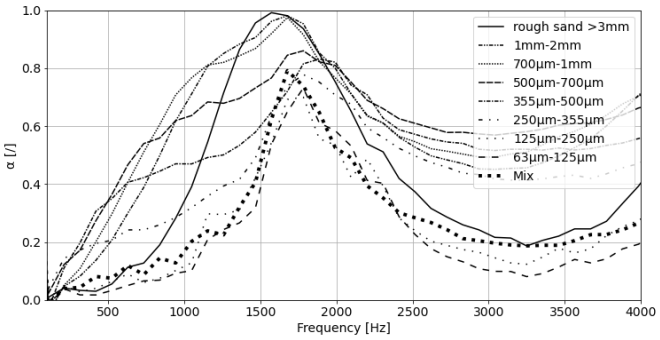

Fig. 7 *Absorption coefficients of the individual grain size fractions (silica sand).*

When mixing two different sizes of particles, a new peak of absorption values is observed in the frequencies lower than the original peak. When more smaller particles are added to the mixture, the new peak moves to lower frequencies but has lower absorption coefficient values. The absorption coefficient when mixing different sand grains is shown in Fig. 8. Smaller particles (125-255µm) were gradually added to rough sand (3 mm).

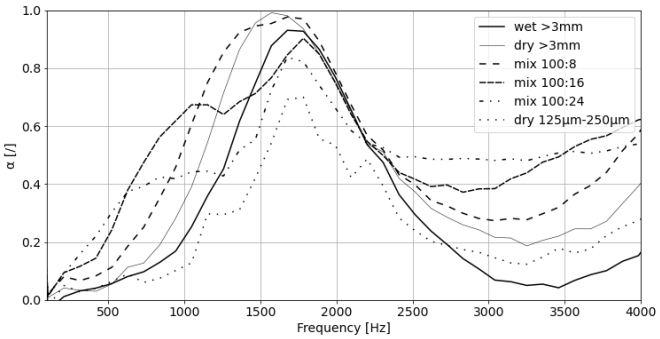

Fig. 8 *Absorption coefficients of different mixtures by mass (silica sand, >3mm and 125-255µm).*

For larger particles, it is evident that not much sound energy is lost inside the samples because of viscous losses, the high absorption coefficient is the result of resonant effects. Fig. 9 shows the comparison of a and at for large particles (>3 mm).

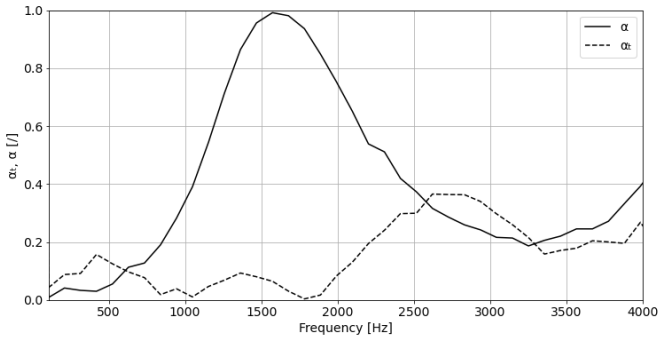

Fig. 9 *Absorption coefficients for large sand particles (>3 mm).*

For size fractions with higher viscous losses, the differences between the two absorption coefficients are greatest at wavelengths coincident with the thickness of the sample. Unlike the larger granules where the absorption peak is measured due to destructive interference between reflected and transmitted sound, much of the sound energy is lost within the material for these sizes. The comparison for sand (500-700 µm) is shown in Fig. 10.

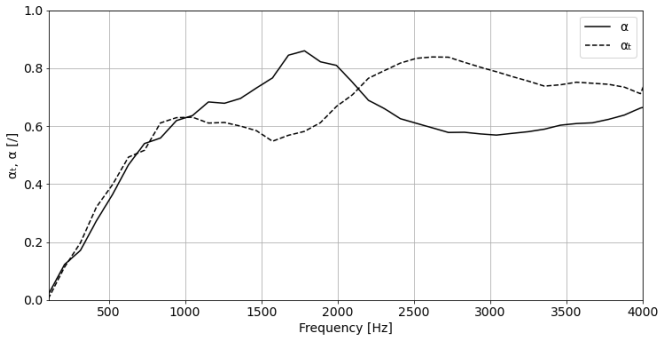

Fig. 10 *Comparison of the absorption coefficient (α) and anechoic absorption coefficient from R and T (α_t) for sand (500-700 µm), layer thickness: 80mm.*

As with the absorption coefficient measurements, mixing two size fractions results in higher energy losses within the granular mixture compared to the two size fractions used. The comparison of the two absorption coefficients for rough sand (< 3mm), fine sand (125-250µm) and the mixture of both is shown in Fig. 11.

Both absorption coefficient values have a similar low frequency peak for the 16% mixture of fine and rough sand. This mixture was chosen because it had the most evident absorption peak at lower frequencies.

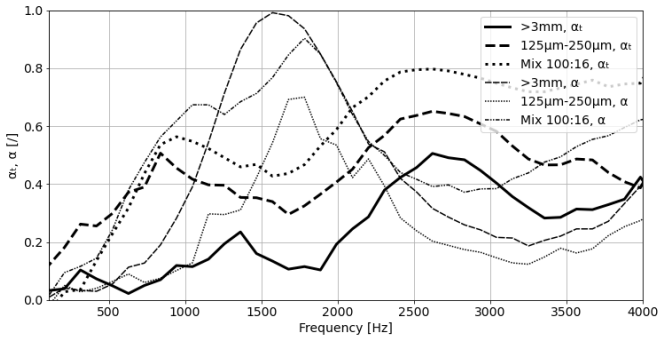

Fig. 11 *Comparison of α_t and α absorption for rough sand (<3mm), fine sand (125-250 µm) and a mixture of both (16% fine sand by mass), layer thickness: 80mm.*

The comparison between transmission loss values of different sizes of granules (both open and enclosed in plastic foil) is shown in Fig. 12. It was found that transmission loss of granular materials is dependent on granule size. Smaller granules create a denser bulk material that blocks sound transmission more effectively. However, when the same granules are enclosed in plastic film, the transmission loss values are similar between different granule sizes, except for the largest granules. This suggests that other material properties, like density, have a greater effect on transmission loss when the sample is not open to airflow.

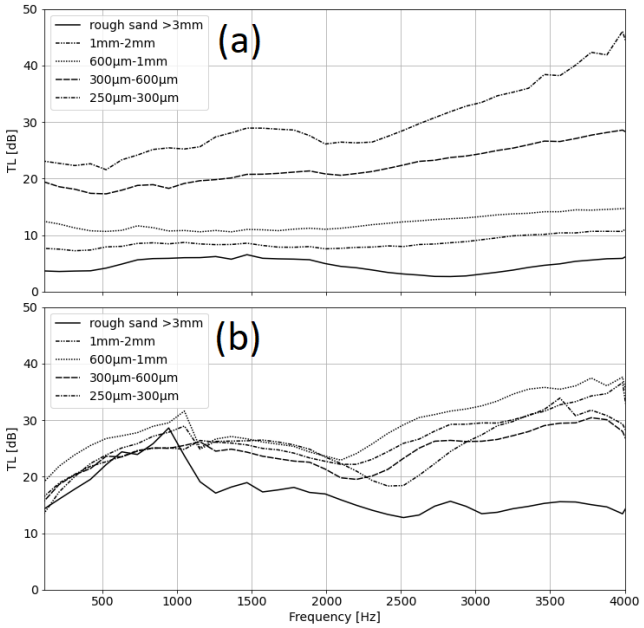

Fig. 12 *Transmission loss values of granular materials, open (a), enclosed in plastic film (b).*

4. DISCUSSION

Silica sand particles have the widest and highest absorption coefficient peaks in a size range between 355 µm and 1 mm. The highest peak absorption occurs when the particle size is larger, and the widest frequency range is achieved with smaller particles. For sizes below 250 µm, the absorption coefficient remains the same for all particle sizes regardless of the material.

When mixing particles of different sizes, a new absorption peak can be created at lower frequencies. For this to occur, the difference between the sizes of the mixed particles must be large enough. It was demonstrated that the new absorption peak is most evident when mixing large granules (larger than 3 mm) and small granules (smaller than 250 µm). The peak is also present in other mixtures but is less pronounced. For this reason, previous studies on granular mixtures [zolanvari2013] did not find this absorption peak. This phenomenon could allow the development of granular absorbers with high absorption coefficients below 1 kHz. This study shows that a wide range of different granular materials could be used for absorbers that exhibit good acoustic performance in the lower frequency range, since the density and type of material do not seem to strongly affect the absorption values of granular mixes.

Existing models for predicting the absorption coefficients of granular materials do not predict the use of multiple granule sizes for sound absorption. Further work in this area is needed

to use the discovered behavior of granule mixtures for the design of new sound absorbing materials.

The comparison between the results obtained with a reflective termination impedance tube and an anechoic impedance tube shows that the interaction between the transmitted and reflected sound plays an important role in the sound absorption of granules. Granules with low viscous losses have a high absorption coefficient at certain frequencies due to the destructive interference between the reflected and transmitted sound, the measured sound absorption for these materials in an impedance tube can be adjusted with the thickness of the sample or an air gap between the reflective termination and the sample. The viability of these granules to be used as an absorption material should be further evaluated in a reverberation room where sound enters the material from multiple directions. Since very little acoustic energy is actually dissipated inside such granular materials, the measurements in an impedance tube likely overestimate their acoustic performance.

If the phase of the reflected and transmitted sound measured in the transmission tube is adjusted to simulate the interaction between the two reflections in the standard method for measuring the absorption coefficient, a high absorption peak is observed that resembles the absorption coefficient measurement in the impedance tube with a reflective termination. This, however, can only be assumed for materials with energy dissipation values close to 0 as the dissipated sound energy is somewhat different when comparing the two absorption coefficients. This comparison does not take into account the fact that a reflective termination in the absorption coefficient measurement will cause the sound pressure at the back of the sample to reach the maximum value. Since the amplitude of the particle velocity at the reflective end is 0, less sound energy can be dissipated inside the material due to viscoelastic losses, especially at low frequencies (under 1 kHz). Since the reflections inside the sample in the transmission tube form a different amplitude profile of the particle velocity, this is difficult to compensate for, and the comparison between measurements does not take this into account. Another consideration is that not all of the measured reflected sound is reflected exactly from the surface, and the delay between reflections could also have an effect on the measurements.

Both the phase difference between the reflected and transmitted sound and the particle velocity amplitude profile do not have a large effect on the measurements of materials with high energy dissipation values, since the absorption coefficients are very similar for the measured frequency range.

Measurements of the two absorption coefficients of bimodal granular mixes confirm that more acoustic energy is dissipated within mixes of different size granules compared to single size fractions. This could be because the pore shape in the bimodal granular mixes allows for higher viscous energy dissipation, or a greater portion of the acoustic energy is lost during mechanical interaction (vibration) between the granules. The peak value in the absorption coefficient measurements is due to the fact that more acoustic energy is dissipated at lower frequencies than in single size granules.

Enclosing granules in plastic film diminishes the influence of viscous losses on the measured transmission loss values. The most influential parameter becomes the sample mass which is similar between samples, except for the biggest granules where the bulk density is lower.

5. CONCLUSIONS

The pulse separation method was modified and used for the measurement of absorption coefficients of granular mixtures. It was observed to be practical for fast measurement of the absorption coefficient and had identical results compared to standardized methods. A new method was proposed for measuring the absorption coefficient in an impedance tube with an anechoic termination using the pulse separation method. The new method can be used to evaluate the kind of dissipation that occurs in an impedance tube when compared to absorption coefficient measurements. It can be used to differentiate between measured absorption that is caused by the destructive interference between two reflections and acoustic energy that is dissipated inside a material. Absorption coefficients of different size particles were examined. The size limit for the transition between a broad absorption frequency range and a narrow frequency range corresponding to the thickness of the granular material layer was observed at about 250 μm. However, for the absorption coefficient in an anechoic impedance tube, even smaller granule sizes had overall higher values compared to large granules, where the absorption peak occurs because of the destructive interference between reflected and transmitted sound. A new way to improve the absorption coefficient of granular materials at low frequencies was discovered. By mixing larger granules and granules with the diameter of about 10% of larger granules, an absorption peak at lower frequencies was observed. Higher sound absorption values compared to single size fractions were observed for these mixes. This could enable the development of purpose-made granular absorbers with customizable absorption characteristics with high absorption coefficient below the resonant frequency.

REFERENCES

[1] S. Sakamoto, Y. Sakuma, K. Yanagimoto, S. Watanabe, Basic study for the acoustic characteristics of granular material (Normal incidence absorption coefficient for multilayer with different grain diameters), Journal of Environment and Engineering 7 (1) (2012) 12-22.

[2] M.J. Swift, P. Bris, K.V. Horoshenkov, Acoustic absorption in re-cycled rubber granulate, Applied Acoustics 57 (3) (1999) 203-212.

[3] J. Sikora, J. Turkiewicz, Sound absorption coefficients of granular materials, Mechanics and control 29 (3) (2010) 149-157.

[4] F. Asdrubali, K.V. Horoshenkov, The acoustic properties of expanded clay granulates, Building Acoustics 9 (2) (2002) 85-98.

[5] H. Zhou, B. Li, G. Huang, Sound absorption characteristics of polymer microparticles, Journal of Applied Polymer Science 101 (4) (2006) 2675-2679.

[6] S.H. Zolanvari, C. Karlstetter, Development of Consolidated Granular Materials as Sound Absorbers: Acoustical and Mechanical Characteristics, in: Proc. AIA-DAGA, 2013.

[7] S. Sakamoto, M. Sasaki, I. Kourakata, K. Yanagimoto, S. Watanabe, Basic study for acoustic absorption characteristics of soft and light granular material (basic characteristics for expanded polystyrene beads), Journal of Advanced Mechanical Design, Systems, and Manufacturing 7 (4) (2013) 677-689.

[8] A. Biskupičová, M. Ledererová, S. Unčík, C. Glorieux, M. Rychtáriková, Sound absorption properties of materials based on recycled plastic granule mixtures, Slovak Journal of Civil Engineering, 29 (1) (2021) 15-19.

[9] C. Bujoreanu, F. Nedeff, M. Benchea, M. Agop, Experimental and theoretical considerations on sound absorption performance of waste materials including the effect of backing plates, Applied Acoustics 119 (2017) 88-93.

[10] A. Boubel, M. Garoum, A. Bybi, N. Laaroussi, Sound absorption measurements of some porous loose granular materials, in: INTER-NOISE and NOISE-CON Congress and Conference Proceedings, 2016.

[11] S. Sakamoto, K. Yamaguchi, K. Ii, R. Takakura, Y. Nakamura, R. Suzuki, Theoretical and experiment analysis on the sound absorption characteristics of a layer of fine lightweight powder, The Journal of the Acoustical Society of America 146 (4) (2019) 2253-2262.

[12] T. Tsuruha, Y. Yamada, M. Otani, Y. Takano, Effect of casing on sound absorption characteristics of fine spherical granular material, The Journal of the Acoustical Society of America 147 (5) (2020) 3418-3428.

[13] M. E. Delany, E. N. Bazley, Acoustical properties of fibrous absorbent materials, Applied Acoustics 3 (1970) 105–116.

[14] K. Attenborough, Acoustical characteristics of rigid fibrous absorbents and granular materials, The Journal of the Acoustical Society of America 73 (3) (1983) 785-799.

[15] J.F. Allard, Y. Champoux, New emperical equations for sound propagation in rigid frame fibrous materials, J. Acoust. Soc. Am. 91 (1992) 3346–3353.

[16] T.G. Zieliński, Microstructure-based calculations and experimental results for sound absorbing porous layers of randomly packed rigid spherical beads, Journal of Applied Physics 116 (3) (2014) 034905.

[17] N.N. Voronina, K.V. Horoshenkov, A new empirical model for the acoustic properties of loose granular media, Applied Acoustics 64 (4) (2003) 415-432.

[18] V.V. Voronina, K.V. Horoshenkov, Acoustic properties of unconsolidated granular mixes, Applied Acoustics 65 (7) (2004) 673-691.

[19] K.V. Horoshenkov, M.J. Swift, The acoustic properties of granular materials with pore size distribution close to log-normal, The journal of the acoustical society of America 110 (5) (2001) 2371-2378.

[20] A. Lefebvre, G.P. Scavone, J. Abel, A. Buckiewicz-Smith, A comparison of impedance measurements using one and two microphones, in: Proceedings of ISMA, 2007.

[21] L. Sun, H. Hou, L.Y. Dong, F.R. Wan, Sound absorption measurement in a circular tube using the echo-pulse method, Acta Acustica united with Acustica 96 (5) (2010) 973-976.

[22] D.B. Sharp, Increasing the length of tubular objects that can be measured using acoustic pulse reflectometry, Measurement Science and Technology 9 (9) (1998) 1469.

[23] M. Garai, Measurement of the sound-absorption coefficient in situ: the reflection method using periodic pseudo-random sequences of maximum length, Applied acoustics 39 (1-2) (1993) 119-139.

[24] Z. Wei, H. Hou, N. Gao, Y. Huang, J. Yang, Sound absorption coefficient measurement by extracting the first reflected wave in a short tube, Applied Acoustics 159 (2020) 107087.

[25] L. Feng, Modified impedance tube measurements and energy dissipation inside absorptive materials, Applied Acoustics 74 (12) (2013) 1480-1485.

[26] J.Y. Chung, D.A. Blaser, Transfer function method of measuring in-duct acoustic properties. I. Theory, The Journal of the Acoustical Society of America 68 (3) (1980) 907-913.

[27] J.Y. Chung, D.A. Blaser, Transfer function method of measuring in-duct acoustic properties. II. Experiment, The Journal of the Acoustical Society of America 68 (3) (1980) 914-921.

УНИВЕРЗИТЕТ У НИШУ
UNIVERSITY OF NIŠ

ФАКУЛТЕТ ЗАШТИТЕ НА РАДУ У НИШУ
FACULTY OF OCCUPATIONAL SAFETY

ФАКУЛТЕТ ЗАШТИТЕ НА РАДУ ЈЕ АКРЕДИТОВАНА ВИСОКОШКОЛСКА УСТАНОВА ЗА ОБАВЉАЊЕ ОБРАЗОВНЕ И НАУЧНОИСТРАЖИВАЧКЕ ДЕЛАТНОСТИ У НАУЧНОЈ ОБЛАСТИ „ИНЖЕЊЕРСТВО ЗАШТИТЕ ЖИВОТНЕ СРЕДИНЕ И ЗАШТИТЕ НА РАДУ".

КОМУНАЛНА ПОЛИЦИЈА

ИНСПЕКЦИЈА РАДА

ОСНОВНЕ АКАДЕМСКЕ СТУДИЈЕ

ЧЕТИРИ ГОДИНЕ (240 ЕСПБ БОДОВА)

- ЗАШТИТА НА РАДУ
- ЗАШТИТА ЖИВОТНЕ СРЕДИНЕ
- ЗАШТИТА ОД ПОЖАРА

ПРОИЗВОДНЕ ДЕЛАТНОСТИ: прерађивачка, прехрамбена индустрија и др.

ЈАВНА КОМУНАЛНА ПРЕДУЗЕЋА

МАСТЕР АКАДЕМСКЕ СТУДИЈЕ

ЈЕДНА ГОДИНА (60 ЕСПБ БОДОВА)

- ИНЖЕЊЕРСТВО ЗАШТИТЕ НА РАДУ
- ИНЖЕЊЕРСТВО ЗАШТИТЕ ЖИВОТНЕ СРЕДИНЕ
- ИНЖЕЊЕРСТВО ЗАШТИТЕ ОД ПОЖАРА
- УПРАВЉАЊЕ ВАНРЕДНИМ СИТУАЦИЈАМА
- МЕНАЏМЕНТ ЗАШТИТЕ ЖИВОТНЕ СРЕДИНЕ

САНИТАРНА ИНСПЕКЦИЈА

КОМУНАЛНА ИНСПЕКЦИЈА

ДОКТОРСКЕ АКАДЕМСКЕ СТУДИЈЕ

ТРИ ГОДИНЕ (180 ЕСПБ БОДОВА)

- ИНЖЕЊЕРСТВО ЗАШТИТЕ НА РАДУ
- ИНЖЕЊЕРСТВО ЗАШТИТЕ ЖИВОТНЕ СРЕДИНЕ

ПРОИЗВОДНЕ ДЕЛАТНОСТИ: грађевинарство, хемијска, петрохемијска, металопрерађивачка, пољопривреда, телекомуникације, нафтна индустрија, саобраћај, шумарство, рударство и др.

МАЛА И СРЕДЊА ПРЕДУЗЕЋА

АГЕНЦИЈЕ И ИНСТИТУТИ

ЗДРАВСТВЕНЕ УСТАНОВЕ

ВЕЛИКА ПРЕДУЗЕЋА

ВАТРОГАСНЕ ЈЕДИНИЦЕ

ОСИГУРАВАЈУЋЕ КОМПАНИЈЕ

18000 Ниш, Чарнојевића 10 А

СЕКТОР ЗА ВАНРЕДНЕ СИТУАЦИЈЕ

Телефон: (+381 18) 529-701

Факс: (+381 18) 249-962

www.znrfak.ni.ac.rs

University of Nis
Faculty of Occupational Safety
„Politechnica“ University of Timisoara
Faculty of Mechanical Engineering
27th International Conference
NOISE AND VIBRATION
Niš, 20 - 21. 10. 2022.

ACOUSTIC PROPERTIES OF STANDARD LOW DENSITY POLYURETHANE LIME FOAM S 2535

Stefan Pajović[1], Mišo Bjelić[1], Vladan Grković[1], Jovana Perić[1]

[1] University of Kragujevac, Faculty of Mechanical and Civil Engineering in Kraljevo, Serbia, pajovic.s@mfkv.kg.ac.rs

Abstract - *This paper presents the results of testing acoustic properties of polyurethane foam samples. Absorption coefficients were measured in an impedance tube - Transfer function method (SRPS EN ISO 10534-2:2008). The samples of standard low-density polyurethane foam with a thickness between 10mm and 100mm were tested. The results show that with increasing sample thickness, the polyurethane foam has excellent acoustic properties in the mid-frequency range.*

1. INTRODUCTION

Environment noise is a big problem in developed cities and densely populated areas. This problem has been very noticeable in recent years due to the rapid development of the industry. Noise pollution continues to grow and affect people's daily life and health. The solution used in noise control is the application of absorption materials. The acoustic performance of porous materials can be characterized by sound absorption and sound transmission loss.

transmission loss.

Polyurethane (PU) foams are characterized by low weight and high porosity, and therefore they are the subject of many studies [1-5]. PU foams are characterized by an internal porous structure that enables an increase in the efficiency of sound absorption. Due to its low price, wide availability of materials from which it is produced and easy manufactured, it is widely used in the field of sound absorption. The acoustic properties of PU foam, fibrous and granular materials, were examined within the project TP 37020 "Development of methodology and means for noise protection in urban areas" financed by the Ministry of Education, Science and Technological Development of the Republic of Serbia [6].

This paper presents the initial results of research into the acoustic properties of low-density PU foam in order to find possibilities for their effective application in noise protection.

2. RESEARCH PLAN

The research plan includes the examination of the acoustic properties of the standard PU foam S 2535 in the frequency range from 125 Hz to 1600 Hz, as well as the dependence of the absorption coefficient on different thicknesses of the sample material.

2.1 Materials – low density foam, type, application

PU foams are made of polyol, isocyanate, water and are most often classified as foams with a density of less than 100 kg/m3. Depending on the production method and intended purpose, the PU foams whose acoustic properties were investigated are divided into four groups. Standard foams (S), foams with increased elasticity (ES), foams with increased hardness (T) and highly elastic foams (HR) [7]. S, ES and T foams are produced as open cell foams. HR foams are produced as foams with a closed cell structure, while under the influence of pressure force, the cell membranes burst and after that, these foams can be considered as foams with an open cell structure.

PU foams are widely used in the electrical, automotive and furniture industries. In conventional use, the most common are foams with densities from 12 kg/m3 to 40 kg/m3 [2].

2.2 Sample preparation

The PU foam from which the test samples were cut was taken from the company "Vapeks d.o.o." - Čačak. Samples cut from a block of foam with a width of 2 m, an average height of 1 m and a length of 1 m were prepared for the research. Three rollers with a diameter of 102 mm were cut along the entire length of the block. Samples with thicknesses of 10, 20, 30, 40, 50, 60, 70, 80, 90 and 100 mm were cut from the roller. In this way, three samples were provided for each of the 10 different material thicknesses (Figure 1) [8].

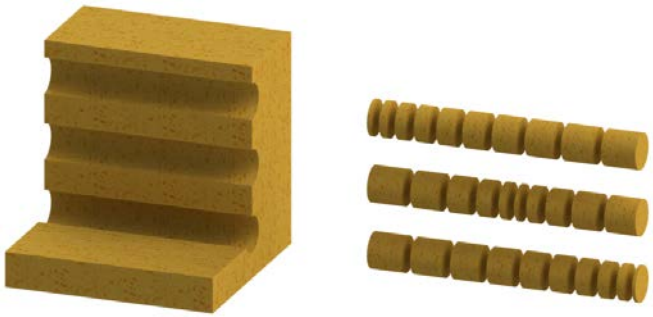

Fig. 1 *Procedure for cutting samples from a block of PU foam [8]*

The basic mechanical characteristics of S foam are shown in Table 1.

Table 1 *Values of mechanical characteristics of standard PU foam [7]*

PU foam type	Sample group label	Density [kg/m3]	Hardness (SLD) [kPa]	Tensile strength [kPa]	Elongation at break [%]	Permanent deformation [%]	Elasticity [%]
		ISO 745	ISO 3386	ISO 1798	ISO 1798	ISO 1856	ISO 8307
Standard foams (S)	S_1	24.4	4.5	156	148	3.2	42
	S_2	29.0	4.1	172	185	2.6	47

Standard PU foam has an open cell structure (Figure 2), which is proven by examining images taken using a microscope and a software device. Based on the recordings, it was also established that the cell structure most often has the shape of a square, pentagon and hexagon.

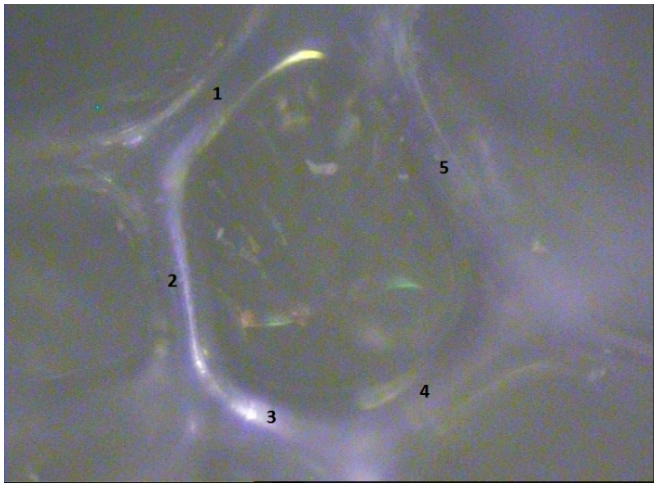

Fig. 2 *Open cell structure of standard PU foam*

2.3 Experimental plan

The measurement of the sound absorption coefficient of low-density PU foam was performed in an impedance tube - transfer function method, according to the standard EN ISO 10534-2:2001 [9] (Figure 3) in the Laboratory for Acoustics of the Faculty of Electrical Engineering in Belgrade.

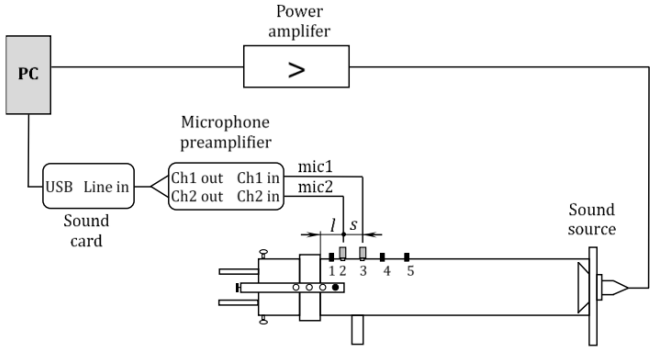

Fig. 3 *Block diagram of the sound absorption measurement system: adapted from [10]*

3. METHOD AND EQUIPMENT

The transfer function method is based on the decompensation of the standing wave which is formed in the tube by recording signals with two microphones and calculating their transfer function. From that transfer function, the reflection coefficient is calculated, and then the absorption coefficient is found under conditions of normal incidence in the frequency range defined by the physical dimensions of the tube and the distance between the microphones. Using this method, it is possible to quickly measure for normal incidence, using small samples.

For an impedance tube with two microphones, the reflection coefficient is calculated according to [10]:

$$R = \frac{H - e^{-jks}}{e^{jks} - H} e^{j2k(l+s)} \tag{1}$$

where is [10]:

- H – the corrected transfer function,
- s – the distance between microphones,
- l – the distance of the closest microphone from the sample, and
- k – the wave number.

The absorption coefficient is determined through the calculated reflection coefficient:

$$\alpha = 1 - |R|^2 \tag{2}$$

The method of impedance tube has numerous advantages, which are described in the literature [11], some of the most important are:

- the measuring device has small dimensions, so it is very practical to use,
- the samples have small dimensions, which facilitates their preparation for measurement,
- the costs of performing the experiment are low.

The disadvantages of this method are:

- only normal incidence of the waves is measured, although it is possible to apply corrections to obtain the values of the absorption coefficient with random incidences,
- different diameters of tube and samples are necessary to cover a wider frequency range.

4. RESULTS AND DISCUSSION

4.1 Experimental results

The experimental values of absorption coefficients by 1/3 of octave bande for different material thicknesses obtained by measuring in an impedance tube are shown in Table 2 and Figure 4.

Table 2 *Values of absorption coefficients for foam S 2535 [8]*

	Material thickness (cm)									
f_c(Hz)	1	2	3	4	5	6	7	8	9	10
125	0.051838	0.071343	0.069233	0.11534	0.12554	0.13017	0.20451	0.20428	0.27103	0.23631
160	0.047356	0.068574	0.081428	0.11805	0.13374	0.17053	0.24863	0.27826	0.37142	0.33666
200	0.054977	0.08146	0.0995	0.1386	0.15279	0.21654	0.31735	0.36527	0.47706	0.44012
250	0.055759	0.086001	0.12003	0.16217	0.18509	0.27497	0.41151	0.47316	0.58595	0.56115
315	0.059219	0.099308	0.14766	0.20141	0.22428	0.35551	0.53553	0.61277	0.63559	0.63448
400	0.06157	0.11274	0.17115	0.25728	0.26599	0.46909	0.67882	0.75032	0.88763	0.78995
500	0.07028	0.14512	0.23154	0.33022	0.35765	0.59031	0.78563	0.8334	0.98411	0.96504
630	0.088069	0.19163	0.32412	0.4178	0.47585	0.71406	0.92102	0.96495	0.9713	0.99422
800	0.10996	0.26301	0.44196	0.58405	0.62189	0.88489	0.99653	0.99235	0.90706	0.95057
1000	0.13364	0.33186	0.58763	0.72818	0.76989	0.94995	0.94328	0.9192	0.82324	0.86785
1250	0.16958	0.47446	0.7898	0.87787	0.87595	0.93178	0.84727	0.86135	0.83354	0.84928
1600	0.21322	0.66003	0.94163	0.93628	0.90703	0.84049	0.77952	0.86477	0.94143	0.93127

α_w	0.1	0.2	0.3(M)	0.35(M)	0.35(M)	0.55(M)	0.7	0.75	0.85	0.8

f_c(Hz)	α_p									
250	0.056652	0.088923	0.122397	0.167393	0.187387	0.28234	0.421463	0.483733	0.5662	0.54525
500	0.073306	0.14983	0.24227	0.3351	0.366497	0.591153	0.795157	0.849557	0.94768	0.916403
1000	0.137727	0.356443	0.606463	0.730033	0.75591	0.922207	0.929027	0.9243	0.854613	0.889233

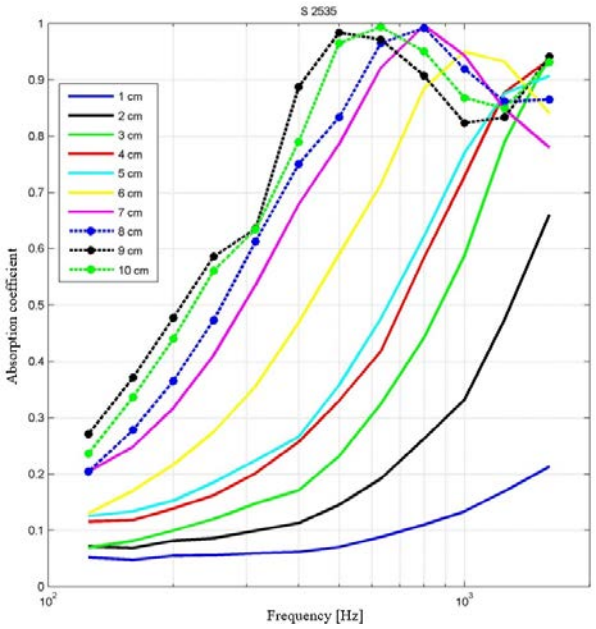

Fig. 4 Value of absorption coefficient for foam S 2535 [8]

From the Table 2 and Figure 4 the following can be observed:

- At low frequencies up to 400 Hz, PU foams do not have pronounced absorption properties and the absorption coefficient ranges from 0.05 for a thickness of 10 mm to 0.4 for a thickness of 60 mm. As the thickness of the material increases, the absorption coefficient at low frequencies also increases, for a PU foam thickness of 90 mm at a frequency of up to 400 Hz, the absorption coefficient is 0.88.
- At high frequencies up to 1600 Hz, PU foam has good absorption properties. For material thickness from 20 mm to 50 mm, the maximum value of the absorption coefficient is at the frequency of 1600 Hz, and for d=20 mm α=0.66, for d=30 mm α=0.94, for d=40 mm α=0.94 and for d=50 mm α=0.91.
- For PU foam thickness d=70 mm, the absorption coefficient is α=0.99 at a frequency of 800 Hz, while this value decreases at higher and lower frequencies.
- PU foam achieves the highest efficiency in the range from 400 Hz to 1600 Hz, where the absorption coefficient is in the range from 0.6 to 0.99.

It can be concluded that the absorption coefficient of PU foam increases with increasing material thickness, but at the same time its maximum shifts towards relatively lower frequencies, up to 500 Hz.

4.2 Procession and analysis of the experimental results

In order to carry out the regression analysis procedure and select an adequate regression model, after selecting the experimental plan and conducting the experimental measurements, it is necessary to carry out the following steps [8]:

- Input of experimental data,
- Summary statistics of possible mathematical models,
- Selection of the stochastic model,
- ANOVA analysis - evaluation of model significance,
- Evaluation of the model adequacy,
- Interval evaluation of model parameters,
- Diagnostics of the model and, if necessary, transformation of the model and repetition of the selection cycle and evaluation of the transformed model,
- Interval evaluation regression function,
- Graphic interpretation and model interpretation.

Data processing was performed in the Desing Expert v.9.0.6.2 software package. From the available mathematical models, models of the 5th and 6th degree are proposed (table 3).

Table 3 *Summary statistics table for foam S 2535*

Model Summary Statistics

Source	Std. Dev.	R-Squared	Adjusted R-Squared	Predicted R-Squared	PRESS	
Linear	0.41	0.8036	0.8002	0.7907	20.78	
2FI	0.38	0.8291	0.8247	0.8099	18.87	
Quadratic	0.23	0.9412	0.9386	0.9318	6.77	
Cubic	0.18	0.9639	0.9609	0.9475	5.21	
Quartic	0.084	0.9926	0.9916	0.9892	1.07	
Fifth	0.075	0.9944	0.9933	0.9903	0.96	Suggested
Sixth	0.072	0.9952	0.9938	0.9896	1.03	Suggested

The 6th grade model was adopted. In order to improve the results, it was necessary to transform the response function using the natural logarithm (Natural Log, k=0, λ=0). After reduction of non-significant members from the proposed model, an analysis of variance (ANOVA) was performed, which is shown in table 4.

Table 4 *ANOVA report for foam S 2535*

Response 4 S2535

Transform: Natural Log Constant: 0

Backward Elimination Regression with Alpha to Exit = 0.100

Removed	F Value	p-value Prob > F	R-Squared	MSE
A^2B	0.043	0.8366	0.9952	5.156E-003
A^3B^2	0.14	0.7105	0.9952	5.103E-003
A^2	0.16	0.6874	0.9952	5.056E-003
A^2B^3	0.19	0.6610	0.9952	5.012E-003
A^2B^4	0.37	0.5454	0.9952	4.970E-003
B^5	0.45	0.5028	0.9952	4.937E-003
A^3	0.61	0.4374	0.9952	4.910E-003
AB^5	1.09	0.2999	0.9951	4.890E-003
A^5B	1.17	0.2820	0.9951	4.894E-003
B^4	1.20	0.2752	0.9950	4.903E-003

Table 4 *ANOVA report for foam S 2535 (continued)*

ANOVA for Response Surface Reduced Sixth model
Analysis of variance table [Partial sum of squares - Type III]

Source	Sum of Squares	df	Mean Square	F Value	p-value Prob > F	
Model	98.78	23	4.29	839.79	< 0.0001	significant
A-d	*0.45*	*1*	*0.45*	*87.40*	*< 0.0001*	
B-f	*0.11*	*1*	*0.11*	*22.21*	*< 0.0001*	
AB	*0.95*	*1*	*0.95*	*186.70*	*< 0.0001*	
A^2	*4.687E-004*	*1*	*4.687E-004*	*0.092*	*0.7627*	
B^2	*0.095*	*1*	*0.095*	*18.58*	*< 0.0001*	
A^2B	*6.112E-004*	*1*	*6.112E-004*	*0.12*	*0.7303*	
AB^2	*0.030*	*1*	*0.030*	*5.81*	*0.0178*	
A^3	*1.444E-005*	*1*	*1.444E-005*	*2.824E-003*	*0.9577*	
B^3	*0.014*	*1*	*0.014*	*2.72*	*0.1021*	
A^2B^2	*0.087*	*1*	*0.087*	*17.03*	*< 0.0001*	
A^3B	*0.26*	*1*	*0.26*	*50.05*	*< 0.0001*	
AB^3	*0.22*	*1*	*0.22*	*42.31*	*< 0.0001*	
A^4	*0.040*	*1*	*0.040*	*7.73*	*0.0065*	
B^4	*7.082E-003*	*1*	*7.082E-003*	*1.38*	*0.2422*	
A^3B^2	*7.073E-004*	*1*	*7.073E-004*	*0.14*	*0.7108*	
A^4B	*0.036*	*1*	*0.036*	*7.01*	*0.0095*	
AB^4	*0.10*	*1*	*0.10*	*19.76*	*< 0.0001*	
A^5	*0.046*	*1*	*0.046*	*9.05*	*0.0034*	
B^5	*2.234E-003*	*1*	*2.234E-003*	*0.44*	*0.5102*	
A^3B^3	*0.025*	*1*	*0.025*	*4.94*	*0.0287*	
A^4B^2	*0.014*	*1*	*0.014*	*2.72*	*0.1025*	
A^6	*0.014*	*1*	*0.014*	*2.82*	*0.0964*	
B^6	*0.011*	*1*	*0.011*	*2.15*	*0.1461*	
Residual	0.49	96	5.114E-003			
Cor Total	99.27	119				

The high F value of the model (F=839.79) and the low probability value (p<0.0001) indicate that the model is significant. The coefficient of determination (R-Squared) and other statistics after ANOVA analysis (Table 5) have good values, which justifies the selection of the adopted mathematical model.

Table 5 *Calculation values of statistics for the evaluation of the mathematical model*

Std. Dev.	0.072	R-Squared	0.9951
Mean	-1.08	Adj R-Squared	0.9939
C.V. %	6.64	Pred R-Squared	0.9924
PRESS	0.75	Adeq Precision	94.518

The final equation of the mathematical model that adequately describes the dependence of the absorption coefficient of PU foam S 2535 on frequency and material thickness is:

$$Ln(a_{2535}) = -3.31800 + 7.63569*d + 6.06169E - 004*f + 0.26953*d*f + 817.77325*d\wedge 2 - 1.28754E - 005*f\wedge 2 - 0.57559*d\wedge 2*f - 2.55283E - 004*d*f\wedge 2 - 73684.41845*d\wedge 3 + 3.88676E - 008*f\wedge 3 - 1.79771E - 003*d\wedge 2*f\wedge 2 - 20.06620*d\wedge 3*f + 1.80161E - 007*d*f\wedge 3 + 1.85161E + 006*d\wedge 4 - 4.68116E - 011*f\wedge 4 + 0.030783*d\wedge 3*f\wedge 2 + 145.31194*d\wedge 4*f - 4.17129E - 011*d*f\wedge 4 - 1.81843E + 007*d\wedge 5 + 2.52487E - 014*f\wedge 5 + 5.54176E - 008*d\wedge 3*f\wedge 3 - 0.14081*d\wedge 4*f\wedge 2 + 6.18407E + 007*d\wedge 6 - 5.09192E - 018*f\wedge 6 \quad (3)$$

The values of the regression coefficient of the mathematical model, the standard error, the 95% confidence interval and the Variance inflation factor (VIF) of the regression coefficient are shown in Table 6.

Table 5 *Values of mathematical model coefficients and confidence intervals*

Factor	Coefficient Estimate	df	Standard Error	95% CI Low	95% CI High	VIF
Intercept	-0.24	1	0.027	-0.29	-0.19	
A-d	0.61	1	0.065	0.48	0.74	40.35
B-f	0.45	1	0.095	0.26	0.64	79.38
AB	-1.71	1	0.12	-1.95	-1.46	74.62
A^2	-0.062	1	0.21	-0.47	0.35	127.18
B^2	-0.94	1	0.22	-1.38	-0.51	145.09
A^2B	0.040	1	0.12	-0.19	0.27	40.75
AB^2	0.36	1	0.15	0.064	0.67	83.11
A^3	-9.789E-003	1	0.18	-0.38	0.36	199.37
B^3	0.75	1	0.45	-0.15	1.65	1284.74
A^2B^2	0.82	1	0.20	0.43	1.22	65.86
A^3B	1.11	1	0.16	0.80	1.42	72.74
AB^3	0.97	1	0.15	0.67	1.26	68.23
A^4	-1.32	1	0.48	-2.27	-0.38	752.19
B^4	0.88	1	0.74	-0.60	2.35	1868.58
A^3B^2	-0.037	1	0.099	-0.23	0.16	21.84
A^4B	-0.30	1	0.11	-0.52	-0.074	30.23
AB^4	-0.56	1	0.12	-0.80	-0.31	42.94
A^5	0.41	1	0.14	0.14	0.68	94.63
B^5	-0.24	1	0.36	-0.96	0.48	728.64
A^3B^3	-0.42	1	0.19	-0.79	-0.045	67.42
A^4B^2	-0.31	1	0.19	-0.69	0.064	55.34
A^6	0.51	1	0.31	-0.094	1.12	323.19
B^6	-0.82	1	0.56	-1.93	0.29	1057.34

The diagnostics of the statistical properties of the model (diagram of normal distribution of residuals, Box-Cox diagram, etc.) show that the residuals are normally distributed and that the model has satisfactory statistical properties (Figures 5 and 6).

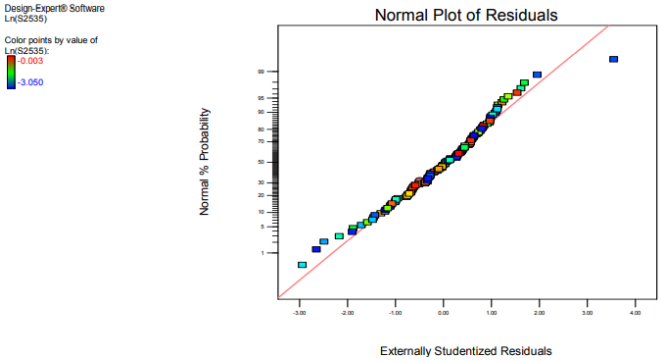

Fig. 5 *Diagram of normal distribution of residuals*

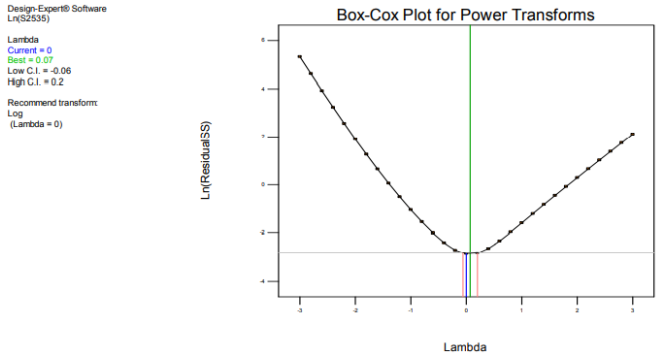

Fig. 6 *Box-Cox plot for the corrected foam model S 2535*

The graphical representation of the mathematical model described by equation (3) is shown in Figures 7 and 8.

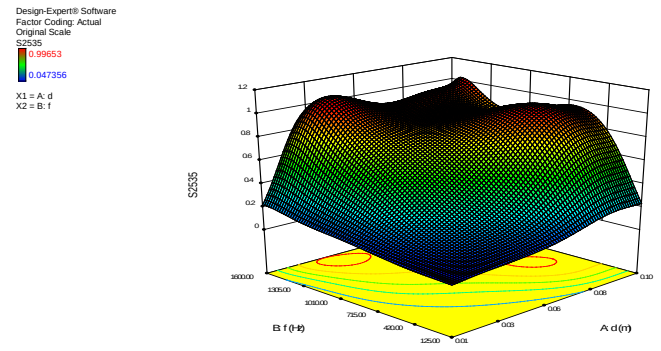

Fig. 7 *3D Graphic representation of the mathematical model for the foam S 2535*

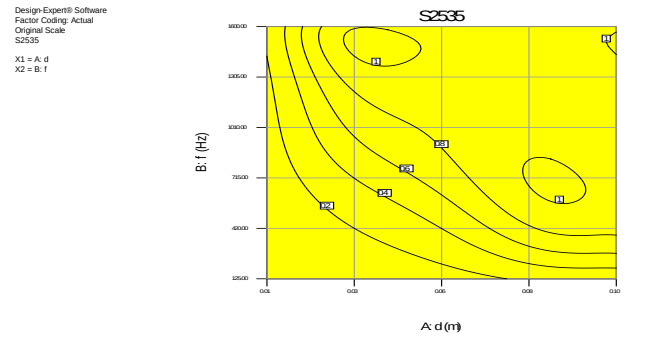

Fig. 8 *Contour 2D representation of the mathematical model for the foam S 2535*

5. CONCLUSION

Experimental results show that the absorption coefficient of PU foam increases with increasing frequency up to a value of 800 Hz and decreases thereafter. The best values of the absorption coefficient are obtained in the interval from 500 Hz to 1200 Hz.

As for the influence of the thickness of the material, it can be stated that the increase in thickness has its purpose up to 70 mm, and after that the absorption coefficient decreases. It also confirms why the test was performed on samples up to 100 mm.

It can be concluded that these materials exhibit a high level of sound absorption in the medium frequency range, which is not characteristic of most absorption materials, and as such can be used in the field of noise protection.

ACKNOWLEDGEMENTS

This work is co-financed by the Ministry of Education, Science and Technological Development of the Republic of Serbia on the base of the contract whose record number is 451-03-68/2022-14/200108. The authors thank the Ministry of Education, Science and Technological Development of the Republic of Serbia for supporting this research.

REFERENCES

[1] Wang C.-N., Torng J.-H., “Experimental study of the absorption characteristics of some porous fibrous materials”, *Appl. Acoust.*, Vol. 62, № 4, p. 447–459, 2001.

[2] Eaves D., “Handbook of Polymer Foams, Rapra Technology Limited”, Shawbury, 289 p., 2004.

[3] Pompoli F., Bonfiglio P., “Acoustical properties of polyurethane open cells materials: Experimental investigation and theoretical models”, *14th Int. Congr. Sound Vib. - ICSV14*, Cairns, 2007.

[4] Lauriks W., Cops A., Verhaegen C., “Acoustical properties of elastic porous materials”, *J. Sound Vib.*, Vol. 131, № 1, p. 143–156, 1989.

[5] Ghaffari Mosanenzadeh S., Doutres O., Naguib H.E., Park C.B., Atalla N., “A numerical scheme for investigating the effect of bimodal structure on acoustic behavior of polylactide foams”, *Appl. Acoust.*, Elsevier Ltd, Vol. 88, p. 75–83, 2015.

[6] M. Kolarević, Z. Šoškić, Z. Petrović, B. Radičević: “Noise Protection in Urban Environment-Description of a Project”, *Mechanics, Transport, Communications*, Sofia, vol. 3, pp. IV-69/IV-78, 2011.

[7] Vapeks d.o.o.; [Electronic resource], URL: http://www.vapeks.rs/en (accessed: 04.02.2016), 2015.

[8] B. Radičević, "Razvoj modela odlučivanja za izbor optimalne smeše zvučno apsorcionih materijala", *Doktorska disertacija*, Fakultet za mašinstvo i građevinarstvo u Kraljevu, Univerzitet u Kragujevcu, Kraljevo, Srbija, 2016.

[9] EN ISO 10534-2:2001, *Acoustics. Determination of sound absorption coefficient and impedance in impedance tubes Transfer-function method.*

[10] Ristanović I., Mijić M., "Jedna realizacija sistema za merenje koeficijenta apsorpcije sa impedansnom cevi", *58. ETRAN*, Vrnjačka Banja, p. AK3.5.1–6, 2014.

[11] SRPS EN ISO 354:2008, *Akustika - Merenje zvučne apsorpcije u reverberacionoj komori.*

University of Nis
Faculty of Occupational Safety
„Politechnica“ University of Timisoara
Faculty of Mechanical Engineering
27th International Conference
NOISE AND VIBRATION
Niš, 20 - 21. 10. 2022.

HYBRID OPTIMIZATION ALGORITHM FOR DETERMINING SOUND ABSORPTION

Tanja Miodragović[1], Branko Radičević[1], Goran Miodragović[2], Marina Ivanović[1]

[1] University of Kragujevac, Faculty of Mechanical and Civil Engineering in Kraljevo, Serbia, miodragovic.t@mfkv.kg.ac.rs
[2] Academy of Applied Study Šumadija, Department Trstenik, Trstenik, Serbia

Abstract - *The great variety of biologically inspired algorithms and the possibility of application in different fields of engineering initiates the application in the search of the space of possible values of the coefficients of empirical models for acoustic impedance. The application of two biologically inspired algorithms: beluga optimization (BWO) and the marine predators algorithm, as well as their hybridization, was investigated in the paper. In order to obtain satisfactory coefficients of empirical models, the BWO algorithm was modified by adding a part of the marine predators algorithm that refers to the change of search agents in the BWO algorithm. The new model provides satisfactory predictions of the sound absorption coefficient of open-cell polyurethane foams, compared to experimental results obtained in an impedance tube. In relation to the known empirical models for impedance where the constants are determined by the linear regression method, the hybrid algorithm provides satisfactory predictions of the sound absorption coefficient of polyurethane foams.*

1. INTRODUCTION

Noise pollution is a serious environmental problem of the modern world. Due to the rapid development of the industry, which directly affects noise pollution, there are consequences for human health such as: stress, sleep disorders, cardiovascular problems and others [1]. Because of the negative impact on human health, it is very important to investigate the acoustic properties of materials that can be used in noise control.

An effective tools used in noise control are porous materials. Porous absorption materials are characterized by a high sound absorption coefficient. Polyurethane foams are widely used in various industries and noise protection systems due to their excellent mechanical properties and availability in a wide range of densities and thicknesses. [2]. Elastic porous foams PU with open cell are generally considered good sound absorbers [3].

With the development of new materials, for application in noise control, it is necessary to find empirical and/or theoretical models, which implementation would enable the determination of the acoustic properties of materials. Empirical models in combination with measurement results are used to determine the dependence of absorption coefficients as a function of frequency and thickness of the material. To determine the coefficients in the empirical model, Radičević [2], using the method of least squares, proposed a new empirical model for determining the acoustic properties of low-density polyurethane foams. The new model provides satisfactory predictions of the sound absorption coefficient of open-cell polyurethane foams, compared to experimental results obtained in an impedance tube.

This paper presents the application of newer biologically inspired algorithms, namely the beluga whale algorithm, BWO (2022, [4]), as well as the marine predator algorithm, MPA (2020, [5]), for determining the coefficients in the empirical model for determiningsound absorption coefficient. In order to obtain the best possible solutions, hybridization of these two algorithms was also carried out. The model for determining the characteristic acoustic impedance was derived based on the known dependencies defined by Delany and Bazley [6].

The accuracy of the results obtained by the proposed algorithms was checked by the results of measuring the absorption coefficients given in [2], and for the material polyurethane foam HR 3744.

2. EMPIRICAL MODELS FOR DETERMINING ACOUSTIC PROPERTIES OF MATERIALS

When selection a material, which is used in noise control, it is necessary to know sound absorption coefficient and the properties of the material under consideration. In the case of polymer foams, aforementioned provides the sound absorption coefficient at normal incidence α_n and the normal surface impedance Z_N. These quantities can be determined by experimental measurements, using the transfer method, described in the standard EN ISO 10534-2 [7]. However, these sizes can be predicted based on material properties: porosity, air flow resistance, pore geometry, etc. Empirical models using these material properties can be used to estimate acoustic properties.

The best-known and one of the first empirical models is the Delany-Bazley model [6], for determining the acoustic impedance and propagation coefficient of fibrous absorption materials. In this model, the only input parameter is the air flow resistance, which can be measured relatively easily. Dunn & Davern [8] retained the same form of equations developed by Delany & Bazley and calculated new values of regression constants for polyurethane foams.

2.1 Model for characteristic acoustic impedance

In order to demonstrate the justification of applying a biologically inspired algorithm to determine the characteristic acoustic impedance, in this work, the model defined by Delany-Bazley was applied[6].

The dependencies in this model are given in Eqs(1) – (4), [2].

$$Z_{CR} = \rho_0 c_0 \left[1 + C_1 \left(\frac{\sigma}{\rho_0 f} \right)^{C_2} \right] \quad (1)$$

$$Z_{CI} = -\rho_0 c_0 \left[C_3 \left(\frac{\sigma}{\rho_0 f} \right)^{C_4} \right] \quad (2)$$

$$\alpha = \left(\frac{2\pi f}{c_0} \right) \left[C_5 \left(\frac{\sigma}{\rho_0 f} \right)^{C_6} \right] \quad (3)$$

$$\beta = \left(\frac{2\pi f}{c_0} \right) \left[1 + C_7 \left(\frac{\sigma}{\rho_0 f} \right)^{C_8} \right] \quad (4)$$

where:

- Z_{CR}, Z_{CI} – real and imaginary part of the characteristic acoustic impedance, Z_C;
- α, β – real and imaginary parts of propagation constant, Γ,
- σ – air flow resistance,
- f – frequency,
- ρ_0 – the density of air and
- c_0 – the speed of sound in the air

The sound absorption coefficient at normal incidence, α_n, for a firmly supported layer of material of thickness *d*, can be obtained using expressions (5) and (6), with knowledge of characteristic acoustic impedance and propagation constant Γ.

$$Z_S = Z_C coth \Gamma o \quad (5)$$

$$\alpha_n = 1 - \left| \frac{Z_S - \rho_0 c_0}{Z_S + \rho_0 c_0} \right|^2 \quad (6)$$

The values of the sound absorption coefficient, which will be used to verify the proposed algorithm, are given in Table 1, [2]. These values were obtained by measuring in an impedance tube using the transfer function method between two microphones, described in the standard SRPS EN ISO 10534-2 [7].

3. OPTIMIZATION ALGORITHMS

In the last decades, methods have been developed that are increasingly better at solving complicated real-world optimization problems. The main characteristic of these methods is that they were created as inspiration from nature and for this reason they are called biologically inspired methods. Biologically inspired optimization algorithms belong to the group of metaheuristic optimization methods that simulate natural processes and systems when performing search activities in the space of potential solutions, [9]. Among the best known, most popular, methods are: genetic algorithms (Genetic Algorithm - GA, John Holland, 1962), differential evolution (Differential Evolution - DE, R. Storn and K. Price 1996), particle swarm optimization (Particle Swarm Optmization - PSO, J. Kennedy and R. Eberhart in 1995), ant colony optimization (ACO M. Dorigo in the late 1990s), cuckoo search (CS – Xin-She Yang and Suash Deb, 2007), firefly algorithm (FA - Xin-She Yang, 2008), bat algorithm (Bat Algorithm – BA - Xin-She Yang, 2010), krill herd hlgorithm – (KHA – Amir H Gandomi and Amir H Alavi, 2012), gray wolf algorithm (Gray Wolf Optimizer, Seyedali Mirjalili, Seyed Mohammad Mirjalili, Andrew Lewis, 2014.

Table 1 *Absorption coefficient values for foam HR 3744, [2]*

	Material thickness (cm)									
f_c(Hz)	1	2	3	4	5	6	7	8	9	10
125	0.078945	0.052273	0.078038	0.091768	0.095615	0.099378	0.14166	0.14739	0.1988	0.23425
160	0.07159	0.064579	0.088787	0.095501	0.1163	0.13339	0.17142	0.1915	0.23306	0.28444
200	0.067147	0.071539	0.095544	0.1082	0.13866	0.16303	0.21552	0.26369	0.29383	0.36679
250	0.062784	0.081199	0.10469	0.12844	0.16959	0.20025	0.26771	0.3203	0.37254	0.47083
315	0.060061	0.082818	0.11674	0.15397	0.20809	0.24824	0.34862	0.41372	0.44536	0.56428
400	0.061533	0.088451	0.13883	0.19781	0.26972	0.31781	0.44411	0.49926	0.59604	0.73095
500	0.062915	0.10462	0.17202	0.25435	0.324	0.38727	0.55493	0.66397	0.75279	0.88024
630	0.07125	0.12535	0.22696	0.3171	0.44179	0.52143	0.74253	0.82768	0.8864	0.96609
800	0.086209	0.15796	0.29957	0.44704	0.59085	0.67178	0.88578	0.93204	0.94498	0.9434
1000	0.089769	0.19083	0.40787	0.5967	0.74673	0.80233	0.92326	0.92662	0.90819	0.8601
1250	0.1146	0.24294	0.56195	0.75699	0.84916	0.8587	0.86797	0.85938	0.83806	0.82517
1600	0.073466	0.30496	0.74481	0.86448	0.85371	0.84389	0.77397	0.80167	0.80959	0.90507

α_w	0.05	0.15	0.25	0.3(M)	0.35(M)	0.4(M)	0.55(M)	0.6(M)	0.65	0.75

f_c(Hz)	α_p									
250	0.063331	0.078519	0.105658	0.130203	0.172113	0.20384	0.277283	0.33257	0.370577	0.4673
500	0.065233	0.10614	0.17927	0.25642	0.34517	0.408837	0.580523	0.663637	0.745077	0.859093
1000	0.096859	0.197243	0.42313	0.600243	0.728913	0.777603	0.892337	0.906013	0.897077	0.876223

The advantage of these algorithms is that they are flexible, can be applied to a large number of optimization problems, as well as their adaptability to the optimization problem. It is important to note here that the function optimized by these methods does not have to be differentiable and continuous, and that there is no limit to the number of variables to be optimized. However, perhaps the most important advantage of these methods is that they are all algorithmically conceived and, as such, can be improved with simple modifications, thus achieving greater efficiency in finding the optimal solution.

In the continuation of the paper, two more recent algorithms are proposed: the beluga whale algorithm, BWO (2022, [4]), the marine predator algorithm, MPA (2020, [5]), as well as their hybridization.

3.1 Beluga whale alghorithm

Inspired by the behavior of the beluga whale while swimming, hunting and "falling", Figure 1, Changting Zhong, Gang Li and Zeng Meng proposed the Beluga Whale Algorithm (Beluga whale optimization – BWO) [4]. Belugas are social animals, living in groups that vary from 2 to 25 members. It is observed that pair of belugas have been swimming in sync or in a "mirror" mode. Beluga whales generally feed in a group and attack prey by directing fish into shallow water, sharing information among themselves taking into account the position of the best candidate. Hence, they share information about the positions considering the best candidate. During migrations and hunting, belugas are threatened by humans, killer whales and polar bears, so a small number of belugas do not survive and end up on the seabed, this phenomenon is called "whale fall".

These three dominant beluga whale behavior are mathematically formulated to form an optimization algorithm, [4].

For behavior modeling, beluga whales are considered as search agents that can move in the search space, changing their position vectors. Therefore, each beluga is a candidate for the best solutions, which is updated during optimization. The matrix to positions of search agents, [4]:

$$X = \begin{bmatrix} x_{1,1} & x_{1,2} & \cdots & x_{1,d} \\ x_{2,1} & x_{2,2} & \cdots & x_{2,d} \\ \cdots & \cdots & \cdots & \cdots \\ x_{n,1} & x_{n,2} & \cdots & x_{n,d} \end{bmatrix}$$

where:

n – the population size of beluga whales,

d – the number of variables being optimized.

For each beluga whale (search agent), the obtained fitness values are stored as follows, [4]:

$$F_X = \begin{bmatrix} f\left(x_{1,1}, x_{1,2}, ..., x_{1,d}\right) \\ f\left(x_{2,1}, x_{2,2}, ..., x_{2,d}\right) \\ \cdots \\ f\left(x_{n,1}, x_{n,2}, ..., x_{n,d}\right) \end{bmatrix}$$

The BWO algorithm can transition from the exploration phase to exploitation depending on the balance factor, which is modeled as given in Eq. (7), [4].

$$B_f = B_0\left(1 - \frac{T}{2T_{\max}}\right) \quad (7)$$

where:

T - the current iteration,

T_{max} – maximum iterative number,

B_0 – randomly changes between (0, 1) at each iteration.

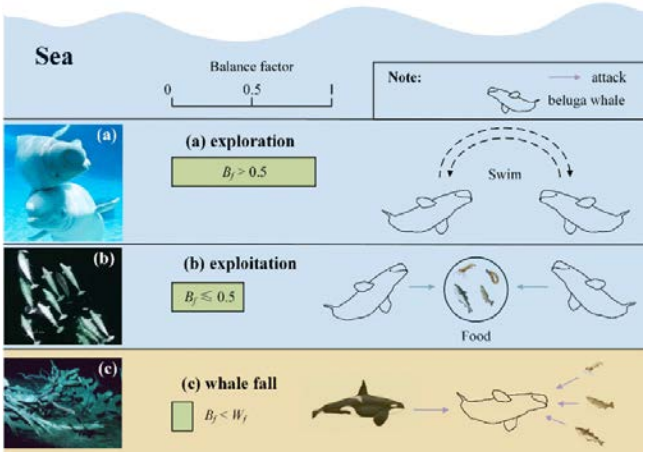

Fig. 1 *Behaviors of beluga whales, (a) swim - exploration phase; (b) foraging - exploitation phase, (c) whale fall- whale fall phase.,[4]*

As previously stated, belugas swim in pairs in a synchronized or mirrored mode. The mathematical model of this behavior is given by the equation (8), [4]

$$\begin{cases} X_{i,j}^{T+1} = X_{i,p_j}^{T} + \left(X_{r,p_1}^{T} - X_{i,p_j}^{T}\right)(1+r)\sin(2\pi r_2), \; j == even \\ X_{i,j}^{T+1} = X_{i,p_j}^{T} + \left(X_{r,p_1}^{T} - X_{i,p_j}^{T}\right)(1+r)\cos(2\pi r_2), \; j == odd \end{cases} \quad (8)$$

where:

T – - the current iteration,

$X_{i,j}^{T+1}$ – the new position for the ith beluga whale on the jth dimension,

p_j, $j = 1,2,\ldots,d$ – is a random number selected from d,

X_{i,p_j}^{T} – position of the ith beluga whale on p_j variable,

X_{i,p_j}^{T} и X_{i,p_j}^{T} – the current positions for ith and rth beluga whale (r - randomly selected beluga whale)

r_1, r_2 – random number between (0,1).

Due to the improvement of convergence, the Levy flight strategy is introduced in the exploitative phase of the BWO. The mathematical model of beluga behavior during feeding is given by the equation (9), [4].

$$X_i^{T+1} = r_3 X_{best}^{T} - r_4 X_i^{T} + C_1 \cdot L_F \cdot \left(X_r^{T} - X_i^{T}\right) \quad (9)$$

where:

T – current iteration,

X_i^T и X_r^T – current position for the ith beluga whale and a random beluga whale,

X_i^{T+1} – the position of new position of the ith beluga whale,

X_{best}^{T} – the best position among beluga whales,,

r_3, r_4 – random number between (0,1)

C_1=2r$_4$ $(1 - T/T_{max})$ – random jump strength that measuring the intensity of Levy flight.

L_F - Levy flight function, [4].

To ensure a constant number of population sizes, beluga positions and step sizes of whale falls are used to determine the updated position. The mathematical model of the whale fall behavior is represented by the equation (10), [4].

$$X_i^{T+1} = r_5 X_i^{T} - r_6 X_r^{T} + r_7 X_{step} \quad (10)$$

где је:

r_5, r_6 и r_7 – random numbers between (0,1)

X_{step} – the step size of whale fall: X_{step}=f(u_b, l_b, C_2)

u_b, l_b – upper and lower boundary of variables

C_2 – step factor which is related to the probability of whale fall and population size, [4].

Based on all the given mathematical models and the mentioned approximations, in Figure 2, the proposed BWO algorithm is given in the form of a pseudo code, [4].

3.2 Marine predator algorithm

The Marine Predator Algorithm (MPA) is a metaheuristic algorithm that is biologically inspired by the feeding behavior of marine predators. This algorithm was proposed by Afshin Faramarzi, Mohammad Heidarinejad, Seyedali Mirjalili, Amir H. Gandomi [5]. When attacking prey, predators follow two strategies: Lévy, when prey concentration is low, and Brownian movement when prey is abundant. In order to make a trade-off between the two strategies, predators measure the ratio of velocity from the prey to them.

```
Initialization of search agents (beluga whale) X_k, k = 1,..,n%% n –the number of agents
Generating the best solution, F_best
Broj_iter=1000; %% maximum number of iterations
While i = 1,...,Broj_iter
    Calculating the probability of failure,W_f
    Calculation of the balance factor, B_f
    While k=1,...,n
      If B_f(k)> 0.5 %% search phase
        Random generation p_j (j = 1,...d); %% d - number of variables
        A random beluga selection X_r;
        Updating the new position of k-th beluga
      Else if B_f(k) ≤ 0.5 %% expoatation phase
        Update random jump strength C_1;
        Calculation of the value of Levy flight
        Updating the new position of k-th beluga;
      End If
      New position limit check and calculation F_c; %% F_c - objective function
    End While
    While k=1,...,n
      If B_f(k) ≤ W_f %% beluga decay phase
        Factor update C_2;
        Step size update, X_step;
        New position update k-th belugas;
        New position limit check and calculation F_c;
      End If
    End While
    Searching for the currently best solution F_c^Best;
End While
```

Fig. 2 *Pseudo code of BWO algorithm,[4]*

The mathematical model of the MPA algorithm is presented below. Like most metaheuristics, MPA starts by initializing a set of solutions in the search space using Eq (11), [10]:

$$X_0 = X_{min} + rand\left(X_{max} - X_{min}\right) \tag{11}$$

where:

X_{min}, X_{max} – lower and upper bound for variables,
rand – uniform random vector in the range (0,1)

Bassed on the survival of the fittest, the top predator is the best one at foraging. Based on this, the matrix of the best solution (top predator), the so-called *Elite* matrix, is formed (12). This matrix array is used to find prey based on information about the position of the prey.

$$Elite = \begin{bmatrix} X_{1,1}^{I} & X_{1,2}^{I} & \ldots & X_{1,d}^{I} \\ X_{2,1}^{I} & X_{2,2}^{I} & \ldots & X_{2,d}^{I} \\ \ldots & \ldots & \ldots & \ldots \\ X_{n,1}^{I} & X_{n,d}^{I} & \ldots & X_{n,d}^{I} \end{bmatrix}_{nxd} \tag{12}$$

where:

$\overrightarrow{X^I}$ - represents the top predator vector,
n – number of search agents,

d – search space.

In this algorithm, there is also a prey matrix, which serves to update the positions of the predators, 14.

$$Prey = \begin{bmatrix} X_{1,1} & X_{1,2} & \ldots & X_{1,d} \\ X_{2,1} & X_{2,2} & \ldots & X_{2,d} \\ \ldots & \ldots & \ldots & \ldots \\ X_{n,1} & X_{n,d} & \ldots & X_{n,d} \end{bmatrix}_{nxd} \tag{13}$$

The MRA optimization process is divided into three main optimization phases taking into account the different velocity ratio between predator and prey. The first stage can be considered when the velocity ratio between predator and prey is high. In contrast, unit ratio, predator and prey move at almost the same pace, and low speed ratios represent the second and third stages. Details of each step are addresed below.

Phase 1. High velocity ratio ($v \geq 10$),

Space search (prey search) is represented by the equation 14.,[5].

$$\begin{gathered} While\ Iter < \frac{1}{3} Max\_iter \\ \overrightarrow{stepsize_i} = \overrightarrow{R_B} \otimes \left(\overrightarrow{Elite_i} - \overrightarrow{R_B} \otimes \overrightarrow{\Pr ey_i}\right),\ i = 1,..,n \\ \overrightarrow{\Pr ey_i} = \overrightarrow{\Pr ey_i} + P \cdot \vec{R} \otimes \overrightarrow{stepsize_i} \end{gathered} \tag{14}$$

where:

$\overrightarrow{R_B}$ – vector containing random numbers based on Normal distribution representing the Brownian motion,
P = 0,5 – constant number,
$\vec{R}$ – vector of uniform random numbers in [0,1],
Iter – the current iteration,
Max_Imer – maximum number of iterations.

Phase 2. Unit velocity ratio ($v \approx 1$),

This phase occurs in the intermediate phase of optimization process, where exploration gradually changes to exploitation. In this phase, both exploration and exploitation are important. Therefore, half of the individuals are designated for research, and the other half for exploitation. In this phase, the prey is responsible for the hunt and the predator is responsible for the search. The mathematical model of this phase is represented by the following equations 15., for the first half of the population [5].

$$\begin{gathered} While \frac{1}{3} Max\_iter < Iter < \frac{2}{3} Max\_iter \\ \overrightarrow{stepsize_i} = \overrightarrow{R_L} \otimes \left(\overrightarrow{Elite_i} - \overrightarrow{R_L} \otimes \overrightarrow{\Pr ey_i}\right),\ i = 1,..,n/2 \\ \overrightarrow{\Pr ey_i} = \overrightarrow{\Pr ey_i} + P \cdot \vec{R} \otimes \overrightarrow{stepsize_i} \end{gathered} \tag{15}$$

For the other half of the population, the model is represented by Eq. 16., [5].

$$\begin{gathered} \overrightarrow{stepsize_i} = \overrightarrow{R_B} \otimes \left(\overrightarrow{R_B} \otimes \overrightarrow{Elite_i} - \overrightarrow{\Pr ey_i}\right),\ i = n/2,..,n \\ \overrightarrow{\Pr ey_i} = \overrightarrow{Elite_i} + P \cdot CF \otimes \overrightarrow{stepsize_i} \end{gathered} \tag{16}$$

where:

$\overrightarrow{R_L}$ – vector of random numbers based on Lévy distribution representing Lévy movement. In this phase, the first half of the prey moves with the Levy strategy, while the other half moves with the Brownian movement strategy.

CF – adaptive parameter to control the step size for predator movement and is generated using Eq. 17., [5].

$$CF = \left(1 - \frac{Iter}{Max\_Iter}\right)^{\left(2 - \frac{Iter}{Max\_Iter}\right)} \tag{17}$$

Phase 3. Low velocity ratio ($v \approx 1$),

This is the exploitation phase and is represented by Eq 18., [5].

$$\begin{gathered} While\ Iter > \frac{2}{3} Max\_iter \\ \overrightarrow{stepsize_i} = \overrightarrow{R_L} \otimes \left(\overrightarrow{R_L} \otimes \overrightarrow{Elite_i} - \overrightarrow{\Pr ey_i}\right),\ i = 1,..,n \\ \overrightarrow{\Pr ey_i} = \overrightarrow{Elite_i} + P \cdot CF \otimes \overrightarrow{stepsize_i} \end{gathered} \tag{18}$$

The behavior of marine predators can be significantly affected by environmental issues, such as eddy formation or

the Fish aggregating Devices (FAD) effect. As a result, the predators spend 80% of their time searching for prey in the vicinity, while the rest of the time they search for prey in other environments. The FADs are considered as local optima and their effect as trapping in these points in search space. Consideration of these longer jumps during simulation avoids stagnation in local optima. The mathematical model of this behavior can be represented by Eq. 19.,[5].

$$\overrightarrow{Prey_i} = \begin{cases} \overrightarrow{Prey_i} + CF\left[\vec{X}_{\min} + \vec{R} \otimes \left(\vec{X}_{\max} - \vec{X}_{\min}\right)\right] \otimes \vec{U}, & if\ r \le FAD_s \\ \overrightarrow{Prey_i} + \left[FAD_s(1-r) + r\right]\left(\overrightarrow{Prey_{r1}} - \overrightarrow{Prey_{r2}}\right), & if\ r > FAD_s \end{cases}, \quad (19)$$

where r is a random number in the range [0,1], a $\vec{U}$ is the binary vector with arrays including zero and one. FADs=0.2 indicates the influence of FADs on the updating process.

MPA saves memory by saving the old prey position. After updating the current solution, the fitness values of the current solution and the previous solution are compared and declared the best, if the value of the previous solution is better than the current solution. The pseudo code of the MPO algorithm is given in Figure 3.

```
Initializing Search Agents - Prey; k = 1,...,n%% n –  number of agents
Broj_iter=1000; %% maximum number of iterations
While i =1,...,Broj_iter
        Calculating the objective function (F_c^□);
        formation of the Elite matrix
        If i < Broj_iter/3
                Prey update, Eq. (16);
        Else if Broj_iter /3 < i < 2
                Broj_iter/3
                While k=1,...,n
                    If j<n/2
                        Prey update, Eq. (17)
                    Else
                        Prey update Eq. (18)
                End While
        Else if i > 2· Broj_iter /3
                Prey update Eq. (19)
        End If
        Memorizing and updating the Elite matrix
        Applying the FADs effect and updating, Eq. (20)
        Find F_c^Best; %% the best predator
End While
```

Fig. 3 *Pseudo code of the MPO algorithm*,[5]

3.3 Hybrid algorithm BW-MPA

Hybridization of optimization algorithms is performed in order to obtain better solutions in a shorter time frame. Usually, similar algorithms are used for the combination of optimization algorithms, that is, algorithms that have the same or similar basis in nature. For this reason, the algorithms presented above were chosen. Namely, beluga whales are members of marine mammals, which can also be said to be predators, except that they hunt in groups.

The hybridization of these two algorithms is reflected in the fact that each search agent, within the BWO algorithm, is positioned as the best predator from the MPA algorithm. Then, the search of the space of possible solutions is performed using the BWO algorithm, where after finding the best solution, an even better position of the agent from the BWO algorithm is checked and searched using the part of the MPA algorithm, Figure 4.

4. RESULTS AND DISCUSSION

The specificity of determining the coefficients of the empirical model of sound absorption is that the exact boundaries of the search space are not known in advance. In other words, the search space is infinite. With the selected empirical model, it is necessary to find eight coefficients, C_i, i = 1,…,8. The limits in which they are searched are in the range of $-\infty$ to $+\infty$. These limits are defined by the vector values l_i for the lower limit, and u_i for the upper limit, Eq. 20.

$$l = \left[-\infty -\infty -\infty -\infty -\infty -\infty -\infty -\infty\right]$$
$$u = \left[+\infty +\infty +\infty +\infty +\infty +\infty +\infty +\infty\right] \quad (20)$$

```
1  Initialization of search agents (beluga whale) X_i, k = 1,..,n%% n –the number of agents
2  Calculating the objective function (F_c^□);
3  Formation of the Elite matrix
4  If i < Broj_iter/3
5          Ažuriranje plena Eq. (16)
6  Else if Broj_iter /3 < i < 2
7          Broj_iter/3
9  While k=1,...,n
10         If j<n/2
11             Ažuriranje plena Eq. (17)
12         Else
13             Ažuriranje plena Eq. (18)
14         Else if i > 2· Broj_iter /3
16             Ažuriranje plena Eq. (19)
17         End If
18 End While
19 Memorizing and updating the Elite matrix
20 Applying the FADs effect and updating, Eq. (20)
21 Find F_c^Best; %% the best predator
22 F_c^Best = Predator_c^Best;
23 l = −rand(1,d) · Predator_c^Best; u = rand(1,d) · Predator_c^Best;
24 %% Modified Beluga algorithm:
25 %% after finding the best solution, F_c^Best, line 29 -  BWO pseudocode
26 %% beluga is seen as a predator and within a cycle While i = 1,...,n
27 %% the part of the MPA algorithm that finds the best predator is inserted
28 While i = 1,...,Broj_iter
29         ...
30         Searching for curent the best solution F_c^Best;
31         Pozicija_plena = Pozicija_beluge_best;
32         Formation of the Elite matrix
33         If i < Broj_iter/3
34                 Ažuriranje plena Eq. (16)
35         Else if Broj_iter /3 < i < 2
36                 Broj_iter/3
37                 While k=1,...,n
38                     If j<n/2
39                         Ažuriranje plena Eq. (17)
40                     Else
41                         Ažuriranje plena Eq. (18)
42                 End While
43         Else if i > 2· Broj_iter /3
44                 Ažuriranje plena Eq. (19)
45         End If
46         Memorizing and updating the Elite matrix
47         Applying the FADs effect and updating, Eq. (20)
48         Finding F_c^Best;
49 End While
```

Fig. 4 *Pseudo code of hybrid BW-MPA algorithm*

For all three algorithms, BWO, MPA and BW-MPA, the algorithm parameters used are:

The number of search agents is 20

The maximum number of iterations is 1000.

Algorithms were applied as suggested in the literature [4] and [5], that is, no modifications were performed. Conventionally speaking, the only modification that has been made is related to the hybridization of these algorithms. The first modification refers to the reduction of the search space, so that, after setting the limits of the variables, equation 20, the positioning of the best search agent was performed, using the MPA algorithm and the fitness values, obtained in this step, are used as a basis for defining the limits of the search space, equation 21, line 23, BW-MPA.

$$l = -rand(1,d) \cdot Predator_c^{Best}$$
$$u = rand(1,d) \cdot Predator_c^{Best} \quad (21)$$

where

d – number of variables,

$Predator_c^{Best}$ – the best solution of the objective function according to the MPA algorithm.

The second modification refers to the incorporation of a part of the MPA algorithm, which attempts to check whether the best solution obtained by the BWO algorithm is also the best predator, lines 30 – 38, BW-MPA pseudocode, Figure 4.

Figure 5 shows a comparative view of the results obtained by the proposed algorithms.

Parameter	BWO	MPA	BW-MPA
Duration of the algorithm [sec]	***407.4369253343***	***1510.8727405994***	***571.7954629894***
C_1	0.65264	0.42371	0.43462
C_2	0.07088	0.30741	0.29065
C_3	-6.38976	-5.00000	-11.71252
C_4	-3.27006	-3.03414	-3.81486
C_5	0.36615	0.30101	0.30681
C_6	0.03847	0.13982	0.13069
C_7	0.10352	0.09744	0.09994
C_8	0.94643	0.94116	0.93413
The objective function Δ	***0.2572380020***	***0.2486829801***	***0.2474991507***
The worst solution	12.4443331703	10.4778114079	26.9913366998
Middle value	0.3145679399	0.3395845575	0.4516901084
Standard deviation	0.4399196086	0.5602260743	1.1194907950

Fig. 5 *Results obtained by the proposed algorithms*

Figures 6, 7 and 8 show convergence curves in the process of searching for the best solution.

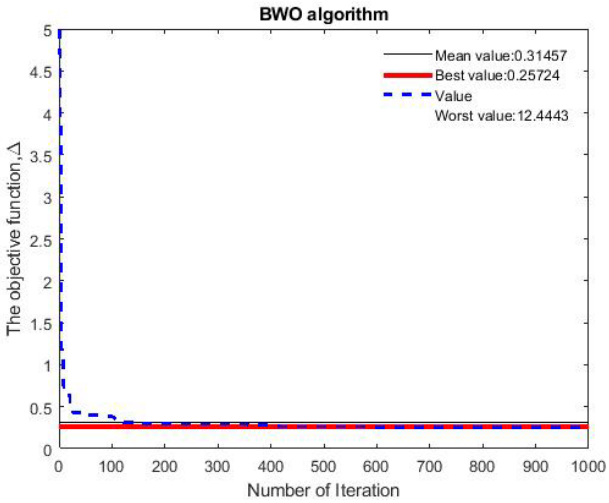

Fig. 6 *Iterative process in determining the coefficients, Ci,i=1,…,8; when implementing the BWO algorithm*

Analyzing the results given in figure 5, as well as the curves given in figures 6, to 8, it is observed that all three diagrams have an excellent convergence. Although, in practice, the search space is unlimited, Eq. 20, all three algorithms already enter the zone of the best possible solution after ten iterations..

By applying these modifications, it was expected that the hybrid algorithm works slower than the individual algorithms. From Figure 5, it can be seen that the search time is slightly longer than that of the BWO algorithm, and significantly less than that of the MPA algorithm. Here we should be honest and say that the duration of the search with the MPA algorithm is determined by the very nature of the algorithm: the number of iterations, at least three cycles of adjustment within one iteration and the like, which in fact leads to an increase in the duration of the search compared to the BWO algorithm.

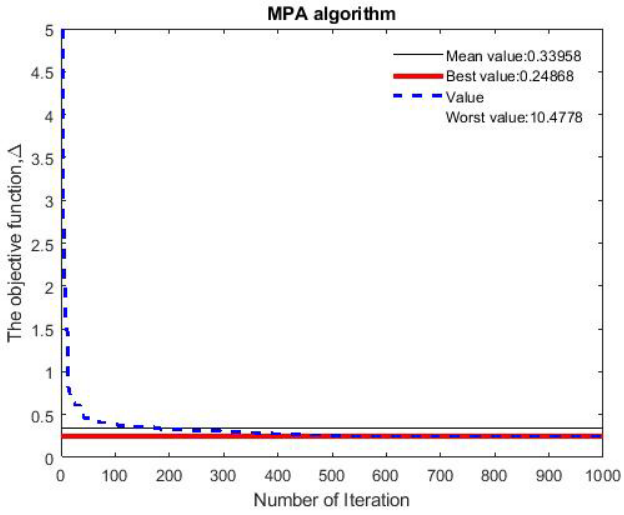

Fig. 7 *Iterative process in determining the coefficients, Ci,i=1,…,8; when implementing the MPA algorithm*

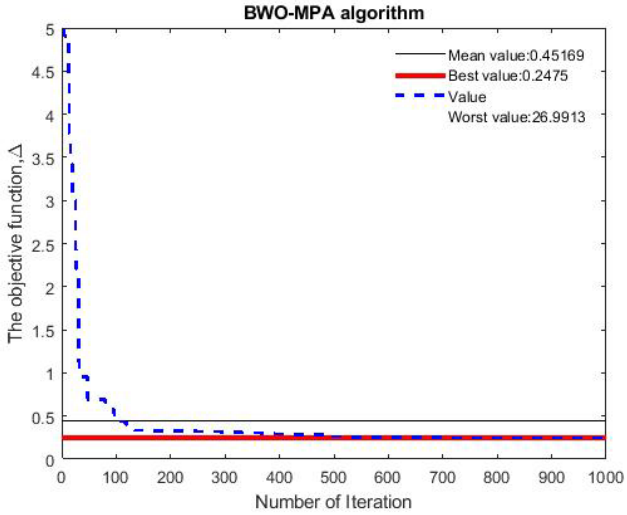

Fig. 8 *Iterative process in determining the coefficients, Ci,i=1,…,8; when applying the hybrid BW-MPA algorithm*

Furthermore, the results obtained by applying these three algorithms to the determination of the coefficients in the empirical model for determining the sound absorption coefficient show that practically all three algorithms give approximate results, with slightly better results obtained by applying the BWO-MPA algorithm Δ = **0.2474991507**. This can be explained by the similar nature of the mentioned algorithms.

The second conclusion can serve as a guideline for further research, and it would refer to the rapid convergence towards the best solution. This actually means that the algorithms can enter the space of possible local minima. In order to avoid this, and especially in the case of an infinite search space, it is necessary to modify these algorithms to avoid the possibility of entering the space of some of the local minima.

Figure 9 shows the dependence of the sound absorption coefficient α_n depending on the thickness of the material, d [m] and the frequency f [Hz], based on the obtained results of the coefficients, C_i, i = 1,..,8., from the Table in the Figure 5.

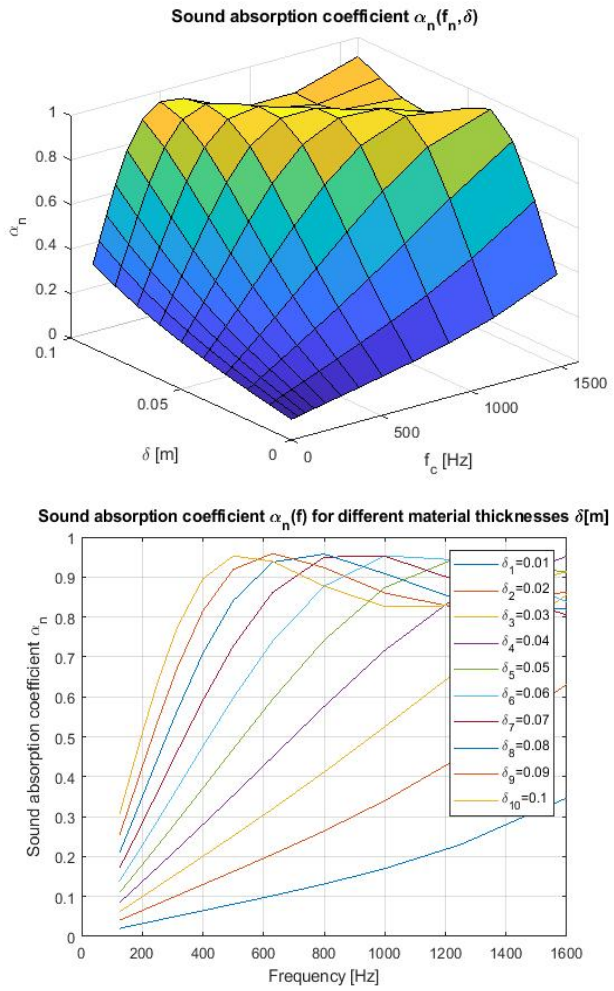

Fig. 9 *Graphical representation of the sound absorption coefficient $\alpha_n=F(f,\delta)$*

5. CONCLUSION

In this paper, the application of the hybridized BWO-MPA algorithm is proposed, by combining a part of the MPA algorithm in the BWO algorithm. The proposed modification was reflected in the fact that the MPA algorithm was used to narrow the infinite search space. This was done by positioning the best search agent, applying the MPA algorithm, and the fitness values, obtained in this step, are used as a basis for defining the boundaries of the search space, equation 21, line 23, pseudocode from Figure 4. A further modification included part of the MPA algorithm in the search cycle of the BWO algorithm, which checks whether the best solution obtained by the BWO algorithm is also the best predator, lines 30 – 38, BW-MPA pseudocode, Figure 4.

Fast convergence, when searching the infinite space of possible solutions, is good, however, it hides the danger of entering the space of a local minimum. Additional modifications of the proposed algorithm, in the continuation of the research, should remove or at least mitigate the danger of entering the local minimum space.

ACKNOWLEDGEMENTS

This work is co-financed by the Ministry of Education, Science and Technological Development of the Republic of Serbia on the base of the contract whose record number is 451-03-68/2022-14/200108. The authors thank the Ministry of Education, Science and Technological Development of the Republic of Serbia for supporting this research.

REFERENCES

[1] W. Yang, J. He, C. He, M. Cai, „Evaluation of urban traffic noise pollution based on noise maps“, Transportation Research Part D: Transport and Environment, Volume 87, 2020, 102516, ISSN 1361-9209.

[2] B. Radičević, “Razvoj modela odlučivanja za izbor optimalne smeše zvučno apsorcionih materijala”, Doktorska disertacija, Fakultet za mašinstvo i građevinarstvo u Kraljevu, Univerzitet u Kragujevcu, Kraljevo, Srbija, 2016.

[3] C. Zhang, J. Li, Z. Hu, F. Zhu, Y. Huang, “Correlation between the acoustic and porous cell morphology of polyurethane foam: Effect of interconnected porosity”, Materials & Design, Volume 41, Pages 319-325, 2012, ISSN 0261-3069.

[4] C. Zhong, G. Li, Z. Meng, “Beluga whale optimization: A novel nature-inspired metaheuristic algorithm”, Knowledge-Based Systems, Volume 251, 2022, 109215, ISSN 0950-7051.

[5] A. Faramarzi, M. Heidarinejad, S. Mirjalili, A.H. Gandomi, “Marine Predators Algorithm: A nature-inspired metaheuristic”, Expert Systems With Applications, Expert Systems with Applications, Volume 152, 2020.

[6] SRPS EN ISO 10534-2, Akustika - Određivanje koeficijenta apsorpcije zvuka i impendanse u Kuntovoj cevi - Deo 2: Metoda transfer-funkcije

[7] M.E. Delany, E.N. Bazley, “Acoustical properties of fibrous absorbent materials”, Appl. Acoust., Vol. 3, № 2, p. 105–116, 1970, DOI:10.1016/0003-682X(70)90031-9

[8] I.P. Dunn, W.A. Davern, “Calculation of acoustic impedance of multi-layer absorbers”, Appl. Acoust., Vol. 19, № 5, p. 321–334, DOI:10.1016/0003-682X(86)90044-7, (1986)

[9] I.Fister Jr., Xin-She Yang, I.Fister, J.Brest, D. Fister, “A Brief Review of Nature-Inspired Algorithms for Optimization”, Elektrotehniški vestnik 80(3), 116–122, 2013.

University of Nis
Faculty of Occupational Safety

„Politechnica“ University of Timisoara
Faculty of Mechanical Engineering

27th International Conference

NOISE AND VIBRATION

Niš, 20 - 21. 10. 2022.

VIBRATION

University of Nis
Faculty of Occupational Safety
„Politechnica“ University of Timisoara
Faculty of Mechanical Engineering
27th International Conference
NOISE AND VIBRATION
Niš, 20 - 21. 10. 2022.

CONDITION MONITORING OF INDUSTRIAL SYSTEM FROM THE VIBRATION ASPECT

Borivoj Novaković[1], Ljiljana Radovanović[1], Luka Đorđević[1], Mića Đurđev[1]

[1] University of Novi Sad, Technical faculty “Mihajlo Pupin” Zrenjanin, email:borivoj.novakovic@tfzr.rs

Abstract - *Condition monitoring of industrial systems is presented in the paper through the aspect of implementation of vibrodiagnostics. Vibrations on the industrial fan system were analyzed, as well as corrective measures performed through the process of dynamic balancing, i.e. impeller balancing. Condition based maintenance greatly increases the efficiency of the system as well as the service life of the system. Most downtime is caused by inadequate maintenance approach, which in this case is avoided by using adequate testing system technology and technology. Vibrations measured on the system were analyzed from the aspect of vibration speed and through the FFT spectrum.*

1. INTRODUCTION

From the aspect of maintenance, it most directly affects potential production downtime due to certain machine failures and machine parts. In order to avoid undesirable delays, it is necessary to plan the maintenance method in a quality and detailed manner, ie. to terminate all elements related to the maintenance of technical systems, starting with people, through equipment and methods. Condition based maintenance is a method that reduces the uncertainty of the operation of equipment and machines, ie increases the reliability of technical systems. Predictive maintenance aims to predict the optimal time point for maintenance actions, taking into account information about the system’s health state and/or historical maintenance data. It tries to avoid the premature and costly repair of a system, while at the same aiming to ensure a timely repair prior to a failure. Conditional monitoring represents a revolution in system maintenance, as well as a methodology that within your system uses modern equipment for diagnostics. In this way, the system leads to constant monitoring, which allows to increase the productivity and efficiency of production [1]. The essence of the predictive concept is reflected in the use of non-destructive techniques in order to determine potential failures very early, so that appropriate corrective actions or repairs are planned in time only when there is a real need for it [2,3]

Vibration-based condition monitoring is an important approach to ensure the reliability of industrial machines [4,5]. These methods are aimed at predicting the state and thus enable the prediction of downtime and failures [6,7]. The method of vibration measurement is probably the best-known method within the scope of this concept, as the most widespread concept in this segment [8].

2. MATERIAL AND METHOD

The task of the modern diagnostic method is to find out the state of the machine and its elements through vibration signals without stopping the process. Spectral analysis gives a clear picture of the problems that occur on rotary machines, in this case it refers to pumps, while for a more detailed state of the system, e.g. bearings uses time domain analysis (Time Waveform Analysis).

When measuring mechanical vibrations, it is necessary to approach the measuring points in detail, first from the aspect of visual control, then by precise placement of sensors, in the places where the bearings are located in the system, in order to fulfill the items of the standards of access to the measurement of mechanical vibrations.

During the measurement and analysis of the collected data, the Adash VA4 device was used.

2.1 Vibration measurement and data analysis

In order to perform the measurement and analysis in the best possible way and in order to carry out an accurate prediction of the state, it is necessary to know the system in detail, operating conditions and operating parameters.

In this paper, measurements were made on pressure pumps in substations that serve to push coolant into the system. The exploitation of these systems is carried out in the time of effective 16 working hours during one working day, which in total time is 24 hours. Such data indicate that these are highly loaded systems whose reliability and availability must be at the highest level. Fig. 1 shows vibrations in the vertical direction on the pump.

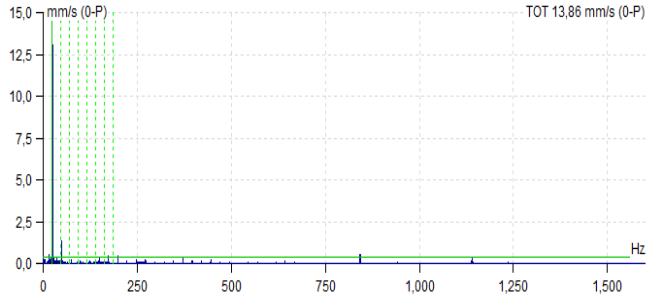

Fig. 1 *Vibrations of the pump in the vertical direction*

From the spectral analysis in Fig. 1, one can see a pronounced first peak at a frequency of 25 Hz, which clearly indicates an imbalance in the system, however, at a frequency of around

800 Hz, a detail appears that may also indicate problems with the bearings.

In order for the picture to be complete, it is necessary to show the spectrum from the horizontal direction, which is shown in Fig. 2.

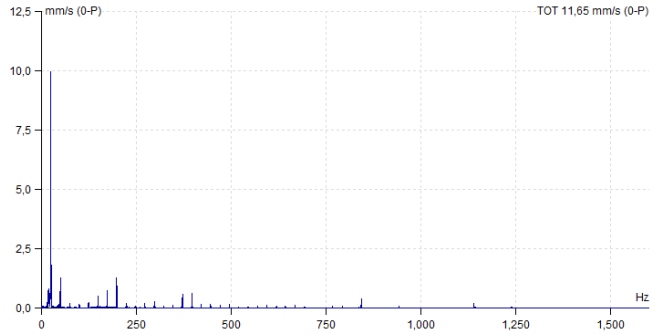

Fig. 2 *Vibrations of the pump in the horizontal direction*

From Fig. 2 it can also be seen as in Fig. 1, so it is necessary to access the detailed analysis of the bearings, through the G method.

The spectrum displayed through acceleration, i.e. the G method, facilitates access to the analysis of the condition of the bearings and the discovery of more detailed data on the bearing failure zone.

Fig. 3 shows the spectrum of vibration acceleration at the measuring points.

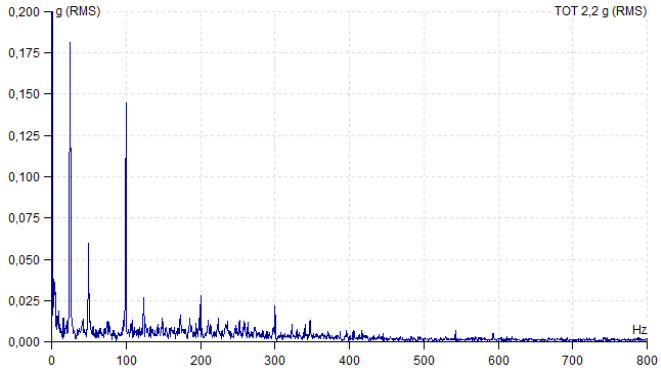

Fig. 3 *Vibrations by the G method in the vertical direction*

Fig. 4 shows the spectrum of vibration acceleration at the measurement points in the horizontal direction.

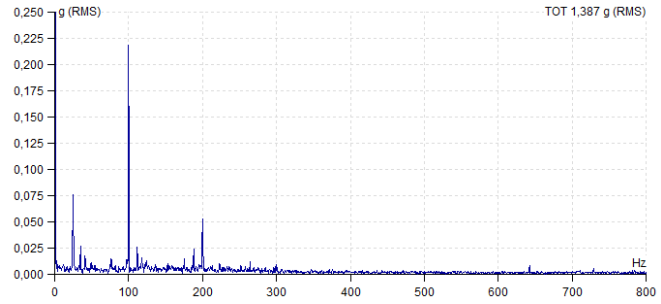

Fig. 4 *Vibrations by the G method in the horizontal direction*

The spectral diagrams from Fig. 3 and 4 indicate that the bearings are in the first stage of failure, that is, there is a high probability that this is related to damage to the outer race of the bearing at some initial stage.

Considering that the analysis of the vibrations from Fig. 1 and 2 established an imbalance of the system at high vibrations, which range in the range of about 12 mm/s, which is far more than is allowed according to the ISO standard, whose limit of permissible vibrations is around 4, 5 mm/s, it is necessary to take measures, i.e. carry out the process of balancing the impeller. During the process of balancing the impeller, it is necessary to replace the bearings in order to carry out the entire maintenance process when stopping the machine and thus avoid unnecessary stopping of the system.

In order to get a clear picture of the actual state of vibrations on the bearings themselves, Time Waveform analysis of the received signals is also used. Fig. 5 shows the spectrum in the time domain for vibrations in the vertical direction.

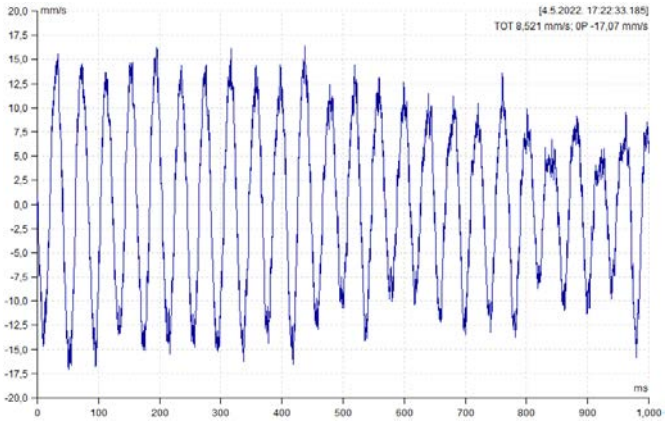

Fig. 5 *Vibrations in the time waveform signal in the vertical direction*

Fig. 6 also shows the time domain in the horizontal direction.

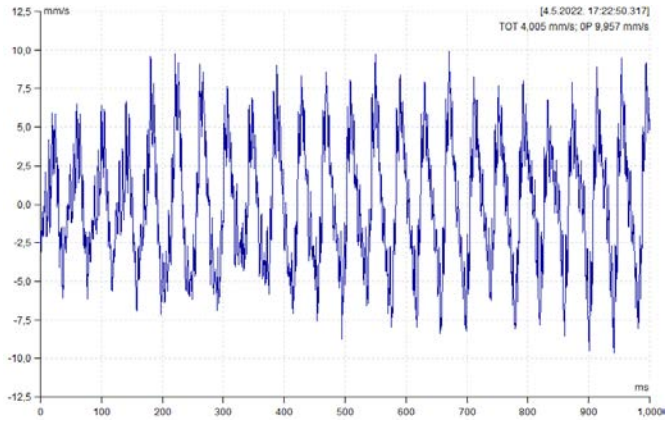

Fig. 6 *Vibrations in the time waveform signal in the horizontal direction*

Fig. 5 and 6 show the vibrations in the time domain from the aspect of the measured values of the vibration speed. In order to fully perform the analysis in the time domain, it is necessary to display the vibration accelerations in the time domain.

Fig. 7 and 8 show vibrations in the time domain from the aspect of vibration acceleration.

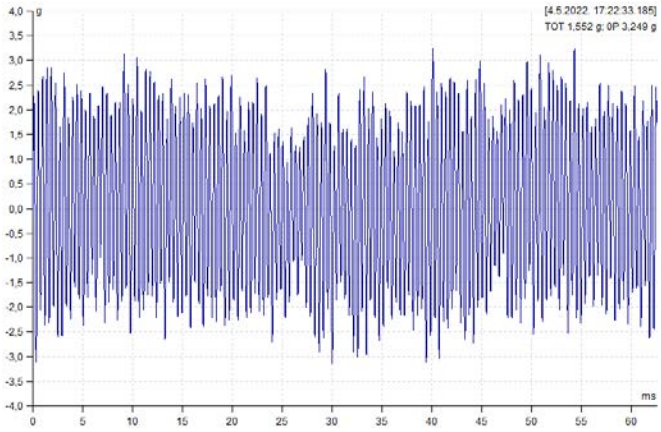

Fig. 7 *Acceleration of vibrations in the time domain in the vertical direction*

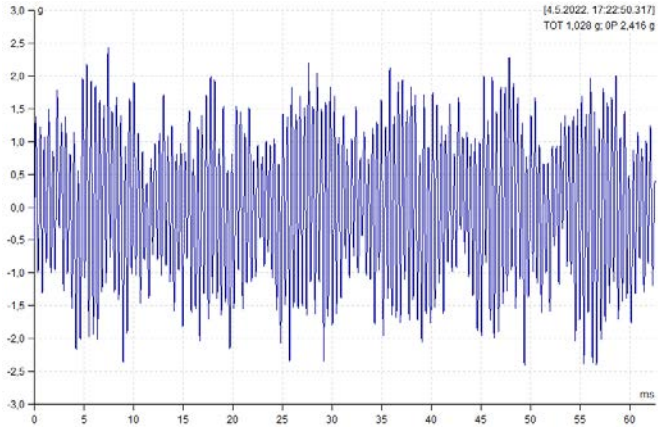

Fig. 8 *Acceleration of vibrations in the time domain in the horizontal direction*

Analyzing the time domains, a detailed analysis identified problems on the outer track of the bearing in the initial phase. The proposed measure is to replace the bearing with a new one during the process of balancing the impeller, in order to achieve optimal pump operating conditions.

3. CONCLUSION

Predictive maintenance is one of the main features of modern ways of maintaining technical systems. In order to implement and carry out predictive maintenance in a quality manner, it is first of all necessary to analyze in detail the System that maintenance deals with. After knowing all the advantages and disadvantages of the technical system that should be subjected to the predictive type of maintenance, a detailed analysis is approached, i.e., technical diagnostics. The importance of vibrodiagnostics and in general detailed system diagnostics is reflected in the prevention of major downtimes, the prediction of major system failures. In this way, unplanned downtime of machines and the so-called indirect maintenance costs, which represent the largest item from the economic aspect, are largely avoided.

REFERENCES

[1] B. Novaković, B., Lj. Radovanović, D. Žikić, S. Vlačić, "Conditional Monitoring in Industry 4.0", *X International Symposium Engineering Management and Competitiveness (EMC 2020)*, pp. 93-97, Zrenjanin, June, 2020.

[2] M. Milovančević, V. Nikolić, D. Petkovic, L.Vracar, E. Veg, N. Tomic, S. Jović, "Vibration Analyzing In Horizontal Pumping Aggregate By Soft Computing", *Measurement*, vol. 125, pp. 454-462, September, 2018.

[3] M. Babić, M. Lazić, "Principi Definisanja Alarma I Limita Stanja Ulja U Eksploa++taciji", *VIII Internacionalna konferencija o Tribologiji*, pp. 177-186, Oktobar, 2003.

[4] B. Novaković, Lj. Radovanović, R. Ivetić, V. Šinik, M. Đurđev, L. Đorđević, „CBM Concept-Predictive Maintenance-Vibration Analysis And Balancing Process Of Industrial Fans", *X International Conference Industrial Engineering and Environmental Protection 2020 (IIZS 2020)*, pp. 208-123, October, 2020.

[5] Q. Huang, B. Tang, L. Deng, "Development Of High Synchronous Acquisition Accuracy Wireless Sensor Network For Machine Vibration Monitoring", *Measurement*, Vol. 66, pp. 35-44, April, 2015.

[6] A. Theissler, J. Pérez-Velázquez, M. Kettelgerdes, Elger, "Predictive Maintenance Enabled By Machine Learning: Use Cases And Challenges In The Automotive Industry", *Reliability Engineering & System Safety*, Vol.215, pp. 107864, November, 2021.

[7] X. Li, Q. Ding, J. Sun, "Remaining Useful Life Estimation In Prognostics Using Deep Convolution Neural Networks", *Reliability Engineering & System Safety*, Vol. 172, pp. 1-11, April, 2018.

[8] S. Amari, L. McLaughlin, H. Pham, "Cost-effective Condition-Based Maintenance Using Markov Decision Processes", *Reliability and Maintainability Symposium*, pp.464-469 , 2006.

BRÜEL & KJÆR
SOUND & VIBRATION
MEASUREMENTS

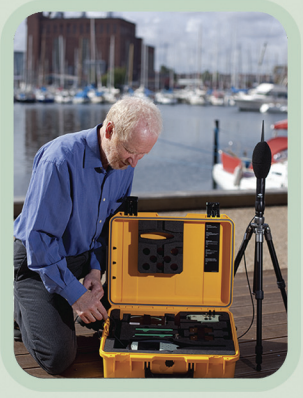

We help our partners and customers
measure and manage
the quality of sound and vibration
in products and enviroment

With more than 90 sales offices or local agents,
we provide immediate and comprehensive
customer support

Contact your local
sales representative:

RMS d.o.o.
Partizanske avijacije 12/3
11070 Novi Beograd, Srbija
Tel.: +381(0)11 2280 951
Fax: +381(0)11 2280 751
www.rms.rs

Brüel & Kjær
an HBK company

University of Nis
Faculty of Occupational Safety
„Politechnica“ University of Timisoara
Faculty of Mechanical Engineering
27th International Conference
NOISE AND VIBRATION
Niš, 20 - 21. 10. 2022.

THE IMPORTANCE OF ADJUSTMENT OF AXIS AND BALANCING ON THE DYNAMIC BEHAVIOR OF THE TURBINE-ELECTRIC GENERATOR ASSEMBLY IN SMALL HYDRO POWER PLANTS

Dragan Jovanović[1], Milena Mančić[2], Miomir Raos[2], Marko Mančić[1], Milan Protić[2], Milena Medenica[2]

[1] University of Nis, Faculty of Mechanical Engineering , Serbia, milena.mancic@znrfak.ni.ac.rs
[2] University of Nis, Faculty of Occupational Safety, Serbia

Abstract - *The importance of renewable energy sources is increasing, especially at the time of the emerging energy crisis. As one of the most important renewable energy sources, hydroelectric power plants that are installed on small watercourses are seen. Small hydropower plants are installed on watercourses with mostly flowing water or with small reservoirs. Their dynamic behavior is specific because they use different types of water turbines. The paper shows the results of adjusting the alignment of the tube and the generator, which resulted in quieter operation of both aggregates and a lower load on the construction object, which prevented the devastation of the building structure, which in this specific case shown is almost a century old. Analysis of the vibration spectrum gives potential causes of vibrations on the turbine generator assembly, which is also shown in the paper. The paper presents the results of the dynamic state of vibrations after alignment adjustment, which indicate that with alignment adjustment measures, even very old aggregates that have been in operation for more than a hundred years can be maintained in full technical and operational readiness.*

1. INTRODUCTION

The energy crisis of 2022 has once again put the importance of renewable energy sources in the foreground, with wind and solar energy occupying a special focus in the whole world, but the construction of these capacities requires significant investment [1]. Serbia has a large number of small watercourses on which the installation of so-called small hydropower plants has been stopped by numerous environmental organizations. That is why it is important to maintain and increase the capacity of already existing hydroelectric power plants that were installed in Serbia at the beginning of the last century. The construction facilities in which those power plants were installed, as well as the dams and reservoirs they use, are at the end of their useful lives. That is why the dynamic behavior of the turbine power unit system is important to be maintained to modern technical standards and to ensure that vibrations due to operation are not transmitted to the environment and the building itself. The technical systems in small hydroelectric power plants were mostly made by the then leading manufacturer of generators, "Siemens & Halske", with years of production, but they are in good condition and the turbines were changed depending on the wear of the materials. This paper presents some modern approaches to improving the functional capabilities of machines whose technical solutions are a century old. The measured parameters are related to: - levels of vibrations, in the directions of coordinate axes, according to ISO 10816-1. - parameters of condition of bearing through the index of bearing condition BCU (Bearing Conditions Unit) and BCS (Bearing Spectrum Conditions) - analysis of the characteristic frequency of vibration in the spectrum, presented by FFT (Fast Fourier Transformation) [2].

2. ANALYSIS OF THE PROBLEMS OF OLD ELECTRICAL POWER STATIONS FROM THE ASPECT OF VIBRATION CONDITIONS

At the time of the creation of today's "small" hydropower plants, they were large because the needs for electricity and the development of industry were of such a scale that they covered. That is why the electric generators were of adequate power and generally ranged from 150 kW to 350 kW at most. Depending on the watercourses, water turbines of different types were used. The main problem in the operation of the power plant is the connection of the water turbine and the power unit, and the problems in operation are mainly caused by the imbalance of parts of the technical system and misalignment at the point of connection of the turbine and the unit. The old technical solutions were mainly based on sliding bearings which were suitable for solutions with low speeds of 250 rpm, while they were later replaced in the middle of the last century with rolling bearings for higher speeds of 750 rpm. Wear phenomena on the sliding bearings cause major problems in the operation of the entire assembly, which are manifested in system resonances, as a result of which high levels of vibration occur on parts of the building foundation, which cause cracks on the foundation plates and can lead to more serious consequences, such as the loosening of the entire building structure. Thus, on the foundation plate of HPP Sveta Petka in Ostrovica near Nis, the level of vibrations rose to 8 mm/s (RMS) at one point, which indicated the need to strengthen the construction of the hydroelectric power plant, which is not an easy and cheap task at all. In technical practice the exact criteria are made for the assessment of the system status based on the measurement of the absolute vibration of the bearings on the outer surface of the machine [3]. By analyzing the spectrum of vibrations, it was

established that the cause of the phenomenon was the electric "shaking" of the generator, which was caused by the asymmetric magnetic field of the machine, which was remedied by special methods for adjusting the gap of the magnetic field of the generator and the axis of rotation, after which the occurrence of vibrations was reduced to the permissible limits. Figure 1 shows the principle diagram of a power unit with a turbine.

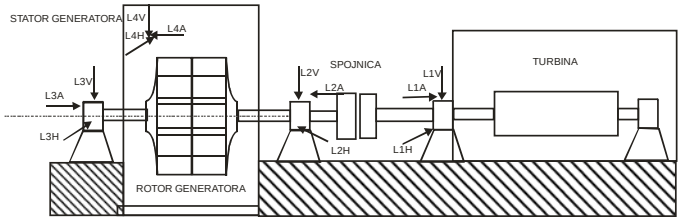

Fig. 1 *Schematic representation of measuring points for measuring vibrations of the turbine power unit system*

As seen in Figure 1 there are predetermined places, measuring points, where the equipment (measuring devices) is situated [2].

The first measuring point is before the RG (rotor generator).

In this paper, the difficulties that three different small hydro power plants are facing are shown.

Figure 2 shows the vibration spectrum of the machine after the correction, where it can be seen that the influence of the electromagnetic field of the generator is reduced.

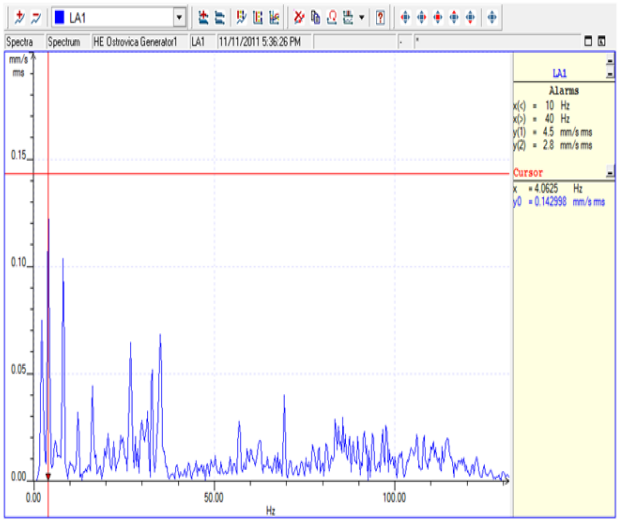

Fig. 2. *Vibration analysis of generator 1 HE Sveta Petka*

By analyzing all the measured vibrations, it was established that the highest peak is at the frequency of the turbine rotation, but that the other harmonics indicate a certain misalignment of the turbine shaft and the generator shaft.

In Figure 3 and Figure 4 is presented the appearance of the unit in real operation, agregate 1 HPP "Sveta Petka" and the real time adjusting the alignment of the same aggregate 1. The first figure, FFT analysis diagram is done for the same spot.

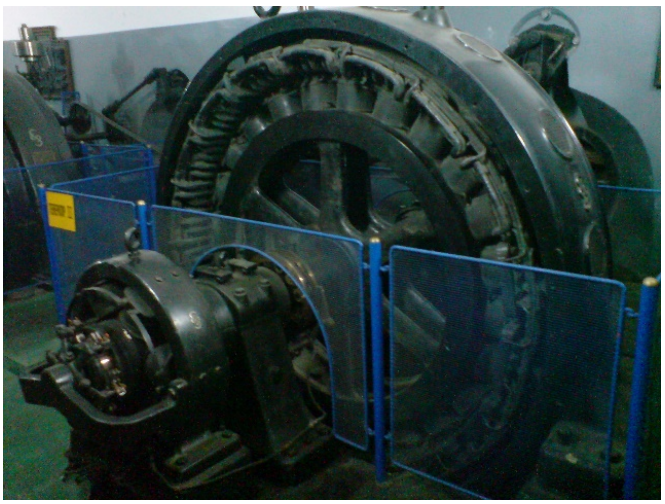

Fig. 3. *Appearance of the unit in real operation, agregate 1 HPP "Sveta Petka"*

Fig. 4. *Adjusting the alignment of aggregate 1 HPP "Sveta Petka"*

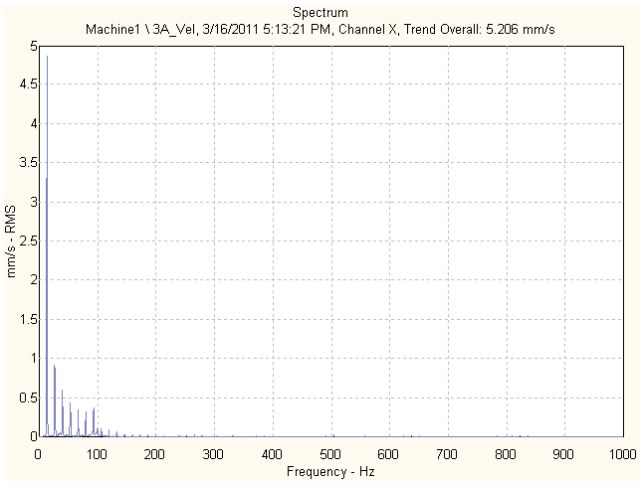

Fig. 5. *Frequency spectrum of turbine 1 HPP Vučje in axial direction*

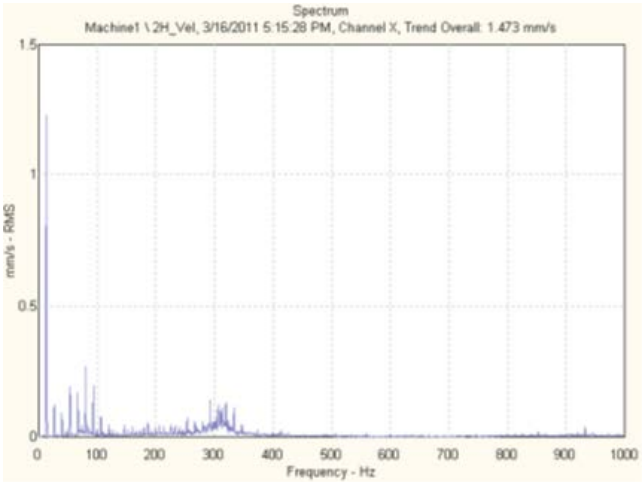

Fig. 6. *Frequency spectrum of turbine 1 HPP Vučje in horizontal direction*

The other type of aggregate in HPP Vučje was treated with the same methodology. Spectral analysis established the influence of the imbalance and misalignment of the shaft of the flywheel mounted on the turbine and the electric generator (Figure 5 and Figure 6).

Based on the analysis, it was established that the cause of the occurrence lies in imbalance and misalignment, so by combining both corrections, the turbine was brought to a functional state. The problem with balancing the machine is that on older machines, masses can only be added or subtracted at points of the magnet poles where there are technical possibilities, so ideal balancing is not always possible because the required mass cannot be accommodated.In the specific case, a mass of 9,000 grams was required, but only a mass of 1,100 grams could be accommodated. By correcting the misalignment, good dynamic behavior of the turbine was obtained.

Figure 7 and figure 8 presents the real time measurements of vibrations, balancing and aligment adjustment of the generator assembly in small HPP „Vučje“.

Fig. 7. *Vibration analysis of the generator assembly*

Fig. 8. *Balancing and alignment adjustment of the generator assembly*

The third type of problem with small hydropower plants is their repair and the increase in generator power. In those cases, the building structure is changed and a new aggregate is installed, which should be brought into the technical standards of the necessary standards, as was done at the HPP “Jelašnica” near Vladičin Han.

Fig. 9 *Alignment adjustment of the new generator and turbine*

In this case the aligment adjustment of the new generator and turbine was done, and in figure 9 it is presented the layout. Figure 10 shows the aligment adjustment in vertical and horizontal axis, and the greater declination is in horizonatal axis.

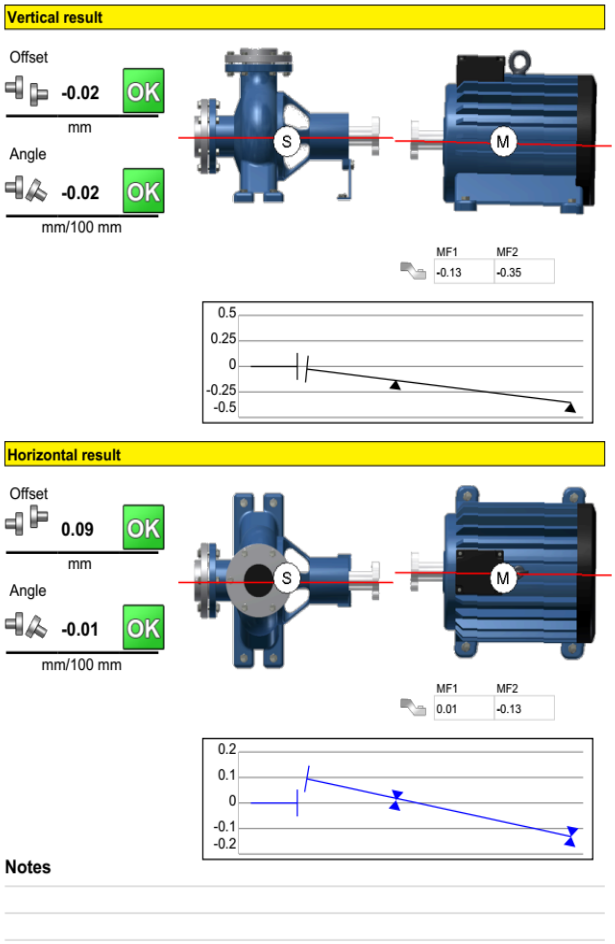

Fig. 10 *Alignment adjustment*

CONCLUSION

This paper shows three different cases of old and still applicable small hydro power plants. The application of modern diagnostic methods and equipment can significantly increase the operational readiness of small hydropower plants and their high-quality work, both with old generators and turbines and with reconstructed generators. Diagnostic methods should indicate the correct choice of improving the dynamic behavior of the machines, and mostly these are problems of alignment and imbalance of rotating masses as shown in this paper. Eliminating these phenomena in old machines requires the application of special procedures considering that at the time of their design, these methods were not present.

REFERENCES

[1] Qi Zhang, Xifeng Wu, Yu Chen, Is economic crisis an opportunity for realizing the low-carbon transition? A simulation study on the interaction between economic cycle and energy regulation policy, Energy Policy, Volume 168, 2022, 113114, ISSN 0301-4215, https://doi.org/10.1016/j.enpol.2022.113114.

[2] P. Girdhar and C. Scheffer, ‘’Practical Machinery Vibration Analysis and Predictive Maintenance’’, ISBN 0 7506 6275 1, Elsevier.

[3] D. Jovanović, N. Živković, M. Raos, Lj. Živković, M. Jovanović, M. Prašćević, ‘’Testing of level of vibration and parameters of bearings in industrial fan’’, Applied Mechanics and Materials, Vol. 430, DOI 10.4028/www.scientific.net/AMM.430.118, pp 118-122, 2013.

[4] ISO 10816-1 - Mechanical vibration -- Evaluation of machine vibration by measurements onnon-rotating parts -- Part 1: General guidelines

[5] S. Jovanović, D. Jovanović, 'Dinamičko uravnoteženje kao najvažniji postupak za poboljšanje dinamičkog ponašanja ventilatora", XXII Konferencija Buka i vibracije, Niš, ISBN 978-86-6093-019-6, pp161-164,

[6] D. Jovanović, M. Jovanović, N. Živković, Lj. Živković, M. Raos, “Belt conveyor drive gearbox problem caused by unpaired gears-a case study”.

[7] D. Jovanovic, M. Jovanovic, M. Raos, N. Zivkovic, M. Stankovic, M. Protic, “Vibration analysis of insufficiently repaired well pump - a case study”, Applied Mechanics and Materials, Vol. 801 (2015) pp 207-212 doi:10.4028/www.scientific.net/AMM.801.207

University of Nis
Faculty of Occupational Safety
„Politechnica“ University of Timisoara
Faculty of Mechanical Engineering
27th International Conference
NOISE AND VIBRATION
Niš, 20 - 21. 10. 2022.

VIBRATIONS APPEARANCE IN SISO CASCADE CONNECTED SYSTEMS WITH RANDOMLY SELECTED PARAMETERS

Bojana M. Zlatkovic[1], *Biljana Samardzic*[2]

[1] University of Nis, Faculty of Occupational Safety, Serbia, bojana.zlatkovic@znrfak.ni.ac.rs
[2] University of Nis, Faculty of Science and Mathematics

Abstract - *The appearance of vibrations in cascade connected SISO systems with randomly chosen parameters is analyzed in this paper. Vibrations are amplified with each successive cascade and they can bring system to instability and eventually to chaos and to a state of failure. Choosing the adequate parameter values the occurrence of vibrations and chaos can be controlled. The appearance of vibrations and chaos is analyzed using the example of rubber strip transportation system which is one of the important system in tyre industry.*

1. INTRODUCTION

Vibrations can appear in a variaty of natural phenomena. The types and sources of vibrations and the propagation of vibrations depend on the characteristic of the analysed system. Vibrations represent continuing motion, often periodic, of a liquid or solid body within certain spatial limits.

As their undesirable and avoided results there are noise, wear and energy waste. Vibrations are very important aspect to take into consideration when designing a system because they can produce failure of components and in general the failure of the whole system. Also, vibrations can bring system into instability and the chaos can appear in the system.

Therefore many vibration control techniques are developed in order to prevent unwanted system behaviour. Vibrations can occure in the presence of parametric uncertainties and disturbances.

In this paper the vibrations appearance in cascade connected SISO (Single Input Single Output) systems with randomly chosen parameters is analysed. Also, system parameters can be random variables with different probability distribution. Vibrations in the systems can be controlled selecting the adequate parameter values. These systems consist of small number of nonlinear SISO subsystems described by equation $x_{k+1} = f(x_k, r)$, where x_k and x_{k+1} are input and output of the k-the cascade respectively, Fig. 1. Nonlinear function f and its parameter r representing the amplification of SISO system are common for all cascades.

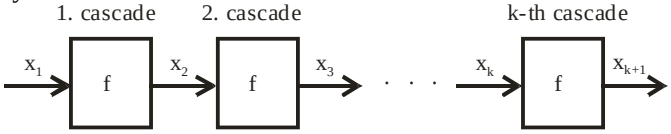

Fig.1 *Block scheme of SISO cascade connected nonlinear system*

In addition to the tendency to oscilations, [1,2], cascade connected SISO systems have one important characteristic and that is the possibility of chaos appearance, [3-7]. As is well known, chaos can occure as a consequence of bifurcation in nonlinear system at certain parameter values.

In cascade connected SISO systems, the iteration is not temporal, but spatial. Each cascade in the system represents one iteration. The passage of the signal through a series of cascade connected subsystems, of the same structure, represents an iterative process. Vibrations are transmitted through the cascades in the same way. The vibrations are amplified with each successive cascade. Choosing the right parameter values the appearance of vibrations can be avoided. This way, other problems such as instability, chaos and, ultimately, system failure can be prevented.

In this paper the appearance of vibrations is analyzed using the example of rubber strip transportation system which is one of the important system in tyre industry, [5].

2. THE RUBBER STRIP TRANSPORTATION SYSTEM

Rubber strip transportation system is the example of cascade connected SISO systems, Fig. 2. This system is very important in the tyre industry because rubber strip forms the external protective part of a tyre. The strip needs to be cooled down to the room temperature in order to be cut into pieces of certain lenght depending on tyre dimension. The specificity of this system is that during transport, due to cooling, the length of the rubber changes. Rubber compresses so the system consists of more subsystems because the tension of the rubber must be avoided, i.e. the rubber is relaxed on the transition from one transporter to another. These systems consist of 7 – 13 cascades.

The rubber length between the transporters determines the velocities of transporters. At great transporters velocities vibrations can appear and they are amplified with each successive transporter.

The causes of the change in the length of the strip are of stochastic nature (ambient temperature, plasticity, elasticity, friction, etc.). Therefore, it is difficult to achieve that the speed ratio of all transporters is constant, which is a technical requirement. The consequence of the high sensitivity of the system to changes in parameters values is the appearance of vibrations and chaotic dynamics.

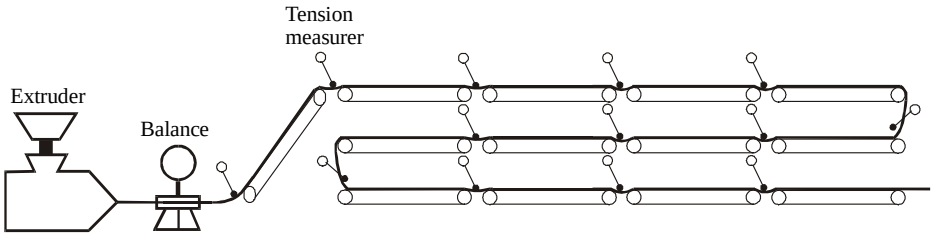

Fig. 2 *Rubber strip transportation system*

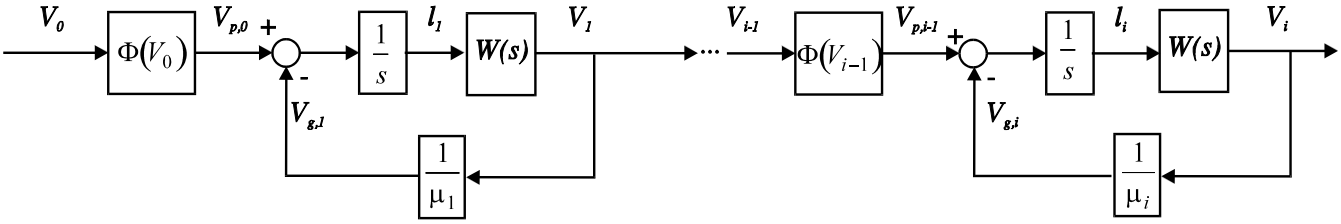

Fig. 3 *Structural scheme of rubber strip transportation system*

The analysis will be performed on the structural scheme of rubber strip transportation system, Fig. 3.

System dynamic is described using next equations:

$$\frac{dl_i}{dt} = \left(\Phi(V_{i-1}) - \frac{1}{\mu_i} V_i \right), \quad i = 1,2,\ldots,n \tag{1}$$

$$T_1 T_2 \frac{d^2 V_i}{dt^2} + (T_1 + T_2)\frac{dV_i}{dt} + V_i = k l_i \tag{2}$$

where:

- l_i is the lenght of the strip between the *i*-th and the *(i+1)*-th transporters,
- V_i is the velocity of the *i*-th transporter,
- μ_i is the strip compression coeficient in the *i*-th transporter,
- k is the gain coefficient of the potentiometer,
- $W(s)$ is the transfer function of the motor with the load,
- T_1, T_2 are the time constants of the subsystem loaded with strip material,
- $\Phi(V_i)$ is the transition nonlinearity.

Vibrations can appear in the beginning cascade at great velocities and they are amplified with each successive cascade. Vibrations of one subsystem cause vibrations of the next subsystem. This is the reason why vibrations increase with increasing the number of cascades, Fig. 4.

High vibrations in the beginning cascades can cause the appearance of chaos in the next cascades. This is illustrated by simulation results, Fig. 5. Vibration is unwanted signal and chaos is random behavior of the system.

Vibration can cause the accumulation or stretching of the rubber strip and it can not be cut into pieces of certain length. To prevent this, the velocity of the first cascade (input) must be adjusted.

Choosing the right input values the appearance of vibrations can be avoided and the appearance of chaos can be prevented.

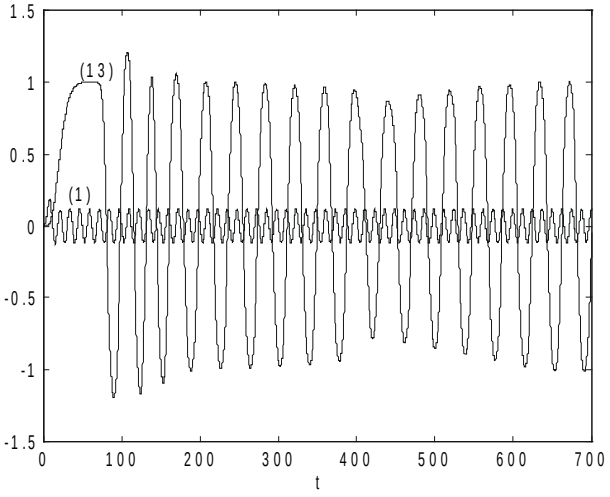

Fig. 4 *Vibrations in the first and thirteenth cascades*

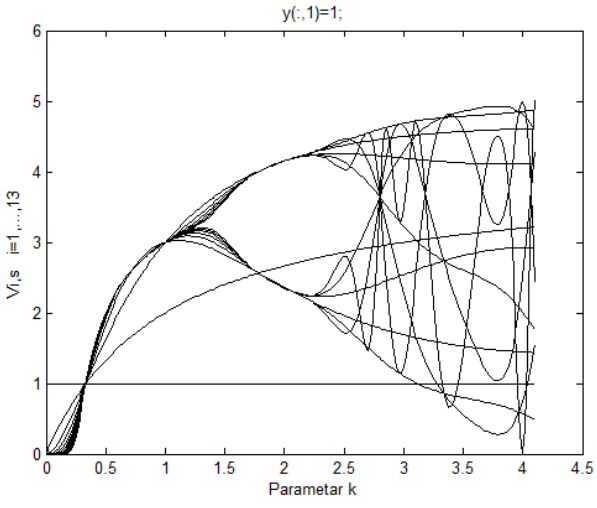

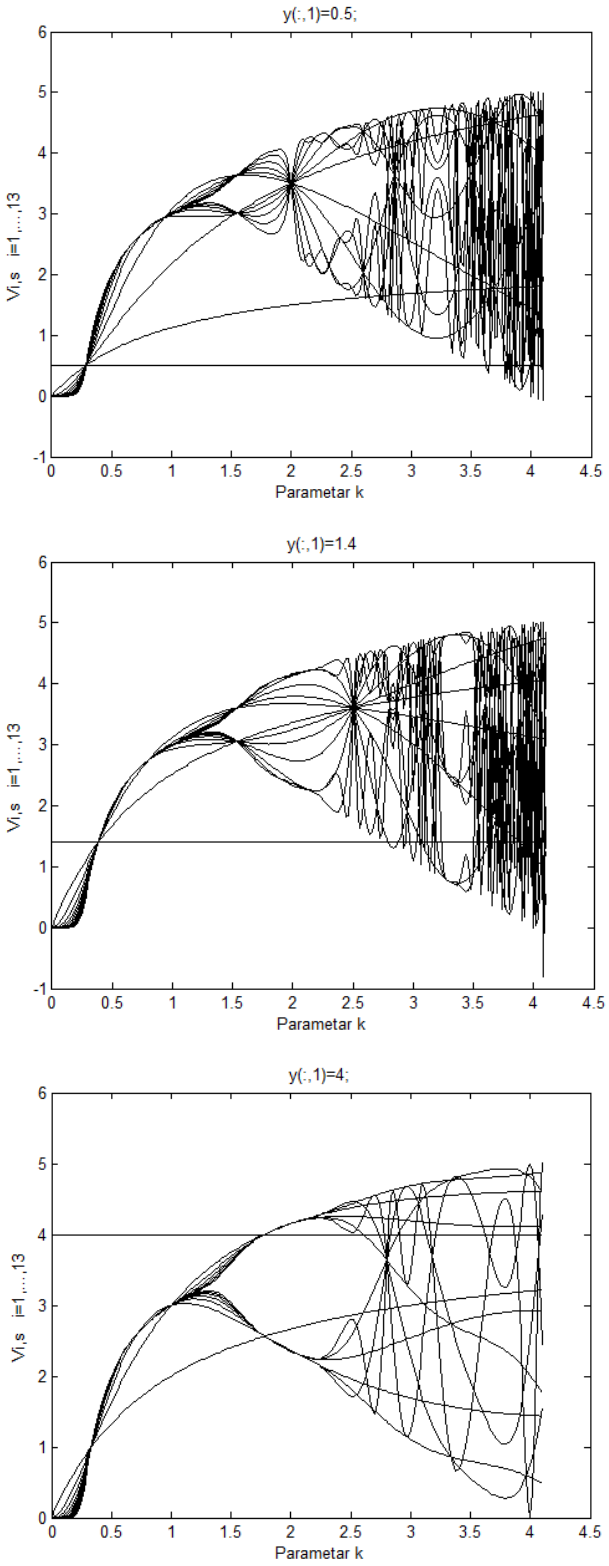

Fig. 5 *Chaos in rubber strip transportation system for different velocity values of the first transporter*

When the velocity of the first transporter has constant value, choosing different values vibrations and chaos can be controlled. In Fig. 5 simulations are given for different input values. It can be seen how different input values affect the occurrence of vibration and chaos.

Also, parameters values change over time and can be presented by some probablity distribution. In Fig. 6 simulations are performed for beta, gamma and exponential distribution of random input.

By analyzing the simulations, it is possible to conclude which parameter values should be avoided in order to prevent vibrations and chaos.

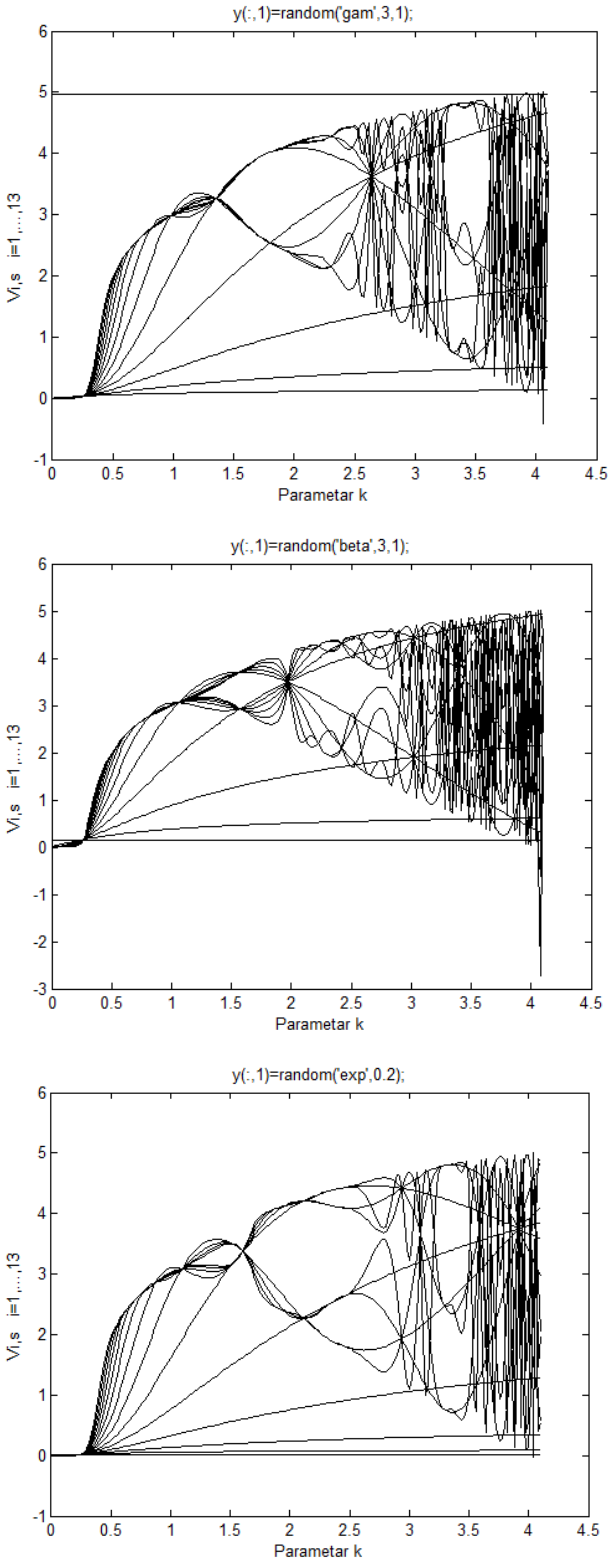

Fig. 6 *Chaos in rubber strip transportation system for different probability density of system input (velocity)*

3. CONCLUSION

Vibrations occur in different types of systems. In this paper the presence of vibrations is shown on example of rubber strip transportation system.

In consideration of the systems structure and the fact that the technological parameters of rubber materials are time variant, one of the characteristic of this system is the possibility of vibrations and chaos appearance.

At higher amplifications, vibrations and chaos can occur. The inadequate choice of parameter values of the system can cause the cracking of rubber strip or its extension, which leads to the system instability, chaos and in an extreme case to the system failure. The results are illustrated by simulations for constant input and random input with beta, gamma and exponential probability distribution.

REFERENCES

[1] B. Danković, "On the appearance of oscillations in cascade systems for transport of rubber strip materials", *Proc. JUREMA* 34, Vol. I, 97-100, 1989.

[2] B. Danković and Z. Jovanović, "O oscilacijama kod automatski upravljanog kaskadno povezanog sistema za transport trakastog materijala", *ELEKTROTEHNIKA* 43 10-11, E1-E3, 1994.

[3] B. Danković, M. Stanković and B. Vidojković, "Simulation of convergent, oscillatory and chaotic dynamics of cascade systems", *Proceedings of the seventh Symposium of Mathematics and its Applications*, Timisoara, pp. 101-106, November, 1997.

[4] B. Vidojković and B. Danković, "Simulacija haotične dinamike kaskadnog sistema primenom programskog paketa MATLAB", *YU INFO* 98, Kopaonik, pp. 497 – 500, Mart 1998.

[5] B. Danković, B. Vidojković and B. M. Vidojković, "On the chaos in cascade systems for rubber strip transportation", *Proceedings of the Fourth International Conference of Heavy Machinery*, Kraljevo, pp. A.97 – A.100, June 2002.

[6] B. Vidojković, B. Danković and Bojana M. Vidojković, "On the Bifurcation Appearance at Nonlinear Cascade Connected Systems", *Proc. TELSIKS 2003, 6th International Conference on Telecommunications in Modern Satellite, Cable and Broadcasting Services*, Niš, Vol. 2, pp. 805 – 808, October, 2003.

[7] B. Samardzic and B. M. Zlatkovic, "Simulation of bifurcation and escape-time diagrams of cascade-connected nonlinear systems for rubber strip transportation", *Nonlinear Dynamics*, Vol. 67, Iss. 2, pp. 1105-1113, 2012.

University of Nis
Faculty of Occupational Safety
„Politechnica“ University of Timisoara
Faculty of Mechanical Engineering
27th International Conference
NOISE AND VIBRATION
Niš, 20 - 21. 10. 2022.

MODELLING AND SIMULATION OF VIBRATIONS IN ELECTRICAL SYSTEMS USING MATLAB/SIMSCAPE

Bojana M. Zlatkovic[1], *Biljana Samardzic*[2]

[1] University of Nis, Faculty of Occupational Safety, Serbia, bojana.zlatkovic@znrfak.ni.ac.rs
[2] University of Nis, Faculty of Science and Mathematics

Abstract - *This paper considers the application of Matlab/Simscape in modelling and simulation of vibrations in electrical systems. The small perturbations of input parameters can greatly change the dynamics of the system. The choice of adequate parameters values can prevent the appearance of vibrations. Simulation is performed on the example of electrical circuit.*

1. INTRODUCTION

The *Matlab/Simscape* is intended for modelling, simulation and analysis of multidomain physical systems, [1]. Instead of the mathematical blocks of *Matlab*'s *Simulink* library, [2, 3], blocks corresponding to physical components such as capacitor, inductor, resistor, damper, spring, etc. are used to form a system model in *Simscape*. Connections are established between the components that correspond to energy flows and signal flows. In this way, the structure of the model corresponds to the structure of the real system and the process of modelling itself resembles the assembly of a real system. The user from the *Simscape* library selects the appropriate blocks and then connects them with lines following the structure of the system.

In this paper the application of *Matlab/Simscape* in modelling and simulation of vibrations in electrical systems is considered. The results are illustrated by the example of an electric circuit

Vibrations are undesirable in electrical curcuits because they can cause energy losses, corrosion and wear, they can change properties of the component or system and lead to failure. That is why is very important to prevent failures due to vibration by eliminating or reducing its effect, [4].

In electrical circuits vibrations are mostly random. They are known as white noise and they are unwanted electrical signal, difficult to predict. In electrical circuits noise can come from anywhere, from external systems as well as from within a circuit itself. In electrical circuits damaged components or loose connections or switches, etc., can be the source of the vibration.

Due to the aging of the component, the values of its parameters change, which affects the proper operation of the component and the entire system. Adequate selection of component parameter values can prevent vibrations or mitigate their effects.
Vibration can be caused by increases in temperatures by physical vibrations, environmental causes, etc. This can, also, change the parameters of the electrical circuit components Vibration that occures due to high temperatures are called thermal noise and it increases with an increase in environmental temperature.

2. SIMSCAPE LIBRARY

Simscape libraries are: *Foundation Library*, *SimDriveline*, *SimElectronics*, *SimHydraulics*, *SimMechanics*, *SimPowerSystems* and *Utilities*. The basic building blocks of *Simscape* are in the *Foundation Library*. There are blocks that represent the real components of different physical domains (electrical, hydraulic, mechanical, pneumatic and thermal domains).

The *Electrical Library* is used for simulation of electrical systems. The blocks of this library are divided into three groups: *electrical elements*, *sources* and *sensors*. The library of *electrical elements* contains the basic elements with which we can realize electrical circuits: resistor, inductor, capacitor, transformer, diode, etc.. The *Electrical Sensors* library contains two sensors: ammeter and voltmeter. Both blocks have three connectors. Two for connection to the electrical circuit (+ and - terminal) and one for measurement and display of measurement results (I-current output, V-voltage output). The *Electrical Sources* library contains DC and AC voltage and current sources.

The *Utilities* library is used to graphically represent the values of physical signals measured by sensors. This library contains the following elements: *Connection Port*, *PS/Simulinc Converter*, *Simulink/PS Converter*, *Solver Configuration* and *Two-Way Connection*. The *PS/Simulinc Converter* element converts *Simscape*'s physical signals (PS) into signals that can be displayed on one of *Simulink's Sinks* blocks (for example, *Scope* - oscilloscope).

The *Simulinc/PS Converter* element converts *Simulinc* signals to physical PS signals, which are inputs to *Simscape* models. The *Solver Configuration* element is a mandatory block in every *Simscape* model. It is connected to any branch of the tested model and serves to define the simulation parameters.

3. MODELLING AND SIMULATION OF VIBRATION IN ELECTRICAL SYSTEM USING SIMSCAPE

The *Simscape* library provides an easier approach to modeling electrical systems. It does not require users to pre-prepared mathematical models for input into a graphic editor, as with *Simulink*. It is only necessary to properly connect the elements of the *Simscape/Electrical* library that resemble real electrical components.

In the following, on the example of specific electrical circuit, we will show the simplicity of modeling and simulation in Simscape and vibration analysis.

Example

A simple approach to modeling the system using the *Matlab-Simscape* and vibration analysis will be explained on the example given in Fig. 1. The components of the system are:

$L = 0.1\text{H}, C = 0.005\text{F}, R = 100\Omega, e_1 = 10\sin\frac{\pi}{10}t, e_2 = 15\sin\frac{\pi}{2}t$

All initial conditions are zero. The output signals of the electrical circuit are current i_1 and voltage on the resistor *R* denoted as u_R.

Simulation results, time dependence of current i_1 and voltage u_R are shown graphically (*Start Time*=0, *Stop Time*=400).
Inductors are one of the critical components of electrical circuit. Their performance has great effect on system performance. That is why inductors should be monitored to detect undesirable conditions such as heating up, saturation, noise and vibration caused by operating conditions.

Resistors are sources of thermal noise. It dependens on three variables: resistance, temperature and bandwidth. Due to agging or heating, the resistance parameters change and vibrations (noise) occur. Because the vibrations are completely random, the electrical signal is noise.

Due to all the above, in this paper the influence of inductor and resistor in given electrical circuit on the occurrence of vibrations is analyzed.

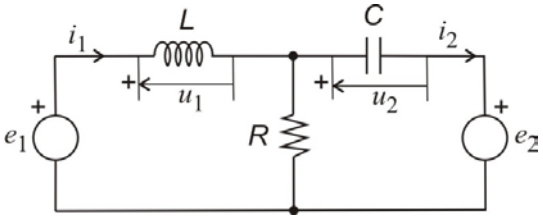

Fig. 1 *Electrical circuit*

Mandatori elements of this *Simscape* model are grounding (*Electrical Reference*) and block *Solver Configuration.*

Since monitoring the waveform of the output voltage on the resistor R is required, we connected the + and - ends of the block *Voltage Sensor* in parallel with it. From the third port of the *Voltage Sensor* block, which is marked with the letter *V*, a physical signal representing the output voltage u_R is brought to the input of the *PS-Simulink Converter block.*
We connected the output of the *PS-Simulink Converter* block to the input of the *Simulink ToWorkspace* block.

It is also required to observe the waveform of the current flowing through the inductor, i_1. Therefore, an ammeter is placed, ie, *Current Sensor* in series, between source e_1 and inductor *L*. From the third port of the *Current Sensor* block, which is marked with the letter *I*, the physical signal representing the output current i_1 is brought to the input of *PS-Simulink Converter* block. We connected the output of the *PS-Simulink Converter* block to the input to the new *Simulink ToWorkspace* block. After starting the simulation, the commands *plot (t, i_1)* and *plot (t, u_R)* are entered in the *Matlab Command Window*, for graphical display of simulation results.

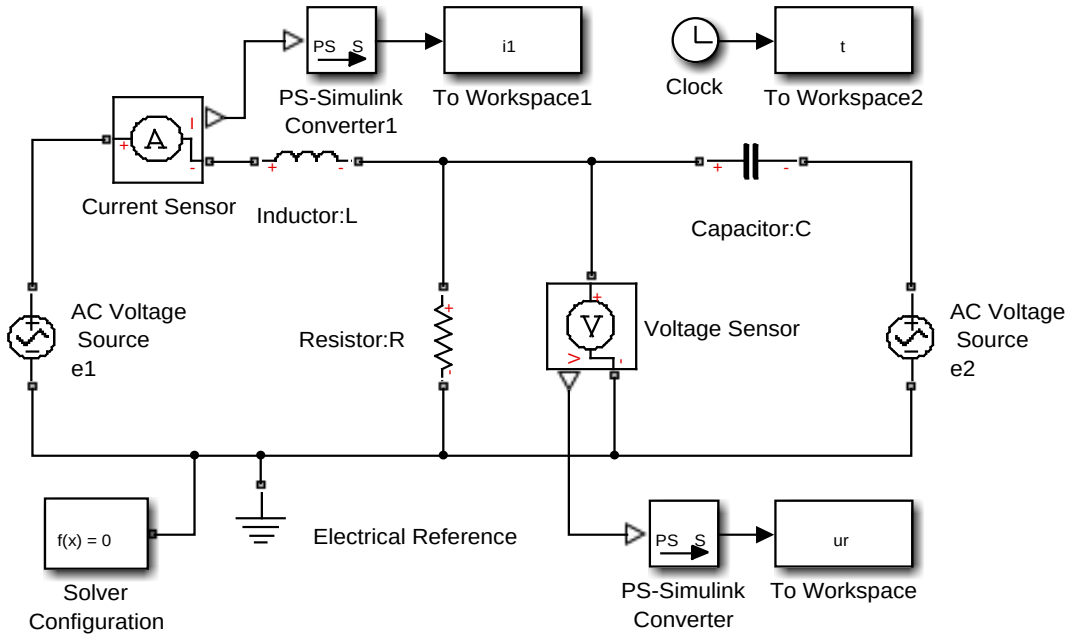

Fig. 2 *Simscape model of electrical circuit*

For the given values of the parameters, vibrations occur only on the inductor as seen in the Fig. 3.

There are no vibrations on the resistor, Fig. 4.

The appearance of vibrations can serve as a test which component of the system causes the vibration.

This way, the occurrence of vibrations can be prevented by choosing the adequate parameter values or by replacing a faulty component.

Thus, serious problems in the circuit such as instability, chaos, system failure can be prevented, also.

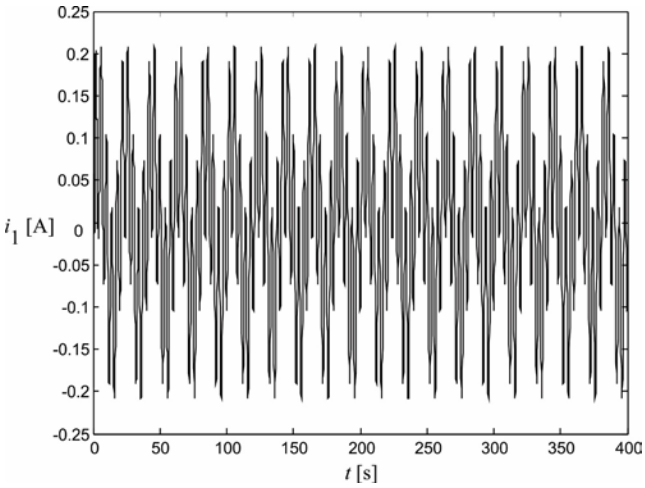

Fig. 3 *Current i_1 time dependence*

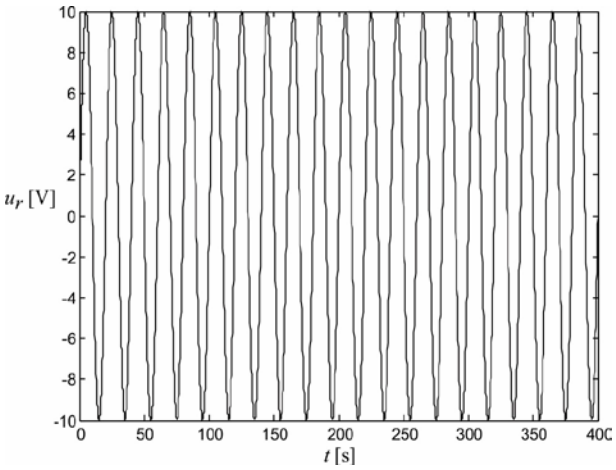

Fig. 4 *Output voltage u_r time dependence*

4. CONCLUSION

Simscape is a simpler approach to system modeling which does not require users to prepare mathematical models in advance for input into a graphics editor. It is only necessary to properly connect the elements of *Simscape* that resemble real components. In this paper using Simscape modelling and simulation of vibration in electrical cuircle is presented.

The choice of adequate parameters values can prevent the appearance of vibrations.

REFERENCES

[1] www.mathworks.com

[2] D. Antić, Priručnik za modeliranje i simulaciju dinamičkih sistema, Niš, 1999.

[3] B. Samardžić and B. M. Zlatković, Automatsko upravljanje, Niš, 2018.

[4] B. M. Zlatković and B. Samardžić: "Vibrations modeling and simulation using stochastic bondsim elements", *Applied mechanics and materials*, vol. 430 (2013), pp. 158-164, Trans. Tech Publications, Switzerland, 2013, *doi: 10.4028/www.scientific.net/AMM.430.158*.

LABORATORIJA ZA BUKU I VIBRACIJE

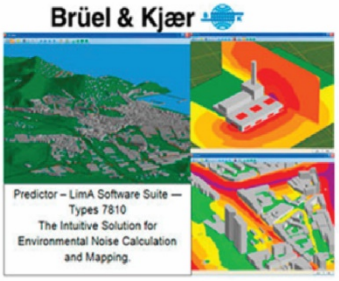

LABORATORY FOR NOISE AND VIBRATION

University of Nis
Faculty of Occupational Safety
„Politechnica“ University of Timisoara
Faculty of Mechanical Engineering
27th International Conference
NOISE AND VIBRATION
Niš, 20 - 21. 10. 2022.

CASE STUDY: EVALUATION OF WBV ACCORDING TO ISO 2631-1 AND ISO 2631-2 FOR WORKERS IN AN OFFICE BUILDING NEAR A CONSTRUCTION SITE

Biljana Beljić Durković [2], Jovan Miočinović [1], Tatjana Radojević [2]

[1] TEHPRO d.o.o., Serbia, biljana.beljic@tehpro.rs
[2] TEHPRO d.o.o., Serbia
[2] TEHPRO d.o.o., Serbia

Abstract - *During the construction of a residential property in a residential and business complex in Belgrade, employees of the one bank's branch office were exposed to the noise and vibrations from the neighbouring construction site. Here the evaluation of WBV for the workers according to standards ISO 2631-1 and ISO 2631-2 is presented.*

1. INTRODUCTION

Whole-Body Vibration exposure is recognized physical risk present in many industries. Though severe vibrations may cause health problems, in the practice of testing of work environment conditions some situations are encountered that require evaluation of vibration effect on comfort and perception. In an office building the employees were exposed to transient environmental conditions during construction of a building in neighbouring construction site. While all the neighbouring residential buildings were temporarily evacuated according to environmental regulations, employed workers were left to their mercy. An assessment was made of noise and vibration impact according to regulations on safety and health at work and a proposal for measures to be taken was given to the employer. Here the results of the evaluation of WBV made both according to ISO 2631-1[1] and ISO 2631-1[2] will be presented.

2. INSTRUMENTATION, SAMPLE AND MEASUREMENT LOCATION AND CONDITIONS

2.1. Instrumentation

For measurements was used SVAN 958 four channels sound (Type 1 IEC 61672-1:2002) and vibration (Type 1 ISO 8041:2005) level meter and analyser with seat accelerometer for whole-body measurements with DYTRAN 3143M1 - IEPE type triaxial accelerometer (Fig. 1).

2.2. Measurement location and conditions

Measurements were made in two offices, one call centre facing the construction site and one training centre that continues the call centre and facing the opposite side of the building relative to the construction site. As the offices are situated at the second floor, additional measurements were made in the building's corridor at the ground floor, first floor and the second floor in front of the entrance to the premises to determine the local variation of the vibration (as required by ISO 2631-2).

Fig. 1 *SVAN 958 four channels sound and vibration level meter and analyser*

Fig. 2 *View of the construction site from the call center office window*

Fig. 3 *Basicentric axes of the human body for standing position according to ISO 2631-1*

Measurements were taken on the floor at the offices, according to ISO 2631-1 in standing position, with the seat accelerometer positioned according to a coordinate system in Fig. 3. The measurement positions are presented in Fig. 4. As a vibration

of limited duration, i. e. during specific construction activities, measurements were taken during such activities, specifically during driving of the steel piles. The duration of measurements was 10 minutes. The workers were exposed to such construction activities two hours a day, between 10:00 and 12:00 or 14:00 and 16:00 depending activity schedule on the construction site.

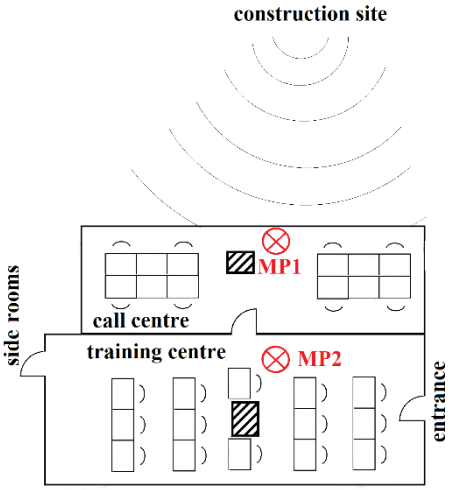

Fig. 4 *Measurement positions in offices in relation to source of vibration*

3. MEASUREMENT RESULTS AND EVALUATION

3.1. Weighted r.m.s. accelerations

Measurements were taken in *x*-, *y*- and *z*-axis oriented as in Fig. 3.

The weighted r.m.s. acceleration is determined for each axis (*x*, *y* and *z*) of translational vibration on the surface which supports the person. When evaluating the effects of vibration on health, assessment of the vibration is made according to equation (1) [1]:

$$a = \left(Max\left\{k_x{}^2 a_{Wd}{}^2 + k_y{}^2 a_{Wd}{}^2 + k_z{}^2 a_{Wk}{}^2\right\}\right)^{1/2} \qquad (1)$$

where multiplying factors k_x = 1,4, k_y = 1,4, and k_z = 1.

When evaluating vibration effect on comfort, for the ISO 2631-1 assessment of the vibration is made according to equation (2) [1]:

$$a_v = (k_x{}^2 a_{Wd}{}^2 + k_y{}^2 a_{Wd}{}^2 + k_z{}^2 a_{Wk}{}^2)^{1/2} \qquad (2)$$

where multiplying factors k_x = 1, k_y = 1, and k_z = 1.

While ISO 2631-1 assessment requires W_k and W_d principal frequency weightings in 1/3 octave bands, ISO 2631-2 assessment requires W_m principal frequency weighting. The instrument setup was to W_k and W_d principal frequency weightings along the corresponding axes with 1/3 octave analysis and logging 200 ms samples. The W_m weighted acceleration is then obtained from 1/3 octave analysis by equation (3) ([1], [2]):

$$a_{W_m} = \left[\sum_i (W_{m_i} a_i)^2\right]^{1/2} \qquad (3)$$

where W_{mi} is the weighting factor for the i-th 1/3 octave band and a_i is the r.m.s. acceleration for the i-th 1/3 octave band. While for the purpose of ISO 2631-1 evaluation the vibration in all three direction is taken into account, for the purpose of ISO 2631-2 evaluation only values obtained in the direction with the highest frequency-weighted vibration magnitude (i.e. *z*-axes) direction are used.

3.2 Measurement results

When taking vibration measurement and analyzing the results certain limitations should be taken into account. Due to mechanical or electrical interferencies when starting the measurement or inadequate measurement interval comparing the dynamic range of the signal-conditioning equipment noise may occur in the measurement result. This should be also kept in mind when calculating the vibration from 1/3 octave bands (equation 2) for low frequencies. For example, to obtain a measurement error of less than 3 dB at a confidence level of 90 % requires a minimum measurement duration of 108 s for a lower limiting frequency (LLF) of 1 Hz and 227 s for a LLF of 0,5 Hz, when the analysis is done with a one-third octave bandwidth ([1]). This noise may easily be seen from logger results as a characteristic “ski slope”. The way of dealing with this apart from proper instrument set up is rewieving measurement loggers and dismissing compromised results, or dismissing compromised parts from logger and performing the calculations on the rest of logged measurement (here logged in 200 ms intervals). In Figures 5. and 6. are given examples of loggers of compromised results for weighted r.m.s. results and 1/3 octave results in low frequencies.

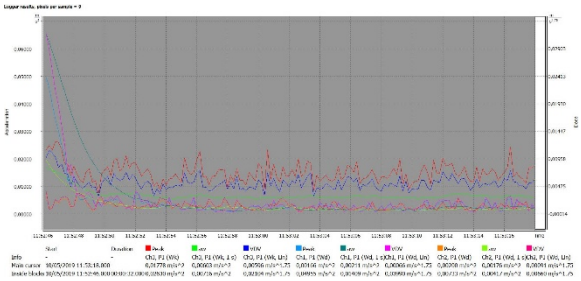

Fig. 4 *Logger results graph for compromised measurement, r.m.s results. A characteristic “ski slope” at the beginning of the graph may be seen.*

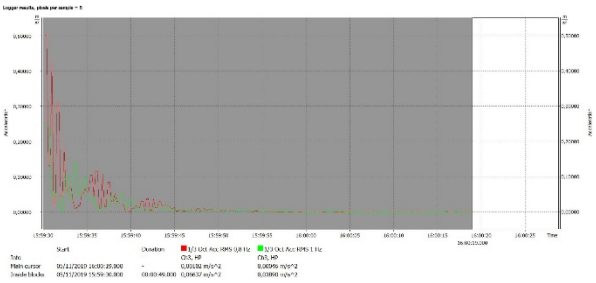

***Fig. 5** Logger results graph for compromised measurement for 0,8 Hz and 1 Hz 1/3 octave bands. A characteristic “ski slope” at the beginning of the graph may be seen.*

In Figure 7. is given a logger results graph for one of the measurements.

From the figure it may be calculated that the shock rate is 39 shocks in minute.

3.3. Evaluation

In Table 1 the measurement and evaluations are given for ISO 2631-1 basic evaluation method with respect to health. The following limit values for comparing with daily vibration exposures are being used. Regulation [3] and Directive 2002/44/EC for basic evaluation method gives daily exposure action value of 0,5 m/s^2 standardised to an eight-hour reference period and daily exposure limit value of 1,15 m/s^2 standardised to an eight-hour reference period.

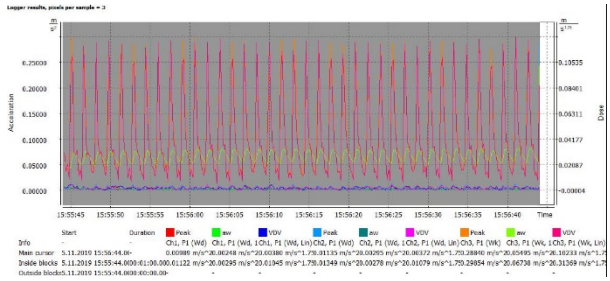

Fig. 7 *Logger results graph for measurement on the position MP2 (Fig.4)*

It may be seen that though containing multiple shocks the additional evaluation according to ISO 2631-1 isn't needed (crest factor is not greater then 9). Daily vibration exposure normalized to a reference period of 8 h, A(8) is calculated for two hours of exposition.

Table 1 *Measurements and evaluation of vibration with respect to health*

Measurement position MP1						
axis	frequency weighting	multi-plying factor	a_w [m/s^2]	Peak value A_w [m/s^2]	*A(8)* [m/s^2]	Crest factor A_w/a_w
x	W_d	1,4	0,00298	0,01533	0,016	5,1
y	W_d	1,4	0,00411	0,02082		5,1
z	W_k	1	0,03221	0,14223		4,4
Measurement position MP2						
axis	frequency weighting	multi-plying factor	a_w [m/s^2]	Peak value A_w [m/s^2]	*A(8)* [m/s^2]	Crest factor A_w/a_w
x	W_d	1,4	0,00295	0,01117	0,034	3,8
y	W_d	1,4	0,00278	0,01354		4,9
z	W_k	1	0,06730	0,29888		4,4

It may be seen that measured values are well below daily exposure action value of 0,5 m/s^2 and limit value 1,15 m/s^2 [3].

With respect to comfort and/or discomfort reactions to vibration in residential and commercial buildings, experience has shown that occupants of residential buildings are likely to complain if the vibration magnitudes are only slightly above the perception threshold. Fifty percent of persons can just detect vibration with a peak magnitude of 0,015 m/s^2 [1]. For the purpose of this evaluation this value is used as a limit for uncomfortable vibration.

In Table 2 the measurement and evaluations are given for ISO 2631-1 and ISO 2631-2 evaluation method with respect to comfort and perception.

It may be seen that measured values are well above this threshold limit so the vibration may be rated as uncomfortable.

4. PROPOSED MEASURES

Based on evaluation of noise and vibration the measures are proposed. Thow the measured values were below legaly binding action and limit values given by regulations on safety and health at work, they were rated as disruptive to work activities (communication with clients and trainning activities). It was suggested to the employer that the workplaces should be temporarily displaced to a location where proper working conditions will be ensured during the construction period.

Table 2 *Measurements and evaluation of vibration with respect to comfort and perception*

Measurement position MP1					
Evaluation according to ISO 2631-1					
axis	frequency weighting	multi-plying factor	a_w [m/s^2]	Peak value A_w [m/s^2]	a_w [m/s^2] (according to (2))
x	W_d	1	0,00298	0,01533	0,033
y	W_d	1	0,00411	0,02082	
z	W_d	1	0,03221	0,14223	
Evaluation according to ISO 2631-2					
axis	frequency weighting	multi-plying factor	a_w [m/s^2]	Peak value A_w [m/s^2]	a_w [m/s^2] (according to (1))
x	W_m	1	0,00390	0,01533	0,0173
y	W_m	1	0,00459	0,02082	
z	W_m	1	0,01734	0,14223	
Measurement position MP2					
Evaluation according to ISO 2631-1					
axis	frequency weighting	multi-plying factor	a_w [m/s^2]	Peak value A_w [m/s^2]	a_w [m/s^2] (according to (2))
x	W_d	1	0,00295	0,01117	0,067
y	W_d	1	0,00278	0,01354	
z	W_d	1	0,06730	0,29888	
Evaluation according to ISO 2631-2					
axis	frequency weighting	multi-plying factor	a_w [m/s^2]	Peak value A_w [m/s^2]	a_w [m/s^2] (according to (1))
x	W_m	1	0,00486	0,01117	0,033
y	W_m	1	0,00496	0,01354	
z	W_m	1	0,03297	0,29888	

4. CONCLUSION

The evaluation of vibration in offices in a residential and business complex in Belgrade during construction works in the neighborhood according to ISO 2631-1 and ISO 2631-2 evaluation method showed that the limits with respect to health were not exceeded. However, evaluation with respect to comfort and perception showed the vibrations as uncomfortable and therefore disruptive to work activities. Based on evaluation a proposal for measures to be taken was given to the employer.

REFERENCES

[1] ISO 2631-1:1997+A1:2010, SRPS ISO 2631-1:2014 Mechanical vibration and shock — Evaluation of human exposure to whole-body vibration — Part 1: General requirements.

[2] ISO 2631-2:2003 Mechanical vibration and shock — Evaluation of human exposure to whole-body vibration — Part 2: Vibration in buildings (1 Hz to 80 Hz).

[3] Regulation on preventive measures for health and safety at work regarding vibration exposure. Off. J. RS. 2011, 93, pp. 30-32

[4] Directive 2002/44/EC of the European Parliament and of the Council of 25 June 2002 on the minimum health and safety requirements regarding the exposure of workers to the risks arising from physical agents (vibration). Off. J. Eur. Commun. 2002, L177, pp. 13-19

УНИВЕРЗИТЕТ У НИШУ
UNIVERSITY OF NIŠ

ФАКУЛТЕТ ЗАШТИТЕ НА РАДУ У НИШУ
FACULTY OF OCCUPATIONAL SAFETY

ФАКУЛТЕТ ЗАШТИТЕ НА РАДУ ЈЕ АКРЕДИТОВАНА ВИСОКОШКОЛСКА УСТАНОВА ЗА ОБАВЉАЊЕ ОБРАЗОВНЕ И НАУЧНОИСТРАЖИВАЧКЕ ДЕЛАТНОСТИ У НАУЧНОЈ ОБЛАСТИ „ИНЖЕЊЕРСТВО ЗАШТИТЕ ЖИВОТНЕ СРЕДИНЕ И ЗАШТИТЕ НА РАДУ".

КОМУНАЛНА ПОЛИЦИЈА

ИНСПЕКЦИЈА РАДА

ОСНОВНЕ АКАДЕМСКЕ СТУДИЈЕ

ЧЕТИРИ ГОДИНЕ (240 ЕСПБ БОДОВА)

- ЗАШТИТА НА РАДУ
- ЗАШТИТА ЖИВОТНЕ СРЕДИНЕ
- ЗАШТИТА ОД ПОЖАРА

ПРОИЗВОДНЕ ДЕЛАТНОСТИ: прерађивачка, прехрамбена индустрија и др.

ЈАВНА КОМУНАЛНА ПРЕДУЗЕЋА

МАСТЕР АКАДЕМСКЕ СТУДИЈЕ

ЈЕДНА ГОДИНА (60 ЕСПБ БОДОВА)

- ИНЖЕЊЕРСТВО ЗАШТИТЕ НА РАДУ
- ИНЖЕЊЕРСТВО ЗАШТИТЕ ЖИВОТНЕ СРЕДИНЕ
- ИНЖЕЊЕРСТВО ЗАШТИТЕ ОД ПОЖАРА
- УПРАВЉАЊЕ ВАНРЕДНИМ СИТУАЦИЈАМА
- МЕНАЏМЕНТ ЗАШТИТЕ ЖИВОТНЕ СРЕДИНЕ

САНИТАРНА ИНСПЕКЦИЈА

КОМУНАЛНА ИНСПЕКЦИЈА

ДОКТОРСКЕ АКАДЕМСКЕ СТУДИЈЕ

ТРИ ГОДИНЕ (180 ЕСПБ БОДОВА)

- ИНЖЕЊЕРСТВО ЗАШТИТЕ НА РАДУ
- ИНЖЕЊЕРСТВО ЗАШТИТЕ ЖИВОТНЕ СРЕДИНЕ

ПРОИЗВОДНЕ ДЕЛАТНОСТИ: грађевинарство, хемијска, петрохемијска, металопрерађивачка, пољопривреда, телекомуникације, нафтна индустрија, саобраћај, шумарство, рударство и др.

МАЛА И СРЕДЊА ПРЕДУЗЕЋА

АГЕНЦИЈЕ И ИНСТИТУТИ

ЗДРАВСТВЕНЕ УСТАНОВЕ

ВЕЛИКА ПРЕДУЗЕЋА

ВАТРОГАСНЕ ЈЕДИНИЦЕ

ОСИГУРАВАЈУЋЕ КОМПАНИЈЕ

18000 Ниш, Чарнојевића 10 А

СЕКТОР ЗА ВАНРЕДНЕ СИТУАЦИЈЕ

Телефон: (+381 18) 529-701

Факс: (+381 18) 249-962

www.znrfak.ni.ac.rs

University of Nis
Faculty of Occupational Safety
„Politechnica“ University of Timisoara
Faculty of Mechanical Engineering
27th International Conference
NOISE AND VIBRATION
Niš, 20 - 21. 10. 2022.

VIBRATION IN INDUSTRIAL TRUCKS: COMPARISON OF EVALUATION OUTCOMES ACCORDING TO ISO 2631-1 AND ISO 2631-5

Jovan Miočinović [1], Biljana Beljić Durković [2]

[1] TEHPRO d.o.o., Serbia, jovan.miocinovic@tehpro.rs
[2] TEHPRO d.o.o., Serbia

Abstract - *Apart from the in Europe legally binding ISO 2631-1 (current SRPS ISO 2631-1:2014 in Serbia) for the evaluation of human exposure to whole-body vibration in workplace, there is also the method for evaluation of vibration containing multiple shocks, ISO 2631-5. Here the methods are being juxtaposed to compare the evaluations for the situations often met in industrial work environment praxis: exposure to vibration containing multiple shocks when driving the vehicle.*

1. INTRODUCTION

Whole-Body Vibration exposure as a common physical risk present in industries may cause not only uncomfortable feeling but also health problems. In addition, task related to driving vehicles expose the professional vehicle operators also to mechanical shocks. The long term exposure to vibration and mechanical shock is related to musculoskeletal disorders, such as sciatica, low back pain and degenerative changes to lumbar spine [1]. Evaluation of the vibration exposure in industrial trucks was made in order to establish vibration exposure levels and estimate the possible resulting health risk. In evaluation made according to ISO 2631-1 [2] basic and the additional evaluation method were applied. Measurement results were compared to daily exposure action and limit values according to Regulation [3] and Directive 2002/44/EC [4]. Also as a vibration containing multiple shocks ISO 2631-5 [5] method was applied and the assessment of health effects was made according to standard. Both method's forecasted health risks were then been compared.

2. INSTRUMENTATION, SAMPLE AND MEASUREMENT LOCATION AND CONDITIONS

2.1. Instrumentation

For measurements was used SVAN 958 four channels sound (Type 1 IEC 61672-1:2002) and vibration (Type 1 ISO 8041:2005) level meter and analyser with seat accelerometer for whole-body measurements with DYTRAN 3143M1 - IEPE type triaxial accelerometer (Fig. 1).

2.2. Sample and measurement location and conditions

Measurements were made in a sample of forklift trucks of different types and load capacities, 14 in one industrial location in beverage packaging company and one in one cement industry plant, and in one dumper truck and in one excavator both on the location of stone quarrying for the construction material industry.

Fig. 1 *SVAN 958 four channels sound and vibration level meter and analyser*

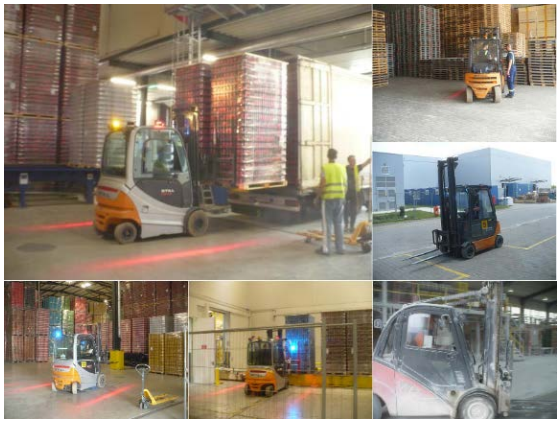

Fig. 2 *Forklift trucks*

Fig. 3 *Dumper truck and excavator*

Measurements were taken on the position of driver's seat.

Measurements were taken according to ISO 2631-1 in seated position, with a person seated on the seat accelerometer according to a coordinate system in Fig. 4.

Measurements were performed in controlled real environment. In forklift trucks measurements were made in time interval representative for usual worktasks as tranportation of products within the warehouse, transportation between production halls including transportation on internal transport roads in the open air, and loading the products into the truck (15 – 30 minutes samples). In dumper truck and excavator measurements included one operational cycle, for dumper one ride all the way from the dumping site in the plant to the ehcavating site in stone quarry and back, and for the excavator one cycle of charging the dumper with the stone (that is, 20 – 40 minutes samples).

Surface roughness, or road condition has a big impact on vibration. As for the forklift trucks, roughness differs between different production halls as well as on the internal roads. As for the dumper and excavator it's about driving on bumpy mountain macadam road, partly heavily damaged turning the ride and maneuvering into off-road ride.

From influences on vibration in vehicle other then roughness / road condition one could specify the driver's experience and vehicle speed. As for the drivers/operators experience it was assumed that all were skilled workers. As for the vehicle speed, the forklift trucks in the plant are speed limited by company rules (10 km/h outdoors and 5 km/h indoors) and for trucks on the mountain bumpy roads by road condition, that is, one can drive only slowly (usually up to 20 km/h) and with outmost care, and that lmits the possible variation due to vehicle speed.

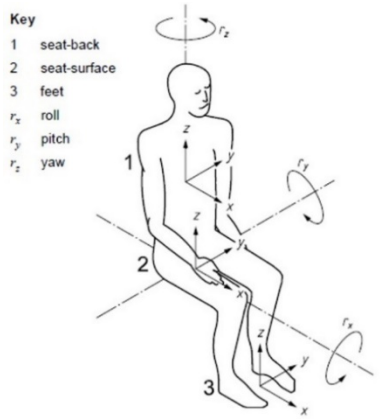

Fig. 4 *Basicentric axes of the human body for seated position according to ISO 2631-1*

3. MEASUREMENT RESULTS AND EVALUATION METHOD

3.1. Weighted r.m.s. accelerations

Measurements were taken in *x*-, *y*- and *z*-axis oriented as in Fig. 4.

The weighted r.m.s. acceleration is determined for each axis (*x*, *y* and *z*) of translational vibration on the surface which supports the person. The assessment of the vibration is made for the forklift trucks with respect to the highest frequency-weighted acceleration determined in any axis on the seat pan (1), and for the dumper truck and excavator, while the vibrations in *x*, *y* and *z* axes are comparable, according to equation (2) [2]:

$$a = \left(Max\{k_x{}^2 a_{Wd}{}^2 + k_y{}^2 a_{Wd}{}^2 + k_z{}^2 a_{Wk}{}^2\}\right)^{1/2} \quad (1)$$

$$a_v = (k_x{}^2 a_{Wd}{}^2 + k_y{}^2 a_{Wd}{}^2 + k_z{}^2 a_{Wk}{}^2)^{1/2} \quad (2)$$

where multiplying factors k_x = 1,4, k_y = 1,4, and k_z = 1.

3.2 ISO 2631-1 basic evaluation method

As for assessment of whole-body vibration with respect to health, the following limit values for comparing with daily vibration exposures are being used.

Regulation [3] and Directive 2002/44/EC for basic evaluation method gives daily exposure action value of 0,5 m/s^2 standardised to an eight-hour reference period and daily exposure limit value of 1,15 m/s^2 standardised to an eight-hour reference period.

3.3 ISO 2631-1 additional evaluation method

As for the additional evaluation of vibration when the basic evaluation method is not sufficient, the fourth power vibration dose method was used. Additional evaluation method is used in cases where the basic evaluation method may underestimate the effects of vibration (high crest factors, occasional shocks, transient vibration). ISO 2631-1 gives two alternative evaluation methods - the running r.m.s. and the fourth power vibration dose. As a third alternative there is the evaluation method described in ISO 2631-5[5]. The indicators for using the additional method according to ISO 2631-1 are: crest factor greater then 9 and $VDV/(a_W{*}T^{1/4})$ of the order or greater then 1,75.

Directive [4] gives daily dose action value of 9,1 m/s^{1,75} and daily dose limit value of 21 m/s^{1,75}.

3.4 ISO 2631-5 evaluation method

ISO 2631-5 [5], [6] method for the evaluation of vibration containing multiple shocks vibration is the sixth power vibration dose method. The acceleration dose (in *k*-direction) is defined as:

$$D_k = [\sum_i Ai^k]^{1/6} \quad (3)$$

where A_{ik} is the ith peak of the response acceleration $a_{ik}(t)$, where $k = x, y$ or z.

The peak is the maximum absolute value of the response acceleration between two consecutive zero crossing for the *x*- and *y*- directions (peak to peak value), and for *z*-direction only the absolute value is to be counted (peak value). That is, for the severity in *z*-direction only the compression of the spine is to be counted. In calculating the dose, peaks of a considerably lower magnitude then highest peak will not significantly contribute to the value associated with 6th power term in equation (3) and may therefore be neglected.

Fort he assessment of health effects the average daily dose to which a person will be exposed, D_{kd}, is to be determined:

$$D_{kd} = D_k \left[\frac{t_d}{t_m}\right]^{1/6} \quad (4)$$

where t_d is the duration of daily exposure and tm is the period over which D_k has been measured.

The daily equivalent static compression dose, S_{ed}, is obtained adding damaging effects on spine in all 3 directions:

$$S_{ed} = \left[\sum_{k=x,y,z}(m_k D_{kd})^6\right]^{1/6} \quad (5)$$

where m_x = 0,015 MPa/(m/s^2), m_y = 0,035 MPa/(m/s^2) and m_z = 0,032 MPa/(m/s^2).

Risk factor R is defined for the assessment of the adverse health efects:

$$R = \left[\sum_{i=1}^{n} \left(\frac{S_{ed} * N^{1/6}}{S_{ui} - c}\right)^6\right]^{1/6} \qquad (6)$$

where N is number of exposure days per year (e.g. 240 for full time job), i is the year counter, n is the number of years of exposure, c is static stress constant due to gravitational force (for the driving posture equals 0,25 MPa), S_{ui} is the ultimate strength of the lumbal spine for a person of age (b+i) years and b is the age at which exposure starts. Relation between S_{ui} and b+i is:

$$S_{ui} = 6{,}75 - 0{,}066(b + i) \qquad (7)$$

R < 0,8 indicates a low probability of an adverse health effect and R > 1,2 indicates a high probability of an adverse health effect.

For the purpose of this paper the calculations were performed according to previous version of ISO 2631-5 [6] followed with some modification.

3.4.1 The modification

The response acceleration $a_{lk}(t)$ is lumbar spinal acceleration response to measured acceleration of the seat pan. $a_{lk}(t)$ is to be calculated according to given formulae and recommended software for sampling rate of 256 samples per second. In Fig. 5 an example of calculated response acceleration is presented.

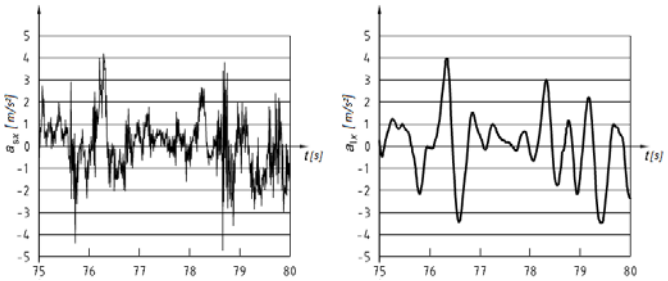

Fig. 5 *Example of calculated spinal response from measured acceleration (ISO 2631-5)[6]*

In Fig. 6 is presented frequency response of the seat to spine transfer function.

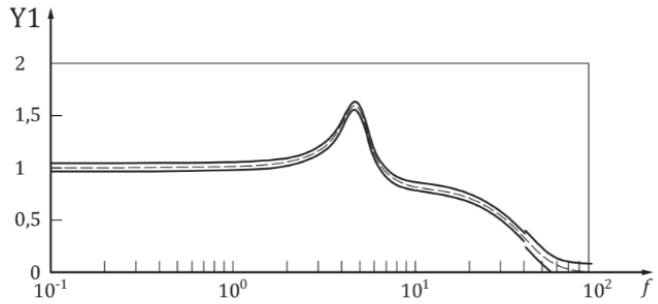

Fig. 6 *Frequency response of the seat to spine transfer function with tolarance bands (ISO 2631-5)[5]*

For the purpose of this paper the following modifications to ISO 2631-5 method have been made.

For A_{ix} and A_{iy} measured values of peak-to-peak values of a_x and a_y have been taken and for A_{iz} measured values of peak value of a_z have been taken. S_{ed} and R were then calculated according to (5) and (6) [6]. The main reason for these modifications is that measurement sampling didn't mach the required 256 samples per second criterion. All measurements were sampled in 5 samples per second rate.

An example of peak measurement is presented in Fig. 7. Here peaks in both directions are presented on positive axis. When comparing it to Fig. 5 (both represent measurement period of 5 seconds) one may easily see that both, the response acceleration (Fig. 5, on the right) and measurement with sampling rate of 5 samples per second (Fig. 6) are straightened comparing to 256 samples per second measurement (Fig. 5, on the left). The difference is that the response acceleration curve is smooth.

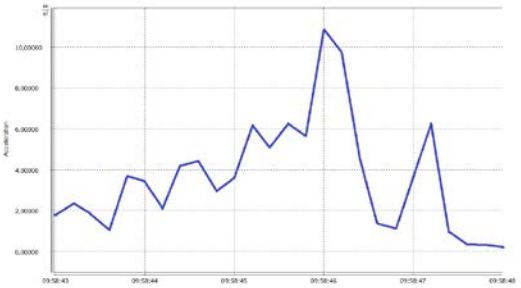

Fig. 7 *Example of measured peak vibration with sampling rate of 5 per second. The measuring interval is 5 seconds*

From Fig. 5 it may easily be seen that highest peaks in spinal response are preserved, and, as has been said before, in the sixth power vibration dose method peaks of lower magnitude then highest peak will not significantly contribute.

Taking all the above into account the modification shouldn't affect the result significantly.

Further, to the values thus calculated a correction factor is applied so the frequency response curve (Fig. 6) would be taken into account. This modification is taken from the current version of ISO 2631-5 [5]. Correction factor was obtained by calculating S_{ed} and R for the vibration values obtained from 1/3 octave measurements when applying transfer function (Fig. 6) and then comparing to those calculated according to (5) directly.

As recently shown [7], there is a small difference in R value calculated by ISO 2631-5 and it's previous version. A comparison is presented in Fig. 8.

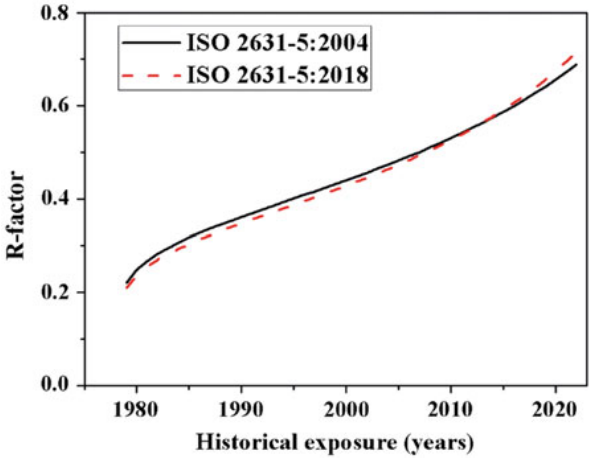

Fig. 8 *Evolution of R over the historical exposure (De la Hoz-Torres et al. [7])*

3.4.1.1 The correction factor

The correction factor is obtained by calculations of S_{ed} and R using (5) and (6) according to frequency response curve (Fig. 6). Following Figure 6, coresonding response factors for 1/3 octave spectrum are given in in Table 1.

First, the sample of 5 from the total of 17 measurements was selected. The sample was chosen so it would cover the range of calculated R values. Then in each measurement selected the subsample of 3 measurement intervals was chosen containing shocks. The idea is while (3) propagates shocks to see the frequency response of tipical shocks contained in vibration.

The results, quotient of spinal response acceleration and acceleration, a_W^*/a_W together with the relation to corresponding values for R factors are presented in Fig. 9. Error bars represent expanded measurement uncertainties. a_W^* is response acceleration obtained from 1/3 octave spectrum of acceleration a_W by additionaly weighting it according to principal frequency weightings given in Table 1. Average a_W^*/a_W for the sample is found to be (1,124 ± 0,082).

Table 1 *Principal frequency weightings in 1/3 octave spectrum according to frequency response curve*

1/3 octave [Hz]	Response factor	1/3 octave [Hz]	Response factor
≤ 1,6	1	12,5	0,78
2	1,06	16	0,74
2,5	1,11	20	0,71
3,15	1,15	25	0,68
4	1,43	31,5	0,53
5	1,5	40	0,32
6,3	1,04	50	0,16
8	0,88	63	0,07
10	0,81	≥ 80	0

All this was done for vibration in z-direction (W_k principal frequency weighting [2]). Similarily, when doing the same procedure on a subsample of vibrations containing shocks in x- and y-direction, with W_d principal frequency weighting (two from first and two from fifth measurement in Fig. 9) the similar quotient is obtained (1,123 ± 0,085).

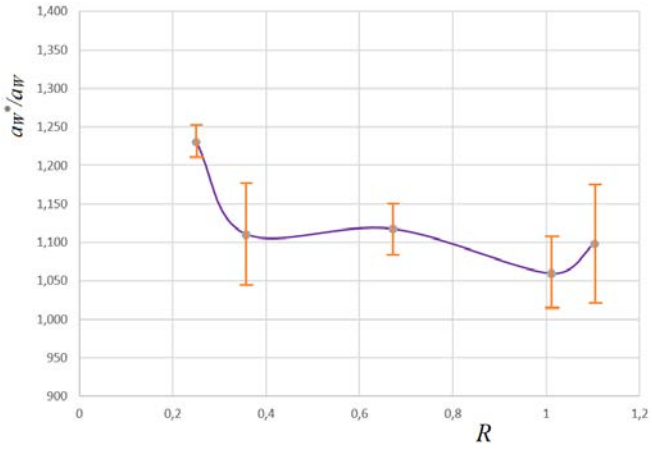

Fig. 9 *Quotient of spinal response acceleration and acceleration, a_W^*/a_W for subsample in 5 measurements containing peaks*

While thus obtained quotient (when the same in x-, y- and z-directions) propagates lineary in equations (5) and (6), it is the wanted correction factor.

3.5 Evaluation results

In Table 2 the results are presented for the trucks under test arranged in ascending order in relation to R. All values for R are calculated for the worker after 10 years of service starting working on the operator job at the age of twenty.

Table 2 *Results for the trucks under test. PL1XY stays for the forklift XY from plant 1, PL2FL01 stays for the forklift from plant 2. The results are arranged in ascending order in relation to R*

Truck under test	S_{ed}	R_{10}	$A(8)$ $[m/s^2]$	VDV $[m/s^{1,75}]$	CF	$VDV/(a_W*T^{1/4})$
PL2FL01	0,327	0,250	0,484	11,36	10,9	1,99
PL1FL01	0,406	0,310	0,393	9,26	13,5	1,97
PL1FL15	0,466	0,356	0,326	7,89	29,6	3,14
PL1FL04	0,504	0,385	0,257	8,67	8,9	1,7
EXCAVATOR	0,658	0,502	0,609	14,88	14,4	2,2
PL1FL12	0,676	0,516	0,464	16,88	27,7	3,43
PL1FL16	0,878	0,671	0,464	17,85	38,9	3,74
PL1FL02	0,904	0,690	0,57	17,22	20,5	2,34
PL1FL17	1,01	0,770	0,549	19,66	30,2	3,11
PL1FL18	1,032	0,788	0,371	14,85	52,8	4,28
PL1FL10	1,269	0,967	0,497	20,43	33,1	3,61
PL1FL07	1,322	1,010	0,5	24,3	13,2	2,6
DUMPER	1,405	1,074	0,691	15,63	10	1,96
PL1FL14	1,443	1,103	0,372	19,94	69	5,26
PL1FL13	1,550	1,184	0,348	17,8	21,4	2,59
PL1FL05	2,330	1,780	0,468	24,79	29,1	2,87
PL1FL11	2,602	1,988	0,81	37,48	45,8	4,75

3.5.1 ISO 2631-1 indicators for using the additional method

In following figure the ISO 2631-1 indicators, crest factor and $VDV/(a_W*T^{1/4})$ are compared to the values indicating need for addition evaluation method.

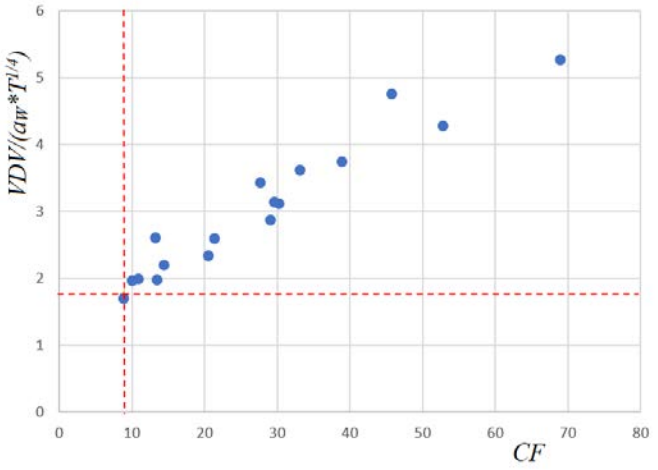

Fig. 10 *Comparing crest factor and $VDV/(a_W*T^{1/4})$ for trucks under test. Compared values are from Table 2. Limit lines are: crest factor 9 and $VDV/(a_W*T^{1/4})$ greater then 1,75. All but one, PL1FL04, meet these criteria*

It may be seen that all but one need the additional evaluation method.

3.5.2 Comparing ISO 2631-1 basic and additional method evaluation results

In Fig. 11 the results of ISO 2631-1 basic evaluation method and of it's additional evaluation method are compared.

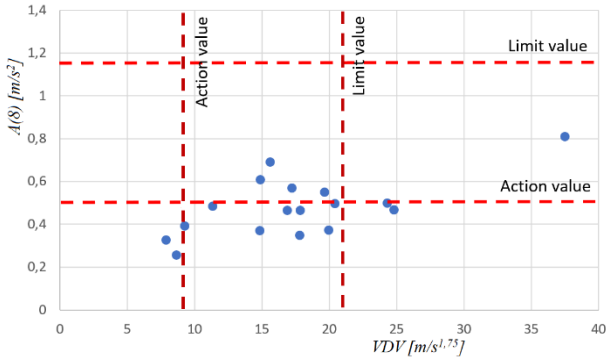

Fig. 11 *Comparing A(8) and VDV results to action and limit values*

We see that while by *A(8)* rating all the results are around action value, by *VDV* rating they are well distributed into 3 categories (below action value, inbetween action and limit values and abow the limit value). For 2 industrial trucks tested (PL1FL04 and PL1FL15) vibrations do not exceed action values. For the others, *VDV* evaluation results exceed the action value for 8 while *A(8)* do not. Four trucks are evaluated between action and limit values in both criteria. While not a single truck exceeds *A(8)* limit value, 3 of them (PL1FL07, PL1FL05 and PL1FL11) exceed *VDV* limit value.

3.5.2 Comparing ISO 2631-1 and ISO 2631-5 evaluation results

In following figures the ISO 2631-1 evaluation results are compared to ISO 2631-5 evaluation results.

When comparing *R* to *A(8)* (Fig. 12) the results seem distributed similar to those of *VDV* (Fig. 11). While all the results are concentrated around action value of *A(8)*, the similar discrimination as by *VDV* (Fig. 11) is made along *R* axis (Fig. 12).

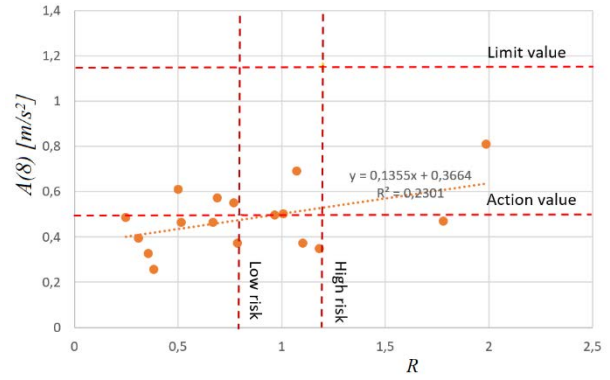

Fig. 12 *Comparing A(8) and R results to action and limit values and risk levels*

The most interesting is comparing *R* to *VDV* as alternative methods for evaluation of vibration containing multiple shock (Fig. 13).

The results are quite grouped together following the same line, (blue dashed in Fig. 13) and thus well separated into categories both by ISO 2631-1 and ISO 2631-5 criteria. For the exposure of 10 consecutive years to vibration starting at the age of twenty, when looking at the vibrations rated according to ISO 2631-1 as between action and limit values, we may see that 8 of them are rated as below the low risk according to ISO 2631-5 (PPL2FL01, PL1FL01, PL1FL04, EXCAVATOR, PL1FL12, PL1FL16, PL1FL02, PL1FL17, and PL1FL18). However, 2 of the operators (PL1FL05, and PL1FL11 operators) are far in high risk, and also overpassing the limit value, while two of operators (of PL1FL16 and PL1FL14) are near entering the high risk zone and also near limit value.

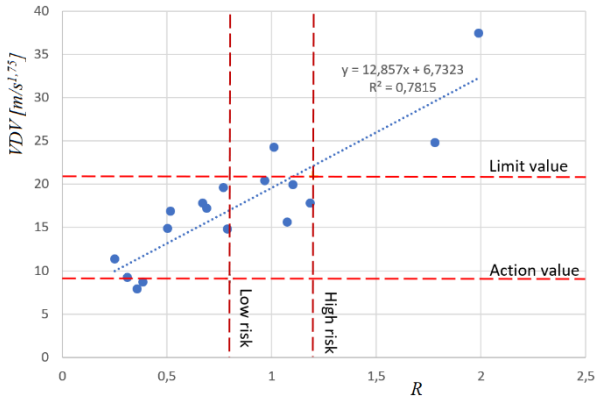

Fig. 13 *Comparing R and VDV results to action and limit values and risk criteria*

ISO 2631-5 takes into account accumulation of risk during the years of exposure. In Fig. 14 evolution of *R* over the historical exposure for the operators of industrial trucks here under test is presented.

It can be seen in Fig. 14 (and comparing to Fig. 13) that both methods give the similar evaluation result, namely, for operators of PL1FL05 and PL1FL11 trucks vibration is evaluated as over the limit (by ISO 23631-1 additional evaluation method) and in high risk (by ISO 23631-5 evaluation method). One ISO 23631-1 rated over the limit is found in ISO 23631-5 middle risk zone (PL1FL07). Additionaly, ISO 23631-5 evaluation method gives us insight in future risks of accumulating vibration effect during the years of exposure. We see that only four of operaters of trucks under test eventually wouldn't overpass low risk after many years of exposure.

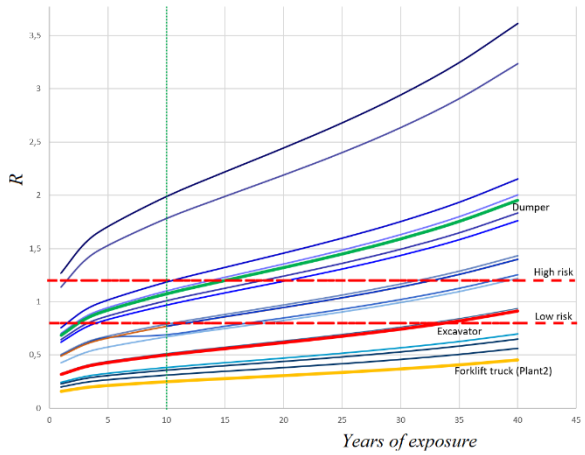

Fig. 14 *Evolution of R over years of exposure. For operators of forklift truck (plant 2) and excavator and dumper trucks operators evolutions are presented as yellow, red and green lines. For the operators of forklift trucks (plant 1) evolution curves are thin lines. Vertical dashed line presents current situation*

4. CONCLUSION

A sample of 17 whole-body vibration measurements made on operators of industrial trucks, 15 of forklift trucks, one dumper truck and one excavator were evaluated both to ISO 2631-1 and 2631-5 evaluation methods. Though most of the sample rated overpassing the action value according to ISO 2631-1 basic evaluation method, almost all needed also an evaluation according to the additional method given in the standard. An alternative method, ISO 2631-5, for evaluation of vibration containing multiple shocks is also carried out. The modification to the method is made to adapt it to measurement set up. It is shown then that the modification in this set up would produce imput values that do not differ significally from the standard set up and therefore should not make a difference in thus calculated *R* values. While using previous version of the standard method, also the modification is made with applying the frequency response curve to get closer to current version of standard. As a result a great match was found in prediction of health risk by both methods. Further, the additional risk arising from the cumulative exposition to vibration during working life, predicted by ISO 2631-5, is assessed.

REFERENCES

[1] Burström, L., Nilsson, T. & Wahlström, J. “Whole-body vibration and the risk of low back pain and sciatica: a systematic review and meta-analysis”, in: Int Arch Occup Environ Health 88, 403–418 (2015).

[2] ISO 2631-1:1997+A1:2010, SRPS ISO 2631-1:2014 Mechanical vibration and shock — Evaluation of human exposure to whole-body vibration — Part 1: General requirements.

[3] Regulation on preventive measures for health and safety at work regarding vibration exposure. Off. J. RS. 2011, 93, pp. 30-32

[4] Directive 2002/44/EC of the European Parliament and of the Council of 25 June 2002 on the minimum health and safety requirements regarding the exposure of workers to the risks arising from physical agents (vibration). Off. J. Eur. Commun. 2002, L177, pp. 13-19

[5] ISO 2631-5:2018 Mechanical vibration and shock -- Evaluation of human exposure to whole-body vibration -- Part 5: Method for evaluation of vibration containing multiple shocks

[6] ISO 2631-5:2004 Mechanical vibration and shock -- Evaluation of human exposure to whole-body vibration -- Part 5: Method for evaluation of vibration containing multiple shocks

[7] De la Hoz-Torres, M.L., Aguilar-Aguilera, A.J., Martínez-Aires, M.D., Ruiz, D.P. (2019). “A Comparison of ISO 2631-5:2004 and ISO 2631-5:2018 Standards for Whole-Body Vibrations Exposure: A Case Study”, in: P. M. Arezes et al. (eds.), Occupational and Environmental Safety and Health. Studies in Systems, Decision and Control, vol 202. Springer, Cham.

University of Nis
Faculty of Occupational Safety
„Politechnica“ University of Timisoara
Faculty of Mechanical Engineering
27th International Conference
NOISE AND VIBRATION
Niš, 20 - 21. 10. 2022.

SHOCK VIBRATION AND ASSESSMENT OF THE RISK OF CREW INJURY WHEN THE VEHICLE HITS A MINE

Snežana Jovanović[1], Aleksandar Đurić[2], Aleksandar Nikolić[3]

[1,3] Technical Test Center, Belgrade, e-mail: sneza.jovanovic.toc@gmail.com
[2] Military Academy, University of defence, Belgrade

Abstract - *In the paper, based on the measured vibrations and the calculated head injury criteria, the survival of crew members in armored combat vehicles (BOV) when encountering explosives is evaluated. Measurements are performed on a sophisticated test dummy, a biodynamic model of a soldier.*

1. INTRODUCTION

Vibrations imply an oscillatory disturbance of longer duration (acceleration longer than 1 second), while shocks are transient mechanical disturbances (with an acceleration of several milliseconds) or vibrations with a large peak factor (the ratio of the maximum acceleration amplitude to the square root of the average acceleration).

The critical factor for the impact vibration effect is the product of the acceleration intensity and its duration (that is, the change in speed).

Modern warfare and attacks with explosive devices on armored vehicles result in a large number of victims and evidence of the danger of shock vibration acceleration to the lives of crew members. In this way, losses are inflicted on the enemy from a distance with minimal risk to one's own forces.

The protection of passengers in a vehicle takes into account several factors that lead to their injury. If the crew members are properly fastened with seat belts and if there are no loose fragments inside the cabin, the main hazard factor to consider is acceleration.

In an explosion under the vehicle (under wheel or chassis), the crew is in direct contact with the accelerated structure and floorboard and is exposed to vertical impact acceleration and the possibility of serious injury.

Values of resistance to vertical impact vibrations shown in Fig. 1 are informative, and realistic endurance ranges depend on many factors. A person's resistance to vibrations and impact accelerations is influenced by: age, gender, physical condition; experience; readiness for an expected impact; magnitude, direction and frequency spectrum of vibrations; the duration of the load and the direction of action of the inertial force vector; the presence of other accompanying disorders (noise, flash, gases, stress, etc.).

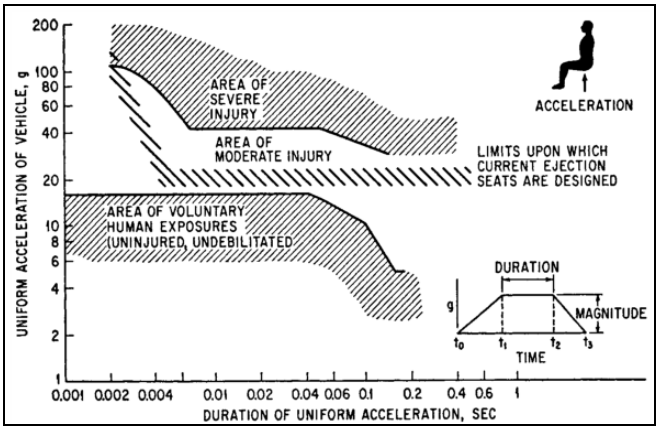

Fig. 1 *Tolerance to headward acceleration as a function of magnitude and duration of impulse*

Modern armored vehicles are adapted to infantry and special units engaged in counter-terrorist and peacekeeping operations in direct and ambush actions of mines and improvised explosives.

The essence of improvement and modification is in strengthening with armor plates and protective glasses, i.e. modular installation of armored parts and subsystems of the vehicle in order to increase the probability and safety of survival of the crew members to the declared level of protection.

The lower part of vehicle the armored body in the shape of the letter "V" (Fig. 2) and in combination with a significant distance from the ground and a rigid vehicle axles, is the first step towards providing anti-mine and generally anti-explosive protection under the wheel and floor of the vehicle.

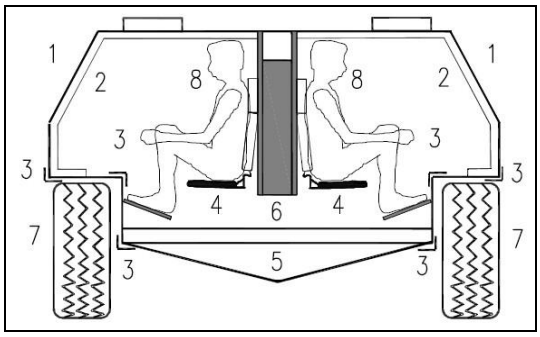

Fig. 2 *Protective measures for armored vehicles*

2. METHODOLOGY

According to the NATO standars method, the explosive-mine protection test of two (larger - four-axle 8x8 and smaller - two-axle 4×4) combat armored vehicles (model BOV) under development was carried out.

The priority was the space for the accommodation of the crew members (commander, driver, gunner and soldiers) and the assessment of their survival and the risk of injury in the case of mines under the wheel or chassis of the vehicle.

For both tests, a vehicle armored body (Fig. 3) was used, which fully corresponds to the finished product in terms of geometry, structure, material and mass. The model had to have wheels and built-in seats, which functlionality was previously checked, as well as the correctness of the fastening system.

Fig. 3 *External appearance of the vehicle armored body of the larger BOV*

The examined vehicles were declared to level 2 (smaller vehicle 4x4) and level 3 (larger vehicle 8x8) of explosive-mine protection.

Categorization of armored vehicles into protection levels is based on 90% crew protection. For the declared level 3 mine protection of the BOV, according to the NATO test standard, 8 kg was activated, while level 2 was tested with 6 kg of explosives. The locations of the explosives were determined based on the worst-estimated outcome.

Examining the level of explosive-mine protection, in addition to vehicles armored body, also includes models of crew members, test dummies that should have appropriate biodynamic responses (Fig. 4) to the action of explosives and the movement of the entire vehicle and its subsystems. The crew member model simulates the behavior of the human body in terms of geometry and mass and in terms of mass distribution.

For a geometric model, it can also be a tst dummy and the combination of geometric and mass equivalent gives the possibility of testing safety systems, such as seat belts.

To measure body load, a test dummy with sensors is necessary. The sensors of the sophisticated test dummy (Fig. 5) provide data on the load on the legs, spine and neck, as well as the performance of the seats, backrests and seat belts.

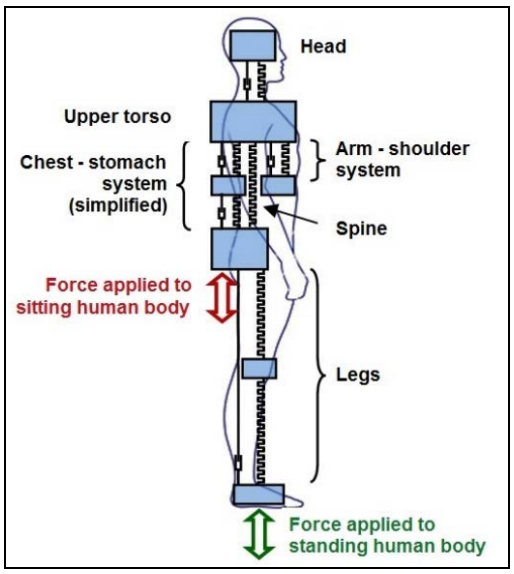

Fig. 4 *Simplified mechanical system of the human body*

The NATO method of testing explosiv- mine protection of BOV accepts a test dummy (Hybrid III) as a model of a male crew member (Fig. 5), which is used in the automotive industry for front frontal collisions, but also for vertical loads (possibility of breaking out seats).

The Hybrid III model is placed in the most common sitting position in military vehicles during an unexpected mine incident, when the direction of the main load is vertical. The seat of the model is the „worst case" position in case of a mine explosion.

The determination of the risk of injury is based on the assessment of the danger to the crew caused by the local deformations of the vehicle and the movement of the vehicle as a whole.

Fig. 5 *Hybrid III dummy, doll for vehicle crash tests*

In addition to force, torque, displacement and pressure sensors, the necessary measurements (Fig. 6) on the model are also performed with three-axis HF accelerometers (A*x*,*y*,*z*) on: neck, pelvis and both lower legs.

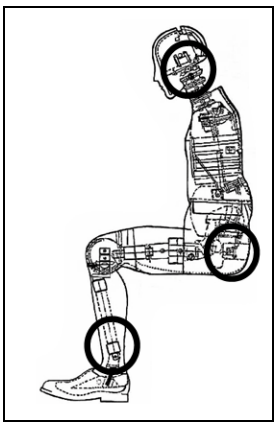

Fig. 6 *Necessary measuring points on the test dummy*

Based on the measurement of impact vibrations (with three-axis HF accelerometers and a measurement speed of 200kHz) at the measuring point of the center of the head (upper part of the neck), the coefficient HIC (Head Injury Criterion) was calculated, which represents the criterion of head injury.

Head Injury Criterion HIC is the maximum value of 2.5 times the increased integral of the resultant triaxial acceleration (a) of the center of the head in time of the occurrence of that maximum (Δt_max = 15 ms), HIC_{15}:

$$HIC_{\Delta t\_max} = \max_{t_1,t_2}\left\{\left[\frac{1}{t_2-t_1}\int_{t_1}^{t_2} a\,dt\right]^{2.5}(t_2-t_1)\right\}$$

$$t_2 - t_1 \le \Delta t\_max$$

$$a = \sqrt{a_x^{\,2} + a_y^{\,2} + a_z^{\,2}}$$

The impact of the explosion on the crew members was evaluated based on measurements of several values on dummies placed in the transport part of a larger (4-axle, Fig. 7) and smaller (2-axle, Fig. 8) armored vehicle.

For the purposes of measuring the largest number of values, a test dummy made according to the model of the Nubrid III standard dummy was used.

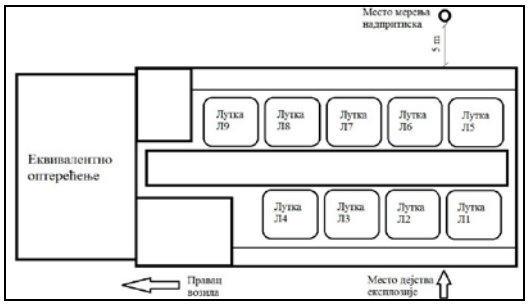

Fig. 7 *Places of measuring test dummies in the armore body of the larger BOV 8×8*

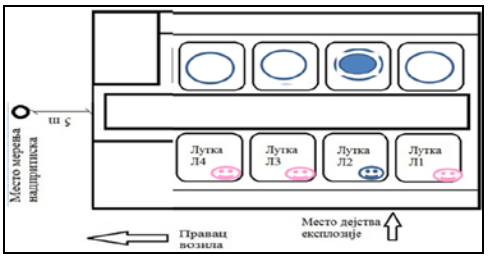

Fig. 8 *Places of measuring test dummies in the armore body of the smaller BOV4×4*

3. RESULTS

In order to verify the declared level (3a for larger and 2a for smaller BOV) of anti-mine protection, the fulfillment of the requirements of the NATO standard was examined:

1. Crew survival - assessed using the HIC criteria, calculated from the measured triaxial head acceleration;
2. That there is no breach in the transport compartment with the crew or passage of fragments and shock wave;
3. That there is no occurrence of flying secondary fragments or insufficiently attached equipment in the crew compartment;
4. That the seats remain attached to the vehicle and that the restraint system keeps the person in the seat.

Fig. 9 *External appearance of the equivalent of the smaller BOV 4x4 after the explosion*

Part of the measurement results (from the aspect of vibrations) and criteria for the impact of the explosion on the crew members is given in Table 1 for the larger and in Table 2 for the smaller BOV.

From the triaxial acceleration measured on the neck of the crew member's head model, the HIC_{15} head injury criterion was calculated.

Table 1 *Results of part of the measurement of the impact of the explosion on the crew members in a larger vehicle (from the aspect of vibrations)*

Measurement place/axis		Acceleration (g)	Result / Criteria
Dummy L2	Neck/X	59,4	**HIC_{15} =233** / HIC_{15} < 250
	Neck/Y	31,3	
	Neck/Z	34	
	Lower leg/Z	333,6	**Velocity=50 m/s** / over crit. < 27 m/s
Dummy L3	Neck/X	23,3	**HIC_{15} =42** / HIC_{15} < 250
	Neck/Y	21,7	
	Neck/Z	20,8	
	Lower leg/Z	131,6	**Velocity=20 m/s** / Crit. < 27 m/s
	Lumbar spine/Z	36,1	**36,1 g** / to 110 g

Table 2 *Results of part of the measurement of the impact of the explosion on the crew members in a smaller vehicle (from the aspect of vibrations)*

Measurement place/axis			Acceleration (g)	Result / Criteria
Dummy L2	Neck	X	74	**HIC_{15} =115** / HIC_{15} < 250
		Y	55	
		Z	195	
	Lumbar spine	X	54	-
		Y	47	-
		Z	77	**77g** / to 110 g
Dummy L4	Neck	X	23,3	**HIC_{15} =42** / HIC_{15} < 250
		Y	21,7	
		Z	20,8	
	Lumbar spine	Z	5	**5g** / to 110 g

4 CONCLUSION

The criterion or permissible value of the HIC coefficient is 250, which theoretically means that there is no risk of head injury up to that value.

Although deformations of the floor plates were noted, no breakthroughs were observed after the detonation of the mine under the wheel, so the criterion of no breakthrough was met.

Within the limits of fulfillment is also the criterion of the absence of parts of equipment that would put the crew in danger if they fall out of the bed.

An examination of the seats and safety belts, immediately after the detonation, confirmed that they were correct.

For the deviation of certain measured sizes on the test dummies from the criteria, it should be taken into account:

The armored body of the larger vehicle was significantly stiffer than the real vehicle (only the wheel had an elastic suspension, while the remaining five supports had rigid connections), so the energy of the detonation was transferred to the floor without any cushioning.

The test dummies approximate the elasticity of the crew members.

For the above reasons, it is estimated that the criterion of the impact of the explosion under the wheel of the BOV on the crew members is in the limit area of fulfillment.

It is theoretically estimated that the armored structure of the vehicle allows the protection of the crew members from the detonation effect of 8 kg (for a 4-axle larger vehicle) and 6 kg (for a 2-axle smaller vehicle) of explosives under the wheel.

REFERENCES

[1] NATO AEP-55 STANAG 4569. Protection Levels for Occupants of Logistic and Light Armored Vehicles.

[2] A.Ramasamy, A.M. Hill, A.E.Hepper, A.M.J. Bull, J.C. Clasper, *Blast mines: Physics, injury mechanisms and vehicle protection*, JR Army Med Corps 155(4): 258 – 264.

[3] McKay B.J., Bir C.A. Lower extremity injury criteria for evaluating military vehicle occupant injury in underbelly blast events // Stapp Car Crash Journal. 2009. № 53. P. 229-249.

University of Nis
Faculty of Occupational Safety
„Politechnica“ University of Timisoara
Faculty of Mechanical Engineering
27th International Conference
NOISE AND VIBRATION
Niš, 20 - 21. 10. 2022.

VIBRATIONS OF THE ARMORED PLATE UNDER THE INFLUENCE OF EXPLOSIVES

Snežana Jovanović [1], Aleksandar Đurić[2], Martin Jovanović[3], Aleksandar Nikolić[4]

[1,4] Technical Test Center, Belgrade, e-mail: sneza.jovanovic.toc@gmail.com
[2] Military Academy, University of defence, Belgrade
[3] VEGRAP, Belgrade

Abstract – *The paper analyzes the shocks measured by accelerometers on a steel plate during the detonation of a mine. The experiment was done with different amounts of explosives and plates of different mass. The non-linear relationship between the amount of explosives and the vibration level of the plate was confirmed. The advantage of elastically attaching the armor plate to the construction of the floor of the armored vehicle has been proven in order to achieve a higher level of anti-mine protection.*

1. INTRODUCTION

The subject of the research study is the vibrations of a steel armor plate under the action of explosives activated below or above it. There have been a lot of diferent researches of the blast waves and it efect on the steel structures [1-6].

The purpose of the test was to contribute to the development of a higher level of armored vehicles mine protection, as well as to determine the possibility of measuring mechanical parameters during the activation of explosives.

Due to the lack of knowledge of the effects of the explosion on the armor plate and the measuring equipment itselfe, so far no direct measurements have been made on the armor plate, but only remote recording with an ultrafast (UF) camera.

2. METHODOLOGY

The research was carried out through several combined experiments with different amounts of explosives and the effect on light (330 kg) and heavy (3,300 kg) armor plates placed on a steel support 4×4 (dimensions 1 m × 1 m × 0.5 m):

- In the first, trial experiment, the effect of an activated TNT explosive under the armor plate (with mass of 330 kg and dimensions 2 m × 1 m × 0.02 m) was observed (visually and by recording the plate with a UF camera).
- In the second phase of the research, a TNT explosive of 200 gr was activated above the plate as in Fig. 1. where the vibrations were measured on the board itself, with HF industrial accelerometers mounted on the underside of the armored plate. Measuring equipment with shielded cables was chosen, which was supposed to monitor the measured phenomenon with the least risk. Accelerometers for measuring impact vibrations are placed via welded adapters (made of armored steel) at three measuring points M1, M2 and M3, as shown in Fig. 2 and then that side of the plate is turned down on the support.

Fig. 1 *The effect of 200 g of TNT explosives activated above the armor plate (placed on a 4×4 support)*

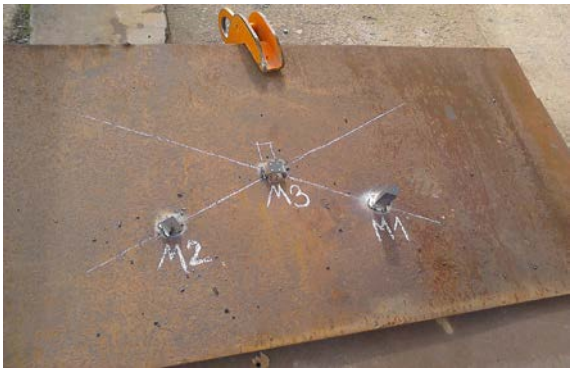

Fig. 2 *Measuring points M1, M2 and M3 of the accelerometers on armor plate of 330 kg*

- In the third experiment, the effect of explosives activated under an armor plate of ten times greater mass (3,300 kg) then previous (2 m × 1 m × 0.2 m) on the same support 4×4 (1 m × 1 m × 0.5 m) was examined. Vibrations were measured at two measuring points M1 (middle of the longitudinal end of the plate) and M2 (center of the plate) as in Fig. 3

with accelerometers on the upper side of the armor plates when activating TNT explosives of: 200 gr with and without gravel, 400 gr with gravel and 600 gr with gravel.

Fig. 3 *Measuring points M1and M2 on armor plate of 3.300 kg mass (dimensions 2 m × 1 m × 0.2 m) set on the support 4×4 (1 m × 1 m × 0.5 m)*

3. RESULTS

From the first trial experiment and based on the height (0.5 m) of the plate support and the UF camera shots, it was concluded that the plate moved (wobbled vertically) up to 1 m under impact with 200 g of TNT, up to 2 m with 400 g of TNT and up to 4 m with 600 gr of TNT, table 1.

Table 1 *Explosion under armor plate (2m × 1m × 0.02m)*

Armored plate (kg)	TNT explosive (gr)	Plate shift (m)	Measurement
330	200	1	UF camera
	400	2	
	600	4	

Fig. 4 *Effect of 600 gr of TNT activated under the armor plate of 330 kg (placed on a 4x4 support)*

Table 2 *Explosion above armor plate (2m × 1m × 0.02m)*

Armored plate (kg)	TNT explosive (gr)	Measurement point of accelerometers under the plate	Acceleration (g)
330	200	M1	1.755
		M2	1.754
		M3	1.688

Table 3 *Explosion under armor plate (2m × 1m × 0.2m)*

Armored plate (kg)	TNT explosive (gr)	Measurement point of accelerometers above the plate	Acceleration (g)
3300	200 (with gravel)	M1	1.220
	200 (with no gravel)	M1	1.515
		M2	1.755
	400 (with gravel)	M1	**777**
		M2	1.013
	600 (with gravel)	M1	137
		M2	139

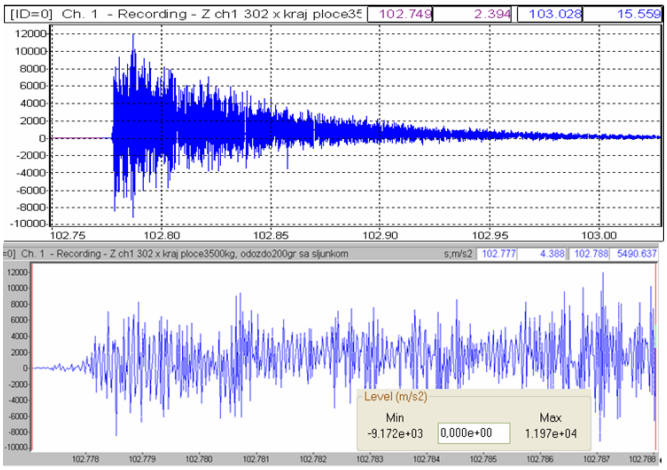

Fig. 5 *Vibrations in the Z axis at the longitudinal end of the plate (M1) under the action of 200 gr TNT (with gravel) under the armor plate of 3,300 kg (2 m × 1 m × 0.2 m)*

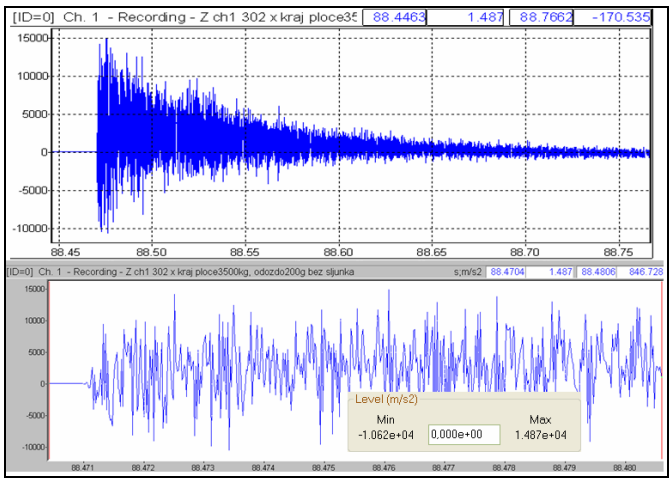

Fig. 6 *Vibrations of the M1 point under the action of 200 gr of TNT (without gravel) under the armor plate of 3,300 kg*

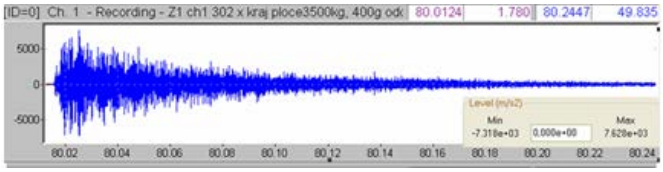

Fig. 7 *Vibrations at the end of the plate (M1) under the action of 400 g of TNT (with gravel) under the armor plate of 3,300 kg*

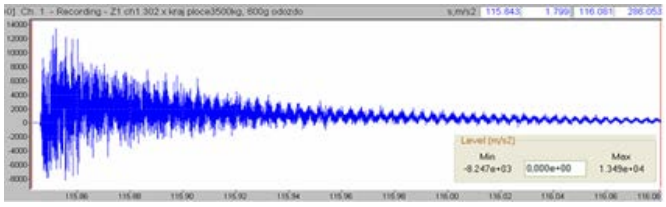

Fig. 8 *Vibrations at the end of the plate (M1) under the action of 600 g of TNT (with gravel) under the armor plate of 3,300 kg*

4. CONCLUSION

The effect of an activated TNT of 200 g below or above a armor plate of 330 kg or 3,300 kg does not damage the armor plate or move it, but is manifested by a huge pressure - a shock, where the direct shock wave is joined together with reflected waves.

Activating explosives above the armored plate gives higher shock amplitudes (due to less energy absorption in the air) than the activating below the plate, in the ground.

Measuring vibrations makes sense only when the armor plate is moving, ie. when activating stronger explosives of 400 gr (and some reasonable step more) under the plate, but this is also risky for sensors and cables (especially when the explosives are in the gravel).

Better results (in terms of analysis and protection in the case of armored vehicles) would be achieved by elastically fastening the plate with as much freedom as possible. This was confirmed by vibration measurements when the 200 gr explosive was activated (when the plate was not moving) and when it was activated explosive of 400 gr, when the plate was moving, and the vibrations were of a significantly smaller amplitude.

REFERENCES

[1] N. Jacob et al, "Scaling aspects of quadrangular plates subjected to localized blast loads-experiments and prediction", International journal of impact engineering, Vol. 30 isues 8-9, sept. 2004, https://doi.org/10.1016/j.ijimpeng.2004.03.012.

[2] Lucia Figuli et al, "Design and analysis of blast loaded windows", Procedia engineering Vol. 192 2017., p 177-182, https://doi.org/10.1016/j.proeng.2017.06.031.

[3] L.M. Mazzarion et al, "A method to represent impacted structures using scaled models made of different materials", International journal of impact engineering, Vol. 90, april 2016, https://doi.org/10.1016/j.ijimpeng.2015.11.018.

[4] C. Wu at al, "Modeling of simultaneous ground shock and airblast presure on nearby structures from surface explosions", International journal of impact engineering, Vol. 31, July 2005., p. 699-717, https://doi.org/10.1016/j.ijimpeng.2004.03.002.

[5] G.R. Johnson at al, "Fracture characteristics of three metals subjected to various strains, strain rates, temperatures and presures", Engineering fracture mechanics, Vol. 21, p 31-48, 1985. https://doi.org/10.1016/0013-7944(85)90052-9.

University of Nis
Faculty of Occupational Safety

„Politechnica“ University of Timisoara
Faculty of Mechanical Engineering

27th International Conference

NOISE AND VIBRATION

Niš, 20 - 21. 10. 2022.

SENVIBE

University of Nis
Faculty of Occupational Safety
„Politechnica“ University of Timisoara
Faculty of Mechanical Engineering
27th International Conference
NOISE AND VIBRATION
Niš, 20 - 21. 10. 2022.

SENVIBE PROJECT: OBJECTIVES AND MAIN ACHIEVEMENTS

Ivana Kovacic[1]

[1] Project Coordinator, University of Novi Sad, Serbia, senvibe@uns.ac.rs

Abstract - *SENVIBE is the acronym of the Erasmus+ Capacity Building project 'Strengthening educational capacities by building competences and cooperation in the field of Noise and Vibration Engineering', coordinated by University of Novi Sad. This paper provides the description of its wider and specific objectives, as well as its main deliverables and outcomes.*

1. INTRODUCTION

The motivation to propose the SENVIBE project [1] was the recognized need to improve national educational capacities and build cooperation and competences in dealing with environmental and occupational noise and vibration (No&Vib) issues in Serbia. The project proposal was approved for financing by the European Education and Culture Executive Agency and implemented during the four-year period 2018 – 2022, with the University of Novi Sad being the coordinating institution. The SENVIBE project has been relying on the synergy between the partners - the two Higher Education Institutions (HEIs) from Europe: University of Southampton, Institute of Sound and Vibration Research ISVR and Kungliga Tekniska Högskolan KTH, Marcus Wallenberg Laboratory for Sound and Vibration Research, who possess the know-how and experience in the area and were expected to transfer the knowledge to boost the practices of four HEIs from Serbia dealing with No&Vib: University of Novi Sad, University of Nis, University of Kragujevac and EDUCONS University from Sremska Kamenica. Besides these academic partners, additional support has been provided by three non-academic partners: the local authority - Provincial Secretariat for Urban Planning and Environmental Protection of Autonomous Province of Vojvodina, stakeholders from industry (Vojvodinian Association of Employers) and the Institute for Occupational Safety and Health from Novi Sad.

The SENVIBE project is at the very end, and this paper summarizes its main objectives and directly related achievements: activites, deliverables and outcomes.

2. PROJECT OBJECTIVES

In order to improve national educational capacities and cooperation, four project objectives were set:

1. To modernise existing courses (modules) in the field of No&Vib as well as to develop and implement new tailor-made ones for undergraduate students of Environmental Engineering, Occupational Safety Engineering, Mechanical Engineering, Electrical Engineering, Civil Engineering and Traffic Engineering at the Serbian HEIs involved;
2. To create and implement two types of Life-Long Learning (LLL) courses;
3. To develop and implement a new MSc programme in Vibro-Acoustic Engineering at the University of Novi Sad;
4. To establish a No&Vib Hub - a central unit launching and facilitating strategic cooperation among the key stakeholders engaged in No&Vib management: academia, local industry and local and national authorities.

Additional objective was to introduce new teaching methodologies, including the use of e-tools and b-learning approaches as well as to purchase, install and use new pieces of equipment or to modernise the existing ones.

3. MAIN ACHIEVEMENTS RELATED TO THE PROJECT OBJECTIVES

3.1 Courses/modules for students

A total of nine existing modules for BSc students were modified. In addition, parts/topics of nine other existing modules were enriched. Three new subjects were developed for BSc students as well as one new subject for MSc students. Various types of new materials for e-learning and b-learning were created and uploaded to the project ICT platform - the so-called, e-SENVIBE platform. Among them are multimedia presentations, web applications, animations and simulations, tests, video material and noise measurement examples. One university textbook (Fig. 1) and one study material were published. Over 1300 students at four universities have been enrolled in modified and new modules and had access to the materials developed.

Fig. 1 *Students with a new SENVIBE textbook*

3.2 LLL courses

The first SENVIBE LLL course developed is entitled 'Environmental & Occupational Noise and Human Vibration Risk Assessment'. It contains six hours of theoretical classes and two hours of practical classes. This LLL course was implemented online twice. The second SENVIBE LLL course is entitled 'Environmental Noise Management', and includes three hours of theoretical classes and one hour of discussion. This course was held in Novi Sad and Kraljevo. Overall, the SENVIBE LLL courses were attended by 119 participants.

The two-part publication 'SENVIBE Glossary' (Fig. 2), was created and published. The first part includes descriptions and translations into English of relevant terms in the field of No&Vib, as well as explanations of accompanying phenomena. The second part of the publication contains a sublimated description of European and domestic regulations in the field of No&Vib in the context of environmental protection and occupational safety.

Fig. 2 *SENVIBE Glossary*

3.3 New MSc programme in Vibro-Acoustic Engineering

The new title of Master Engineer of Vibro-Acoustic Engineering was registered and included in the list of professional, academic and scientific titles in Serbia. The content of a new MSc Academic Programme Vibro-Acoustic Engineering (MASVAE) was developed and accredited. Its curriculum contains 12 modules and enables profiling towards Vibration Engineering, Acoustic Engineering or Environmental No&Vib. The programme is run at the University of Novi Sad, and 25 students were enrolled as the first generation in 2021/22. The vibration lab was established (Fig. 3) and a mini-anechoic chamber purchased. The e-SENVIBE platform was enriched with newly developed materials and used for teaching and learning purposes.

Fig. 3 *MASVAE students in a new vibration lab*

3.4 No&Vib Hub

The No&Vib Hub's mission includes developing effective mechanisms for cooperation through astudent internship programmes, industrial scholarship/fellowship programmes, realisation of joint projects, monitoring of reform policies, development and implementation of professional training, seminars and workshops, dissemination activities and exchange of knowledge on the related legislation, monitoring results, new issues, etc. The No&Vib Hub was established at the University of Novi Sad in November 2020. So far, 45 members from the governmental, academic, research, economic, professional and non-governmental sector have joined the platform (joining can be done online via the No&Vib Hub website [2]). Various activites have been realized, among which is the publication of three brochures (Fig. 4): 'Occupational Noise – Guide for Employees and Employers', 'Occupational Vibration – Guide for Employees and Employers' and 'Guide for the Local Self-Government Units – Environmental Noise'. In addition, a leaflet about noise for a wider community has been created, published and distributed.

Fig. 4 *One of the SENVIBE brochures published*

4. CONCLUSIONS

The SENVIBE project has addressed the need for strengthening educational capacities by building competences and cooperation in Serbia in the No&Vib fields via new/ modernised modules/topics, LLL courses, a new MSc programme in Vibro-Acoustic Engineering, and a newly established No&Vib Hub. The existing and future challenge is to attract students and attendees to the aforementioned courses as well as to assure that the Hub continues to grow and attract more stakeholders within the No&Vib fields, aspiring to assure a better cooperation between HEIs and other sectors.

ACKNOWLEDGEMENT: This SENVIBE project (598241-EPP-1-2018-1-RS-EPPKA2-CBHE-JP) has been funded by the European Commission. This publication reflects the views only of the author, and the Commission cannot be held responsible for any use which may be made of the information contained therein.

REFERENCES

[1] www.senvibe.uns.ac.rs

[2] https://senvibe.uns.ac.rs/procedura-za-pridruzivanje-novib-hub-u/

SeNVibe

https://senvibe.uns.ac.rs

AUSPICE

Ministry of Education,
Science and Technological Development
Republic Serbia

www.mpn.gov.rs

GENERAL SPONSOR

Brüel & Kjær
an HBK company

www.bksv.com